



Wild Fish Conservancy
N O R T H W E S T
S C I E N C E E D U C A T I O N A D V O C A C Y

September 6th, 2024

Submitted via Electronic Filing to the [Federal Registrar](#)

Re: Comments re: 90-Day Finding on a Petition to List Gulf of Alaska Chinook Salmon as Threatened or Endangered Under the Endangered Species Act (NOAA-NMFS-2024-0042-0001)

Dear NMFS Office of Protected Resources,

Wild Fish Conservancy (WFC) submits these comments on National Marine Fisheries Service's (NMFS) 90-Day Finding on a Petition to list Gulf of Alaska (GOA) Chinook salmon as threatened or endangered under the Endangered Species Act (ESA). WFC is a nonprofit conservation organization headquartered in Washington State and working from California to Alaska to preserve, protect and restore the northwest's wild fish and the ecosystems they depend on, through science, education, and advocacy.

I. INTRODUCTION

On May 24, 2024, NMFS announced a 90-day finding on a petition from WFC to list GOA Chinook salmon (*Oncorhynchus tshawytscha*) as threatened or endangered under the ESA. The petition also requested that NMFS designate critical habitat concurrently with the listing. NMFS is soliciting scientific and commercial data, including traditional ecological knowledge pertaining to Chinook salmon that spawn in the rivers of Southern Alaska

WFC is highly qualified to comment on the 90-day finding announced by NMFS regarding the petition to list the GOA Chinook salmon under the ESA and possesses the expertise to assess the legal requirements for the listing, ensuring that it aligns with national laws. WFC's focus on the region's wild fish provides them with the scientific and practical insight necessary to contribute valuable data and perspectives on the ecological needs of the Chinook salmon and the potential impacts of their listing and habitat designation under the ESA.

II. DISCUSSION

Facing the critical situation of GOA Chinook salmon, and with the troubling bycatch by trawl fisheries, WFC urges NMFS to take urgent, decisive action to list Chinook salmon under the ESA.

A. The ESA mandates a strict, time-bound process for listing endangered species, and adherence to timelines is crucial for conservation of GOA Chinook salmon.

The ESA serves as a cornerstone of environmental legislation in the United States, aimed at conserving endangered and threatened species and the ecosystems upon which they depend.¹ To ensure the timely protection of species, Congress mandated **a detailed and time-bound process for listing species under the ESA**. Congress described this listing process as “[t]he cornerstone of effective implementation of the Endangered Species Act.”²

The listing process begins with NMFS making a preliminary 90-day finding to determine if a petition presents substantial scientific or commercial information indicating that the action may be warranted.³ Upon determining that the petition contains substantial information, NMFS must publish this finding in the Federal Register, opening the process to public review and comment. *Id.*

Subsequently, NMFS has a maximum of 12 months from the date the petition was received to make a further determination.⁴ This period involves a thorough review of the species’ status, culminating in one of three possible outcomes: (1) the petitioned action is not warranted; (2) the petitioned action is warranted, leading NMFS to propose a rule to list the species as threatened or endangered; or (3) the petitioned action is warranted but precluded by other higher priority actions. Significantly, this statutory period is not discretionary. If the agency fails to timely issue its 12-month finding, it is in violation of the ESA.⁵ If NMFS decides to list the species, it publishes a proposed rule in the Federal Register for public comment.⁶ The final listing determination must be made within one year of publishing the proposed rule.⁷

The case of GOA Chinook salmon is particularly urgent. On May 24, 2024, NMFS announced a 90-day finding on a petition from WFC, highlighting the critical status of Chinook salmon populations. These populations are integral not only to the ecosystem but also to the cultural and economic fabric of the region. Any delay in the 12-month finding, as observed in past instances such as the failure to timely address the listing of the cauliflower coral,⁸ could

¹ 16 U.S.C. § 1531(b).

² S. Rep. No. 418, 97th Cong., 2d Sess. at 10; see also H. Rep. No. 567, 97th Cong., 2d Sess. at 10 (describing section 4 of the ESA, 16 U.S.C. § 1533).

³ 16 U.S.C. § 1533(b)(3)(A).

⁴ 16 U.S.C. § 1533(b)(3)(B).

⁵ See 16 U.S.C. §§ 1533(b)(3)(B) & 1540(g). The failure to meet this deadline is also agency action “unlawfully withheld or unreasonably delayed” within the meaning of the Administrative Procedure Act, 5 U.S.C. § 706(1).

⁶ 16 U.S.C. § 1533(b)(5).

⁷ 16 U.S.C. § 1533(b)(6)(A)(i).

⁸ Center for Biological Diversity, *Lawsuit Advances Protections for Hawaii’s Cauliflower Coral* (2020), available at: <https://biologicaldiversity.org/w/news/press-releases/lawsuit-advances-protections-for-hawaiis-cauliflower-coral-2020-03-04>. The case of the cauliflower coral (*Pocillopora meandrina*), known as Ko‘a in Hawaiian, is a recent and relevant example of NMFS’s failure to meet its legal obligations under the ESA. In that instance, NMFS did not

have severe consequences for the survival of Chinook salmon populations. WFC urge NMFS to strictly adhere to the ESA's mandatory timelines to avoid a repeat of past delays, which can significantly endanger vital species.

B. The ESA requires a comprehensive analysis of all mortality sources, including indirect take, for listing GOA's Chinook salmon under the ESA.

ESA Section 4(b)(1)(A) requires that the decision to list a species under the ESA be made on a comprehensive analysis of "the best scientific and commercial data available."⁹ This includes evaluating factors like "present or threatened destruction, modification, or curtailment of its habitat or range" and "overutilization for commercial, recreational, scientific, or educational purposes."¹⁰ In the context of assessing the status of GOA Chinook salmon within the GOA Evolutionarily Significant Unit(s) (ESU), this provision requires a thorough examination of all mortality sources impacting these populations.

The current exploitation rates (ERs) reported by fisheries targeting specific species do not adequately account for the indirect take, or bycatch, of non-target species such as Chinook salmon. This is particularly significant due to the tendency of Chinook salmon populations to aggregate densely in certain areas. Because of this spatial clustering, catch figures may not accurately reflect the severe impact of fishing activities on small, localized Chinook populations. Therefore, a detailed analysis at the level of individual fishing vessel's catch and/or source population is necessary to understand the impact on Chinook salmon. To comply with the ESA, the status review must extend beyond direct mortality rates to encompass indirect mortality, a critical concern highlighted by the substantial bycatch of Chinook salmon in British Columbia (BC) and Alaska fisheries.

Additionally, a new, standardized international Pacific Rim baseline for genetic stock identification (GSI) of Chinook Salmon has recently been published. We recommend any past GSI analysis take into account any difference in reporting groups this new baseline may reveal. In addition, special attention is warranted in regard to some of the inaccuracies reported for the new baseline in regards to the Taku, Stikine, and SE Alaska stocks based on the results reported by Van Doornick et al (2024) in figure 4. Additional genetic analyses use next generation genetic analysis techniques (more loci across the entire Chinook salmon genome) may be necessary to adequately identify ESU's.

adhere to the mandatory 12-month finding deadline following a positive 90-day finding that listing the coral species might be warranted. This delay not only violated the express statutory requirements of the ESA but also potentially exacerbated the threats to the species' survival. The Center for Biological Diversity had to resort to legal action to compel NMFS to fulfill its duty. This situation should serve as a cautionary tale in the current deliberations over the Chinook salmon.

⁹ 16 U.S.C. § 1533(b)(1)(A).

¹⁰ 16 U.S.C. § 1533(a)(1)(A)-(B).

1. NMFS should consider Chinook bycatch data in BC fisheries for ESA evaluations of GOA stocks.

A draft report by Fisheries and Oceans Canada (DFO Report), recently shared with the WFC by an independent journalist, highlights the concerning levels of bycatch involving Chinook salmon in the BC groundfish trawl fisheries.¹¹ The DFO Report analyzed tissue samples recovered from the BC groundfish fisheries conducted from September 26, 2022 to February 20, 2023. During that time period, a total of 28,117 Pacific salmon were captured, of which 26,273 were Chinook.¹² The majority of Chinook caught were from the mid-water troll fleet.¹³ This represents a tripling of the previous 14-year average and the highest level of bycatch since 2008.

Stock composition analyses of the Chinook caught included both coded wire tag (CWT) recoveries from Pacific Salmon Treaty exploitation rate indicator stocks in BC, Puget Sound, and the Washington Coast, and genetic assignment methods (for Chinook that lacked a coded-wire tag).¹⁴ Genetic stock identification analyses included parent-based tagging (PBT) analyses and genetic stock identification (GSI) analyses.¹⁵ PBT analyses were applicable only for BC hatchery stocks for which appropriate parental genetic data had been acquired.¹⁶ GSI analyses were applied to the remaining Chinook samples that were not resolved by PBT.¹⁷

This method allowed researchers to determine the stock composition for Chinook salmon that originated in Canada. While the study did not determine the stock composition for Chinook salmon that originated in the United States, it is reasonable to infer that Chinook salmon that did not originate in Canada, originated in the United States, some of which could have been from GOA Chinook populations.¹⁸ As noted in the DFO report, “stock composition of Chinook salmon represented by Canadian-origin stocks, as estimated based upon combined CWT and PBT-GSI information, varied from 21% to 83% among catch strata.”¹⁹

These results suggest that significant numbers of US stocks, including the petitioned GOA stocks, were also taken by the BC groundfish fishery. Accordingly, as part of its review, NMFS should acquire the BC groundfish bycatch data evidenced by the DFO Report and conduct appropriate stock identification analyses on all Chinook samples not identified as belonging to BC Chinook stocks.

¹¹ C.R. Lagasse et al., *Review of Salmon Bycatch in the Pacific Region 2022/23 Groundfish Trawl Fishery and Preliminary Results of an Enhanced Monitoring Program*, Can. Manusc. Rep. Fish. Aquat. Sci. 273 (2023).

¹² *Id.* at 14.

¹³ *Id.*

¹⁴ *Id.* at 5.

¹⁵ *Id.*

¹⁶ *Id.*

¹⁷ *Id.*

¹⁸ *Id.* at 30.

¹⁹ *Id.* at 8.

2. NMFS should consider bycatch data from the Alaska Bering Sea (BSAI) and GOA groundfish trawl fisheries for ESA evaluations of GOA stocks.

In addition to the recent Chinook bycatch in the BC groundfish fisheries, there has been significant bycatch of Chinook in the Alaska groundfish fisheries, notably within the Bering Sea and Aleutian Islands (BSAI) and the GOA Pollock fisheries. The latest data from Guthrie et al. shows estimated stock contributions of Chinook bycatch across the Northwest Gulf of Alaska, Copper, Coastal Southeast Alaska, among others.^{20,21} NMFS should evaluate the two reports by Guthrie et al. and include the catches of both adult, and subadult, Chinook salmon that are likely captured from populations being evaluated for listing in the Petition.

3. Additional scientific publications relevant to the evaluation of the petition.

We recommend adding the following publications to the list of relevant scientific information that should be considered by the Biological Review Team:

Brendan Byrne, Junjie Liu, Kevin W. Bowman, Madeleine Pascolini-Campbell, Abhishek Chatterjee, Sudhanshu Pandey, Kazuyuki Miyazaki, Guido R. van der Werf, Debra Wunch, Paul O. Wennberg, Coleen M. Roehl & Saptarshi Sinha. Nature 2024. Carbon emissions from the 2023 Canadian wildfires.

Davies, B., McNabb, R., Bendle, J., Carrivick, J., Ely, J., Holt, T., Markle, B., McNeil, C., Nicholson, L., Pelto, M. 2024. Accelerating glacier volume loss on Juneau Icefield driven by hypsometry and melt-accelerating feedbacks. Nature Communications.

Gayeski, N., Swanson, D., MacDuffee, M., Rosenberger, A. Productivity and resilience of Chinook salmon compromised by ‘Mixed-Maturation fisheries in marine waters.’ In review, 2024. BioRxiv

Van Doornik, D.M., Moran, P., Rondeau, E.B., Nichols, K.M., Narum, S.R., Campbell, M.R., Clemento, A.J., Hargrove, J.S., Hess, J.E., Horn, R.L., Seeb, L.W., Stephenson, J.J., McKinney, G.J. 2024. A new, standardized international Pacific Rim baseline for genetic stock identification (GSI) of Chinook Salmon. North American Journal of Fisheries Management. 44:857-869.

Von Biela, V. R., L. Bowen, S. D. McCormick, M. P. Carey, D. S. Donnelly, S. Waters, A. M. Regish, S. M. Laske, R. J. Brown, S. Larson, S. Zuray, and C. E. Zimmerman. 2020. Evidence of prevalent heat stress in Yukon River Chinook Salmon. Canadian Journal of Fisheries and Aquatic Sciences 77:1878–1892.

²⁰ C. M. Guthrie III et al., *Genetic stock composition analysis of Chinook salmon (*Oncorhynchus tshawytscha*) bycatch samples from the 2020 Bering Sea pollock trawl fisheries*, US Department of Commerce, NOAA Technical Memo NMFS-AFSC-446 (2022), 30.

²¹ C. M. Guthrie III et al., *Genetic stock composition analysis of Chinook salmon (*Oncorhynchus tshawytscha*) bycatch samples from the 2020 Gulf of Alaska trawl fisheries*, US Department of Commerce, NOAA Technical Memo NMFS-AFSC-445 (2022), 30.

Von Biela et al. Fisheries 2021. Premature Mortality Observations among Alaska's Pacific Salmon During Record Heat and Drought in 2019.

III. CONCLUSION

WFC strongly support the prompt listing of GOA Chinook salmon under the ESA. Given the substantial evidence of high bycatch rates in both domestic and international fisheries, WFC urge NMFS to adhere strictly to the ESA-mandated timelines and procedures. It is imperative that NMFS incorporates comprehensive bycatch data and all other relevant scientific and commercial information in its status review to ensure a well-informed and timely decision. Prompt and thorough attention to this process will not only serve the immediate needs of the Chinook salmon but will also positively reinforce the commitment to conservation efforts for similarly situated species in the future.

Attached:

1. Additional References
2. References from Footnotes

Carbon emissions from the 2023 Canadian wildfires

<https://doi.org/10.1038/s41586-024-07878-z>

Received: 29 November 2023

Accepted: 25 July 2024

Published online: 28 August 2024

Open access

 Check for updates

Brendan Byrne^{1✉}, Junjie Liu^{1,2}, Kevin W. Bowman^{1,3}, Madeleine Pascolini-Campbell¹, Abhishek Chatterjee¹, Sudhanshu Pandey¹, Kazuyuki Miyazaki¹, Guido R. van der Werf⁴, Debra Wunch⁵, Paul O. Wennberg^{2,6}, Coleen M. Roehl² & Saptarshi Sinha⁷

The 2023 Canadian forest fires have been extreme in scale and intensity with more than seven times the average annual area burned compared to the previous four decades¹. Here, we quantify the carbon emissions from these fires from May to September 2023 on the basis of inverse modelling of satellite carbon monoxide observations. We find that the magnitude of the carbon emissions is 647 TgC (570–727 TgC), comparable to the annual fossil fuel emissions of large nations, with only India, China and the USA releasing more carbon per year². We find that widespread hot–dry weather was a principal driver of fire spread, with 2023 being the warmest and driest year since at least 1980³. Although temperatures were extreme relative to the historical record, climate projections indicate that these temperatures are likely to be typical during the 2050s, even under a moderate climate mitigation scenario (shared socioeconomic pathway, SSP 2–4.5)⁴. Such conditions are likely to drive increased fire activity and suppress carbon uptake by Canadian forests, adding to concerns about the long-term durability of these forests as a carbon sink^{5–8}.

Canadian forests cover a vast area of nearly 362 million ha (ref. 9), amounting to 8.5% of the global forested area¹⁰. These forests are an important sink of carbon, absorbing fossil carbon dioxide (CO₂) from the atmosphere and slowing the pace of climate warming^{11,12}. However, climate change is increasing forest fire activity, acting to suppress the carbon uptake capacity of these forests¹³. Although more frequent fires have been widespread, 2023 has seen forest fires on an extreme scale. With 15 million ha of Canadian forests burned (about 4% of forest area)¹, 2023 saw more than seven times (8 σ) the average burned area over the preceding 40 years (1983–2022 mean, 2.2 million ha; range, 0.2–7.1 million ha)¹. The adverse societal impacts of these fires are clear: 232,000 evacuations and poor air quality affecting millions¹⁴. However, the carbon emissions from the fire events remain uncertain. In this study, we quantify these emissions through inverse modelling of satellite observations of carbon monoxide (CO). Then, we examine concurrent climate anomalies and projected changes in the prevalence of hot–dry weather under climate change. Finally, we discuss the implications of fires for the Canadian carbon budget.

Fire emissions

Fire carbon emissions can be tracked from space using bottom-up and top-down approaches. Bottom-up approaches use satellite observations to track fire activity, such as burned area¹⁵ or fire radiative power¹⁶. Emissions of CO₂, CO and other trace gases are then estimated by combining the estimates of fire activity with quantities such as fuel loads and emission factors. Although these bottom-up estimates are continually improving, inventories can vary significantly

in global and regional trace gas and aerosol emission estimates^{15,17}. Top-down approaches provide a method for refining bottom-up trace gas emission estimates by optimally scaling emission estimates to be consistent with the observed concentrations of trace gases in fire plumes. A strength of this approach is that it integrates emissions from both flaming and smouldering combustion to capture net emissions.

In this study, we perform top-down estimates of CO emissions from the 2023 Canadian fires based on observational constraints from the Tropospheric Monitoring Instrument (TROPOMI) space-based CO retrievals (Fig. 1a,b). These estimates are performed using three different bottom-up fire emission inventories: the global fire emissions database (GFED4.1s)¹⁵, the global fire assimilation system v.1.2 (GFAS)¹⁶ and the quick fire emissions dataset v.2.6r1 (QFED)¹⁸. For each inversion, the combined carbon emissions released as CO and CO₂ (CO₂ + CO) are then estimated using the CO₂/CO emission factors from the same bottom-up database. The CO₂/CO emission ratios can be highly variable, adding uncertainty to our analysis. We incorporate some of this uncertainty here as each bottom-up database has different mean emission ratios for Canadian forests (range, 7.7–10.8 gC of CO₂ per gC of CO₂). Details for these inversions are provided in the methods and a description of the inversion results and evaluation of the performance of the top-down estimates are provided in Supplementary Information sections 1 and 2). We find the top-down estimates are relatively insensitive to choices about inversion configuration but do show sensitivity to prescribed hydroxyl radical (OH) abundances¹⁹, which determine the atmospheric lifetime of the CO emitted (Supplementary Information section 1 and Supplementary Fig. 1).

¹Jet Propulsion Laboratory, California Institute of Technology, Pasadena, CA, USA. ²Division of Geological and Planetary Sciences, California Institute of Technology, Pasadena, CA, USA.

³Joint Institute for Regional Earth System Science and Engineering, University of California, Los Angeles, CA, USA. ⁴Meteorology & Air Quality Group, Wageningen University and Research, Wageningen, The Netherlands. ⁵Department of Physics, University of Toronto, Toronto, Ontario, Canada. ⁶Division of Engineering and Applied Science, California Institute of Technology, Pasadena, CA, USA. ⁷Department of Energy, Environmental, and Chemical Engineering, Washington University in St. Louis, St. Louis, MO, USA. ✉e-mail: brendan.k.byrne@jpl.nasa.gov

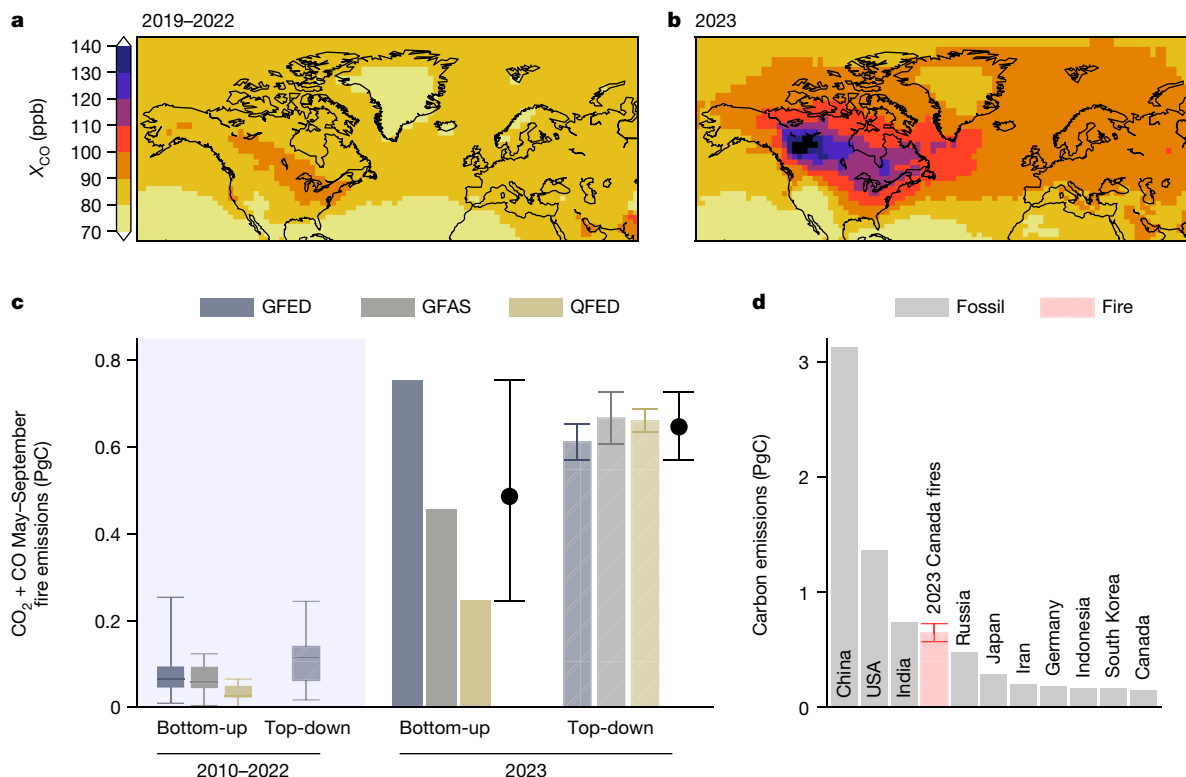


Fig. 1 | CO enhancements and fire emission estimates. **a–c**, May–September TROPOMI dry-air mole fractions of CO (X_{CO}) averaged over 2019–2022 (**a**) and for 2023 (**b**) aggregated to a $2^\circ \times 2.5^\circ$ grid. **c**, Canadian forest fire carbon emissions (from CO and CO_2) for the 2023 May–September fire season, compared with fire emissions during 2010–2022 (distribution shown by box-and-whisker plots).

Top-down emissions over 2010–2022 are estimated from MOPITT (2010–2021) and TROPOMI (2019–2022) CO retrievals. **d**, A comparison of May–September Canadian fire emissions with 2022 territorial fossil carbon emissions for the ten largest emitting countries, obtained from Global Carbon Budget 2022³.

Figure 1c shows the bottom-up and top-down $CO_2 + CO$ carbon emissions from fires during May–September 2023. The bottom-up datasets show large differences, ranging from 234 to 735 TgC (mean of 469 TgC). This range is reduced by 69% in the top-down estimates (570–727 TgC), which also give a larger mean estimate of 647 TgC. Emissions during 2023 far exceed typical Canadian forest fire emissions, with 2010–2022 average emissions of 29–82 TgC for the bottom-up inventories and 121 TgC for top-down estimates (Supplementary Fig. 2). To contextualize these numbers, we compare the top-down estimates to annual national fossil fuel emissions for the ten largest emitters (Fig. 1d). The 5 month 2023 emissions are more than four times larger than Canadian annual fossil fuel emissions (149 TgC yr^{-1}) and comparable to India’s annual emissions (740 TgC yr^{-1}).

Fire activity is affected by several complex drivers, including fuel traits²⁰ and ignition probability²¹. However, fire weather—hot and dry conditions—has been shown to be extremely important in driving fire behaviour²². Climate data show an exceptionally hot and dry fire season for Canadian forests during 2023 (Fig. 2). This was the driest January–September period for Canadian forests since at least 1980, with about 86% of forested area having below-average precipitation and about 52% being more than 1 s.d. below the 2003–2022 average (Supplementary Fig. 4). May–September 2023 was the warmest since at least 1980, with about 100% of the forest area above average and about 90% being more than 1 s.d. above the 2003–2022 average. Similarly, the vapour pressure deficit (VPD), which is closely associated with fire activity^{22–24}, was the third highest since 1980, including 85% of the forest area being above average and about 54% being more than 1 s.d. above the 2003–2022 average.

Although hot–dry conditions were widespread across Canadian forests, there are two notable regional patterns. Western Quebec (49°–55° N, 72°–80° W), which is typically relatively wet (Supplementary

Fig. 5a), had exceptionally dry conditions during 2023, with precipitation through September being 23.7 cm (49%) below average. Coupled with extreme heat and VPD during June–July, fire emissions in this region contributed about 15% of the national total (Supplementary Fig. 6). The other notable region was northwestern Canada near the Great Slave Lake (57°–62° N, 110°–125° W). This region is drier than western Quebec on average, with about half the annual precipitation. However, 2023 was exceptional, with both a large precipitation deficit of 8.1 cm (27% of January–September total) and exceptionally warm conditions throughout May–September (+2.6 °C) (Supplementary Fig. 6). This region contributed about 61% of the total Canadian forest fire emissions.

Fires and climate

The relationship between climate variability and fire emissions for Canadian forests is examined in Fig. 3, which shows fire emissions as a function of temperature and precipitation Z-scores over 2003–2023 for the $0.5^\circ \times 0.625^\circ$ grid cells, in which Z-scores are the anomalies divided by the standard deviation. May–September emissions are lowest for combined cool–wet conditions (5.2 gC m^{-2}), whereas emissions increase when either temperature is above average (19.5 gC m^{-2}) or precipitation is below average (9.2 gC m^{-2}). However, emissions are largest for combined warm–dry conditions (35.7 gC m^{-2}). In particular, fire emissions are much increased during exceptionally hot and dry conditions (99.6 gC m^{-2} , temperature $Z > 1$ and precipitation $Z < -1$). These hot–dry conditions were much more prevalent in 2023 than in preceding years, with a mean May–September T2M Z-score of 2.3 and a precipitation Z-score of –1.1 across grid cells, explaining why fire emissions were extreme during 2023. Notably, the number of individual fires during 2023 was not unusual, with 6,623 relative to a 10 yr average of

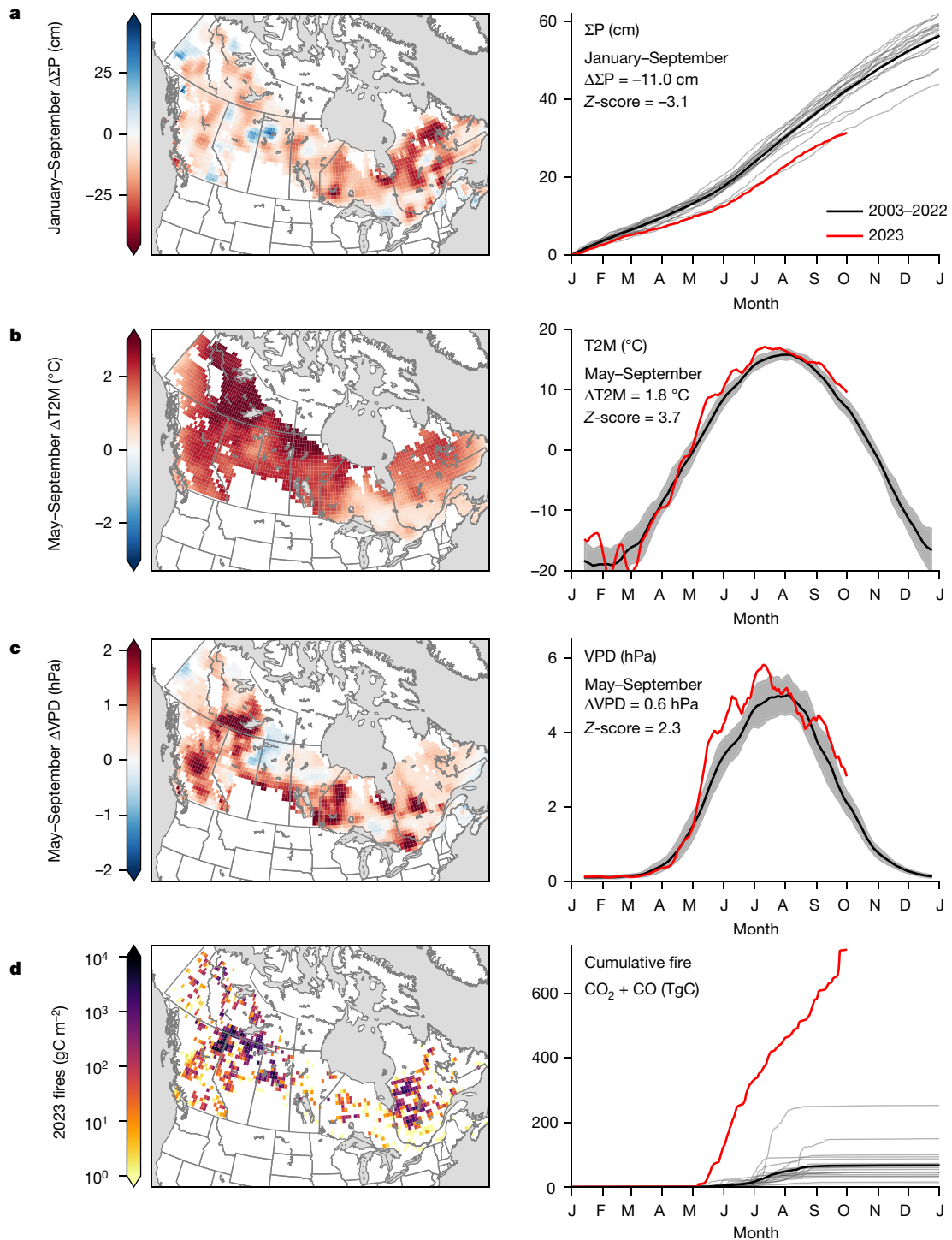


Fig. 2 | Canadian forests climate anomalies for 2023 relative to 2003–2022 mean. a–d, Maps (left) and time series (right) of CPC global unified gauge-based cumulative precipitation (ΣP) (a), MERRA-2 2 m temperature (with 2 week running mean) (b), MERRA-2 VPD (with 2 week running mean) (c) and fire $\text{CO}_2 + \text{CO}$ emissions from the GFED4.1s database (d). All maps are shown at a

spatial resolution of $0.5^\circ \times 0.625^\circ$ and Z-scores are for the area-mean of Canadian forests. Note that GFED4.1s is shown instead of the inversion results because those are at a coarser spatial resolution and cover a shorter time period, maps of prior and posterior mean fire emissions are shown in Supplementary Fig. 14. Months are shown from January (J) to December (D).

5,597 (ref. 25). Yet, probably primarily driven by these hot-dry conditions²⁴, many of these fires grew to enormous sizes with hundreds of megafires (greater than 10,000 ha) recorded.

Next, we examine future climate conditions in the region and how they compare to the concurrent climate conditions that led to the massive fires. Figure 3 shows the decadal mean temperature and precipitation Z-scores for the median of 27 models from the

coupled model intercomparison project phase 6 (CMIP6)²⁶ under the moderate-warming shared socioeconomic pathway (SSP) 2–4.5 (ref. 4). Large projected temperature increases are found to occur, with average temperatures in the 2050s similar to 2023. More modest increases in precipitation are projected, indicating a ‘speeding up’ of the water cycle, in which both evaporation and precipitation rates increase (Supplementary Fig. 12 shows ensemble distribution). Studies indicate that

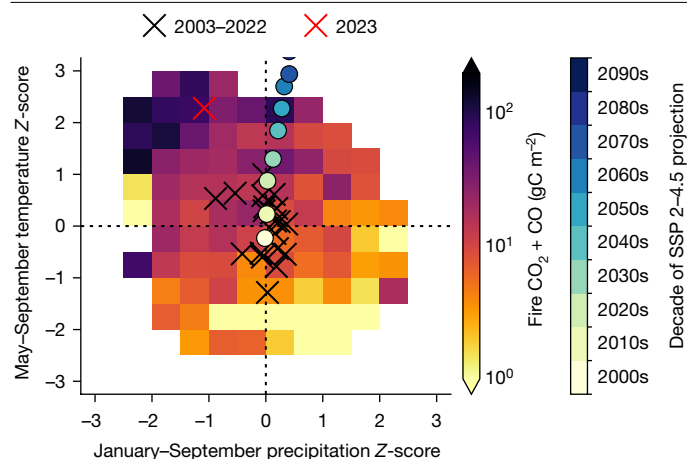


Fig. 3 | Relationship between fire emissions and climate anomalies. Mean May–September GFED4.1s CO₂ + CO fire emissions as a function of May–September T2M Z-score and January–September precipitation Z-score for each 0.5° × 0.625° forested grid cell during 2003–2023 (using 2003–2022 as a baseline). For individual years, the mean Z-scores across forested grid cells are shown with 'X'. The projected decadal-mean temperature and precipitation Z-scores for the median CMIP6 model under SSP 2–4.5 are shown by the circles. The CMIP6 Z-scores are calculated using the 2000–2019 period as a baseline but use the reanalysis 2003–2022 standard deviations (see section on 'Climate data'). The historical and projected T2M and precipitation over the Canadian boreal forests simulated by the CMIP6 ensemble are shown in Supplementary Fig. 12.

the combined effect will result in regional increases in moisture deficits for Canadian forests through the end of the twenty-first century^{6,27,28}. Beyond the 2050s, average temperature and precipitation conditions are projected to exceed the historical range. These changes will impact the boreal carbon cycle in many ways, such as changing fuel loads and species composition, which complicates projections of future fire activity. However, increases in boreal fire emissions linked to warming have been reported over recent decades^{13,27,29,30} and several studies have projected further increases in Canadian fire activity with future warming^{5–8}. Thus, we find that warming, coupled with regionally increasing moisture deficits, is likely to drive increased fire carbon emissions from Canadian forests.

Canadian carbon budget implications

As a party to the Paris Agreement, Canada is obligated to track economy-wide greenhouse gas (GHG) emissions and removals in a national GHG inventory (NGHGI). This includes tracking emissions and removals from 'managed' lands, for which human interventions and practices have been applied to perform production, ecological or social functions³¹. However, the 2006 Intergovernmental Panel on Climate Change (IPCC) guidelines for national GHG inventories³¹ and Canadian NGHGI³² differ in how emissions and removals over managed lands are categorized. The IPCC guidelines treat all emissions and removals on managed land as anthropogenic, whereas the Canadian NGHGI treats 'natural disturbances' as non-anthropogenic. This difference in categorization leads to large differences between the Canadian NGHGI and an estimate using the IPCC guideline definitions.

Figure 4 shows that NGHGI removals on managed forest land are almost exactly compensated by emissions from harvested wood products, such that the total CO₂ emissions for Canada are dominated by the energy sector (more than 90% of net emissions). However, we see that natural disturbances are shown to be of considerable magnitude, amounting to nearly 60% of total CO₂ emissions in 2021. The 2023 CO + CO₂ fire emissions across managed Canadian forests (see section

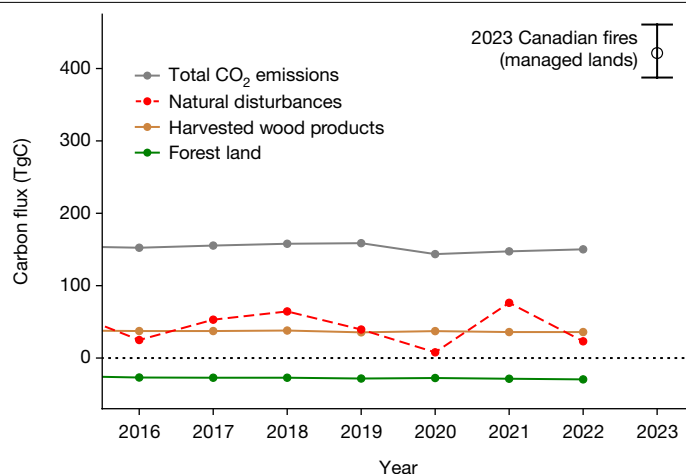


Fig. 4 | Canada's NGHGI CO₂ emissions and removals compared with the 2023 Canadian fires. Lines show the annual net emissions or removals from managed forest land (green), harvested wood products (brown), natural disturbances that are not counted towards Canada's emissions (red) and the economy-wide net CO₂ emissions (grey). The top-down estimates of the 2023 CO₂ + CO fires emissions over managed land are shown in black. Total CO₂ emissions, harvested wood products and forest land emissions and removals were obtained from Table A11-1 of the NGHGI³², whereas natural disturbances were obtained from Table 6-5 of the NGHGI. All quantities presented are in units of teragrams of carbon (1 TgC = 1 MtC = 1,012 gC), which can be converted to units of megatonnes of CO₂ (MtCO₂) by multiplying by a factor of 3.664.

on 'Managed land') are estimated to be 421 (388–461) TgC, amounting to 2.5–3 years of economy-wide CO₂ emissions.

Regardless of their characterization, fire carbon emissions will affect the growth rate atmospheric CO₂. As such, monitoring changes in the carbon budget across both managed and unmanaged land is important. Including all land in the Canadian carbon budget, top-down estimates find that Canadian ecosystems are a sink of CO₂ when constrained by either in situ or space-based CO₂ observations. Using both data types, an ensemble of atmospheric CO₂ inversion systems report that Canadian carbon stocks increased 366 ± 88.6 TgC yr⁻¹ over 2015–2020¹¹, contributing about 30% of the net land carbon sink. Similarly, space-based biomass estimates find carbon accumulation in Canadian boreal forests, although smaller in magnitude^{13,33,34}. Thus, Canadian forests play an important role in mitigating anthropogenic emissions, slowing the rise of atmospheric CO₂. The large carbon release resulting from the 2023 Canadian fires puts into question the durability of this sink. Others¹³ showed that fires have acted to suppress the carbon uptake potential of Canadian forests over the past 30 years. Although Canadian forests have historically experienced large stand-replacing fires at infrequent intervals of 30 to more than 100 years^{35–37}, increases in fire frequency will probably reduce biomass recovery and affect species composition^{37–40}. It has also been argued that fire, insects and droughts may already be driving Canadian forests into a carbon source^{41,42}. In the extreme case that expansive fires, such as that of 2023, become the norm (burning 4% of Canadian forest area), all Canadian forests could burn every 25 years. So, although the magnitude is uncertain, it is likely that increasing fire activity in Canadian forests will reduce the capacity of these Canadian forests to continue to act as a carbon sink.

The role of Canada's fire management strategy in managing fire carbon emissions also deserves some discussion. Fire management strategies require balancing several considerations, including socio-economic costs, ecological impacts and carbon emissions. Canada's present strategy adopts a risk-based approach, for which decisions on whether or not to suppress fires are made on a fire-by-fire basis⁴³, with

differing priorities across provinces and territories. Understanding how fire regimes will change with climate change is thus of high importance, for future decision criteria and costing.

Conclusions


The 2023 fire season was the warmest and driest for Canadian forests since at least 1980, resulting in vast carbon emissions from forest fires. Using TROPOMI CO retrievals, we estimate the total May–September CO₂ + CO emissions from these fires to be 647 TgC (range 570–727 TgC), comparable in magnitude to India's annual fossil fuel CO₂ emissions. The 2023 warmth was exceptional based on the last 44 years but CMIP6 climate models project that the temperatures of 2023 will become normal by the 2050s. Such changes are likely to increase fire activity^{5–8}, risking the carbon uptake potential of Canadian forests. This will impact allowable emissions for reaching warming targets, as reduced carbon sequestration by ecosystems must be compensated for by adjusting anthropogenic emissions reductions.

Online content

Any methods, additional references, Nature Portfolio reporting summaries, source data, extended data, supplementary information, acknowledgements, peer review information; details of author contributions and competing interests; and statements of data and code availability are available at <https://doi.org/10.1038/s41586-024-07878-z>.

- Jain, P. et al. Canada under fire—drivers and impacts of the record-breaking 2023 wildfire season. *ESS Open Archive* <https://doi.org/10.22541/essoar.170914412.27504349/v1> (2024).
- Friedlingstein, P. et al. Global carbon budget 2022. *Earth Syst. Sci. Data* **14**, 4811–4900 (2022).
- MERRA-2 *tavg1_2d_slv_Nx: 2d, 1-Hourly, Time-Averaged, Single-Level, Assimilation, Single-Level Diagnostics V5.12.4* (GSFC DAAC, accessed 24 October 2023); <https://doi.org/10.5067/VJAFPL1ICSIV>.
- Meinshausen, M. et al. The shared socio-economic pathway (SSP) greenhouse gas concentrations and their extensions to 2500. *Geosci. Model Dev.* **13**, 3571–3605 (2020).
- Wang, X. et al. Projected changes in fire size from daily spread potential in Canada over the 21st century. *Environ. Res. Lett.* **15**, 104048 (2020).
- Kitzberger, T., Falk, D. A., Westerling, A. L. & Swetnam, T. W. Direct and indirect climate controls predict heterogeneous early-mid 21st century wildfire burned area across western and boreal North America. *PLoS ONE* **12**, 0188486 (2017).
- Nitschke, C. R. & Innes, J. L. Climatic change and fire potential in south-central British Columbia, Canada. *Glob. Change Biol.* **14**, 841–855 (2008).
- Phillips, C. A. et al. Escalating carbon emissions from North American boreal forest wildfires and the climate mitigation potential of fire management. *Sci. Adv.* **8**, 7161 (2022).
- The State of Canada's Forests Annual Report 2022* (Government of Canada, 2022); <https://natural-resources.canada.ca/our-natural-resources/forests/state-canadas-forests-report/16496>.
- Global Forest Resources Assessment 2020: Main Report* (FAO, 2020); <https://doi.org/10.4060/ca9825en>.
- Byrne, B. et al. National CO₂ budgets (2015–2020) inferred from atmospheric CO₂ observations in support of the global stocktake. *Earth Syst. Sci. Data* **15**, 963–1004 (2023).
- Deng, Z. et al. Comparing national greenhouse gas budgets reported in UNFCCC inventories against atmospheric inversions. *Earth Syst. Sci. Data* **14**, 1639–1675 (2022).
- Wang, J. A., Baccini, A., Farina, M., Randerson, J. T. & Friedl, M. A. Disturbance suppresses the aboveground carbon sink in North American boreal forests. *Nat. Clim. Change* **11**, 435–441 (2021).
- O'Neill, N. & Otis, D. Military deploys 350 soldiers to Northwest Territories, 68 per cent of population evacuated. *CTV News* (22 August 2023).
- Werf, G. R. et al. Global fire emissions estimates during 1997–2016. *Earth Syst. Sci. Data* **9**, 697–720 (2017).
- Kaiser, J. W. et al. Biomass burning emissions estimated with a global fire assimilation system based on observed fire radiative power. *Biogeosciences* **9**, 527–554 (2012).
- Pan, X. et al. Six global biomass burning emission datasets: intercomparison and application in one global aerosol model. *Atmos. Chem. Phys.* **20**, 969–994 (2020).
- Darmenov, A. S. & Silva, A. M. *The Quick Fire Emissions Dataset (QFED): Documentation of Versions 2.1, 2.2 and 2.4* (NASA Global Modeling and Assimilation Office, accessed 10 November 2023); <https://gmao.gsfc.nasa.gov/pubs/docs/Darmenov796.pdf>.
- Voulgarakis, A. et al. Analysis of present day and future OH and methane lifetime in the ACCMIP simulations. *Atmos. Chem. Phys.* **13**, 2563–2587 (2013).
- Varner, J. M., Kane, J. M., Kreye, J. K. & Engber, E. The flammability of forest and woodland litter: a synthesis. *Curr. For. Rep.* **1**, 91–99 (2015).
- Veraverbeke, S. et al. Lightning as a major driver of recent large fire years in North American boreal forests. *Nat. Clim. Change* **7**, 529–534 (2017).
- Williams, A. P. et al. Observed impacts of anthropogenic climate change on wildfire in California. *Earth's Future* **7**, 892–910 (2019).
- Clarke, H. et al. Forest fire threatens global carbon sinks and population centres under rising atmospheric water demand. *Nat. Commun.* **13**, 7161 (2022).
- Juang, C. S. et al. Rapid growth of large forest fires drives the exponential response of annual forestfire area to aridity in the western United States. *Geophys. Res. Lett.* **49**, e2021GL097131 (2022).
- Fire Statistics* (Canadian Interagency Forest Fire Centre, accessed 3 November 2023); <https://ciffc.net/statistics>.
- Eyring, V. et al. Overview of the coupled model intercomparison project phase 6 (CMIP6) experimental design and organization. *Geosci. Model Dev.* **9**, 1937–1958 (2016).
- Parisien, M.-A. et al. Abrupt, climate-induced increase in wildfires in British Columbia since the mid-2000s. *Commun. Earth Environ.* **4**, 309 (2023).
- Haughian, S. R., Burton, P. J., Taylor, S. W. & Curry, C. Expected effects of climate change on forest disturbance regimes in British Columbia. *J. Ecosyst. Manag.* <https://doi.org/10.22230/jem.2012v13n1a152> (2012).
- Zheng, B. et al. Record-high CO₂ emissions from boreal fires in 2021. *Science* **379**, 912–917 (2023).
- Eyring, V. et al. Coumou, D., Luo, F. & Veraverbeke, S. Early snowmelt and polar jet dynamics co-influence recent extreme Siberian fire seasons. *Science* **378**, 1005–1009 (2022).
- 2006 IPCC Guidelines for National Greenhouse Gas Inventories* (IGES, 2006).
- National Inventory Report: Greenhouse Gas Sources and Sinks in Canada* (Environment Canada, 2023); <https://publications.gc.ca/site/eng/9.506002/publication.html>.
- Xu, L. et al. Changes in global terrestrial live biomass over the 21st century. *Sci. Adv.* **7**, 9829 (2021).
- Tagesson, T. et al. Recent divergence in the contributions of tropical and boreal forests to the terrestrial carbon sink. *Nat. Ecol. Evol.* **4**, 202–209 (2020).
- Larsen, C. & MacDonald, G. An 840-year record of fire and vegetation in a boreal white spruce forest. *Ecology* **79**, 106–118 (1998).
- Stocks, B. et al. Large forest fires in Canada, 1959–1997. *J. Geophys. Res. Atmos.* **107**, 5 (2002).
- Johnstone, J. F. et al. Fire, climate change, and forest resilience in interior Alaska. *Can. J. For. Res.* **40**, 1302–1312 (2010).
- Whitman, E., Parisien, M.-A., Thompson, D. K. & Flannigan, M. D. Short-interval wildfire and drought overwhelm boreal forest resilience. *Sci. Rep.* **9**, 18796 (2019).
- Walker, X. J. et al. Increasing wildfires threaten historic carbon sink of boreal forest soils. *Nature* **572**, 520–523 (2019).
- Wang, J. A. et al. Extensive land cover change across arctic–boreal northwestern North America from disturbance and climate forcing. *Glob. Change Biol.* **26**, 807–822 (2020).
- Kurz, W. A. et al. Mountain pine beetle and forest carbon feedback to climate change. *Nature* **452**, 987–990 (2008).
- Kurz, W. A., Stinson, G., Rampley, G. J., Dymond, C. C. & Neilson, E. T. Risk of natural disturbances makes future contribution of Canada's forests to the global carbon cycle highly uncertain. *Proc. Natl Acad. Sci. USA* **105**, 1551–1555 (2008).
- Tymstra, C., Stocks, B. J., Cai, X. & Flannigan, M. D. Wildfire management in Canada: review, challenges and opportunities. *Prog. Disaster Sci.* **5**, 100045 (2020).

Publisher's note Springer Nature remains neutral with regard to jurisdictional claims in published maps and institutional affiliations.

 **Open Access** This article is licensed under a Creative Commons Attribution 4.0 International License, which permits use, sharing, adaptation, distribution and reproduction in any medium or format, as long as you give appropriate credit to the original author(s) and the source, provide a link to the Creative Commons licence, and indicate if changes were made. The images or other third party material in this article are included in the article's Creative Commons licence, unless indicated otherwise in a credit line to the material. If material is not included in the article's Creative Commons licence and your intended use is not permitted by statutory regulation or exceeds the permitted use, you will need to obtain permission directly from the copyright holder. To view a copy of this licence, visit <http://creativecommons.org/licenses/by/4.0/>.

© The Author(s) 2024

Methods

Climate data

Precipitation estimates were derived from Climate Prediction Center (CPC) global unified gauge-based analysis of daily precipitation data provided by the National Oceanic and Atmospheric Administration from their website at <https://psl.noaa.gov> (refs. 44,45). MERRA-2 2 m temperature (T2M) and dew point temperature at 2 m (T2MDEW) were obtained from the single-level diagnostics file³. VPD was calculated from these quantities using:

$$\text{VPD} = e_s - e_a,$$

where e_s is the saturation vapour pressure and e_a is the vapour pressure, calculated from T2MDEW and T2M, respectively, using the formulation of ref. 46. The Z-scores for precipitation, T2M and VPD were calculated relative to the 20-year baseline of 2003–2022; for example, for T2M this is calculated as:

$$Z\text{-score}_{\text{year}} = \frac{\text{T2M}_{\text{year}} - \text{mean}(\text{T2M}_{2003-2022})}{\text{std}(\text{T2M}_{2003-2022})},$$

where T2M_{year} is the May–September mean T2M for a given year and $\text{T2M}_{2003-2022}$ is the 20-element ensemble of May–September mean T2Ms during 2003–2022.

CMIP6 data were downloaded from the Canadian Climate Data and Scenarios website (<https://climate-scenarios.canada.ca/?page=cmip6-scenarios>). We examine the ensemble median of 27 models provided on a $1^\circ \times 1^\circ$ grid (technical documentation at <https://climate-scenarios.canada.ca/?page=pred-cmip6-notes>). The models included are based on data availability and are tabulated at <https://climate-scenarios.canada.ca/?page=cmip6-model-list>. T2M and precipitation are analysed for the historical and future scenarios. We combine the historical simulation with SSP 2–4.5 (ref. 4), shown in the main text or SSP 5–8.5 as shown in Supplementary Fig. 7.

The Z-scores are calculated from the median of the CMIP6 ensemble by calculating the temporal mean of the median model mean over 2000–2019 for a given grid cell, whereas the reanalysis data are used to estimate internal variability. Therefore, the T2M Z-score is calculated as:

$$Z\text{-score}_{\text{year}} = \frac{\text{T2M}_{\text{CMIP year}} - \text{mean}(\text{T2M}_{\text{CMIP}2000-2019})}{\text{std}(\text{T2M}_{\text{MERRA}2003-2022})}$$

Sources and sinks

Fossil CO emissions. Anthropogenic CO emissions are obtained from the community emissions data system (CEDS) for historical emissions⁴⁷; specifically we use version CEDS-2021-04-21 (ref. 48).

Prior fire CO₂ and CO emissions. Fire CO₂ and CO emissions are obtained from the GFED, GFAS and QFED databases. GFED4.1s¹⁵ provides estimates of biomass burning using a biogeochemical model ingesting MODIS 500 m burned area⁴⁹ in combination with 1 km thermal anomalies and 500 m surface reflectance observations to estimate burned area associated with small fires using a statistical model⁵⁰. These data were downloaded from <https://www.globalfiredata.org/>. GFAS v.1.2 provides estimates of daily biomass burning emissions by assimilating MODIS fire radiative power observations¹⁶. These data were downloaded from the atmosphere data store (<https://ads.atmosphere.copernicus.eu>). We use v.2.6 of the QFED gridded emission estimates¹⁸. These data were downloaded from <https://portal.nccs.nasa.gov/datashare/iesa/aerosol/emissions/QFED/v2.6r1/0.25/QFED/>. For all biomass burning datasets, we release fire emissions at the model surface but incorporate a 3 hourly diurnal cycle based on ref. 51. Year-specific emissions are used for the prior in the atmospheric CO inversions.

Biogenic emissions, atmospheric CO production and OH data.

Biogenic emissions, atmospheric CO production and OH data were all derived from the outputs of the MOMO-Chem chemical data assimilation⁵². An updated version of the tropospheric chemistry reanalysis v.2 (TCR-2)⁵³ produced using MOMO-Chem is used to evaluate the atmospheric production and loss of CO. The reanalysis is produced through the assimilation of several satellite measurements of ozone, CO, NO₂, HNO₃ and SO₂. The chemical loss of CO was estimated using the reanalysis OH fields. Because of the multiconstituent data assimilation, the reanalysis OH shows improved agreements in global distributions over remote oceans in comparison with the ATom aircraft measurements from the surface to the upper troposphere⁵³. Constraints obtained for OH profiles have a large potential to influence the chemistry of the entire troposphere, including oxidation of non-methane hydrocarbons (NMHCs) to estimate the chemical production of CO. The biogenic emissions at the surface were obtained from the model of emissions of gases and aerosols from Nature v.2.1 (MEGAN2.1)⁵⁴. Year-specific fields were only available through 2018 and estimates for that year are repeated for more recent years. We also perform a supplemental sensitivity analysis for the impact of prescribed OH abundances on inferred emissions using the fields of ref. 55, which are commonly used for GEOS-Chem methane inversions⁵⁶.

CO retrievals

TROPOMI. TROPOMI is a grating spectrometer aboard the ESA Sentinel-5 Precursor (S5P) satellite which measures Earth-reflected radiances⁵⁷. CO total column densities are retrieved in the shortwave infrared (around 2.3 μm) using the shortwave infrared CO retrieval algorithm^{58,59}. TROPOMI CO retrievals⁶⁰ were downloaded from the Copernicus data space ecosystem (<https://dataspace.copernicus.eu/>). We use SSP RPRO L2 CO (processor v.2.4.0) through 25 July 2022, then switch to S5P OFFL L2 CO for more recent data (processor v.2.5.0 or 2.5.0). Retrieved CO total column densities are then converted to dry-air mole fractions of CO (X_{CO}) using the dry-air surface pressure and hypsometric equation. The column averaging kernel is similarly converted to mole-fraction space. Individual retrievals (quality flag ≥ 0.5) from each orbit are aggregated into super-observations using the model grid ($2^\circ \times 2.5^\circ$).

The retrieval uncertainty on super-observations is taken to be the mean uncertainty on all retrievals in a given super-observation. This approach is used because systematic errors may exist between retrievals, such that assuming random errors would underestimate the true retrieval error. For assimilation into NASA carbon monitoring system-flux (CMS-Flux), we calculate observational errors that incorporate error in the atmospheric transport model. For this, we follow the approach of ref. 61. First, we perform a forward model simulation with the prior fluxes for 2019–2023. Then we take the observational uncertainty to be the standard deviation between the simulated and real TROPOMI super-observations over a moving window of 30° latitude, 30° longitude and 30 days (across all years). The uncertainties estimated using this approach range over 3.5–14.3 ppb (5–95 percentiles), whereas retrieval errors range over 1.4–4.9 ppb. Thus, the observational errors are dominated by representativeness errors.

MOPITT. We use the MOPITT (measurements of pollution in the troposphere) satellite thermal-infrared–near-infrared (TIR–NIR) CO retrieval. Version 9 (L2V19.9.3)⁶² is used from 2009 to 31 October 2022, whereas L2V19.10.3.beta is used from 1 November 2022 onwards. These data were downloaded from the EarthData ASDC (<https://asdc.larc.nasa.gov/data/MOPITT/>). As with TROPOMI, profile retrievals were converted into dry-air mole fractions of CO (X_{CO}) for assimilation; however, unlike TROPOMI, we do not generate super-observations but instead assimilate individual observations. This is because the footprint of MOPITT retrievals ($22 \times 22 \text{ km}^2$) is much coarser than TROPOMI retrievals ($3 \times 7 \text{ km}^2$).

TCCON. The total carbon column observing network (TCCON) consists of ground-based Fourier transform spectrometers which retrieve X_{CO} , X_{CO_2} and other species from observations of solar radiation⁶³. In this study, we examine GGG2020 (ref. 64) TCCON data from Park Falls⁶⁵ and East Trout Lake⁶⁶. These data were obtained from the TCCON Data Archive hosted by CaltechDATA at <https://tccodata.org>. Super-observations are created for each site as hourly averages; we only include hours with five or more observations.

Atmospheric CO inversions

We perform a series of CO inversion analyses using the CMS-Flux atmospheric inversion system. This inversion model is descended from the GEOS-Chem adjoint model⁶⁷ and has been used for CO₂ (refs. 68,69) and CO inversion analyses⁷⁰. The inversions in this study are all performed globally at 2° × 2.5° spatial resolution using MERRA-2 reanalysis. CEDS anthropogenic emissions, biogenic atmospheric CO production, direct biogenic CO emissions and fire emissions (from GFED4.1s, GFAS or QFED) and atmospheric OH fields are all prescribed in the forward simulations (see section on ‘Sources and sinks’). Four-dimensional variational data assimilation (4D-Var) is used to optimize scaling factors on the net surface flux for each grid cell (combined anthropogenic, fire and direct biogenic CO flux). The posterior CO fluxes are then decomposed into anthropogenic, fire and biogenic fluxes using the fractional contribution of the prior (an approach widely used for CO inversions).

A series of MOPITT X_{CO} inversions are performed over 2010–2021. Weekly fluxes are optimized over the period 7 November of the preceding year (YYYY – 1) to 1 February of the next year (YYYY + 1), the optimized fluxes in the desired year are retained (YYYY) and the fluxes outside this period are discarded as spin-up or spin-down. These inversions are performed using the GFED4.1s fire inventory. Prior uncertainties on emissions are assumed to be proportional to the emissions, with a scale factor uncertainty of 200%.

TROPOMI X_{CO} inversions are performed over 2019–2023. These inversions are performed over a truncated period of 1 April to 30 September, with April then being discarded as spin-up. Several different inversion configurations are used to quantify the uncertainty in posterior fluxes due to both Bayesian posterior uncertainties and systematic choices about error specification and inversion configuration, both of which have been shown to contribute significantly to inversion error estimates¹¹.

Three ensembles of inversions are performed on the basis of the three different prior fire inventories: GFED4.1s, GFAS or QFED (Extended Data Fig. 1a). Each prior inventory was subjected to four different experimental configurations (Extended Data Fig. 1b). In one case, the X_{CO} super-observations error is taken to be the mean retrieval uncertainty across all retrievals included in a given super-observation. This approach typically gives an uncertainty of 1.3–4.9 ppb. The other case uses an observational error estimate that incorporates representativeness errors (see section on ‘TROPOMI’), which are typically between 3.5 and 14.3 ppb. The experimental configurations also differ by the treatment of prior uncertainties on the fluxes. These uncertainties are not well known a priori, thus we use two very different approaches. In the first approach, we assume that the errors on fluxes are equal to 200% of the prior flux estimate. In the second approach, we assume that flux uncertainties are near constant in flux units (scale factor uncertainty times control flux is constant, this is truncated to scale factors uncertainties between 0.25 and 1,000). Finally, we also vary the temporal optimization to either 3 or 7 days. As with the prior flux uncertainties, there are many possible choices for temporal optimization, so we choose two reasonable estimates to quantify the sensitivity to this choice. The spread in maximum a posteriori estimates across these different set-ups gives an indication of the uncertainty in estimated fluxes due to the set-up decisions.

We also estimate the Bayesian posterior uncertainty (Extended Data Fig. 1c), which derives from uncertainties in the prior fluxes and

observations. This uncertainty is estimated using the Monte Carlo method introduced by ref. 71 and formalized by ref. 72. We perform the experiment during 2023 for each prior inventory and use 40 inversion ensemble members using the inversion configuration with TROPOMI X_{CO} representativeness errors and 7 day optimization.

Finally, for each prior inventory, we calculate the posterior best estimates and uncertainties from the experiments described above (Extended Data Fig. 1d). The best estimate is taken to be the mean across the four different inversion configurations. The uncertainty on this estimate is taken as the square-root of the sum of the variances resulting from the different inversion configurations and Monte Carlo posterior covariance estimate. The overall best estimate is taken to be the average across the best estimates for the prior inventory ensembles and the overall uncertainty is taken to be the range of 1 σ uncertainties across the three prior inventory ensembles.

We estimate posterior CO₂ fluxes from the posterior CO emissions using the CO₂/CO emission ratios provided by the prior GFED4.1s, GFAS and QFED inventories. Each inventory has different CO₂/CO emission; thus, we use the emission ratio to estimate the posterior CO₂ from the same inventory that was used as the prior inventory. This incorporates some uncertainty CO₂/CO emission ratio into the CO₂ emission estimates.

Regional masks

Forest area. Forest area is defined using v.6.1 of the MODIS MCD12C1 product⁷³. On the basis of the type 1 majority land cover, we define forests to include the categories evergreen needleleaf forests, evergreen broadleaf forests, deciduous needleleaf forests, deciduous broadleaf forests, mixed forests, woody savannas and savannas.

Managed land. The map of managed lands⁷⁴ was accessed through personal communication with M. Hafer and A. Dyk (the map was only created for cartographic communication purposes). The extent of land considered managed forest in Canada for the purposes of GHG reporting to the United Nations Framework Convention on Climate Change cannot be mapped in detail. That information comes from provincial/territorial forest inventories that are not spatially explicit and cannot be mapped. Supplementary Fig. 13 shows the managed land map and the fractional managed/unmanaged for 2° × 2.5° grid cells.

Data availability

The dataset produced for this study can be accessed at JPL Open Repository, <https://doi.org/10.48577/jpl.V5GR9F>.

Code availability

The Python and Bash codes used in this study are available at Zenodo (<https://doi.org/10.5281/zenodo.12709398>)⁷⁵.

- Xie, P. et al. A gauge-based analysis of daily precipitation over East Asia. *J. Hydrometeorol.* **8**, 607–626 (2007).
- Chen, M. et al. Assessing objective techniques for gauge-based analyses of global daily precipitation. *J. Geophys. Res. Atmos.* <https://doi.org/10.1029/2007JD009132> (2008).
- Buck, A. *Buck Research CR-1A User's Manual (Appendix 1)* (Buck Research Instruments, 1996).
- Hoesly, R. M. et al. Historical (1750–2014) anthropogenic emissions of reactive gases and aerosols from the community emissions data system. *Geosci. Model Dev.* **11**, 369–408 (2018).
- Smith, S. J., Ahsan, H. & Mott, A. CEDS v 2021 04 21 gridded emissions data. *PNNL Datahub* <https://doi.org/10.25584/PNNLDataHub/1779095> (2021).
- Giglio, L., Randerson, J. T. & Van Der Werf, G. R. Analysis of daily, monthly, and annual burned area using the fourth-generation global fire emissions database (GFED4). *J. Geophys. Res. Biogeosci.* **118**, 317–328 (2013).
- Randerson, J. T., Chen, Y., Van Der Werf, G., Rogers, B. & Morton, D. Global burned area and biomass burning emissions from small fires. *J. Geophys. Res. Biogeosci.* <https://doi.org/10.1029/2012JG002128> (2012).
- Mu, M. et al. Daily and 3-hourly variability in global fire emissions and consequences for atmospheric model predictions of carbon monoxide. *J. Geophys. Res. Atmos.* <https://doi.org/10.1029/2011JD016245> (2011).

52. Miyazaki, K., Bowman, K. W., Yumimoto, K., Walker, T. & Sudo, K. Evaluation of a multi-model, multi-constituent assimilation framework for tropospheric chemical reanalysis. *Atmos. Chem. Phys.* **20**, 931–967 (2020).
53. Miyazaki, K. et al. Updated tropospheric chemistry reanalysis and emission estimates, TCR-2, for 2005–2018. *Earth Syst. Sci. Data* **12**, 2223–2259 (2020).
54. Guenther, A. B. et al. The model of emissions of gases and aerosols from Nature version 2.1 (MEGAN2.1): an extended and updated framework for modeling biogenic emissions. *Geosci. Model Dev.* **5**, 1471–1492 (2012).
55. Park, R. J., Jacob, D. J., Field, B. D., Yantosca, R. M. & Chin, M. Natural and transboundary pollution influences on sulfate-nitrate-ammonium aerosols in the United States: implications for policy. *J. Geophys. Res. Atmos.* <https://doi.org/10.1029/2003JD004473> (2004).
56. Wecht, K. J., Jacob, D. J., Frankenberg, C., Jiang, Z. & Blake, D. R. Mapping of North American methane emissions with high spatial resolution by inversion of SCIAMACHY satellite data. *J. Geophys. Res. Atmos.* **119**, 7741–7756 (2014).
57. Veeckind, J. et al. TROPOMI on the ESA Sentinel-5 Precursor: a GMES mission for global observations of the atmospheric composition for climate, air quality and ozone layer applications. *Remote Sens. Environ.* **120**, 70–83 (2012).
58. Landgraf, J. et al. Carbon monoxide total column retrievals from TROPOMI shortwave infrared measurements. *Atmos. Meas. Tech.* **9**, 4955–4975 (2016).
59. Borsdorff, T. et al. Improving the TROPOMI CO data product: update of the spectroscopic database and destriping of single orbits. *Atmos. Meas. Tech.* **12**, 5443–5455 (2019).
60. Copernicus Sentinel-5P (Processed by ESA): TROPOMI Level 2 Carbon Monoxide Total Column Products. Version 02 (European Space Agency, 2021); <https://doi.org/10.5270/S5P-bj3nry0>.
61. Heald, C. L. et al. Comparative inverse analysis of satellite (MOPITT) and aircraft (TRACE-P) observations to estimate Asian sources of carbon monoxide. *J. Geophys. Res. Atmos.* <https://doi.org/10.1029/2004JD005185> (2004).
62. Deeter, M. et al. The MOPITT version 9 CO product: sampling enhancements and validation. *Atmos. Meas. Tech.* **15**, 2325–2344 (2022).
63. Wunch, D. et al. The total carbon column observing network. *Phil. Trans. R. Soc. A* **369**, 2087–2112 (2011).
64. Laughner, J. L. et al. The total carbon column observing network's GGG2020 data version. *Earth Syst. Sci. Data* **16**, 2197–2260 (2024).
65. Wennberg, P. O. et al. TCCON Data From Park Falls (US), Release GGG2020.R1 (CaltechDATA, 2022); <https://doi.org/10.14291/tcon.ggg2020.parkfalls01.R1>.
66. Wunch, D. et al. TCCON Data From East Trout Lake, SK (CA), Release GGG2020.R0 (CaltechDATA, 2022).
67. Henze, D. K., Hakami, A. & Seinfeld, J. H. Development of the adjoint of GEOS-CHEM. *Atmos. Chem. Phys.* **7**, 2413–2433 (2007).
68. Liu, J. et al. Carbon monitoring system flux estimation and attribution: impact of ACOS GOSAT XCO₂ sampling on the inference of terrestrial biospheric sources and sinks. *Tellus B Chem. Phys. Meteorol.* **66**, 22486 (2014).
69. Liu, J. et al. Carbon monitoring system flux net biosphere exchange 2020. *Earth Syst. Sci. Data* **13**, 299–330 (2021).
70. Byrne, B. et al. The carbon cycle of southeast Australia during 2019–2020: drought, fires, and subsequent recovery. *AGU Adv.* **2**, e2021AV000469 (2021).
71. Chevallier, F., BrÅLeon, F.-M. & Rayner, P. J. Contribution of the orbiting carbon observatory to the estimation of CO₂ sources and sinks: theoretical study in a variational data assimilation framework. *J. Geophys. Res. Atmos.* <https://doi.org/10.1029/2006JD007375> (2007).
72. Stanley, M., Kuusela, M., Byrne, B. & Liu, J. Technical note: posterior uncertainty estimation via a monte carlo procedure specialized for data assimilation. *EGUsphere* **2024**, 1–20 (2024).
73. Friedl, M. & Sulla-Menashe, D. MODIS/Terra+Aqua Land Cover Type Yearly L3 Global 0.05Deg CMG V061 [Data set]. (NASA EOSDIS Land Processes Distributed Active Archive Center, accessed 11 November 2023); <https://doi.org/10.5067/MODIS/MCD12C1.061>.
74. *Inventory and Land-use Change* (Natural Resources Canada, accessed 2 April 2024; <https://natural-resources.canada.ca/climate-change-adapting-impacts-and-reducing-emissions/climate-change-impacts-forests/carbon-accounting/inventory-and-land-use-change/13111>).
75. Byrne, B. bkbyrne/2023CanadaFires: v1.0.0. Zenodo <https://doi.org/10.5281/zenodo.12709398> (2024).

Acknowledgements The research carried out at the Jet Propulsion Laboratory, California Institute of Technology, was under a contract with the National Aeronautics and Space Administration. Resources supporting this work were provided by the NASA High-End Computing programme through the NASA Advanced Supercomputing Division at Ames Research Center. Authors B.B., A.C., J.L. and K.B. acknowledge the support from NASA Orbiting Carbon Observatory Science Team Program and the Carbon Monitoring System Program (grant no. NNH20ZDA001N-CMS). We acknowledge the World Climate Research Programme, which, through its Working Group on Coupled Modelling, coordinated and promoted CMIP6. We thank the climate modelling groups for producing and making available their model output, the Earth System Grid Federation (ESGF) for archiving the data and providing access and the many funding agencies who support CMIP6 and ESGF. GFAS is generated using Copernicus Atmosphere Monitoring Service Information 2020; neither the European Commission nor ECMWF is responsible for any use that may be made of the information it contains. The East Trout Lake TCCON station is funded through an infrastructure grant from the Canada Foundation for Innovation (grant no. 35278) and the Ontario Research Fund (grant no. 35278). The Park Falls TCCON site was supported by NASA (grant no. 80NSSC22K1066). We thank J. L. Laughner for guidance with the TCCON data. We thank M. Hafer and A. Dyk for providing information on Canada's managed land. And we thank L. Baskaran for help in rasterizing these data.

Author contributions B.B., J.L., K.W.B., M. P.-C., A.C. and S.P. conceptualized and designed the study. K.M. provided atmospheric CO production and OH estimates. G.R.v.d.W. extended the GFED4.1s dataset for this experiment. D.W., P.O.W. and C.M.R. provided TCCON data. S.S. provided MERRA-2 reanalysis for the model. B.B. conducted the analysis and wrote the paper, with input from all authors.

Competing interests The authors declare no competing interests.

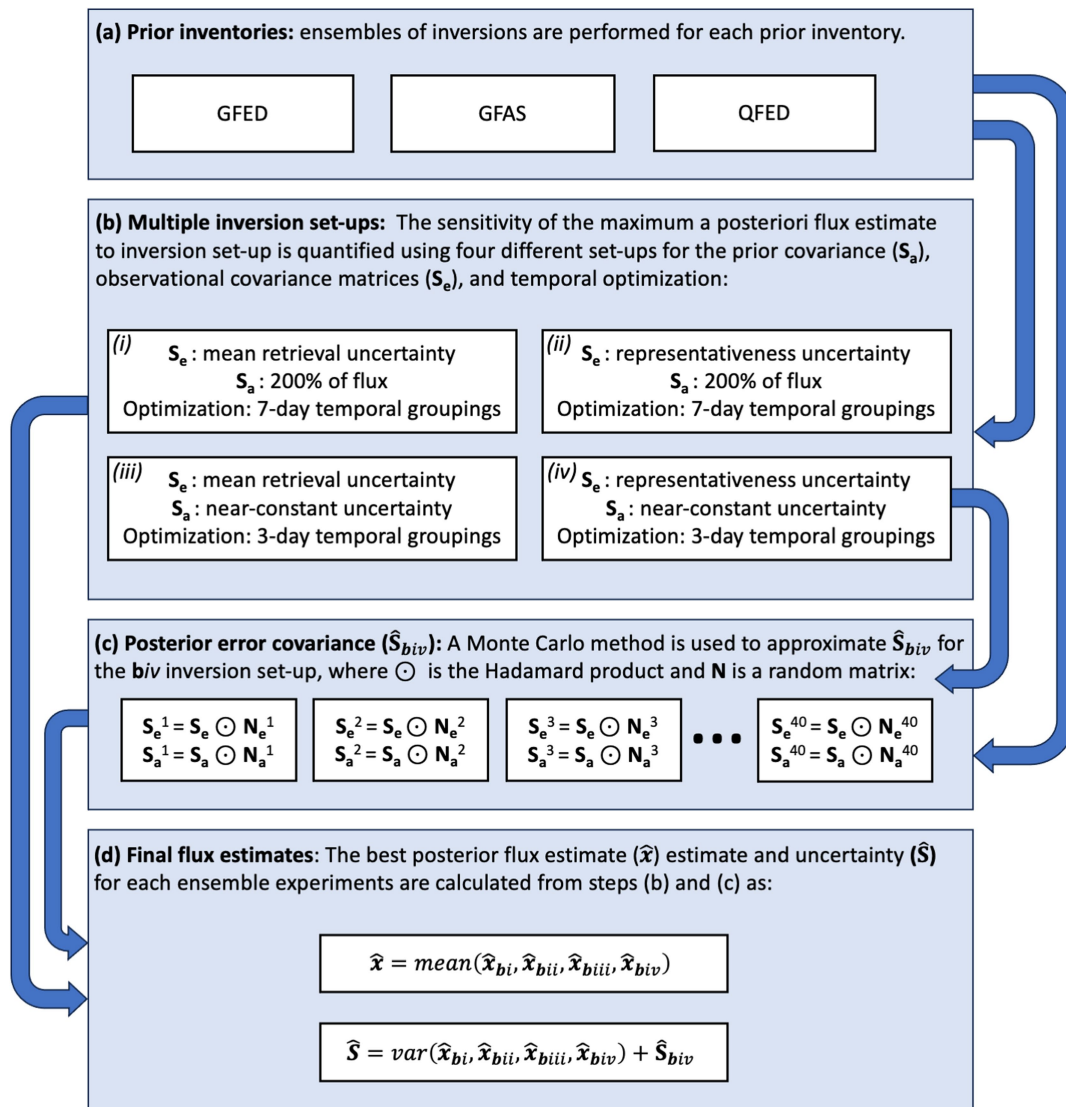
Additional information

Supplementary information The online version contains supplementary material available at <https://doi.org/10.1038/s41586-024-07878-z>.

Correspondence and requests for materials should be addressed to Brendan Byrne.

Peer review information *Nature* thanks Mike Flannigan, Johannes Kaiser and the other, anonymous, reviewer(s) for their contribution to the peer review of this work. Peer reviewer reports are available.

Reprints and permissions information is available at <http://www.nature.com/reprints>.



Extended Data Fig. 1 | Schematic diagram of the TROPOMIXCO inversion procedure. (a) Ensembles of inversions are performed based on three different flux inventories. (b) To quantify the sensitivity to systematic error sources, four inversions are performed that differ in observational error constraints, prior error constraints, and temporal optimization frequency. (c) Bayesian


posterior error estimates are estimate for 2023 by following the Monte Carlo approach for 4D-Var of Chevalier et al.⁷¹. (d) The posterior best estimates are taken as the average maximum a posteriori estimate across inversion configurations while the uncertainty is taken to be the sum-of-squares of the error components estimated in (b) and (c).

Accelerating glacier volume loss on Juneau Icefield driven by hypsometry and melt-accelerating feedbacks

Received: 16 August 2023

Accepted: 26 May 2024

Published online: 02 July 2024

 Check for updates

Bethan Davies¹✉, Robert McNabb², Jacob Bendle³, Jonathan Carrivick⁴, Jeremy Ely⁵, Tom Holt⁶, Bradley Markle⁷, Christopher McNeil⁸, Lindsey Nicholson⁹ & Mauri Pelto¹⁰

Globally, glaciers and icefields contribute significantly to sea level rise. Here we show that ice loss from Juneau Icefield, a plateau icefield in Alaska, accelerated after 2005 AD. Rates of area shrinkage were 5 times faster from 2015–2019 than from 1979–1990. Glacier volume loss remained fairly consistent ($0.65\text{--}1.01\text{ km}^3\text{ a}^{-1}$) from 1770–1979 AD, rising to $3.08\text{--}3.72\text{ km}^3\text{ a}^{-1}$ from 1979–2010, and then doubling after 2010 AD, reaching $5.91 \pm 0.80\text{ km}^3\text{ a}^{-1}$ (2010–2020). Thinning has become pervasive across the icefield plateau since 2005, accompanied by glacier recession and fragmentation. Rising equilibrium line altitudes and increasing ablation across the plateau has driven a series of hypsometrically controlled melt-accelerating feedbacks and resulted in the observed acceleration in mass loss. As glacier thinning on the plateau continues, a mass balance-elevation feedback is likely to inhibit future glacier regrowth, potentially pushing glaciers beyond a dynamic tipping point.

Globally, mountain glaciers and ice caps dominate loss of land ice¹, and were responsible for 21% of observed global sea level rise from 1993–2017¹. The largest contributions (8 mm from 1961–2016) were from Alaskan and Western Canadian glaciers^{1,2}, which hold a large volume of ice ($46.4 \pm 15.3\text{ mm}$ sea-level equivalent)³, and which will contribute to sea level rise for centuries to come^{4,5}. Alaska will likely remain the largest regional contributor to 2100 AD⁶. Model projections indicate that, with emissions policies defined under the Paris Agreement, land ice will drive 25 cm (11, 40 cm at 5th, 95th percentiles) sea-level rise by 2100 AD. Of this, 13 cm will come from glaciers, 25% of which will come from Alaska alone⁴. Under the higher-emission scenario RCP 4.5, around 30% of glacier ice will have disappeared from Alaska by the year 2100 (relative to 2015 AD), causing $17 \pm 4\text{ mm}$ of global sea level rise⁷.

Alaskan icefields may be particularly vulnerable to accelerated melt as the climate warms. Firstly, a large ice volume in Alaska is in hypsometrically top-heavy or plateau icefields (cf.^{3,8}, Fig. 1) with a low-slope accumulation area, making them likely vulnerable to small changes in equilibrium line altitude (ELA)^{8,9}. Secondly, a decrease in height of a flatter icefield or ice cap will theoretically result in a decrease in surface mass balance (SMB) as the ice surface lowers into warmer air, which reinforces itself as an SMB-elevation positive feedback¹⁰. Thirdly, due to an absence of higher topography, flatter ice caps and icefields cannot retreat to higher elevations and find a new equilibrium¹¹. Icefields therefore are likely to exhibit threshold behaviour^{10,12}, with tipping points for rapid and irreversible recession. However, a paucity of long, multi-decadal empirical observations of icefield change impedes our ability to accurately constrain and

¹School of Geography, Politics and Sociology, Newcastle University, Newcastle-upon-Tyne, UK. ²School of Geography and Environmental Sciences, Ulster University, Colrairie, Northern Ireland, UK. ³Geological Survey of Norway, Trondheim, Norway. ⁴School of Geography and water@leeds, University of Leeds, Leeds, UK. ⁵Department of Geography, University of Sheffield, Sheffield, UK. ⁶Centre for Glaciology, Aberystwyth University, Aberystwyth, UK. ⁷Geological Sciences, University of Colorado Boulder, Boulder, CO, USA. ⁸U.S. Geological Survey, Alaska Science Center, Anchorage, AK, USA. ⁹Department of Atmospheric and Cryospheric Sciences, Universität Innsbruck, Innsbruck, Austria. ¹⁰Nichols College, Dudley, Massachusetts, USA.

✉ e-mail: bethan.davies@newcastle.ac.uk

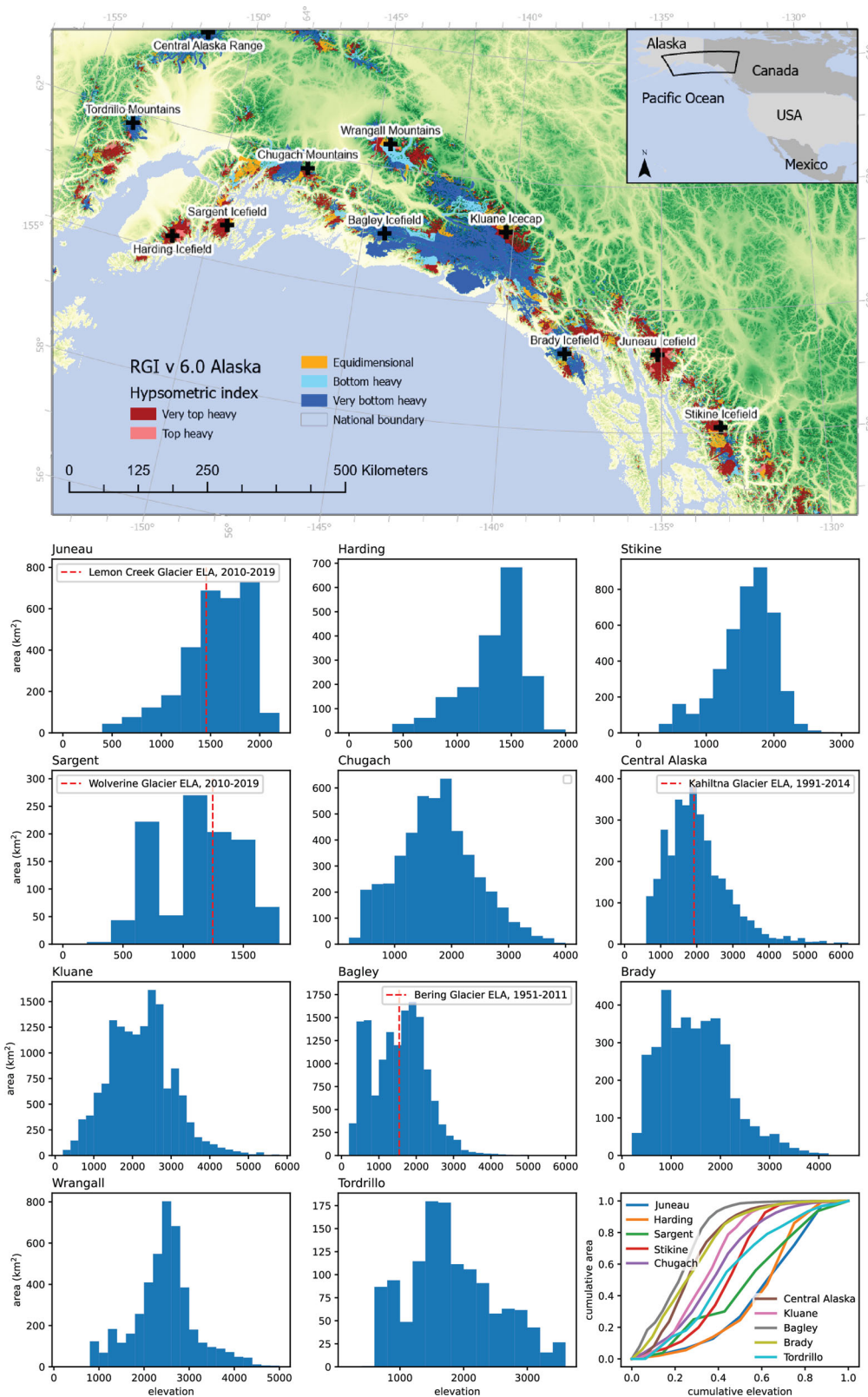


Fig. 1 | Hypsometry of major Alaskan icefields. Top: hypsometric index of individual glaciers in the RGI (Randolph Glacier Inventory) v6.0⁶⁷. Hypsometric index defined after ref. 63. Visualised on background of void-filled 3" Viewfinder Panorama DEMs (Digital Elevation Models), comprising SRTM DEM (Shuttle Radar Topography Mission Digital Elevation Model) south of 60°20'N. Below: area-elevation histograms for major ice bodies in Alaska. Measured Equilibrium Line

Altitudes (ELAs)^{25,33,35,94,95} shown with red dashed line. Juneau, Kluane, Brady, Sargent and Bagley icefields all have a significant low-slope plateau in their accumulation areas. Juneau, Stikine, Harding, Sargent and parts of Kluane Icefield are all very top-heavy icefields. Bottom right: normalised cumulative area-elevation plots for each icefield. The top-heavy Juneau, Stikine, Harding and Sargeant icefields alone make up 2589 km³ of ice.

evidence these processes and identify tipping points and thresholds of change. Understanding the physical processes that affect the different way icefields and ice caps respond to climate change is key to improving our ability to estimate icefield response to future climate change^{13–15}.

Upskilling our ability to predict future glacier behaviour using model-data comparisons requires detailed observations for model parameterisation and calibration or weighting of projections^{16,17}. In Alaska, the largest Holocene glacier expansion occurred during the “Little Ice Age” (LIA)¹⁸, AD 1770–1850 AD^{18–20}, with temperatures 1.3 °C¹⁹ to 2 °C²⁰ cooler than modern (Supplementary Information Section 3). The geomorphological imprint of this expansion is clearly observable in Sentinel satellite imagery and the fine-resolution ArcticDEM product²¹. Temperature changes during this historical period were of a similar amplitude of forcing (± 2 °C) to those projected in the next two centuries²². Datasets of glacier change through this historical period, with a measure of uncertainty, are required for understanding the behaviour of ice caps and icefields under a changing climate, and for upskilling projections through data-model comparisons^{4,14,16,23,24}, but few exist with a long (more than a few decades) and high (decadal) temporal resolution. The aim of this study is therefore to quantify “Little Ice Age” to recent (2020 AD) glacier change at Juneau Icefield (Alaska and British Columbia, Figs. 1, 2a) to determine the rates of, and controls on, icefield-wide shrinkage and thinning.

Juneau Icefield (northern Coast Mountains) straddles the boundary between Alaska (USA) and British Columbia (Canada) (Figs. 1, 2 and Supplementary Fig. 1). It is a temperate, maritime icefield, though the eastern side has a more continental climate^{25,26}. The icefield spans an elevation range of 0–2300 m asl, with a large, low-slope accumulation area covering 1400 km². It comprised 1050 glaciers in 2019²¹, covering 3816.3 km² and with an ice volume of 1051.1 \pm 301.7 km³ (calculated using data from ref. 3; Supplementary Fig. 2). Most of the glacier area is held in 40 topographically confined outlet glaciers (2939.1 \pm 4.2 km²), which drain directly from the main plateau. Separate to this plateau are smaller ice bodies; 145 valley glaciers (570.9 \pm 2.3 km²), 584 mountain glaciers (279.2 \pm 6.4 km²) and 281 glacierets (27.2 \pm 3.0 km²)²¹. The northern accumulation plateau area lies above 1500 m and has modelled ice thicknesses reaching 420 m³, while the southern plateau is lower, above 1200 m, but ice here is approximately 950 m thick (Supplementary Fig. 1, 2). Taku Glacier has a maximum measured thickness of 1477 m, with a bed up to 600 m below sea level²⁷. Icefalls occur on 23 outlet glaciers (including 13 outlet glaciers draining from the main interconnected plateau) and the study region as a whole contains 150 icefalls observed on 55 glaciers²¹. These icefalls have a mean elevation of 1481 m asl (range 810–2121 m) and many occur around the rim of the icefield plateau²¹.

Outlet glaciers around Juneau Icefield were at their neoglacial maximum at around 1770 AD (Supplementary Information Section 3)^{28–31}, with some historical observations of outlet glacier extent also mapped in the early 20th century³². Juneau Icefield has an especially long and detailed mass balance record since 1946^{25,33–35} and an exceptional database of glaciological observations (e.g., refs. 25,36–42). Positive annual balance was recorded between 1946 to 1949, with high winter cyclonic activity. From 1950 to 1957, annual mass balances were negative, due to decreased cyclonic activity, and below-normal accumulation temperatures⁴⁰. Between 1958 to 1962, warmer winter temperatures and increased precipitation led to increasing annual mass balance. From 1964 to 1975, cool ablation season temperatures and above average winter precipitation caused increased annual balances⁴⁰. Young et al. calculate a rate of -0.57 (-0.11 , $+0.12$) m w. e. a⁻¹ for the icefield from 1980–2016, with ice west of the topographic divide undergoing a greater rate of mass loss than the more interior glaciers⁴³. In comparison, Berthier et al. calculate a mass balance of -0.65 m yr⁻¹ for the Coast mountain range from 1962 to 2006⁴⁴. Glaciers today continue to thin and recede in response to an

overall warming^{33,45}. From 2000 to 2016, Juneau Icefield had a mass balance of -0.68 ± 0.15 m w. e. a⁻¹⁴⁶. Lemon Creek had a cumulative annual mass balance of -1.03 m w. e. from 1990 to 2018, with increasing rates of mass loss, primarily driven by increases in glacier ablation and summer warming³³ (Supplementary Fig. 3d). After decades of glacier advance, Taku Glacier is now receding, with thinning across its entire elevation range between 2013 and 2018, with an average rate of -1.3 m ice equivalent per annum^{25,37}.

Measured equilibrium line altitudes (ELAs) reach 1499 m asl (mean 2011–2020 AD) on Lemon Creek Glacier and 1159 m asl on Taku Glacier^{25,35}, with ELAs over 1500 m reported in warm years. The equilibrium line altitude (ELA) at Taku Glacier has risen from 912 m asl (mean 1940–1950 AD) to 1000 m (mean 1986–2018) and to 1159 m asl (mean 2011–2020 AD)³⁸. The ELA at Lemon Creek Glacier has risen from 1038 m asl (mean 1961–1970) to 1499 m asl (mean 2011–2020)²⁵. This means that the ELA of outlet glaciers is now more frequently reaching the rim of the plateau around the icefield (1200 m asl; cf.²¹). Independent hydrological measurements indicate that glacier ice melt volumes are increasing, with spring glacier melt volume increasing at 16% decade⁻¹⁴⁷, and an increasing trend in annual glacier ice melt production.

Southern Alaska has a maritime, high-latitude climate regime, characterised by abundant snowfall and cooler summers³³. Climate in southern Alaska and in the Gulf of Alaska region is largely controlled by the North Pacific Decadal Variability⁴⁸. The dominant modes of the North Pacific Decadal Variability are largely determined by the wintertime strength of the Aleutian Low and sea surface temperature anomalies related to the Pacific Decadal Oscillation.

Precipitation patterns in Juneau are dominated by the Aleutian Low, which is a region of winter-time low pressure near the Aleutian Islands⁴⁹. These low-pressure conditions increase the frequency and intensity of winter storms. A strong Aleutian Low, with a positive Pacific Decadal Oscillation, therefore brings enhanced winter storms and increased precipitation along the Gulf of Alaska⁵⁰. There is strong interannual to multidecadal variability in the Aleutian Low, with a shift in 1976 from mainly negative values (1951–1975) to mainly positive values (1977–2001), leading to increased coastal precipitation⁵¹ and winter snowfall⁵². Since 2015, the Aleutian Low has been weaker⁵³. The shift in the Aleutian Low after 1976 is reflected in snowfall received at Juneau; analysis of three-month winter (DJF) precipitation data from the meteorological station at Juneau Airport (NOAA⁵⁴) show mean values of 10,300 \pm 1300 mm w. e. (with a 95% confidence interval) from 1951–1975, and 13,200 \pm 1200 mm, 1977–2020 AD. A Student's *t*-test showed a statistically significant increase in precipitation between these two time periods (*t* stat 3.36 > *t* Critical one-tail 1.67) (Supplementary Fig. 3b). The increase in precipitation occurs mostly in September to November (Supplementary Fig. 3c).

Temperatures from Juneau Airport meteorological station (NOAA⁵⁴; Supplementary Tables 1, 2) are available from 1941–present at a monthly resolution. Mean summer temperatures (1986–2005) reach 13.34 °C, with a mean annual air temperature of 5.67 °C. Winter temperatures show a strong increase in warming, with a trend of 0.35 °C per decade from 1941–2020 (*p* < 0.05). There was an increase in mean winter temperatures of 2.07 °C from 2001–2020 relative to 1941–1970 (Supplementary Table 1), which has lengthened the summer melt season. For mean annual air temperatures, six of the ten warmest years have occurred since the year 2000, and the ten coolest years all occurred prior to 1973 (Supplementary Fig. 3a). Since records began at Juneau Airport, summer temperatures have also increased, with temperatures from 2001 to 2020 0.97 °C warmer than from 1941 to 1970. This trend is in line with observations across Alaska, which shows warming temperatures since the 1970s and exceptionally warm recent years, a shrinking snow-season state-wide, and a longer melt season⁵⁵.

This climate shift is also clearly visible in the ERA5 climate reanalysis data⁵⁶ (Supplementary Fig. 4). Here, the mean climate

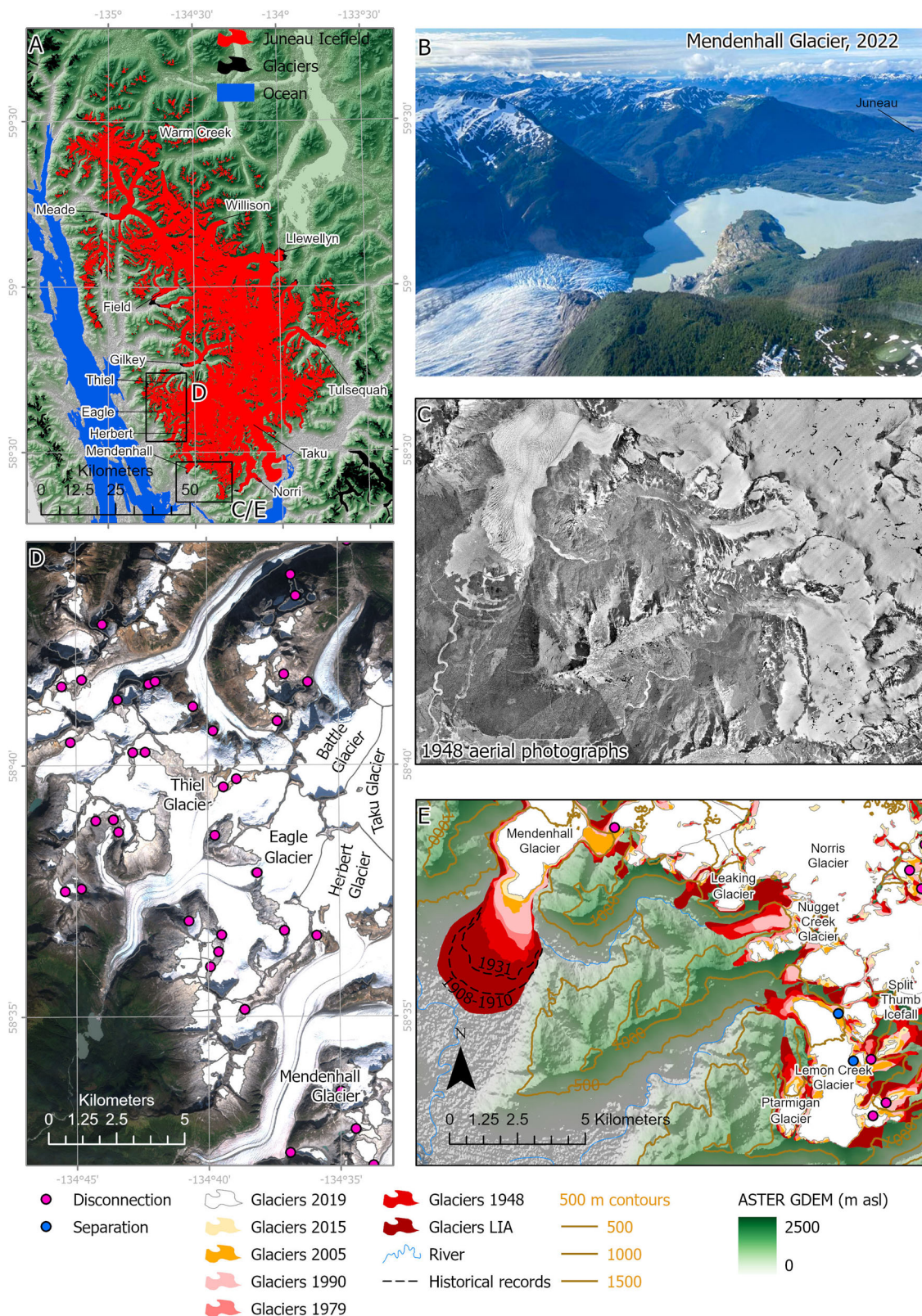


Fig. 2 | The Juneau Icefield and its evolution over time. **A** Overview of Juneau Icefield; glacier extent in 2019 is shown in red. Key glacier names are shown. Glaciers in black not included in the study area. Overlain on background of ASTER GDEM. **B** Field photograph (credit Bethan Davies) of Mendenhall Glacier, in June 2022. **C** Examples of aerial imagery used in glacier reconstruction (1948) for Mendenhall Glacier and Lemon Creek Glacier. Image courtesy of the U.S. Geological

Survey. **D** Example of satellite imagery (Sentinel-2A, 2019) for Thiel Glacier (north-flowing) and Eagle Glacier (south-flowing). **E** Example of reconstructed glacier area loss for Mendenhall Glacier and Lemon Creek Glacier. Historical glacier positions from ref. 28. **C, E** have the same scale and extent. Extents are shown in (A). See also Supplementary Figs. 1, 2. ASTER GDEM is the Global Digital Elevation Model produced by ASTER, courtesy of NASA/JPL-Caltech.

(temperature, precipitation and vertically integrated moisture difference) of 1990–2005 and 2015–2019 are compared with the mean 1950–1980 climate. The post-1976 climate shift is clearly apparent, with warming and increased precipitation in 1990–2005 relative to 1950–1980. However, the difference is much greater for the 2015–2019 period, when temperatures, at both 2 m and 850 mb, are substantially higher. This period sees especially warm temperatures around Juneau (Supplementary Fig. 4e, f) as well as decreased precipitation (Supplementary Fig. 4h).

Results

LIA glacial reconstruction

The reconstructed LIA icefield (Figs. 3, 4 and Supplementary Figs. 9–10) covered $5414.95 \pm 111.76 \text{ km}^2$; 29.5% larger than in 2019 AD (Table 1), with reconstructed ablation areas adding $95.26 \pm 17.01 \text{ km}^2$ compared with 2013 AD (Table 2). At this time, Juneau Icefield outlet glaciers extended down onto the plain in several valleys, with many forming large unconstrained piedmont lobes; for example, Hole-in-the-Wall and East and West Twin Glaciers, Mendenhall Glacier, Herbert Glacier, Llewellyn Glacier and Eagle Glacier (Supplementary Fig. 10). At these piedmont glacier lobes, large concentric moraines represent a substantial period of stability and moraine building for the glacier. In many of these places, the moraines display multiple closely spaced ridge crests. There are some moraines visible between the innermost of these concentric piedmont glacier moraines and the 1948 glacier outlines, for example at Herbert Glacier (Supplementary Figs. 1h, 9), suggesting that the ice may have temporarily stabilized during recession into the valleys, potentially due to changing topographic constraints on the margin. Recessional moraines are also evident at Llewellyn Glacier, but within the 1948 extent.

For the most part, over-deepenings inside the main moraine crests are infilled with proglacial lake water. Taku and Norris glaciers were the only two glaciers to reach the ocean and to calve directly into a marine fjord. East and West Twin Glacier and Hole-in-the-Wall Glacier drained into an ice-dammed lake, but the remaining piedmont glaciers were land-terminating. Kettle lakes occur frequently within the piedmont glacier moraine crests. The remainder of the outlet glaciers (e.g., Field, Gilkey and Meade glaciers) remained constrained as land-terminating valley glaciers at their most recent neoglacial maximum (Figs. 3, 4, Supplementary Fig. 10). These glaciers terminated on land and had a long, narrow, low-slope glacier snout. Again, as the glaciers have receded from their most recent maximum position, proglacial lakes have formed within the over-deepening, impeding observation of younger recessional moraines.

Taku Glacier shrank by 6.4% (49.95 km^2) but was slightly thinner at the terminus during the LIA than today, potentially reflecting its different configuration and marine-terminating environment, compared with the thicker, terrestrially terminating glacier present today^{25,37}. Recent recession now sees the formation of lagoons at the ice margin and the onset of a lacustrine or lagoonal terminus. At the LIA, Taku Glacier was coalescent with Norris Glacier in Taku Inlet²⁸, calving into the fjord (Supplementary Fig. 11). It is likely that this marine-terminating glacier had a long, low-slope, low-elevation snout, as is typical for water-terminating glaciers. We suspect that the glacier was grounded, given the shallow fjord, though this is not constrained. Behind the terminus, we reconstruct an ice-dammed lake at 15 m elevation, following the clear break in slope between the forested mountainside and the low-slope boggy valley floor, as originally mapped by Lawrence, 1950²⁸. This is in line with ice-contact fans observed at Twin Glacier Lake moraines and at Wright Glacier terminus further up-valley (Supplementary Fig. 10), which provide additional geomorphological evidence for an ice-dammed lake at 15 m asl. However, little geomorphological evidence of shorelines is visible in the ArcticDEM or satellite imagery. Reconstructing the lake following the 15 m contour generates a lake 95.84 km^2 in size.

Around the periphery of the main plateau, the LIA extent of valley glaciers and mountain glaciers is generally well constrained by substantial and clear moraines, enclosing ice-scoured bedrock or fluted glacial sedimentary surfaces. There are occasional recessional moraines within these larger moraines. For some glaciers, such as Denver Glacier, limited clear geomorphology visible on satellite imagery precluded reconstruction of the glacier extent, and so the 1948 extent is used as the earliest data source.

Reconstructed geometric equilibrium line altitudes (ELA_{LIA}) ranged from 1070 m (Taku Glacier, Lemon Creek Glacier) to 932 m (Mendenhall Glacier) and 1494 m (Llewellyn Glacier) (Supplementary Fig. 10). In comparison, the average ELA for Lemon Creek Glacier from 1998–2019 was 1327 m asl^{25,35}. This represents an ELA lowering of -150 m at Lemon Creek Glacier, relative to today^{25,35}. Peripheral glaciers to the east of the icefield had an ELA_{LIA} higher than 1500 m, compared with under 1250 m in the west (Supplementary Fig. 10).

Overall changes since the “Little Ice Age”

Between the AD 1770 and AD 2019 inventories, 108 glaciers disappeared (Fig. 5), and only 70.53% of glacier area now remains relative to the Neoglacial maximum. 100% of glaciers mapped in 2019 had receded relative to their LIA position, with 47 new ice-contact proglacial lakes developing as glacier termini receded. The largest areal losses (52.5%) were from the Icefield’s outlet glaciers (which made up 64.25% of the area during the LIA). Of all the glacier area lost between 1770 and 2019 AD, $538.0 \pm 32.4 \text{ km}^2$ was from outlet glaciers. The main outlet glacier termini all receded by -4 to 5 km , shrinking by up to 69 km^2 (Supplementary Table 9).

The total cumulative ice loss from across Juneau Icefield is $315.3 \pm 237.5 \text{ km}^3$; this equates to a loss of 24.25% of the ice volume (from ref. 3) between the LIA maximum and 2020 AD. There has been thinning of 150 m at the terminus of Field Glacier, 220 m on Ogive Glacier, 150 m on Gilkey Glacier, and 200 m on Meade Glacier. Bacon Glacier has thinned by 190 m, and Tulsequah by 180 m.

Accelerating change through the 20th and 21st Centuries

Most glaciers (91%) receded substantially from their LIA extent between 1770 and 1948 AD (Fig. 5), during a period of warming (Fig. 6a). Total glacier area shrank by 12.18% at a rate of 0.07 a^{-1} ($3.70 \text{ km}^2 \text{ a}^{-1}$). This was accompanied by a conservative estimate of volume loss of $0.65 \pm 0.92 \text{ km}^3 \text{ a}^{-1}$ (Fig. 6b–g). Between 1948 and 1979 AD, 342 (30.6%) glaciers advanced, and overall rates of glacier recession were slow (0.12 a^{-1}) (Fig. 6b–g; Table 1). This was likely caused by an increase in snowfall relative to the period before 1948 (Supplementary Table 2, Fig. 6f). Most advancing glaciers were either small mountain glaciers or glacierets, likely reflecting their faster response time. Despite these changes, a comparatively low rate of thinning persisted, at an icefield-wide average of 0.11 m a^{-1} (Fig. 6c). Rates of recession before 1948 remain well below those experienced by most outlet glaciers after the year 2005 (Supplementary Table 10).

Slower rates of area loss and thinning continued until 1979, followed by an acceleration of ice loss during the latter 20th and start of the 21st centuries (Table 1). Fewer (8.5%) glaciers advanced between 1990 and 2005 ($n = 95$). Rates of glacier area loss rose, reaching 0.18 a^{-1} ($8.33 \text{ km}^2 \text{ a}^{-1}$, 1979–1990), and then sharply accelerated to 0.39 a^{-1} ($17.54 \text{ km}^2 \text{ a}^{-1}$, 1990–2005). From 1979–2000, icefield-wide volume loss reached $3.7 \pm 1.6 \text{ km}^3 \text{ a}^{-1}$ (Fig. 6d), also indicating a sharp acceleration from the preceding periods, with a mean thinning of -0.48 m a^{-1} across all glaciers (Fig. 6c). Glacier tongues thinned across the icefield (Fig. 7), with thinning reaching higher elevations up-glacier than before (Fig. 7). Thinning reached elevations of 1380 m asl on Mendenhall Glacier, 1490 m for Tulsequah Glacier, and the plateau at 1550 m for Meade Glacier.

This rate of ice loss continued into the 21st century. Between 2005–2015 AD, 99% of glaciers receded, and 10% of glaciers

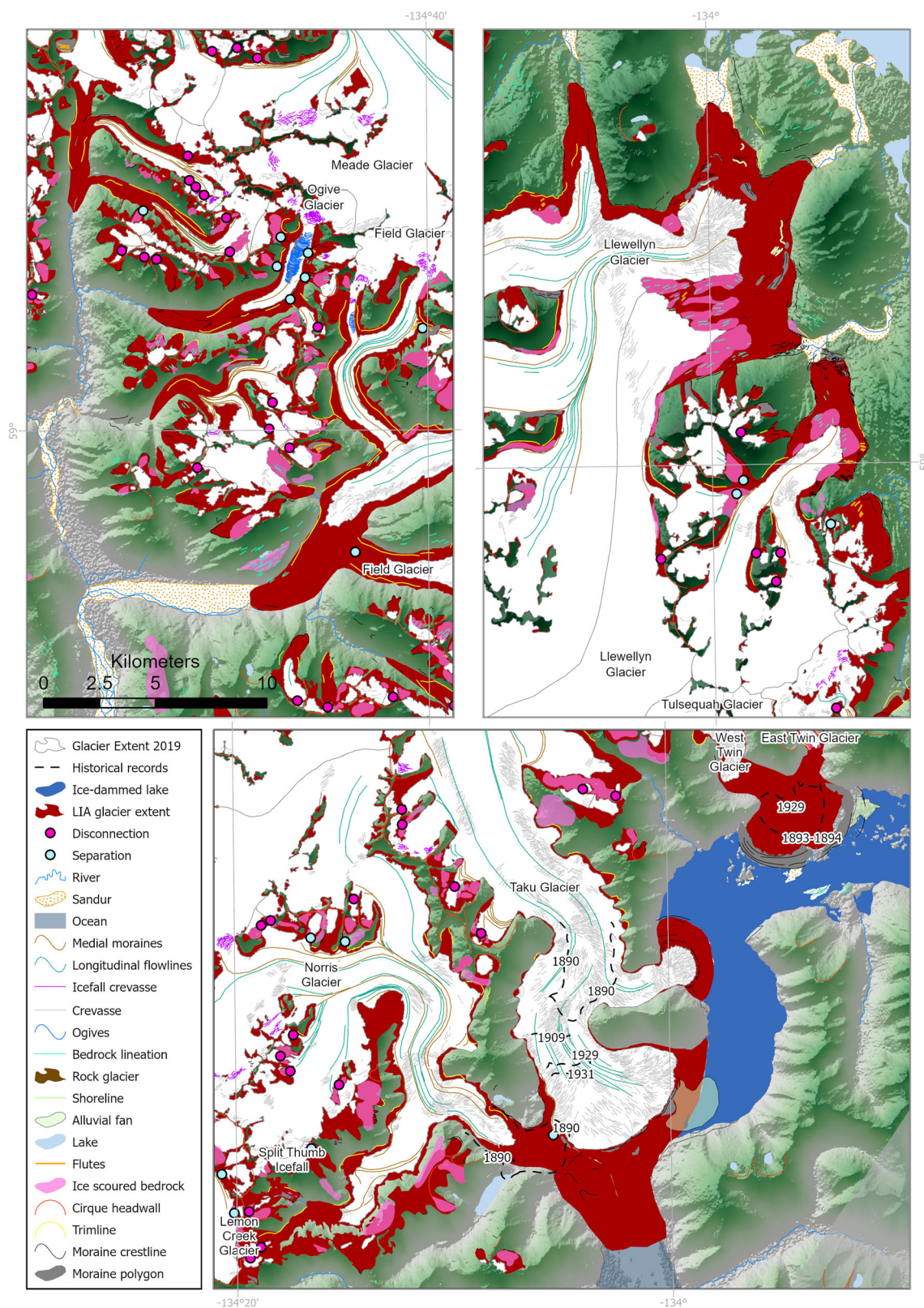


Fig. 3 | Details and examples of the geomorphological data and icefield reconstruction for the “Little Ice Age” (LIA) maximum. Geomorphological data, including all shapefiles, are available from ref. 21. Overlain on ASTER GDEM, the Global Digital Elevation Model produced by ASTER, courtesy of NASA/JPL-Caltech.

disappeared between 2005 and 2019 AD. From 2005 onwards, glacier areal loss accelerated sharply relative to previous time periods, reaching $0.60\% \text{ a}^{-1}$ ($25.36 \text{ km}^2 \text{ a}^{-1}$, 2005–2015) and then $0.96\% \text{ a}^{-1}$ ($38.47 \text{ km}^2 \text{ a}^{-1}$, 2015–2019) (Fig. 6b–g). Rates of recession were 1.5 times

faster from 2015–2019 (Mean (M) = 5.88, Standard Deviation (SD) = 5.26) than from 2005–2015 (M = 2.48, SD = 2.11), $t(1097)$, $p < 0.001$.

Icefield outlet glaciers experienced severe volume loss after 2010 (Fig. 6c, g; Table 2), with thinning across the icefield plateau at

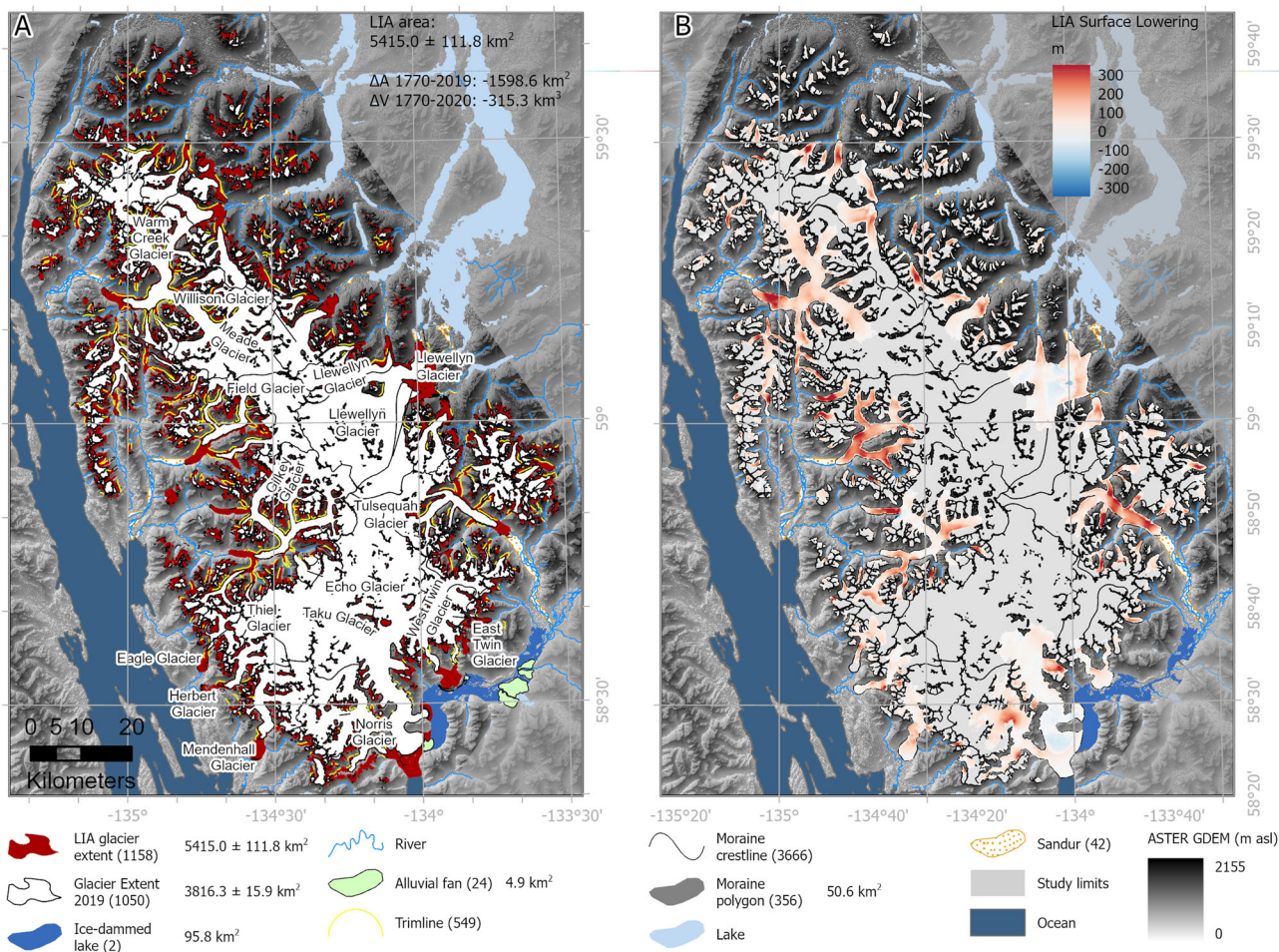


Fig. 4 | “Little Ice Age” (LIA) reconstruction of Juneau Icefield. **A** Reconstruction of Juneau Icefield during the Little Ice Age. Geomorphic data from ref. 21. Legend shows number of features in brackets. **B** ice surface lowering (m), LIA (1770) to present (year 2013; comparison with Copernicus DEM). More information on the

LIA reconstruction is available in Supplementary Information with glacier equilibrium line altitudes (ELAs) from the LIA shown in Supplementary Figs. 9–11. Feature counts are shown in brackets in the legend. ASTER GDEM is the Global Digital Elevation Model produced by ASTER, courtesy of NASA/JPL-Caltech.

elevations of up to 1800 m asl (Fig. 7) and volume loss at a rate of $5.91 \pm 0.8 \text{ km}^3 \text{ a}^{-1}$ (2010–2020). The whole icefield loss equated to 5% of the total volume reconstructed in 2017–18 by ref. 3 from 2010–2020. Alongside this thinning we observe increased glacier fragmentation, with both terminus separation and glacier disconnections (*sensu* ref. 21), where glacier tributaries are detached from their accumulation areas, occurring increasingly frequently (Fig. 6h, i).

Overall, rates of glacier areal recession rose slowly from 1948–2005, followed by a sharp acceleration in rates of glacier area loss after 2005. Icefield-wide, rates of glacier area shrinkage were 7 times faster from 2015–2019 relative to 1948–1979, and 5 times faster relative to 1979–1990 (Table 1, Fig. 6b–g). There are three distinct periods in icefield volume loss, with relatively consistent rates from LIA-1979, followed by a rise from 1979–2010, and a doubling of rates of volume loss after 2010 (Fig. 6d). There has thus been a steep acceleration in the rate of ice mass loss across the icefield since the early twenty-first century.

Snowline and Albedo change

This rapid glacier recession was accompanied by ELAs rising to the plateau height in the period 2005–2020^{25,35} (Fig. 6i), and exceptionally high snowlines on the plateau in 2018³⁸ and 2019 (Figs. 5, 6k, Supplementary Table 13; Supplementary Fig. 14). Late summer snowlines mapped in 2019 from Sentinel-2 imagery (Figs. 5, 6k) had a mean altitude of 1612 m asl (SD 162 m; $n = 178$). Snowlines on Taku Glacier

were a mean altitude of 1445 m in 2019, compared with a measured ELA in 2019 of 1528 m³⁵. The snowline here is therefore well above the southern plateau at 1200 m asl. No snow was observed in the Sentinel-2 imagery on Lemon Creek Glacier at the end of the ablation season in 2019, in line with the measured ELA of 2023 m that year³⁵. Snowlines on Meade, Llewellyn and Field Glacier had a mean elevation of 1671 m (SD 119 m), well above the height of the northern plateau at 1500 m asl (Fig. 5). This icefield-wide trend has continued in subsequent years (Fig. 6k, Supplementary Tables 13, 14 and Supplementary Figs. 13, 14). These datasets show that, although snowline elevation was unusually high in 2019, snowlines are reaching the plateau frequently, with both snowlines and ELAs regularly occurring above the plateau height of 1200 m since 2005 and increasingly frequently in the last decade of the study period.

Alongside this trend of rising snowlines, we also observe a decrease in icefield wide average albedo (Fig. 6l, Supplementary Tables 15–17). When clipped to the 1990 glacier outlines, and thus taking into account terminus recession and icefield fragmentation as well as the impact of darkening snow and ice surfaces, the mean albedo from 1987–2009 was 0.81 ± 0.03 (95% confidence interval). From 2010 to 2023, this decreased to 0.67 ± 0.03 . The albedo of the plateau above 1500 m (compared with the Copernicus DEM) also decreased from 0.92 ± 0.02 (1987–2009) to 0.78 ± 0.04 (2010–2023). The months of September and August in 2018 and 2019, which were characterised by exceptionally high snowlines, likewise had exceptionally low icefield-

Table 1 | Total summed areas and rates of change across Juneau Icefield, with climate data from each period

Year	Total glacier area (km ²)	Mean glacier area (SD), km ²	Count of glaciers	Δ Area (km ²)	% change	Total rate of glacier ΔA (km ² a ⁻¹)	Mean rate of glacier change (km ² a ⁻¹)	Rate of glacier ΔA (% a ⁻¹)	Mean % change per annum	No. Advancing years (SD)	Median no. years (SD)	Summer temperature anomaly (°C)
1770	5415.0 ± 111.8	4.7 (32.4)	1158									
1948	4755.5 ± 26.0	4.1 (31.0)	1118	-659.0 ± 137.7	-12.18	-3.70	-0.003 ± 0.001	-0.068	0.20	67	178.0 (0)	-0.83
1979	4584.0 ± 97.6	34.0 (30.7)	1118	-171.6 ± 123.6	-3.61	-5.48	-0.007 ± 0.002	-0.115	-0.03	342	31.0 (14.3)	-1.02
1990	4496.1 ± 55.8	3.9 (30.4)	1117	-87.9 ± 153.4	-1.92	-8.33	-0.007 ± 0.002	-0.182	0.18	387	11.1 (1.0)	-0.30
2005	4238.7 ± 47.7	3.7 (29.8)	1114	-258.8 ± 103.5	-5.76	-17.37	-0.015 ± 0.003	-0.390	1.14	95	14.9 (0.3)	0.01
2015	4001.5 ± 69.4	3.5 (29.3)	1102	-235.8 ± 117.1	-5.56	-25.76	-0.022 ± 0.005	-0.598	2.54	0	9.0 (0.5)	-0.40
2019	3816.3 ± 15.9	3.3 (28.9)	1050	-185.1 ± 85.3	-4.63	-38.47	-0.033 ± 0.006	-0.961	5.88	5	5.0 (0.4)	0.55
Total change			-108	-1598.6 ± 127.6								

“Advancing” is the number of glaciers with increased glacier area. Mean rate of glacier area change (km² a⁻¹) is shown with the 95% confidence interval. Summer temperature anomaly is compared with the 1986–2005 AD mean. SD standard deviation.

wide mean albedos of 0.44 to 0.48, respectively (LC08 sensor). In contrast, the lower icefield average snowline in August 2021 (Supplementary Table 16) is reflected with a higher albedo of 0.66 in the LC08 sensor.

When comparing the time periods 1987–2009 and 2010–2023, the icefield-wide albedo within the 2019 glacier outlines was lower from 2010–2013 (mean = 0.71, standard deviation = 0.14) than from 1987–2009 (mean = 0.84, standard deviation = 0.08); $t(90) = 5.48$, $p < 0.05$. This decrease is caused by more pixels with a lower albedo in summer, especially on the plateau; here, a regression for average albedo over time results in an r^2 value of 0.23 ($p < 0.05$). Many bright pixels with high albedo however remain throughout the study period, especially at higher altitudes on the plateau.

Icefield fragmentation

The recession and thinning of Juneau Icefield glaciers has resulted in increasing icefield fragmentation. This includes the separation of glacier tongues in the valleys, and disconnections higher up the glacier, where bare rock appears within the glacier polygon as a result of thinning, usually over thin, steep and heavily crevassed ice such as in icefalls²¹. While 291 disconnections were first mapped in ref. 21, which were frequently observed in association with icefalls, here we calculate the timing of disconnection by comparing the mapped disconnections with the new glacier outlines, and analyse the thinning occurring at the site of the disconnections. The mean elevation of the disconnections has remained relatively constant over time (Fig. 6i), with a total mean elevation of 1299 m asl (1362 m in disconnections after 2005); this is controlled by the location of steep ice around the rim of the plateau²¹. This altitudinal range (1200–1400 m asl) was subjected to thinning in the period 2010–2020 (Fig. 7). For example, in a subsidiary accumulation basin on Gilkey Glacier, thinning of 1.4 m a⁻¹ is observed at a height of 1340 m adjacent to a glacier disconnection. At Thiel Glacier, thinning of 1.7 m a⁻¹ is observed at an altitude of 1034 m adjacent to the site of a pre-2019 disconnection.

These disconnections are occurring at a uniform altitude and slope through time (Fig. 6i) but are occurring more frequently after 2005 AD as glacier ELAs increasingly intersect this altitudinal range (Fig. 6h; refs. 21,35) and thinning occurs at higher elevations (Fig. 7). Glacier snowlines in 2019 AD were above the elevation of icefalls around the rim of the plateau²¹ (Fig. 5), resulting in net ablation at the height of many of the icefalls. Glacier tongues down-stream of glacier disconnections show increasing debris cover and thinning. For example, thinning of up to 9 m a⁻¹ on Thiel Glacier tongue, with a glacier-wide mean of -3.33 m a⁻¹, is far above the mean of 1.3 m a⁻¹ for outlet glaciers (2010–2020, Fig. 6c).

Discussion

This Juneau Icefield-wide examination of glacier and climate change over this 250-year time period reveals that rates of glacier recession have sharply accelerated since 2005, relative to earlier time periods (Fig. 6b, g). Observed rates of glacier volume and area loss are rapidly accelerating, demonstrating a threshold response to a warming climate, a rising ELA and snowlines, and decreasing regional albedos, in contrast to published modelling studies, which suggest a linear rate of volume loss to 2040 AD and acceleration only after 2070 AD^{6,14}. In summary, temperatures rose by 1.39 °C at Juneau Airport (1941–2020, Figs. 5 and 6f), with a shift occurring in the 1970s, in line with regional observations across Alaska³⁵. This is related to a shift to mainly positive values in the Pacific Decadal Oscillation from 1976⁵¹, bringing increased precipitation and warmer temperatures to Alaska^{50,51} and to Juneau (Supplementary Tables 1, 2; Supplementary Figs. 3, 4). Temperatures were relatively stable from 1990–2005 (Fig. 6f). Icefield thinning and area loss remained stable during this time period (Fig. 6b–d). From 2010–2020, there was another rise in temperature, and in ELA^{25,33,35}, with the ELA and late-summer snowlines now intersecting with the

Table 2 | Total volume change for Juneau Icefield, LIA to 2020 AD

Time period	Volume Change			Mean glacier area-averaged dh/dt (m) ± 95% confidence interval ^a				
	ΔV (km ³ a ⁻¹)	Total volume change (km ³)	Cumulative volume change (km ³)	All glaciers	Glacierets	Mountain Glaciers	Valley Glaciers	Outlet Glaciers
1770–2013 ^b	-0.4 ± 0.1	-95.26 ± 17.01						
1770–1948	-0.7 ± 0.9	-115.9 ± 163.4	-115.9	-0.11 ± 0.01	-0.12 ± 0.03	-0.12 ± 0.01	-0.11 ± 0.03	-0.10 ± 0.02
1650–1948	-0.4 ± 0.6							
1880–1948	-1.7 ± 2.4							
1948–1979	-1.0 ± 0.7	-31.3 ± 23.0	-147.2	-0.28 ± 0.03	-0.17 ± 0.06	-0.28 ± 0.03	-0.44 ± 0.09	-0.33 ± 0.11
1979–2000	-3.7 ± 1.6	-78.2 ± 33.0	-225.4	-0.51 ± 0.02	-0.37 ± 0.05	-0.49 ± 0.03	-0.73 ± 0.07	-0.69 ± 0.14
2000–2010	-3.1 ± 1.0	-30.8 ± 10.1	-256.2	-0.21 ± 0.04	-0.10 ± 0.07	-0.17 ± 0.05	-0.50 ± 0.09	-0.45 ± 0.22
2010–2020	-5.9 ± 0.8	-59.1 ± 8.0	-315.3	-0.74 ± 0.03	-0.58 ± 0.05	-0.69 ± 0.03	-1.10 ± 0.09	-1.21 ± 0.21

^aMean dh/dt is the glacier area-averaged thinning, averaged for all glaciers, provided with 95% confidence interval. Glaciers with no data coverage are excluded. The low spread in the data results in a small value for the uncertainty in the mean.

^bChange from LIA ("Little Ice Age") to 2013 is the difference between the reconstructed LIA ice surface (ablation areas only) and the Copernicus DEM, with an approximate date of 2013 AD. Note that this is only for the area of the glacier ablation areas (shown in Fig. 2).

icefield plateau (Figs. 5, 6; ref. 38), driving lower albedos and widespread thinning across the plateau (Fig. 7), with a thinning rate 1.9 times higher than from 1979–2000, and a sharp and substantial increase in rates of glacier recession. Glaciers receded 2.2 times faster in 2015–2019 relative to 1990–2005, with an increase in mean summer temperature anomaly of just 0.55 °C (2015–2019, from NOAA data⁵⁴, Fig. 6f, j, l; Supplementary Tables 1, 2) relative to the 1986–2006 mean.

The critical driver of the accelerating glacier mass decline at Juneau Icefield is that the rising ELA (mean 1437 m asl at Lemon Creek Glacier, and 1188.5 m at Taku Glacier, with highs of 2023 and 1528 m respectively, 2011–2020 AD³⁵) and late summer snowline now intersects the elevations of the icefield plateau (1200 m to 1500 m) (Figs. 5, 6i), driving thinning across the plateau (Fig. 8) and increased glacier fragmentation at points of key vulnerabilities (i.e., at sites of steep, heavily crevassed ice). This rising ELA drives a reduced accumulation area ratio (cf. ref. 25). Icefield hypsometry then creates conditions prone to a strong mass balance response to moderate climate forcing^{8,12}, because the low-slope icefield plateau is susceptible to significant loss of accumulation area. In coming decades, this will drive further decrease of the icefield's accumulation area, and will continue to drive accelerated glacier mass change.

We hypothesise that the dramatic reduction in icefield accumulation area is decreasing overall icefield albedo. As snow cover duration and extent is reduced (cf. Fig. 5), darker rock, firn and ice surfaces are increasingly exposed, which absorb more solar radiation, enhancing the ablation rate. This albedo feedback (cf.^{15,57} and illustrated in Fig. 8) is likely to then contribute to further icefield thinning. This effect is compounded by deposition of black carbon⁵⁸ and dust⁵⁹, which is set to increase in future, due to a rise in tourism and wildfires⁶⁰.

Thinning on low-slope icefield plateaux, as observed in Fig. 7, is likely to drive an elevation-SMB feedback by lowering the icefield surface and driving increased melt in warmer air temperatures (due to the lapse-rate induced rise in air temperature at lower elevations^{10,11,61}) (Fig. 8). This response is fundamentally unstable, as thinning drives increasingly negative mass balances, even in the absence of further climate forcing⁶¹. In some places across the Juneau plateau, the ice is over 600 m thick³ (Supplementary Fig. 2), so the ice-elevation feedback has a large range over which to operate. This topographic feedback can lead to an increased frequency of extreme negative mass balance rates, especially when the climate data diverges from the mean¹¹. Once initiated, long-term thinning is inevitable, because even in the event of climate stabilisation, the mass balance-elevation feedback will inhibit glacier regrowth (cf.¹⁴), likely forming an irreversible tipping point in glacier dynamics.

Thinning in vulnerable areas of thin, heavily crevassed ice such as the icefalls that surround the plateau is encouraging icefield

fragmentation and disconnection of glacier accumulation and ablation areas^{8,9,21,62,63}. Bare rock appearing within the glacier boundaries indicates reduced nourishment between the accumulation basin and glacier outlet tongues and is likely to enhance melt through radiative forcing, encouraging a positive melt feedback^{15,62}. Disconnected glaciers stagnate and downwaste once detached in this manner⁶². Thin debris accumulates on the ice surface, darkening the surface and thereby enhancing melt. In some places, debris accumulates to the point that the glacier becomes debris-covered (>50% of the tongue is covered in thin debris²¹). Thicker debris cover on glacier ice encourages in situ down-wasting but slows rates of glacier area loss due to the insulating impact of debris cover on surface melt⁶⁴. The proportion of debris-covered glacier area to clean-ice glacier area will likely increase as glacier shrinkage continues, increasing the relative importance of debris cover. We hypothesise that increased bare rock exposure and the loss of ice within and around glaciers will act to darken the region, resulting in the observed reduced regional albedo, which may contribute to further local warming. Finally, structural mapping across Juneau Icefield indicates areas of weakness associated with steep icefalls²¹. Their abundance indicates that further disconnections, fragmentation, and downwasting are inevitable²¹. Further thinning will drive the development of new icefalls across topographic steps, as the ice surface becomes increasingly influenced by bed topography. Increased glacier disconnection at icefalls and subsequent down-wasting of remnant glacier tongues is therefore expected to become more frequent in future decades, and will form a hysteresis behaviour, whereby glacier regrowth is inhibited.

These processes may be exacerbated as further increases in temperature alter the ratio between solid and liquid precipitation across Juneau Icefield, reducing the amount of snowfall and decreasing accumulation. Top-heavy icefield glaciers are predicted to experience the most significant losses of glacier area over coming decades⁸, and the accelerating trends observed in the recent past at Juneau Icefield are likely to continue. The hypsometrically controlled melt-accelerating feedbacks will contribute to a hysteresis in the system, impeding glacier regrowth even in the event of climate cooling.

The acceleration in mass change observed at Juneau Icefield has significant implications for understanding how other icefields may behave in our warming world. Significantly, Alaska is not only a major contributor to ongoing sea level rise, but also contains some of the world's largest plateau icefields (Fig. 1), which will also be susceptible to rising ELAs and SMB and altitude feedbacks. Equilibrium line altitudes are already approaching the plateau for Sargent Icefield and Bagley Icefield. Substantial low-slope icefields are also present in Canada (Devon Island Ice Cap⁶⁵, Agassiz Ice Cap, Penny Ice Cap), Greenland (Hans Tausen Iskappe¹⁰) and Norway (Svartisen,

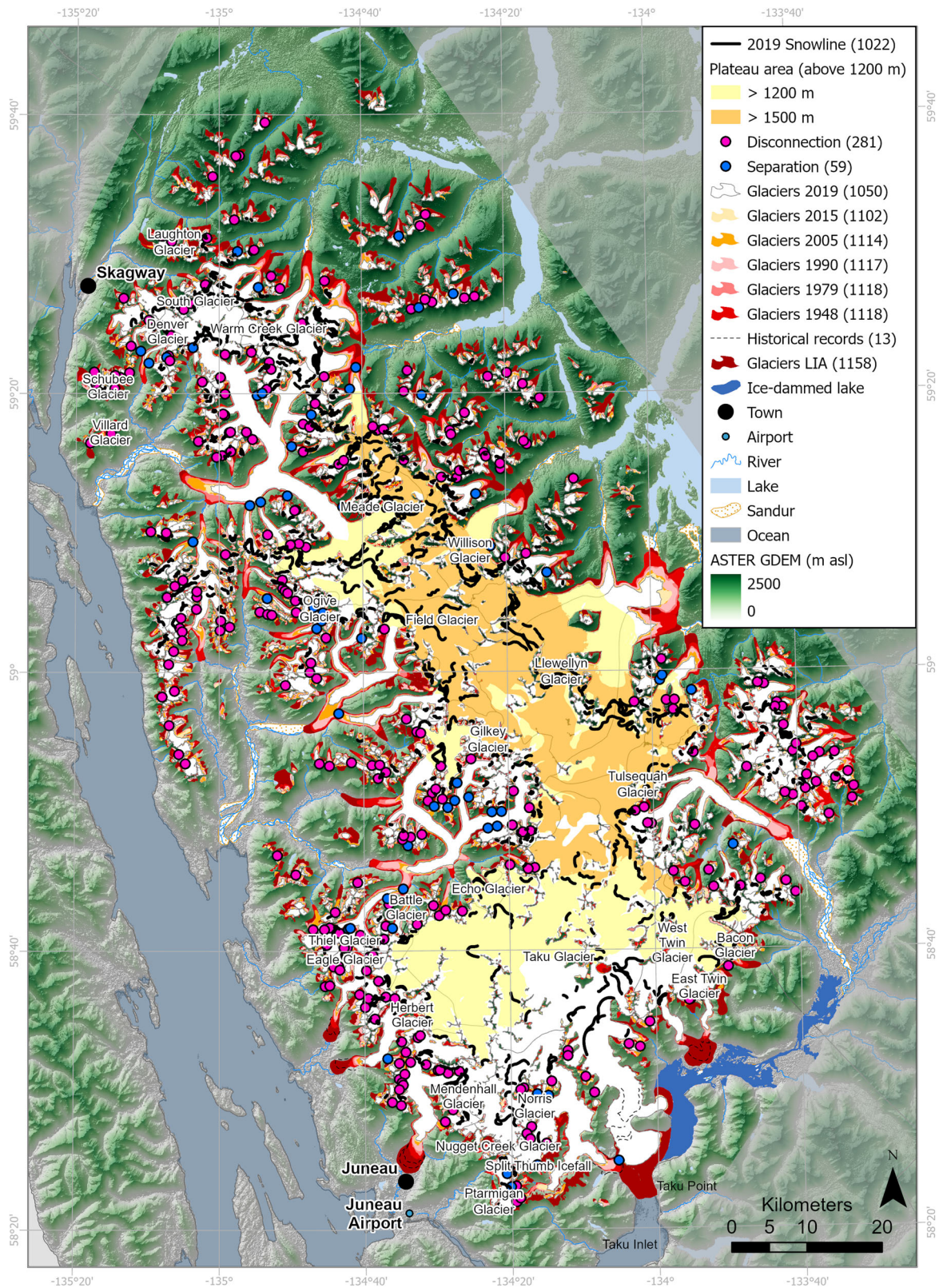
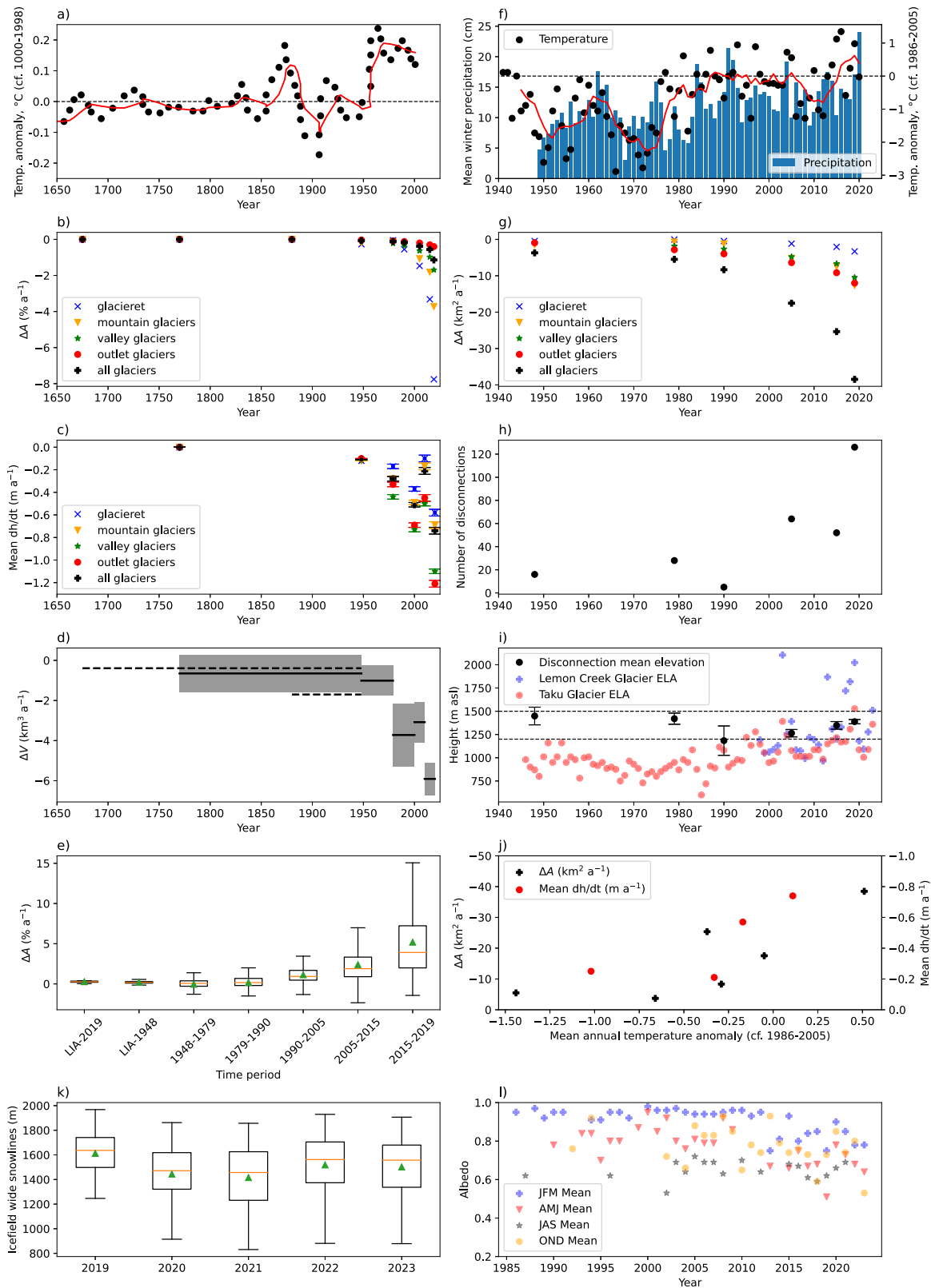


Fig. 5 | Glacier area change for Juneau Icefield, LIA (“Little Ice Age”) to 2019 AD. Number of glaciers in each time slice is shown in the legend in brackets. Late summer snowline for 2019 AD is shown. Historical recorded glacier extents are available for Eagle Glacier, Herbert Glacier, Mendenhall Glacier, Taku Glacier and

East and West Twin Glaciers^{28,96,97} (see Supplementary Information Section 3.2). Overlain on ASTER GDEM, the Global Digital Elevation Model produced by ASTER, courtesy of NASA/JPL-Caltech.



Jostedalbreen). Plateau ice masses are also important along the Antarctic Peninsula and on James Ross Island. Glacier disconnections may also be critical in bottom-heavy plateau icefields with substantial low-lying outlet glaciers, such as Kluane, Yakutat, Brady and Bagley icefields (cf.⁸; Fig. 1). Conversely, loss of low-lying ablation regions may in some situations have a stabilising impact, because as the low-lying high-ablation areas are lost, this could lead to less negative specific

mass balances¹⁴, emphasising how these complex processes can be icefield-specific. However, this stabilising influence will not offset the pervasive effects of the SMB, albedo and altitude feedbacks if ELAs reach the plateau.

By examining the observed centennial changes in an Alaskan plateau icefield to climate, we show that glacier recession and volume loss have accelerated dramatically in the last 20 years, with marked and

Fig. 6 | Summary plots of climate and glacier area and volume change. Time frames (x axes) are consistent in both columns to allow comparison of climate, volume and area change through time. **a** Summer air temperature anomalies from varved proglacial lake sediments in southern Alaska⁹⁸. Red line is the 5-year moving average. Anomaly is computed for the year 1000–1998 AD. **b** Glacier area change through time ($\% \text{ a}^{-1}$) for different types of glaciers. **c** Glacier area-averaged thinning through time (dh/dt) for different classes of glacier. The mean dh/dt (m a^{-1}) is calculated for each glacier, and these values are then averaged for each glacier class for each time period. 95% confidence interval is shown. **d** Total glacier volume change, with uncertainties. Dashed lines show rates for an earlier and a later LIA (“Little Ice Age”) maximum, respectively. **e** Boxplots of annualised rates of glacier recession for all glaciers where data exist. Mean is shown as green triangle and median as an orange line. **f** Temperature anomaly (scatter plot with 5 year moving average, red line), compared with the 1986–2005 mean, from Juneau airport

weather station⁵⁴ (see Fig. 5), and mean winter precipitation (bars) as measured at Juneau airport meteorological station. **g** Glacier total summed area change ($\text{km}^2 \text{ a}^{-1}$), focused on the time period 1940–2020 AD. **h** Number of glacier disconnections observed in each time slice. **i** Glacier equilibrium line altitudes from Lemon Creek Glacier and Taku Glacier. Derived from the USGS Benchmark Glacier Programme³⁵; see also reference publications^{25,33}. Mean elevation of observed disconnections, with error bars of one standard deviation, also shown. Dashed lines indicate the plateau at 1200 m and 1500 m, respectively (refer to Fig. 5 for the mapped plateau area). **j** Temperature and mean rate of glacier recession ($\text{km}^2 \text{ a}^{-1}$; black) and glacier thinning (dh/dt (m a^{-1}); red). **k** Boxplots of mapped snowlines, 2019–2023. Further information in Supplementary Tables 13–14 and Supplementary Figs. 13 and 14. **l** Seasonal means each year for albedo for Juneau Icefield. Further data available in Supplementary Tables 15–18. Source data are provided as a Source Data file.

accelerating thinning and recession, compared with the rest of the twentieth century. This accelerated mass change is induced by a number of hypsometrically controlled melt-accelerating feedbacks that drive accelerated thinning and volume across the plateau. The destabilising surface mass balance-elevation feedback, loss of accumulation area, albedo feedback, and glacier disconnections associated with plateau icefields are therefore already occurring here.

Alaska is the largest regional sea-level contributor from glaciers in GlacierMIP⁵, with a linear decrease in glacier area and volume predicted to the year 2100 AD, with high uncertainty in rates of mass loss for any given climate scenario, due to the high ice volume in this region. However, once ELAs rise and thinning occurs on the plateau, accelerated mass change occurs due to a series of feedbacks that accelerate melt. Other large icefields and icecaps in Alaska (such as the Harding, Bagley and Kluane icefields, Fig. 1) and the Arctic (e.g., Devon Ice Cap, Agassiz Ice Cap, Penny Ice Cap, Hans Tausen Iskappe), which also occur at low elevations and have similar low-slope plateau accumulation areas, are likely to also display an accelerating rate of future volume loss. Therefore, the outputs of existing large scale regional to global glacier model projects and ensembles should be interpreted with care, and we suggest that more historical data are integrated into future simulations through data-model comparisons to ensure that melt-accelerating behaviours are anticipated, evaluated, and accounted for. The results of this work could have large implications given the important sea-level contributions of Alaska, Canada and Greenland’s icefields and the important water resources provided by plateau icefields in the Rocky Mountains (e.g., Columbia Icefield), which could all be subject to similar processes as snowlines rise under ongoing climate warming and these major icefields reach regional tipping points in mass change and volume loss.

Methods

Baseline glacier outlines were derived from the Randolph Glacier Inventory (RGI) v. 6.0^{66,67}. We used glacial geomorphological mapping (ref. 21 and reviewed in Supplementary Information Sections 3 and 5) and historical records²⁸ to reconstruct LIA extent and then volume^{68,69}. We then applied structure-from-motion algorithms in MicMac^{70,71} to 20th Century archival aerial photographs (1948 and 1979 AD) as well as topographic maps to reconstruct glacier area and surface elevation in 1948 and 1979 (see Supplementary Fig. 6 for data coverage). Satellite imagery was also used in 1990, 2005, 2015 and 2019 to altogether yield glacier outlines from 1770, 1948, 1979, 1990, 2005, 2015 and 2019 AD (Supplementary Fig. 7), and original icefield surface DEMs at -1770, 1948, and 1979 AD. We combined these with datasets of ice surface elevation derived from structure-from-motion algorithms using ASTER imagery from 2000, 2010 and 2020⁷².

Remote sensing datasets

Glaciers in 2019 AD, glacial structures, glacial geomorphology and lakes were used from ref. 21. These features were mapped in ESRI

ArcGIS (projection WGS 84, UTM zone 8 N), using 10 m resolution Sentinel-2 imagery (swath 290 km), and these data and methods are published in full in ref. 21; methods and datasets are summarised here for completeness. Late-summer satellite images with limited cloud cover and snow on the glacier ablation regions were chosen. Landsat imagery was used to map glacier extent in 2015 (Landsat 8), 2005 (Landsat 7 ETM+), 1990 (Landsat 4–5 MSS), and 1980–1982 (using a combination of archival aerial photographs and Landsat 3 MSS imagery where there was no coverage). Landsat imagery was acquired pre-registered to Universal Transverse Mercator (UTM) World Geodetic System 1984 ellipsoidal elevation (WGS84) zone 8 N projection. Image resolution ranged from 4 m (aerial orthomosaics) to 10 m (Sentinel-2), and 30–80 m (Landsat).

Stereo aerial photographs from the 1979 Alaska High Altitude Photography (AHAP) survey were used to map glacier extent and structures from 11th–12th August 1979, especially in areas where significant glacier changes have occurred. This campaign acquired black and white photography at 1:120,000 scale resolution. Cloud cover is minimal and snow patches are limited in area and scope. These photographs were scanned by the USGS EROS Data Centre at 25 microns (1200 dpi).

Aerial stereo photographs from the 1948 aerial photography survey of Alaska were used to map glacier area. Photographs were acquired on 13th August 1948. USGS topographic maps dating from 1948 were used to supplement the 1948 aerial photographs, where the orthomosaic was poor, or where original aerial photographs were unavailable on the USGS server (Supplementary Fig. 6). This was mostly the case in Canada. Here, USGS maps (AK_Atlin_360559_1960_250000) were used, where the topographic maps were deemed sufficiently high in quality (see Supplementary Tables 3, 5), with a good correspondence between mapped lakes, rivers and topography. Where topographic maps showed a low correspondence, the 1979 AHAP mosaics were used, and, where these were also unavailable (in the eastern-most parts of the study area), Landsat imagery was used (Supplementary Fig. 6). Overall, 66.6% of the glacier area was mapped from the 1948 ortho mosaics, and 27.8% of glacier area was mapped from topographic maps (Supplementary Table 3). This means that the glacier extent in 1948 is the best available estimate given the data availability. Annual rates of recession are calculated using the date of the imagery or data source used to map glacier extent. The glacier extent in 1948 is considered a minimum; use of later datasets results in some glaciers being underestimated due to continued glacier recession.

Topographic data were derived from the 2 m resolution ArcticDEM v3.0 release⁷³, except where tiles were missing, and ASTER GDEM⁷⁴, ALOS DEM⁷⁵ and novel DEMs derived from the aerial photographs using structure-from-motion methods. A derived composite DEM is mostly ArcticDEM, with data gaps being filled with a void-filled 30 m resolution ASTER GDEM v2.0⁷⁴. For this process, both DEMs were projected in UTM Zone 8 N, and clipped to the same extent. All

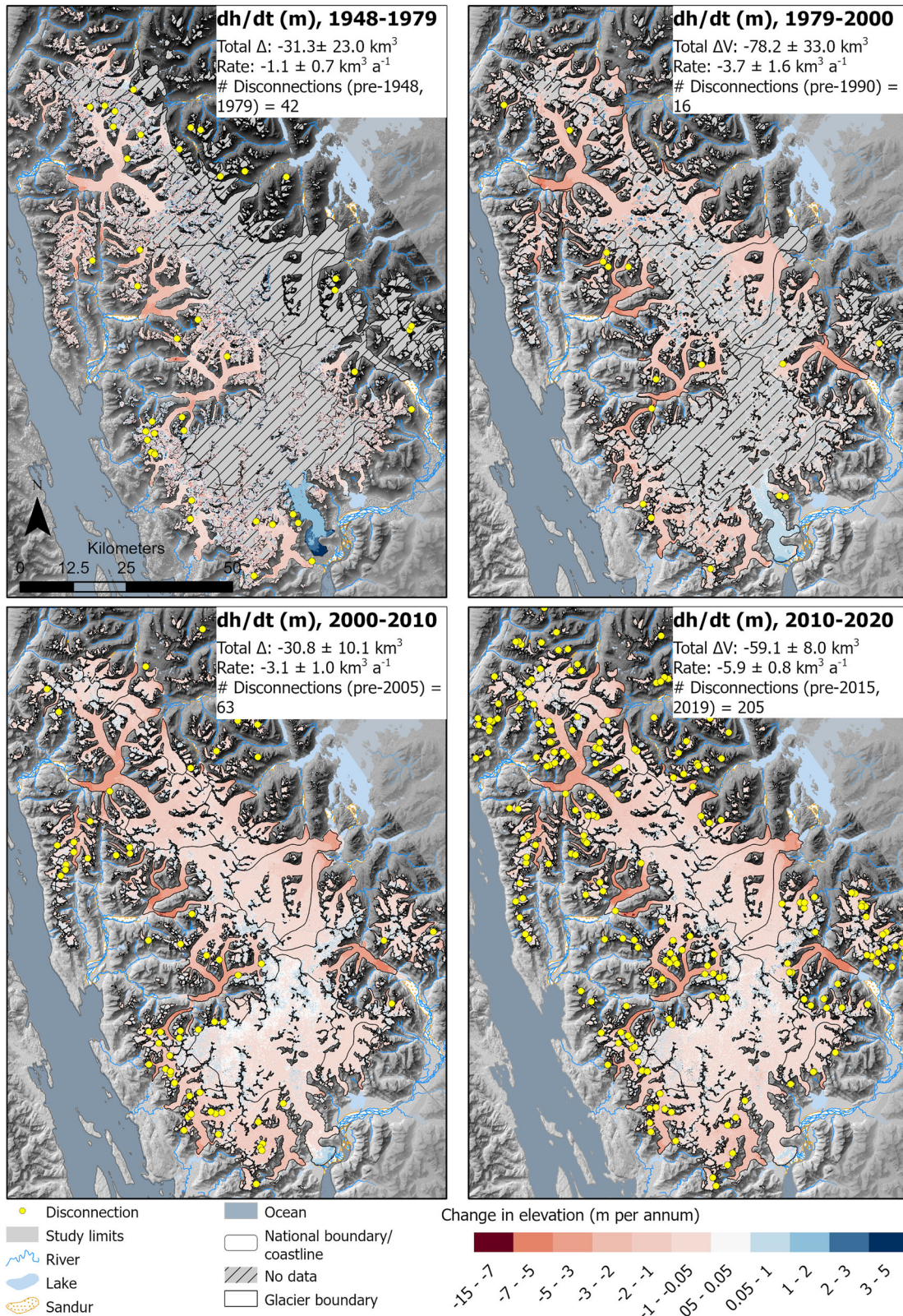


Fig. 7 | Glacier surface elevation change per year (dh/dt) for each glacier in each time period. Values are given in metres. Yellow circles are the glacier disconnections observed within each timeslice. Zero elevation change shows as colourless; negative change (thinning) as red and positive change (thickening) as blue.

Number of disconnections is shown in each panel; however, as date of disconnection is taken from the area change datasets, the timings do not precisely match. Overlain on ASTER GDEM, the Global Digital Elevation Model produced by ASTER, courtesy of NASA/JPL-Caltech.

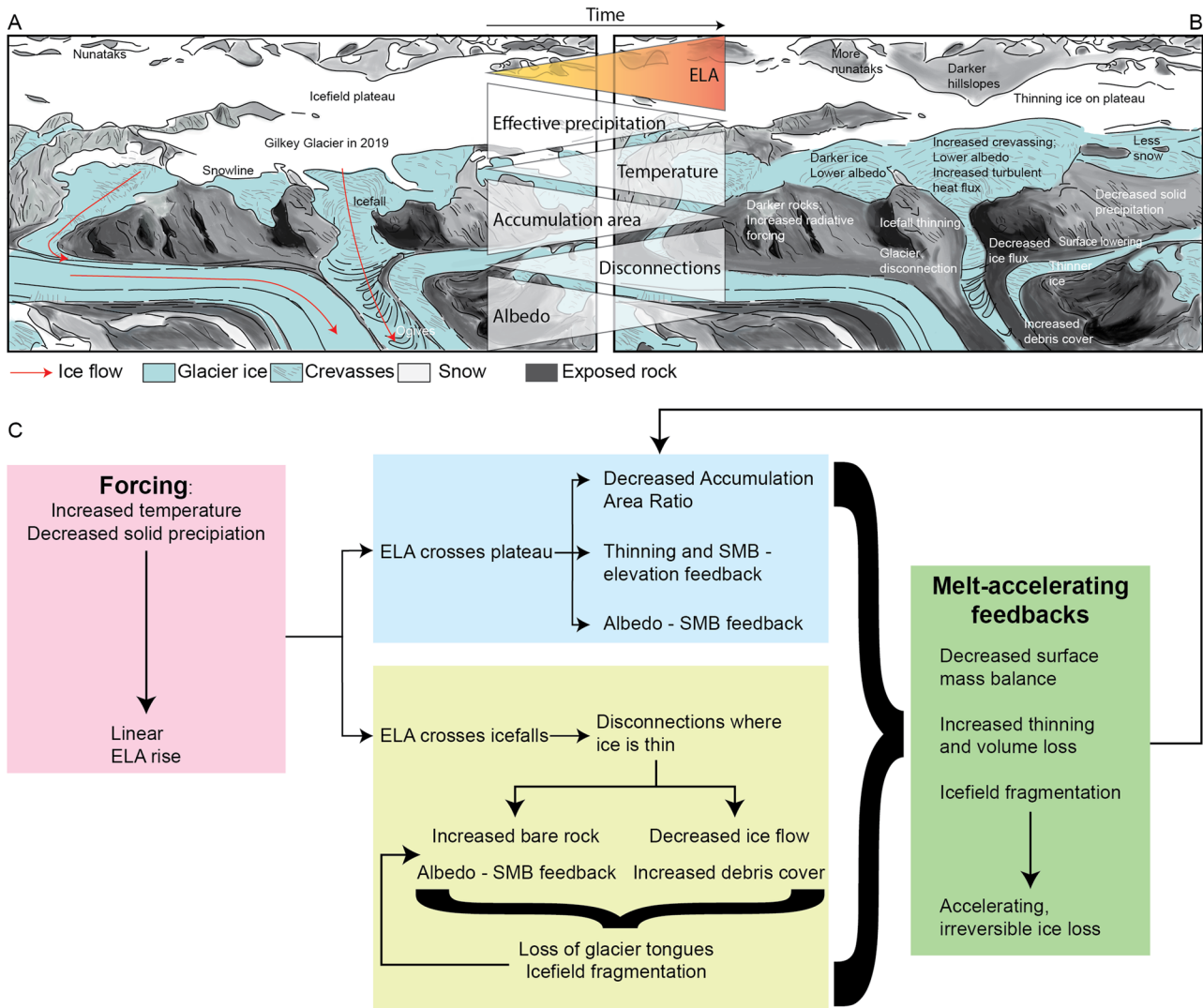


Fig. 8 | The key processes operating on the low-slope plateau on Juneau Icefield. **A** Schematic conceptual sketch of Vaughan Lewis Icefall and tongue on Gilkey Glacier, Juneau Icefield, in 2019. **B** Schematic sketch of same site to illustrate how it might look in a few decades, highlighting some of the key processes. **C** Flow chart

illustrating the different processes contributing to the accelerating recession of Juneau Icefield and at other low-slope icefields. See Supplementary Fig. S1D for a field photograph of the Vaughan Lewis Icefall and Gilkey Glacier.

ArcticDEM ‘nodata’ values were converted to 0. The ArcticDEM holes were then filled with the ASTER GDEM data (filled output upsampled to 2 m cell size to match ArcticDEM) using raster calculator. Comparison of the composite DEM with the original, unmodified GDEM raster yield differences for individual pixels of up to 15 m, which is within GDEM resolution. This likely stems from the resampling carried out as part of the final raster calculation. Hillshade and slope models were derived from the composite DEM mosaic to aid interpretation of glaciological features.

For some glaciers, historical maps and surveys prior to 1948 are available. Here, the maps provided in historical sources (e.g., ref. 28) were scanned, georeferenced, and the termini digitised and included in the available data. As only terminus positions are available, these are provided as polylines at the glacier terminus, annotated with the year (e.g., Fig. 2E, Supplementary Fig. 5).

Photogrammetry and generation of orthomosaics and DEMs

Aerial photographs from surveys flown in 1948 and 1979 are available in Earth Explorer (USGS). They are scanned images, without any geospatial data attached. The files are not georeferenced but the database includes an approximate footprint for some images. The

surveys were undertaken in July–August 1948 and from a single flight in August 1979, during a period of minimal snow and cloud cover. We selected all available images from the Earth Explorer database (1446 from 1948 AD and 103 from 1979 AD) that intersected a polygon drawn around our study region, along with images that had no footprints in the database but were part of the same flight roll, and that were not damaged, torn or had holes.

For 1979, we used the calibration reports provided by NASA along with the fiducial markers to resample the images to a consistent size. The 1948 images do not have calibration reports but do have fiducial markers, so we used the average position of the fiducial marks to resample the images. We then applied contrast limit adaptive histogram equalization (CLAHE) to ensure the images had consistent brightness. Using MicMac⁷¹, we found tiepoints and calculated the relative camera orientations for each image and processed a relative orthophoto and DEM, using camera coordinates rather than geographic coordinates. The 1948 images were processed in four separate blocks due to the number of images involved. We then automatically registered the resultant orthophotos to a Sentinel-2 image to find ground control points. Elevation was determined using the Copernicus 30 m DEM (<https://spacedata.copernicus.eu/collections/copernicus->

digital-elevation-model). From these control points, we extracted the DEMs for each of the four blocks in 1948 and in 1979, using MicMac. For 1948 we co-registered to the Copernicus DEM and cropped the edges of the DEM to deal with edge effects, before stitching the DEMs together, using an established approach⁷⁶. In post-processing, we masked the errors (largely in the accumulation area) and these are given as 'no data'. Voids are filled using the local mean elevation change method⁷⁷.

DEMs of difference were then produced for LIA-1948, 1948–1979, 1979–2000 AD. Volume change from 1979–2000 uses the STRM. DEMs for volume change analysis from 2000–2020 are derived from ref. 72, using ASTER imagery and ArcticDEM. DEMs were resampled prior to differencing to the extent of a Copernicus DEM over the study domain, which includes resampling to the 30 m pixel size of the Copernicus DEM. This is undertaken using bilinear resampling. The 1948 and 1979 DEMs are therefore upsampled, as they are higher resolution than the Copernicus DEM.

Glacier area determination and uncertainty

Initial ice divides and glacier outlines were downloaded from the Randolph Glacier Inventory (RGI) version 6.0^{66,67}, which has a census date of AD 2005⁷⁸. This historical inventory is our baseline from which recent changes are assessed. The RGI outlines were updated and removed since some were incorrect; they were misclassified snow cover or shadow, or inappropriately subdivided into glaciers. Some glaciers were missing, or were incorrectly delineated, or had overlapping outlines with another glacier polygon. These errors are clear when comparing outlines to the higher resolution, more recently acquired satellite imagery. RGI 6.0 glacier outlines were therefore manually edited to be consistent with Landsat 7 ETM+ imagery from 2005 (updated outlines published²¹, see Supplementary Table 6). Glacier outlines were then manually edited in ArcGIS according to observed changes around the glacier margin from the satellite imagery, aerial photograph orthomosaics, 1948 USGS topographic maps, both in the terminus and forefield, and at higher elevations, to reflect glacier extent in 2019, 2015, 2005, 1990, 1979, and 1948 AD. RGI IDs were maintained for each glacier polygon. Where glaciers had separated into separate polygons, the same RGI ID was used for both and the glacier was treated as a multipart polygon in ESRI ArcGIS. The high pixel resolution of the recent Sentinel-2 images and archival aerial photographs allowed a more detailed glaciological analysis and smaller minimum glacier and lake area for mapping than earlier inventories, which relied on coarser-resolution Landsat imagery⁷⁸. The minimum glacier and lake size mappable was 0.001 km². The date for each glacier is noted in the attribute information and is used to calculate annualised rates of change. Glaciers were categorised as glacierets, mountain glaciers, valley glaciers or outlet glaciers, following GLIMS guidelines⁷⁹ and previous work²¹.

To generate glacier outlines for the latest neoglacial maximum (the LIA), the RGI v6.0 2005⁶⁷ outlines were manually edited to extend to the crests of LIA-associated moraines, bare ice-scoured rock and associated trimlines, using published geomorphological mapping²¹ and published chronological and geological data^{28,32,34,80,81}, which are reviewed comprehensively in the Supplementary Information (e.g., Supplementary Fig. 5). The more subtle geomorphological evidence included stripped bedrock at elevations beneath surrounding vegetated hillslopes, and locally-depressed treelines. Glacier moraines at Herbert, Eagle and Twin Glacier Lake were ground truthed and field-checked during fieldwork in July 2022. Published ages were gleaned from the literature and included in the geodatabase. Radiocarbon ages were recalibrated using CALIB⁸². Calibrated mean ages (2σ) are presented as 'cal. ka BP'. Morphostratigraphic principles^{83–85} were applied to differentiate between the most recent, LIA Neoglacial moraines, and older moraines deposited in the Younger Dryas or earlier Holocene glaciations. In most cases, Holocene neoglaciations are likely to have

been within the limits of the LIA¹⁸, which makes confusion of older ice limits less likely. Where it was unclear which moraine related to the LIA, the innermost was chosen, to provide a conservative estimate of LIA area. Cross-checks were then performed against sites that have been documented as dating from the LIA.

Uncertainty in glacier area was calculated following the methods outlined by ref. 86. Eleven representative glaciers, across the spectrum of glacier sizes and including typical examples of debris-covered and clean-ice glaciers, were digitised seven times, with a minimum of one day between each round of digitising (Supplementary Fig. 8). The mean, standard deviation and 95% confidence interval was then calculated for each glacier for each timeslice. There was a significant correlation between glacier size and confidence interval (Supplementary Table 7). A regression through the data points provided an equation that was used for size-class specific up-scaling to the full dataset^{66,86,87}. As a comparison, we also calculated the standard error and standard error of the forecast for each timeslice. This gave a similar, but smaller, estimate of the uncertainty, and so the confidence interval, the more conservative estimate of uncertainty, was used.

Glacier recession, defined in terms of area change per annum (km² a⁻¹) and proportional rates of area change (% a⁻¹), was calculated for each glacier. Note that where we refer to terminus retreat (i.e., a glacier length change) this is specifically stated. Annual rates of area change were calculated by dividing area change (km²) by the time between analyses for each glacier (time was taken from date of satellite or aerial photograph image acquisition). This allows results to be compared between different times and different glacier areas. For 1948 and 1979, where the same imagery is used for a few glaciers in each timeslice due to a lack of coverage, this means that rates of glacier recession are 0 and are removed from our analysis. However, all glaciers are included in the total summed areas given for each timeslice, and the total summed rates of change. Rates of glacier recession for individual glaciers (% a⁻¹ and km² a⁻¹) are normally distributed. Mean rates are presented with the 95% confidence interval.

Snowlines

The late summer snowline from 2019 AD was mapped from the cloud-free Sentinel-2 imagery (Supplementary Table 6), using black and white band 4 imagery (in line with structural mapping conducted in ref. 21). These images, from 30th August to 7th September 2019, provided clear, cloud-free coverage of the entire icefield. The short timeframe between image acquisitions allowed temporal continuity and clear visualization of icefield snowlines. Snowlines were identified as a wavy, discontinuous boundary between bright white and duller grey; the higher albedo snow reflecting a brighter white colour.

Glacier disconnections

Glacier disconnections, where the tongue of a glacier had become separated from its accumulation area^{62,63,88}, were mapped across the icefield published in ref. 21 without a date stamp. Individual disconnections were mapped that occurred prior to each timeslice. We classified glacier tongues as 'disconnected' if they were associated with one or more of these disconnections from the accumulation area. In the case of disconnected glaciers, multipart polylines were used to record glacier length along the same flowline. The timing of disconnection was calculated through comparison with the glacier area outlines, and the slope and elevation of the disconnection calculated through automated tools using tools within the GIS. Elevations were derived from ASTER GDEM⁷⁴.

Surface albedo

We derived a stack of 299 Landsat 5–9 images in Google Earth Engine for the years 1986–2023, limited to WRS path/row 57/19 and 58/19, for all available scenes with less than 20% cloud cover on land (Supplementary Table 15). Clouds were masked using a cloud cover filter using

the USGS QA_Mask, removing any pixels identified as cloud by the USGS algorithm. We calculated albedo for each pixel in the stack using the albedo equation developed for Landsat 7^{89,90} bands blue, red, and infrared, and applied this across the TM, ETM+ and OLI sensors for Landsats 5–9. We then calculated average albedo for every scene within the icefield boundaries as of 1990, 2005 and 2019 AD (not including the peripheral ice masses). This captured the plateau and glacier tongues. Using the average albedos calculated within the 2019 outlines effectively analyses the darkening of snow and glacier ice only, whereas using the 1990 outlines captures glacier recession and fragmentation in addition to darkening snow and ice. We also calculated the average albedo in each scene for pixels above 1500 m in the Copernicus DEM (~2013 AD), this capturing just the plateau. Observations were limited to at least 60% of the plateau being covered and not masked out by cloud.

LIA volume reconstruction

Our LIA outlines were converted to lines with points along them at intervals of 100 m, and those points were used to extract elevations from the ALOS DEM⁷⁵, which was selected for its seamless coverage. A surface to represent the LIA glacier ice surface below the ELA was interpolated between those points. Carrivick et al.^{68,69} have shown that there is a negligible effect of which DEM (resolution and date) is used in these types of analyses, because the points are preferentially located from the high-resolution 2 m Arctic DEM⁷³ even if the elevation values are extracted from a coarser resolution DEM. However, Carrivick et al.^{68,69} have also shown that there is an effect on volume loss calculations of the choice of interpolation method and in this study, we followed their advice using a Natural Neighbour interpolation.

Due to an absence of moraines and trimlines above the equilibrium line altitude of glaciers, our mapping of a LIA glacier outline, our LIA ice surface and our analysis of elevation changes and hence volume loss only pertains to LIA ablation area. Following the method of Carrivick et al.^{68,69}, LIA glacier ablation areas were produced by automatically estimating glacier-specific equilibrium line altitudes (ELA_{LIA}) using the Area-Altitude Balance Ratio (AABR) method⁹¹. The AABR method was chosen to explicitly consider (spatially-distributed) glacier hypsometry. The glacier-specific ELA_{LIA} were subsequently merged with our mapped moraine crests and trimlines to create a single polygon for each glacier ablation area. We estimated the ELA_{LIA} using a BR of 1.88 for all glaciers as suggested to be typical of maritime glaciers⁹². Published work shows that the choice of balance ratio has little influence on glacier ELA⁹³.

Volume change estimates presented in this study can only be considered as a proxy for mass balance if it is assumed that glacier surfaces above the ELA have not changed since the LIA. Thus, volume change using the methods in this work should be considered as minimum estimates because probably some mass loss has occurred above the ELA_{LIA} as they have risen in elevation due to atmospheric 20th Century warming. That mass loss above the ELA_{LIA} would likely be via surface lowering, rather than areal contraction, and so we would not detect it with our mapping.

Glacier volume change calculation

To determine volume changes (LIA-1948, 1948–1979, 1979–2000 AD), we used the LIA, 1948 and 1979 glacier outlines, using the outlines that correspond to the start date of the DEMs of difference for each time period. For each glacier, the outline was divided into elevation bands of either 50 m or, 10% of the glacier elevation range, whichever was smaller. In effect, glaciers with an elevation range of greater than 500 m were divided into 50 m elevation bands. The mean elevation change was calculated for each elevation band, removing outliers that were more than 3 normalised median absolute deviations (NMAD) away from the median of the band. We use the mean value for the elevation band if there is 25% or more coverage by area within the

elevation band. If there is less than 25% coverage by area within the elevation band, then we use the icefield-wide average for that elevation band.

For each elevation band, this mean elevation change value was multiplied by the area of the band, to calculate volume change, per elevation band. Each band's volume change was summed, and the sum of this is the total volume change for each glacier. For glaciers with no DEM coverage at all, we use the icefield-wide area-averaged thinning rate to scale up the total volume change for the region. This amounts to 44.6% of glacier area for LIA-1948, 16.8% for 1948–1979, 4.4% for 1979–2000, and 0% for 2000–2020 (Supplementary Table 8).

The sum of the total volume change for each glacier was then summed to calculate total volume change for each time period. Mean dh/dt per glacier was calculated by dividing the mean elevation change value by the time period. Mass change was not calculated. For LIA-1948, where pixels showed a positive elevation change, this was assumed to be erroneous, due to the substantial area change, these pixels were masked out. The LIA-1948 elevation change will be a minimum, because the LIA DEM only covers ablation areas.

We use the normalized median absolute deviation of off-glacier pixels to estimate the uncertainty in the DEMs of difference. To estimate the uncertainty in elevation change (σ_{dz}) introduced by interpolating elevation bands with no data, we adapt the approach utilised in ref. 33 in Eq. (1):

$$\sigma_{dz} = N_z(1 - f) + (M + N_z)f \quad (1)$$

Where N_z is the NMAD of off-glacier elevation differences calculated between the two DEMs, f is the fraction of the glacier that required interpolation, M is the standard deviation of all on-glacier pixels.

We estimate the total uncertainty in each glacier's volume change as the quadratic sum of the elevation change and the area parts (Eq. 2).

$$\sigma_{dv} = \sqrt{(\sigma_{dz}A)^2 + (\sigma_A \bar{dh})^2} \quad (2)$$

Where A is the glacier area, σ_A is the uncertainty in glacier area (following the methods above), and \bar{dh} is the area-averaged elevation change on the glacier.

Uncertainty is higher in the LIA-1948 period due to the interpolation of the datasets over areas with no data. The LIA DEM is calculated only over the icefield ablation areas, and the 1948 DEM is likewise not available over Canada. This does not mean that the change is insignificant, but we emphasise that the uncertainty is large because of interpolation, not because of variability of the elevation differences.

Volume change, and uncertainty, from 2000–2010 and 2010–2020 AD was derived directly from ref. 72. Glacier outlines were taken as the RGI v6.0, as explained in the original publication. Glacier-averaged mean volume change and mean elevation change through time (mean dh/dt) was calculated following the method above. Thus they do not take into account area changes through this time period and should be considered a minimum value.

Data availability

All data used in this work are available open access and source data are provided with this paper. The glacier outlines, source data, and the novel digital elevation models and orthomosaics from the LIA, 1948 and 1979 are available from Mendeley Data (Davies, Bethan (2024), "Juneau Icefield 1770-2020", Mendeley Data, V3, doi: 10.17632/4djw8z3jrb.3; <https://data.mendeley.com/datasets/4djw8z3jrb/2>). Source data are provided with this paper. The updated Juneau Icefield glacier outlines are also available from GLIMS. Shapefiles of geomorphological mapping used in the neoglacial LIA reconstruction are available from Davies et al. 2022 (ref. 21). Historical topographic maps are available from the USGS map viewer (<https://ngmdb.usgs.gov/>)

[topoview/viewer/#4/52.19/-123.71](#)) as georeferenced GEOTIFFS. Aerial photographs and Landsat and Sentinel satellite imagery are available from USGS Earth Explorer (<https://earthexplorer.usgs.gov/>). SRTM available from the USGS EROS archive (<https://www.usgs.gov/centers/eros/science/usgs-eros-archive-digital-elevation-shuttle-radar-topography-mission-srtm-1>) and the 3" Viewfinder Panorama DEMs are available from <https://viewfinderpanoramas.org/dem3.html>. ASTER GDEM V3 available from the NASA Jet Propulsion Laboratory (<https://asterweb.jpl.nasa.gov/gdem.asp>). DEMs of difference from 2000–2010 and 2010–2020 are available from Hugonnet et al 2021 (ref. 72). Source data are provided with this paper.

Code availability

The software used in this manuscript includes ESRI ArcGIS, QGIS, MicMac and MatPlotLib, as well as standard MS Office programmes. Information on installation, system requirements and instructions for use are all available with these software packages. Information on MicMac is available here: <https://github.com/micmacIGN/micmac>. Code to derive albedo in Google Earth Engine (GEE account needed): <https://code.earthengine.google.com/?scriptPath=users%2Frobertmcnabb%2Fjuneau%3Aalbedo.js>

References

- Slater, T. et al. Review article: Earth's ice imbalance. *Cryosphere* **15**, 233–246 (2021).
- Zemp, M. et al. Global glacier mass changes and their contributions to sea-level rise from 1961 to 2016. *Nature* **568**, 382–386 (2019).
- Millan, R., Mouginit, J., Rabatel, A. & Morlighem, M. Ice velocity and thickness of the world's glaciers. *Nat. Geosci.* <https://doi.org/10.1038/s41561-021-00885-z> (2022).
- Edwards, T. L. et al. Projected land ice contributions to twenty-first-century sea level rise. *Nature* **593**, 74–82 (2021).
- Marzeion, B. et al. Partitioning the uncertainty of ensemble projections of global glacier mass change. *Earth's Future* **8** <https://doi.org/10.1029/2019EF001470> (2020).
- Rounce, D. R. et al. Global glacier change in the 21st century: Every increase in temperature matters. *Science* **379**, 78–83 (2023).
- Hock, R. et al. in *IPCC Special Report on the Ocean and Cryosphere in a Changing Climate* (eds Portner, H. O. et al.) 131–202 (The IPCC, 2019).
- McGrath, D., Sass, L., O'Neel, S., Arendt, A. & Kienholz, C. Hypsometric control on glacier mass balance sensitivity in Alaska and northwest Canada. *Earth's Future* **5**, 324–336 (2017).
- Boston, C. M. & Lukas, S. Topographic controls on plateau icefield recession: insights from the Younger Dryas Monadhliath Icefield, Scotland. *J. Quat. Sci.* **34**, 433–451 (2019).
- Zekollari, H., Huybrechts, P., Noël, B., van de Berg, W. J. & van den Broeke, M. R. Sensitivity, stability and future evolution of the world's northernmost ice cap, Hans Tausen Iskappe (Greenland). *Cryosphere* **11**, 805–825 (2017).
- Bolibar, J., Rabatel, A., Gouttevin, I., Zekollari, H. & Galiez, C. Nonlinear sensitivity of glacier mass balance to future climate change unveiled by deep learning. *Nat. Commun.* **13**, 409 (2022).
- Åkesson, H., Nisancioglu, K. H. & Morlighem, M. Simulating the evolution of Hardangerjøkulen ice cap in southern Norway since the mid-Holocene and its sensitivity to climate change. *Cryosphere* **11**, 281–302 (2017).
- Clarke, G. K. C., Jarosch, A. H., Anslow, F. S., Radić, V. & Menounos, B. Projected deglaciation of western Canada in the twenty-first century. *Nat. Geosci.* **8**, 372–377 (2015).
- Ziemen, F. A. et al. Modeling the evolution of the Juneau Icefield between 1971 and 2100 using the Parallel Ice Sheet Model (PISM). *J. Glaciol.* **62**, 199–214 (2016).
- Marshall, S. J. Regime shifts in glacier and ice sheet response to climate change: examples from the Northern Hemisphere. *Front. Clim.* **3** <https://doi.org/10.3389/fclim.2021.702585> (2021).
- Aschwanden, A. & Brinkerhoff, D. J. Calibrated mass loss predictions for the Greenland ice sheet. *Geophys. Res. Lett.* **49**, e2022GL099058 (2022).
- Aschwanden, A., Bartholomäus, T. C., Brinkerhoff, D. J. & Truffer, M. Brief communication: a roadmap towards credible projections of ice sheet contribution to sea level. *Cryosphere* **15**, 5705–5715 (2021).
- Barclay, D. J., Wiles, G. C. & Calkin, P. E. Holocene glacier fluctuations in Alaska. *Quat. Sci. Rev.* **28**, 2034–2048 (2009).
- Forbes, V., Ledger, P. M., Cretu, D. & Elias, S. A sub-centennial, Little Ice Age climate reconstruction using beetle subfossil data from Nunalleq, southwestern Alaska. *Quat. Int.* **549**, 118–129 (2020).
- Winski, D. et al. A 400-year ice core melt layer record of summertime warming in the Alaska range. *J. Geophys. Res. Atmos.* **123**, 3594–3611 (2018).
- Davies, B. et al. Topographic controls on ice flow and recession for Juneau Icefield (Alaska/British Columbia). *Earth Surf. Process. Landf.* **47**, 2357–2390 (2022).
- Almazroui, M. et al. Projected changes in temperature and precipitation over the United States, Central America, and the Caribbean in CMIP6 GCMs. *Earth Syst. Environ.* **5**, 1–24 (2021).
- Rounce, D. R. et al. Quantifying parameter uncertainty in a large-scale glacier evolution model using Bayesian inference: application to High Mountain Asia. *J. Glaciol.* **66**, 175–187 (2020).
- Albrecht, T., Winkelmann, R. & Levermann, A. Glacial-cycle simulations of the Antarctic Ice Sheet with the Parallel Ice Sheet Model (PISM)–Part 2: Parameter ensemble analysis. *Cryosphere* **14**, 633–656 (2020).
- McNeil, C. et al. Explaining mass balance and retreat dichotomies at Taku and Lemon Creek Glaciers, Alaska. *J. Glaciol.* **66**, 530–542 (2020).
- Roth, A., et al. Modeling winter precipitation over the Juneau Icefield, Alaska, using a linear model of orographic precipitation. *Front. Earth Sci.* **6** <https://doi.org/10.3389/feart.2018.00020> (2018).
- Nolan, M., Motkya, R. J., Echelmeyer, K. & Trabant, D. C. Ice-thickness measurements of Taku Glacier, Alaska, USA, and their relevance to its recent behavior. *J. Glaciol.* **41**, 541–553 (1995).
- Lawrence, D. B. Glacier fluctuation for six centuries in southeastern Alaska and its relation to solar activity. *Geogr. Rev.* **40**, 191–223 (1950).
- Heusser, C. J. & Marcus, M. G. Historical variations of Lemon Creek Glacier, Alaska, and their relationship to the climatic record. *J. Glaciol.* **5**, 77–86 (1964).
- Motyka, R. J. & Begét, J. E. Taku Glacier, Southeast Alaska, U.S.A.: late Holocene history of a tidewater glacier. *Arct. Alp. Res.* **28**, 42–51 (1996).
- Motyka, R. J. Little Ice Age subsidence and post Little Ice Age uplift at Juneau, Alaska, inferred from dendrochronology and geomorphology. *Quat. Res.* **59**, 300–309 (2003).
- Knopf, A. The Eagle River region, southeastern Alaska: US Geol. Surv. Bull. **502**, 36–40 (1912).
- O'Neel, S. et al. Reanalysis of the US Geological Survey Benchmark Glaciers: long-term insight into climate forcing of glacier mass balance. *J. Glaciol.* **65**, 850–866 (2019).
- Pelto, M., Kavanaugh, J. & McNeil, C. Juneau Icefield mass balance program 1946–2011. *Earth System Science. Data* **5**, 319–330 (2013).
- U.S. Geological Survey, B. G. P. *Glacier-wide mass balance and compiled data inputs (ver. 8.0, November 2023)*: U.S. Geological Survey data release. (2016).
- Criscitello, A. S., Kelly, M. A. & Tremblay, B. The response of Taku and Lemon Creek glaciers to climate. *Arct. Antarct. Alp. Res.* **42**, 34–44 (2010).

37. McNeil, C. et al. The Imminent Calving Retreat of Taku Glacier. *Eos, Transactions of the American Geophysical Union* 102 (2021).
38. Pelto, M. Exceptionally High 2018 Equilibrium Line Altitude on Taku Glacier, Alaska. *Remote Sens.* **11**, 2378–2378 (2019).
39. U. S. Geological Survey Benchmark Glacier Program. *USGS benchmark glacier project comprehensive data collection.* (2020).
40. Miller, M. M. & Pelto, M. S. Mass balance measurements on the Lemon Creek glacier, Juneau Icefield, Alaska 1953–1998. *Geogr. Ann. A Phys. Geogr.* **81**, 671–681 (1999).
41. Boyce, E. S., Motyka, R. J. & Truffer, M. Flotation and retreat of a lake-calving terminus, Mendenhall Glacier, southeast Alaska, USA. *J. Glaciol.* **53**, 211–224 (2007).
42. Motyka, R. J., O’Neel, S., Connor, C. L. & Echelmeyer, K. A. Twentieth century thinning of Mendenhall Glacier, Alaska, and its relationship to climate, lake calving, and glacier run-off. *Glob. Planet. Change* **35**, 93–112 (2002).
43. Young, J. C. et al. A changing hydrological regime: trends in magnitude and timing of Glacier ice melt and glacier runoff in a high latitude coastal watershed. *Water Resour. Res.* **57**, e2020WR027404 (2021).
44. Berthier, E., Schiefer, E., Clarke, G. K. C., Menounos, B. & Remy, F. Contribution of Alaskan glaciers to sea-level rise derived from satellite imagery. *Nat. Geosci.* **3**, 92–95 (2010).
45. Jakob, L., Gourmelen, N., Ewart, M. & Plummer, S. Spatially and temporally resolved ice loss in High Mountain Asia and the Gulf of Alaska observed by CryoSat-2 swath altimetry between 2010 and 2019. *Cryosphere* **15**, 1845–1862 (2021).
46. Berthier, E., Larsen, C., Durkin, W. J., Willis, M. J. & Pritchard, M. E. Brief communication: Unabated wastage of the Juneau and Stikine icefields (southeast Alaska) in the early 21st century. *Cryosphere* **12**, 1523–1530 (2018).
47. Young, R., Foster, T., Mieno, T., Valocchi, A. & Brozović, N. Hydrologic-economic trade-offs in groundwater allocation policy design. *Water Resour. Res.* **57**, e2020WR027941 (2021).
48. Gaglioti, B. V. et al. Timing and potential causes of 19th-century glacier advances in coastal Alaska based on tree-ring dating and historical accounts. *Front. Earth Sci.* **7**, 82–82 (2019).
49. Overland, J. E., Adams, J. M. & Bond, N. A. Decadal variability of the Aleutian low and its relation to high-latitude circulation. *J. Clim.* **12**, 1542–1548 (1999).
50. Winski, D. et al. Industrial-age doubling of snow accumulation in the Alaska Range linked to tropical ocean warming. *Sci. Rep.* **7**, 1–12 (2017).
51. Hartmann, B. & Wendler, G. The significance of the 1976 Pacific climate shift in the climatology of Alaska. *J. Clim.* **18**, 4824–4839 (2005).
52. Pelto, M. S. & Miller, M. M. Mass balance of the Taku Glacier, Alaska from 1946 to 1986. *Northwest Science*, **64**, 121–130 (1990).
53. Hurrell, J., & National Center for Atmospheric Research Staff. (2020). The climate data guide: North Pacific (NP) index by Trenberth and Hurrell; monthly and winter. National Center for Atmospheric Research, Boulder, Colorado. Available: <https://climatedataguide.ucar.edu/climate-data/north-pacific-np-index-trenberth-and-hurrell-monthly-and-winter>.
54. National Oceanic and Atmospheric Administration (NOAA). *Climate at a Glance: City Time Series* <https://www.ncei.noaa.gov/access/monitoring/climate-at-a-glance/> (2021).
55. Thoman, R. & Walsh, J. E. *Alaska’s Changing Environment: Documenting Alaska’s Physical and Biological Changes Through Observations* (International Arctic Research Center, University of Alaska Fairbanks, 2019).
56. Hersbach, H. et al. The ERA5 global reanalysis. *Q. J. R. Meteorol. Soc.* **146**, 1999–2049 (2020).
57. Johnson, E. & Rupper, S. An examination of physical processes that trigger the albedo-feedback on glacier surfaces and implications for regional glacier mass balance across High Mountain Asia. *Front. Earth Sci.* **8** <https://doi.org/10.3389/feart.2020.00129> (2020).
58. Nagorski, S. A., Kaspari, S. D., Hood, E., Fellman, J. B. & Skiles, S. M. Radiative forcing by dust and black carbon on the Juneau Icefield, Alaska. *J. Geophys. Res. Atmos.* **124**, 3943–3959 (2019).
59. Skiles, S. M., Flanner, M., Cook, J. M., Dumont, M. & Painter, T. H. Radiative forcing by light-absorbing particles in snow. *Nat. Clim. Change* **8**, 964–971 (2018).
60. Kehrwald, N. M. et al. Boreal blazes: biomass burning and vegetation types archived in the Juneau Icefield. *Environ. Res. Lett.* **15**, 085005 (2020).
61. Sass, L. C., Loso, M. G., Geck, J., Thoms, E. E. & McGrath, D. Geometry, mass balance and thinning at Eklutna Glacier, Alaska: an altitude-mass-balance feedback with implications for water resources. *J. Glaciol.* **63**, 343–354 (2017).
62. Rippin, D. M., Sharp, M., Van Wychen, W. & Zubot, D. Detachment of icefield outlet glaciers: catastrophic thinning and retreat of the Columbia Glacier (Canada). *Earth Surf. Process. Landf.* **45**, 459–472 (2020).
63. Jiskoot, H., Curran, C. J., Tessler, D. L. & Shenton, L. R. Changes in Clemenceau Icefield and Chaba Group glaciers, Canada, related to hypsometry, tributary detachment, length-slope and area-aspect relations. *Ann. Glaciol.* **50**, 133–143 (2009).
64. Benn, D. I. & Nicholson, L. Calculating ice melt beneath a debris layer using meteorological data. *J. Glaciol.* **52**, 463–470 (2006).
65. Van Wychen, W. et al. Spatial and temporal variation of ice motion and ice flux from Devon Ice Cap, Nunavut, Canada. *J. Glaciol.* **58**, 657–664 (2012).
66. Pfeffer, W. T. et al. The Randolph Glacier Inventory: a globally complete inventory of glaciers. *J. Glaciol.* **60**, 537–552 (2014).
67. Randolph Glacier Inventory Consortium et al. *Randolph glacier inventory—a dataset of global glacier outlines: Version 6.0: technical report* (RGI Consortium, 2017).
68. Carrivick, J. L., James, W. H. M., Grimes, M., Sutherland, J. L. & Lorrey, A. M. Ice thickness and volume changes across the Southern Alps, New Zealand, from the Little Ice Age to present. *Sci. Rep.* **10**, 13392–13392 (2020).
69. Carrivick, J. L. et al. Accelerated volume loss in glacier Ablation Zones of NE Greenland, little ice age to present. *Geophys. Res. Lett.* **46**, 1476–1484 (2019).
70. Jaud, M. et al. Assessing the accuracy of high resolution digital surface models computed by PhotoScan® and MicMac® in sub-optimal survey conditions. *Remote Sens.* **8**, 465–465 (2016).
71. Rupnik, E., Daakir, M. & Deseilligny, M. P. MicMac—a free, open-source solution for photogrammetry. *Open Geospatial Data Softw. Stand.* **2**, 1–9 (2017).
72. Hugonnet, R. et al. Accelerated global glacier mass loss in the early twenty-first century. *Nature* **592**, 726–731 (2021).
73. Porter, C. et al. ArcticDEM, Version 3. *Harvard Dataverse* **1**, <https://doi.org/10.7910/DVN/OHHUKH> (2018).
74. Aster Gdem Validation Team, Meti/Ersdac, Nasa/Lpdaac & Usgs/Eros. *ASTER Global DEM Validation Summary Report 28–28* (2009).
75. Tadono, T. et al. Precise global DEM generation by ALOS PRISM. *ISPRS Ann. Photogramm. Remote Sens. Spat. Inf. Sci.* **2**, 71–76 (2014).
76. Nuth, C. & Kääh, A. Co-registration and bias corrections of satellite elevation data sets for quantifying glacier thickness change. *Cryosphere* **5**, 271–290 (2011).
77. McNabb, R., Nuth, C., Kääh, A. & Girod, L. Sensitivity of glacier volume change estimation to DEM void interpolation. *Cryosphere* **13**, 895–910 (2019).
78. Kienholz, C. et al. Derivation and analysis of a complete modern-date glacier inventory for Alaska and northwest Canada. *J. Glaciol.* **61**, 403–420 (2015).

79. Raup, B. et al. Remote sensing and GIS technology in the Global Land Ice Measurements from. *Space (GLIMS) Proj. Comput. Geosci.* **33**, 104–125 (2007).
80. Miller, M. M. Inventory of terminal position changes in Alaskan coastal Glaciers since the 1750's. *Proc. Am. Philos. Soc.* **108**, 257–273 (1964).
81. Molnia, B. F. Late nineteenth to early twenty-first century behavior of Alaskan glaciers as indicators of changing regional climate. *Glob. Planet. Change* **56**, 23–56 (2007).
82. Stuiver, M., Reimer, P. J. & Reimer, R. W. *CALIB 5.0.1. Program and Documentation*. 09 March 2 <http://www.calib.qub.ac.uk/> (2009).
83. Boston, C. M., Lukas, S. & Carr, S. J. A Younger Dryas plateau icefield in the Monadhliath, Scotland, and implications for regional palaeoclimate. *Quat. Sci. Rev.* **108**, 139–162 (2015).
84. Lüthgens, C. & Böse, M. From morphostratigraphy to geochronology—on the dating of ice marginal positions. *Quat. Sci. Rev.* **44**, 26–36 (2012).
85. Lukas, S. Morphostratigraphic principles in glacier reconstruction—a perspective from the British Younger Dryas. *Prog. Phys. Geogr.* **30**, 719–736 (2006).
86. Paul, F. et al. Error sources and guidelines for quality assessment of glacier area, elevation change, and velocity products derived from satellite data in the Glaciers_cci project. *Remote Sens. Environ.* **203**, 256–275 (2017).
87. Paul, F. et al. On the accuracy of glacier outlines derived from remote-sensing data. *Ann. Glaciol.* **54**, 171–182 (2013).
88. Le Heron, D. P., Kettler, C., Wawra, A., Schöpfer, M. & Grasmann, B. The sedimentological death mask of a dying glacier. *Depos. Rec.* **8**, 992–1007 (2022).
89. Liang, S. Narrowband to broadband conversions of land surface albedo I: Algorithms. *Remote Sens. Environ.* **76**, 213–238 (2001).
90. Naegeli, K. et al. Cross-comparison of albedo products for glacier surfaces derived from airborne and satellite (Sentinel-2 and Landsat 8) optical data. *Remote Sens.* **9**, 110 (2017).
91. Pellitero, R. et al. A GIS tool for automatic calculation of glacier equilibrium-line altitudes. *Comput. Geosci.* **82**, 55–62 (2015).
92. Rea, B. R. Defining modern day Area-Altitude Balance Ratios (AABRs) and their use in glacier-climate reconstructions. *Quat. Sci. Rev.* **28**, 237–248 (2009).
93. Carrivick, J. L. et al. Mass loss of glaciers and ice caps across Greenland since the Little Ice Age. *Geophys. Res. Lett.* **50**, e2023GL103950 (2023).
94. Young, J. C., Arendt, A., Hock, R. & Pettit, E. The challenge of monitoring glaciers with extreme altitudinal range: mass-balance reconstruction for Kahiltna Glacier, Alaska. *J. Glaciol.* **64**, 75–88 (2018).
95. Tangborn, W. Mass balance, runoff and surges of Bering Glacier, Alaska. *Cryosphere* **7**, 867–875 (2013).
96. Gilmore, R. A. Descriptive report: Southeast Alaska, *Taku River to Flat Point*. Register Number 8032. (U.S. Coast and Geodetic Survey, 1953).
97. Motyka, R. J. *Taku Glacier Advance: preliminary analysis*. 32 (Alaska Division of Geological and Geophysical Surveys, Juneau, Alaska 99801, 1989).
98. Loso, M. G. Summer temperatures during the Medieval Warm Period and Little Ice Age inferred from varved proglacial lake sediments in southern Alaska. *J. Paleolimnol.* **41**, 117–117 (2009).
- Council (NERC) independent fellowship (NE/R014574/1). L.N. was supported by research funds from the Faculty of Geo- and Atmospheric Sciences at the University of Innsbruck. Fieldwork to Juneau Icefield by Bethan Davies and Lindsey Nicholson was supported by the Royal Geographical Society and the Geological Society, as well as the Juneau Icefield Research Project. Any use of trade, firm or product names is for descriptive purposes only and does not imply endorsement by the US Government.

Author contributions

B.D. and R.M. conceived and designed the study. B.D. mapped the glacial geomorphology, snowlines and other glacial features. B.D. and J.B. compiled satellite data and mapped glacier extents. J.B. compiled ERA5 reanalysis datasets. R.M. supported methodological development and processed aerial photography and satellite imagery to derive glacier volume changes, and calculated albedo. J.C. reconstructed ice surface at the LIA. B.D. visualised and analysed the data. C.M. supported methods development and analysed and validated the data. B.D. and L.N. undertook fieldwork to ground-truth geomorphological mapping. M.P. validated ELA measurements and historic ELA observations. T.H. supported data analysis. B.D., L.N., J.C., J.E., B.M. and C.M. supported funding acquisition for fieldwork. B.D. wrote the main manuscript with support from R.M.; B.D., R.M., J.B., J.C., J.E., T.H., B.M., C.M., L.N. and M.P. contributed to scientific discussion and interpretation of the results and all authors contributed to the manuscript.

Competing interests

The authors declare no competing interests.

Additional information

Supplementary information The online version contains supplementary material available at <https://doi.org/10.1038/s41467-024-49269-y>.

Correspondence and requests for materials should be addressed to Bethan Davies.

Peer review information *Nature Communications* thanks Catherine Delaney and the other, anonymous, reviewer(s) for their contribution to the peer review of this work. A peer review file is available.

Reprints and permissions information is available at <http://www.nature.com/reprints>

Publisher's note Springer Nature remains neutral with regard to jurisdictional claims in published maps and institutional affiliations.

Open Access This article is licensed under a Creative Commons Attribution 4.0 International License, which permits use, sharing, adaptation, distribution and reproduction in any medium or format, as long as you give appropriate credit to the original author(s) and the source, provide a link to the Creative Commons licence, and indicate if changes were made. The images or other third party material in this article are included in the article's Creative Commons licence, unless indicated otherwise in a credit line to the material. If material is not included in the article's Creative Commons licence and your intended use is not permitted by statutory regulation or exceeds the permitted use, you will need to obtain permission directly from the copyright holder. To view a copy of this licence, visit <http://creativecommons.org/licenses/by/4.0/>.

© The Author(s) 2024

Acknowledgements

We thank numerous colleagues and collaborators for fruitful discussions and support, including Fabien Maussion, Tamsin Edwards, Seth Campbell, and faculty and students from the Juneau Icefield Research Project. J.E. acknowledges support from a Natural Environment Research

1
2
3
4
5
6
7
8
9
10
11
12
13
14
15
16
17
18
19
20
21

Productivity and resilience

of Chinook salmon compromised by ‘Mixed-Maturation’ fisheries in marine waters

Nick Gayeski^{1*}, Devin Swanson², Misty MacDuffee³, and Andrew Rosenberger^{3,#b}

¹Fisheries Scientist, Wild Fish Conservancy, P.O. Box 402, Duvall, WA, USA;

²Software Engineer, Wild Fish Conservancy, P.O. Box 402, Duvall, WA, USA;

³Biologist, Raincoast Conservation Foundation, P.O. Box 2429, Sidney, Canada;

^{#b}Principal, Coastland Research, PO Box 4592, Smithers, Canada

* Corresponding author

Email: nick@wildfishconservancy.org (NG)

22

23 **Abstract**

24 Most Chinook salmon (*Oncorhynchus tshawytscha*) in the northeast Pacific Ocean are
25 harvested in mixed-stock marine fisheries. Here, multiple populations with varying abundance
26 and productivities are encountered. In addition, many of these fisheries generally encounter both
27 mature and immature Chinook. Hence, these fisheries are better described as mixed-stock and
28 “mixed-maturation” (MM) fisheries. Harvest of immature fish can skew the age composition of
29 Chinook populations towards younger, and hence smaller, individuals. Older Chinook are
30 generally larger and contribute disproportionately to the productivity of their populations. We
31 developed an individual-based demographic-genetic model of ocean-type Chinook to evaluate
32 the effects of fisheries that harvest immature Chinook. We then compared those effects to
33 terminal fisheries that harvest only mature fish. Our model provides the ability to assess the
34 benefits of terminal Chinook fisheries to both landed catch and Chinook rebuilding. Recovered
35 populations show a more archetypal age- and sex-structure than contemporary ocean-type
36 Chinook subject to marine mixed-maturation fisheries. In our modeled scenarios of mixed-
37 maturation fisheries, we found that immature Chinook can comprise up to 59% of the total
38 numbers of fish caught, and 47% of the total weight of the catch. If instead, these Chinook were
39 not harvested until they mature and reach terminal fisheries, they would contribute greater
40 biomass to landed catches. These terminal fisheries allow a higher percentage of larger, older
41 Chinook to escape, and would increase the fecundity and productivities of their populations. The
42 benefits of terminal fisheries would accrue to fishers, sustainable wild harvesting, wildlife, and
43 the rebuilding of depleted Chinook runs.

44

45 Key words: Age-and-size overfishing, fisheries-induced selection, mixed-maturation fisheries,

46 Chinook, Individual-based model, Demographic-genetic model

47 **Introduction**

48 A number of wild Pacific salmon species and populations have declined in adult body size over
49 recent decades. Such observations in Chinook salmon (*O. tshawytscha*) have been documented
50 since the 1920s. Chinook salmon have displayed marked declines in size-at-age and declines in
51 the proportion of older, larger individuals, particularly females, in many populations across their
52 range in the eastern Pacific and watersheds from the Pacific Northwest to Alaska [1-12].

53 A number of likely factors affecting salmon body size over this time have been identified,
54 including marine environmental conditions, interactions with large numbers of hatchery salmon
55 in marine waters [13-15], adverse genetic and ecological interactions with hatchery salmon, and
56 the direct and indirect effects of fisheries that impose selection [8, 9,16-20]. While there have
57 undoubtedly been major changes in the marine ecosystems of the northeastern Pacific in which
58 Chinook populations rear for the majority of their lives, and many of these changes are likely to
59 adversely affect the marine growth of Chinook, such processes do not rule out a significant role
60 for fisheries induced demographic change and/or selection (FIS) (e.g., [18, 21, 22]).

61 Of particular relevance to ocean-type Chinook salmon populations originating in British
62 Columbia (BC) and the southern US (Washington, Oregon and California, including the lower
63 and middle Columbia River) are coastal mixed-stock fisheries that occur in territorial waters (3
64 nautical miles) of provincial and state coasts and in the Pacific Coast EEZs of Canada and the

65 US. These fisheries are managed pursuant to the Pacific Salmon Treaty (PST), and domestically
66 through the US Pacific Fisheries Management Council (PFMC) Salmon Plan and Canada's
67 Integrated Fisheries Management Planning (IFMP) process. The majority of ocean-type
68 Chinook (also called Fall Chinook [23, 24]) from these populations migrate north as sub-
69 yearlings to rear inside of the continental shelf in the coastal marine waters of BC and Southeast
70 Alaska (SEAK) before attaining their maturation size and age and migrating back to their natal
71 rivers. These immature Chinook are subject to harvest in marine troll and net fisheries conducted
72 in SEAK and BC that are managed under the Aggregate Abundance-Based Management
73 (AABM) regime of the PST. Hence, these coastal mixed-stock fisheries are also "mixed-
74 maturation (MM) marine fisheries." Fall Chinook bound for rivers in the southern US and BC
75 that escape the AABM fisheries are then subject to one or more state, tribal or provincial
76 fisheries managed pursuant to the PFMC or the IFMP Salmon Plans. As a result of this life-
77 history and migratory pattern, immature ocean-type Chinook are vulnerable to capture in coastal
78 mixed-stock fisheries at similar rates as mature individuals.

79 **Direct and indirect age overfishing**

80 Harvest of large numbers of immature salmon, i.e., individuals captured one or more
81 years before they have completed their marine growth and become mature adults, results in
82 indirect age-overfishing and consequent growth-overfishing (lowered productivity and yield per
83 recruit). Indirect age- and/or size-overfishing is a distinct phenomenon from direct age-
84 overfishing.

85 Direct age-overfishing occurs when older, typically larger individuals are targeted by harvesters
86 through gear selectivity and/or fishing at times or in areas where older, larger fish are known to

87 occur in numbers disproportionate to their abundance in the total harvestable population. This
88 directly reduces the proportion of older, larger fish in the remaining unharvested population,
89 especially the spawning population. This can also select for an earlier age at maturity either by
90 selecting on the growth rate or on the maturation size, or both. Indirect age- (and thus size-)
91 overfishing, by contrast, reduces the proportion and total abundance of older, larger adults in the
92 harvestable and the spawning population by removing individuals one or more years before they
93 are scheduled to mature when they are at smaller sizes.

94 Independent of ecological conditions in marine waters that may result in adverse growth
95 conditions, age- and growth-overfishing (direct or indirect) is a result of fishing mortality alone.
96 The effect of intensive and age- and size-selective harvesting on downsizing body size is well
97 documented in the fisheries literature [25-32], as life-history theory predicts that increased
98 mortality in older age and size classes generally favors earlier sexual maturation at smaller size
99 [27, 29, 33]. Indirect age over-fishing is less likely to occur in terminal (e.g., river) or near-
100 terminal (e.g., estuary) fisheries as all, or a majority of, Chinook present are returning mature
101 spawners, (although direct size over-fishing may still occur if the gear and/or the fishers
102 differentially select for larger fish [34]). Further, indirect age-overfishing is less likely than direct
103 age-overfishing to select for faster growth rates (and thus younger maturation age) because when
104 immature individuals are at sizes vulnerable to the fishing gear there is generally no benefit to
105 faster growth, as larger fish are likely to be equally or more vulnerable to fishing gear.

106 To date, the potential selective and demographic effects of age-overfishing in coastal mixed-
107 maturation Chinook fisheries have not been closely analyzed, though the potential for adverse
108 selective and/or demographic consequences has been acknowledged [2, 8, 18, 25, 35]. We
109 hypothesize that (indirect) age-overfishing in mixed maturation (MM) fisheries results in

110 changes in the demographics of affected Chinook populations, selecting for younger age-at-
111 maturity as a result of the reduction in fitness of immature Chinook genetically programmed to
112 mature at older ages. That is, genes that select for older ages at maturity are reduced in frequency
113 in the population as immature individuals are removed from the population. As a result of
114 adverse impacts on the fitness of older, larger Chinook, indirect age overfishing shifts the age
115 structure of the spawning population toward a younger mean age, with resultant reductions in
116 mean body size, thereby reducing catch biomass and the productivity of the spawning
117 population. Reductions in the proportion and size of older females in particular are likely to have
118 adverse consequences for population productivity, as fecundity is related to the length of female
119 Chinook salmon [6, 12, 36], as well as having adverse impacts on the value of the landed catch
120 (e.g. [37]). If correct, MM fisheries in general are likely to have adverse impacts on the
121 productivity and resilience of extant Chinook populations in comparison to terminal/near-
122 terminal fisheries. This affects the potential for recovery of depressed Chinook populations in
123 BC and the Southern US. In addition, such loss of productivity and resilience is likely to inhibit
124 future returns of harvestable Chinook populations to terminal and near-terminal areas that may
125 provide long-term, sustainable fisheries that support small-scale local fishing economies and
126 communities.

127 To investigate the potential of MM fisheries to effect harvest-induced change, we developed an
128 individual-based demographic-genetic model [21, 38, 39] based on the life-history of ocean-type
129 Chinook. We then applied the model to evaluate MM harvest of immature and maturing
130 individuals relative to a terminal fishery harvesting only mature adults. An individual-based
131 model simulates demographic and selected genetic processes of each individual in the
132 population, and is thus capable of considering individual variation in demographic and relevant

133 genetic characteristics within size- and/or age-classes. This approach is particularly valuable for
134 addressing issues related to fisheries induced demographic change and selection. To facilitate
135 informative modeling of different fishing gears— particularly troll and gill net fisheries – we
136 parameterized our model based on fork length.

137 Our primary focus is on the demographic effects of the various harvest regimes. In particular, we
138 are interested in changes in the age-and size-structure of the population due to the effects of
139 harvest mortality on the fitness of the phenotypes produced by the suite of available genotypes
140 that control daily growth rates and maturation lengths. To provide a clear focus on the
141 contrasting effects of MM and terminal fisheries, we conduct our harvest simulation on a single
142 population. Hence, we do not address the additional issues that surround the effects of harvest in
143 mixed stock marine fisheries.

144 We first describe the basic features of the model and then report on the results of six harvest
145 simulation scenarios, ranging from typical coastal MM Chinook fisheries to terminal fisheries.
146 We evaluate harvest impacts on size- and-age- of maturity of males and females, the proportions
147 of sex and age class in the annual adult return, the proportions of sex and age class on the
148 spawning grounds, and how this relates to reproductive potential. We refer to the model as an
149 “individual-based Chinook demographic-genetic model (IBCDM) for length-based ocean-type
150 life-history”.

151 **Methods**

152 **Development of the Individual-based Chinook Demographic-genetic**

153 **Model (IBCDM)**

154 **General model features**

155 Our model was derived in large part from the IBSEM model of [39] and parameterized to reflect
156 the life-history of ocean-type Chinook salmon. Juvenile ocean-type Chinook become smolts as
157 sub-yearlings, migrating seaward within several weeks or months of emerging from the
158 spawning gravel [23, 24, 40]. We also incorporated some of the model approaches developed by
159 [41] to evaluate fisheries selectivity of an in-river gillnet fishery for Yukon River Chinook. The
160 model was written in C++. For brevity, in the rest of this paper we refer to our model either as
161 IBCDM or simply as “the model”.

162 Our focus is on comparing mixed-maturation (MM) marine and terminal fisheries and not on
163 mixed-stock fisheries, *per se*. We therefore model a single population with an ocean-type life-
164 history and a size- and age-structure likely to be representative of a 19th century population prior
165 to the development of intensive coastal mixed-stock and MM fisheries. Most importantly, the
166 model population contains a higher proportion of older individuals (ages 5 and 6) than the
167 majority of ocean-type Chinook populations in the latter half of the 20th century and the first 2
168 decades of the 21st century. The model population is based on a combination of data for ocean-
169 type Chinook salmon from the Fraser River (BC) from the mid-1960s [42] and the Hanford
170 Reach Upriver Bright population in the middle Columbia River provided by [43], who analyzed
171 several data sources between 1920 and 1990. This data was used to build a model we believe is
172 generally representative of an ocean-type Chinook population that may have existed prior to
173 modern fisheries occurring in the Columbia River mainstem, Georgia Strait and the lower Fraser
174 River by the 1920s [3, 23]. Consequently, similar to [41], our model population is best viewed as
175 representing a generic historical ocean-type Chinook population. The model has the flexibility to

176 be parameterized with stock-specific data when that is of interest. For the objectives of this
177 paper, the generic model is appropriate.

178 The model population consists of the following stages: eggs, parr (post-emergent fry), smolts,
179 and post-smolts of ages 1 to 6 (Supplementary File S2, Table A). Males and females are modeled
180 separately. Males mature between the ages of 2 (ocean age 1) and the maximum age of 6 (ocean
181 age 5); females between the ages of 3 (ocean age 2) and 6 (ocean age 5). Spawning is modeled as
182 occurring on November 1 of each model year, and fry (called “parr”) are modeled as emerging
183 from the gravel and completing yolk absorption on May 1 of the following calendar year. All
184 parr are assumed to have a common size (weight and fork length) at the time of emergence.

185 Genetics control the probability of maturing at an adult size within length intervals reflective of
186 the growth trajectories of the majority of males and females at each possible age of maturity.

187 Size at maturity is greater than 350 millimeters (mm) fork length (FL) for males and greater than
188 520 mm for females. Genetic control is parameterized following the approach of [39] and [44].

189 The general features are described in the **Genetics** section below. Additional details are given in
190 Supplementary File S1.

191 Both growth and survival are modeled from the parr stage forward. Ricker-type density
192 dependence is included and applies to survival of newly emerged parr from May 1 to smolt at
193 July 1 (60 days) at which time smolts migrate to marine waters. Growth and density-independent
194 survival of smolts is calculated to November 1 of the year of migration (123 days) at which time
195 smolts are referred to as “age 1”, the age they will attain if they survive to their next birthday on
196 May 1 of the following calendar year. Growth and survival from the smolt stage forward is
197 modeled using the joint growth-and-mortality model of McGurk [45]. Parr are assumed to grow

198 in accordance with the growth rate component of the McGurk model but survival to the smolt
199 stage is subject to the size-independent Ricker density-dependent survival equation. From age-1
200 forward growth, survival, potential harvest and maturation occur at annual time steps. Harvest
201 occurs immediately prior to adult spawning. Ricker-type juvenile density dependence, and
202 growth and post-smolt density independent survival are described in Supplement File S1, A4.
203 We parameterized the model so that it results in an adult population with a Ricker spawner
204 recruit relationship with an alpha value of 5.24, a beta value of 604, and a deterministic
205 equilibrium adult population size of 1000 (Supplementary File S2, Table K). Fig 1 shows the
206 general life cycle of the population. The model life-stages and related parameters and values are
207 shown in Supplementary File S2 (Tables A, B, and C).

208

209 **Fig 1. Generalized life history of ocean-type Chinook salmon.**

210

211 **Model logic**

212 The model is initialized as a colonization process by a spawning population of 508 males ages 2
213 to 6, and 492 females ages 3 to 6. The proportions of ages in each sex are chosen to achieve a
214 target adult equilibrium population of approximately 1000 individuals, a sex ratio of
215 approximately 1:1 and target age/sex proportions. Since the model is length- and not age-based,
216 we refer to the initial spawning population by length-intervals associated with the dominant
217 maturation age within each interval (abbreviated L2, L3, etc.), as shown below in Fig 2. At
218 initialization these can be thought of as equal to the mean fork length in millimeters of the
219 maturation age of each sex, listed in Table 1 and Supplementary File S2, Table C.

220 **Table 1. Mean age-specific lengths and weights (standard deviation) of the ocean-type**
221 **Chinook model population pre 20th century.**

	Age 2	Age 3	Age 4	Age 5	Age 6
Mean Fork Length, mm (inches)	450 (18)	650 (26)	850 (33.5)	950 (37.4)	1050 (41.3)
Mean Weight, grams (lbs.)	1020 (2.25)	3283 (7.24)	7712 (17.0)	10984 (24.2)	15094 (33.3)

222

223

224 **Fig 2. Maturation lengths in mm at ages 2 to 6 from 10000 simulated random values drawn**
225 **from each of the five possible bivariate-normal distributions of daily growth rates and**
226 **maturation lengths. age groups L2 to L6 from left to right.**

227

228 Due to random growth of individuals and size-dependent density independent post-smolt
229 mortality (described in Supplement File S1, and **Post-smolt growth and survival** below), the
230 unfished equilibrium abundance will vary around the target of 500 male and 500 female
231 spawners, but will rarely be exactly these values. We evaluated the time it takes to attain a
232 stochastic equilibrium by running the model without harvest for 1000 time-steps (years) and
233 examining the distributions of spawner sexes and ages at several 25-year (approximately 6
234 generation) intervals and at the final year of each 25-year period. We determined that the model
235 achieves its stochastic equilibrium by year 100. Data for a 1000-year non-harvest simulation is
236 provided in Supplement File S4.

237 In the simulations reported below, we run the model for 100 years without harvest, allowing the
238 population to achieve a stochastic equilibrium following the initial colonization. We then run the
239 selected harvest scenarios for 25 years, followed by 25 years of no harvest. We chose 25 years
240 for the harvest period as a reasonable length of time for harvest to impact the demographics of
241 the population in a time frame relevant to short-term management interests, but short enough that
242 fisheries-induced evolution is not likely to occur. Similarly, we chose 25 years for the post-
243 harvest evaluation period as a time frame relevant to a management evaluation of the ability of
244 the harvested population to respond demographically to the cessation of harvest, assuming that
245 no fishery- induced selection occurs during the harvest period. This provides a realistic measure
246 of the demographic impact of the 25-year harvest regime on the population and the population's
247 ability to recover from those impacts.

248 **Genetics**

249 Individuals are diploid. Daily growth rate and maturation size (weight) is defined by a single set
250 of 20 genes. Length is determined from weight following an allometric length-weight equation
251 ($L = aW^b$). For computational efficiency sex is randomly assigned at the smolt stage with an
252 equal (mean) sex ratio. Individuals inherit a maternal and a paternal allele at each locus.

253 We follow [39] in employing an additive quantitative genetics model. The genotypic effect
254 (breeding value) is determined using a simple additive model with exponentially declining
255 weights, such that there are a small number of genes (loci) which have relatively large effect on
256 daily growth rate and size-at-maturity, and the remaining genes having exponentially smaller
257 influence as shown in Supplement File S1, Table A and Fig A.

258

259 Maturation age and size (weight, WMat) are determined by quantitative genetic parameters
260 controlling the daily growth rate in weight and the weight- (and hence length-) at-maturity
261 assigned to offspring. Maturation is determined by the “total allelic (genotypic) value” measured
262 across the 20 bi-allelic (0, 1) loci, which is equal to the individual’s breeding value. Each
263 fertilized egg inherits one allele (0 or 1) with equal probability from each parent at each of the 20
264 loci, by successively choosing at random one parental allele from each locus using a uniform
265 distribution on [0,1]. Following [39] the “allelic value” of each locus is determined by
266 multiplying the genotypic value of each locus (0, 0.5, or 1) by a locus-specific weight. The
267 weights decline exponentially from a maximum value at locus 1 to a minimum at locus 20.
268 (Supplement File S1, Table A and Fig A.) The sum of all weighted allelic values (the sum of “1”
269 alleles weighted by the locus-specific weight of influence, [46]) constitutes the “total allelic
270 value” of an individual’s genotype. Following [39], we name this total genetic value S^ϕ (S^ϕ).
271 The values of S^ϕ range from a minimum of 0 (when all 20 loci are homozygous for the “0”
272 allele) to a maximum of 1 (when all 20 loci are homozygous for the “1” allele).

273 Each S^ϕ value within a specified range (e.g., >0.2 and ≤ 0.4) then determines the probability of
274 an individual maturing at one of three length intervals by virtue of inheriting a daily growth rate
275 (GR) in weight (g/g body weight) and a target maturation weight (WMat) and length (LMat)
276 from a bivariate normal distribution with mean growth rate (GR_x) and mean maturation weight
277 (W_xMat). Maturation weight is then converted to maturation length (L_xMat) via the
278 deterministic allometric length-weight equation (Supplemental File S2, equation 1.2). L_xMat is
279 equal to the maturation length that an individual with mean growth rate GR_x would attain at age
280 x , for $x = 2$ to 6 for males and 3 to 6 for females. Thus, we model the genetic determination of
281 the mean GR and WMat values assigned to offspring as canalized as an evolutionary response to

282 the environmental variability experienced by the founder population during its evolutionary
283 history. This constitutes a form of “diversification bet-hedging” against unpredictable
284 environmental variability that can fundamentally affect the fitness of different maturation ages
285 [47-51].

286 Additionally, when desired, phenotypic plasticity in growth rate and target maturation weight
287 and length can be allowed to occur based on stochasticity in individual daily growth and annual
288 survival rates that may be experienced in the post-smolt marine environment. This feature is
289 described in the Supplement File S1, **Incorporating environmental stochasticity in**
290 **maturation weight and length.**

291 After mating and spawning occur, parr emerge, undergo density-dependent survival to the smolt
292 stage and sex is assigned to each smolt, daily growth rate, maturation weight, and length is
293 determined according to each individual’s total allelic value as described above and in
294 Supplement File S1, Section A2.

295

296 **Spawning and mating**

297 The mean fecundity of a female (mf) is determined by its fork length [36] based on the Pearson
298 equation used by [41]. The actual number of eggs is determined from a normal distribution with
299 mean mf and a standard deviation (mfsd) chosen to achieve an appropriate random variation in
300 fecundity at each female age.

301 Mating is modeled as size-selective following the approach of [41]. Each female spawner is
302 chosen at random, then a male is chosen at random. whether or not the male “proposes” to the

303 female is determined based on the relative (fork) lengths of each individual. If the female
304 “accepts” the male’s proposal mating occurs and each of the females’ eggs receives one allele
305 from each parent at each of the 20 loci that determine the offspring’s probability of maturing
306 within a specific length-interval Once mating occurs, the female is removed from the class of
307 potential mates and placed in the spawner population. Males remain in the candidate pool and
308 may mate with one or more other females. The equations for fecundity and mate choice are
309 described in Supplement File S1, Section A1 and parameter values are listed in Supplementary
310 File S2, Tables H and I.

311

312 **Egg development and parr emergence**

313 All fertilized eggs are assumed to be the same size and survive to become parr (post-emergent
314 fry) on May 1 according to a random binomial survival probability, $segg$. Surviving parr are
315 assigned a common fork length of 37 mm and weight of 0.3545 grams. The value of $segg$ is
316 listed in Supplementary File S2, Table J.

317

318 **Parr-to-smolt growth and survival**

319 Parr survive to become smolts on July 1 according to a Ricker density-dependent function and
320 grow according to the growth component of the McGurk equation, as described in the following
321 section and Supplementary File S1, A5. Parameter values are given in Supplementary File S2,
322 Tables K and L.

323

324 **Post-smolt growth and survival**

325 Smolts and sub-adults up to the age/length of maturity grow and survive according to the
326 McGurk integrated growth-and-survival model [45]. The equations of the McGurk model are
327 derived from the allometries of growth and mortality. The growth coefficient is the value of GR
328 assigned on the basis of the individual's maturation genotype (S^ϕ) that determines which
329 bivariate normal distribution of growth rate (GR) and target maturation length (LMat) the
330 individual inherits (described in Supplement Files S1, **Logic and governing equations for**
331 **genetic assignment of growth and length**). Details of the McGurk model are provided in
332 Supplementary File S1, A5, and parameter values are listed in Supplementary File S2, Table L.
333 Daily growth rates and maturation lengths are assigned such that individuals genetically
334 programmed to mature at smaller sizes and younger ages have higher growth rates than
335 individuals programmed to mature at longer lengths (and greater weights) and generally older
336 ages. This is expected for most semelparous anadromous salmon [24, 57]. Analysis of 1000
337 simulated values of each of the five GR/WMat BVNs demonstrate that the parameterization of
338 these distributions produce the expected negative correlation between maturation age and length
339 on the one hand and daily growth rate on the other (Table 2).

340 **Table 2. Correlation coefficients between maturation length-at-age and daily growth rate of**
341 **each mature age class and of the entire set of age classes combined from 1000 simulated**
342 **values of GR and LMat for each age-/length-at-maturation class (L2 to L6).**

Age-/length class:	Corr(Lmat, GR):
All	-0.901

L2	0.899
L3	0.902
L4	0.894
L5	0.906
L6	0.907

343

344 The McGurk integrated growth and mortality model generates stage-to-stage survival rates that
345 incorporate the effects of both size and rate of growth between life-history stages. The
346 integration of the two effects quantifies the trade-off between 1) reducing future predation risk
347 by rapid growth in the near term in order to obtain a larger size and 2) increasing the mortality
348 risk in the short run due to faster growth that increases predation risk and possible metabolic
349 risks due to reduced tissue maintenance. All else being equal, individuals of a given size that
350 grow relatively fast incur greater mortality rates than same size individuals that grow slower;
351 and, conversely, individuals of small size foraging at a given rate incur greater mortality rates
352 than larger individuals that forage at the same rate in the same or similar environment.

353

354 **Harvest, maturation and spawning**

355 Harvest is modeled to occur annually immediately prior to spawning November 1. Harvest of
356 each vulnerable individual is modeled randomly based on a global exploitation rate (hg) that
357 applies equally to all vulnerable individuals. The global exploitation rate may be modified for
358 each of 5 contiguous length intervals of mature individuals and each of 4 contiguous length
359 intervals of immature individuals. The intervals may be chosen to correspond to the range of

360 lengths of the majority of each age at maturity (2 to 6) and each age of immature individuals (2
361 to 5), or be otherwise chosen for length intervals for which different harvest rates are applied.
362 For each interval, the target harvest rate is determined by multiplying the global exploitation rate
363 by a user-chosen length-interval state variable v between 0 and 1 to yield the actual harvest rate
364 $h_a (= h_g * v)$ to which individuals in the specific length-intervals are vulnerable. This provides the
365 flexibility to model harvest scenarios with different length interval and maturation status-specific
366 harvest vulnerabilities, which in turn allows modeling of different harvest management regimes
367 and gear selectivity. Specifically, terminal fishery scenarios are modeled only on mature adults,
368 with harvest vulnerabilities of immatures of all length intervals set equal to 0. Mixed-maturation
369 fishery scenarios can explore a range of vulnerabilities of both mature and immature individuals,
370 including minimum length thresholds and drop-off and non-retention mortalities of sub-legal size
371 matures and immatures.

372 Mature individuals that survive harvest move to the mating/spawning population at the end of
373 each annual time-step. Unharvested immatures undergo growth and survival to the next time
374 step.

375

376 **Model initialization**

377 **The unfished equilibrium population**

378 The model is initialized with a mix of mature individuals of various ages and sexes in their target
379 equilibrium proportions, numbering 1000 in total. For both sexes, the mean lengths of each age
380 are shown in Table 1. These initial abundances and the proportions of both sexes combined are

381 listed in Supplementary File S2 (B.6, Tables O, P, and Q). Individuals in each age-/length- class
382 are initialized with distinct age-/length-specific mean alleles frequencies at the 20 loci
383 controlling the maturation probabilities. Supplementary File S3 provides additional information.

384 **Heritability of maturation age and length**

385 Heritabilities for life-history traits are known to be smaller than heritabilities for morphological
386 and behavioral traits [16, 58, 59]. This is consistent with the expectation that selection should
387 deplete standing genetic variation in fitness [60, 61]. It is also expected from the bet-hedging
388 parameterization of the genetic control of daily growth rates and size at maturity. We estimated
389 heritabilities of smolts and recruited adult spawners of the same cohort for length- and age-at-
390 maturation, and daily growth rate (GR). Estimates were made separately for each sex and for
391 both sexes combined using mid-parent/offspring regression. Heritabilities were reasonably low,
392 ranging from 0.07 to 0.20 (Supplementary File S2, Table R).

394 **Harvest scenarios**

395 The model provides for the ability to model harvest with either a minimum threshold length
396 limit, as appropriate to a troll fishery, or a fishery with both a lower and an upper size limit, as
397 may occur in a gillnet fishery. To provide a robust evaluation of the impact to Chinook
398 demographics from both troll and gillnet harvest in terminal and mixed-maturation fisheries, we
399 evaluate 6 harvest scenarios that explore the main features of these 2 kinds of harvest regimes.
400 All scenarios were run with the same seed for the random number generator and initiated with
401 100 years of no harvest (pre-fishery scenario), to attain the adult equilibrium spawner abundance

402 and age/sex composition. This was followed by 25 years of harvest with a constant global
403 harvest rate, hg , and a set of vulnerabilities to the global rate, v , of matures and immatures in
404 each maturation length interval ranging from $v = 0$ for completely invulnerable to $v = 1.0$ for
405 fully vulnerable. This yielded one or more length-interval and maturation-state-specific harvest
406 rates $h_a (=hg*v)$. Catch of individuals vulnerable to harvest was modeled in all scenarios by
407 drawing a uniform random number, u , on $[0, 1]$ and considering an individual caught if u is less
408 than or equal the value of h_a to which the individual is vulnerable.

409 The 6 scenarios consist of 3 basic troll fishery scenarios (H1, H3, and H5) and 3 similar basic
410 gillnet fishery scenarios (H2, H4, and H6). The 3 types of fisheries modeled for both troll and
411 gillnet scenarios are, in order: 1) a terminal fishery harvesting matures at a global harvest rate
412 (hg) that achieves maximum sustained yield in the total weight of the catch (scenarios H1 and
413 H2); 2) a mixed maturation fishery harvesting immature and mature Chinook at a global harvest
414 rate (hg) that achieves maximum sustained yield in the total weight of the catch (scenarios H3
415 and H4); and, 3) a terminal fishery harvesting matures at a global harvest rate that approximates
416 the total weight of the MSY catch of the corresponding MM scenario (scenarios H5 and H6). We
417 refer to this latter harvest rate and corresponding harvest scenario as the “mixed-maturation-
418 MSY-catch-weight-equivalent (MMCWE)”. For scenarios H1 to H4, the approximate global
419 MSY harvest rate (hg) was estimated by trial-and-error by running each 150-year simulation
420 with the global harvest rate (applied in years 101 to 125) set to several different values over
421 intervals of 0.05 (e.g., 0.60, 0.65, 0.70) and choosing as the global MSY harvest rate (H_{msy}) the
422 value of hg that generated the largest total weight of the catch. In the case of scenarios H5 (troll
423 MMCWE) and H6 (gillnet MMCWE), the global harvest rate was further refined at intervals less

424 than 0.05 as necessary to achieve a close approximation to the corresponding MM scenario total
425 catch weight.

426 Scenarios H1 to H6 were first run with no post-smolt environmental variation, simulating the
427 average environmental conditions affecting density-independent growth and survival. We then
428 ran each scenario with environmental variation affecting daily growth rates and annual survival
429 rates. Details are described in Supplementary File S1, A7 and A8. Parameter values are
430 described in Supplementary File S2, B5.

431 The features of each of the 6 scenarios are listed in Table 3. For terminal fishery scenarios,
432 vulnerabilities (v) of all immatures were set equal to 0, and all matures were set to 1.0. For
433 mixed-maturation fishery scenarios, v of all matures and immatures were set equal to 1.0. We
434 provide further details in the Discussion.

435

436 **Table 3. Harvest scenarios H1 through H6 with their global harvest rates and**
437 **vulnerabilities of immature fish. hg is the global harvest rate; v is the length range-specific**
438 **modifier of the global harvest rate applied to immature and mature fish. The actual**
439 **harvest rate for individuals in length ranges for which v is less than 1.0, ha , is equal to**
440 **$hg*v$.**

441

Scenario	Type	Gear Type	hg	Immature Vulnerability (v)
H1	Terminal MSY	Troll	0.65	0.0

H2	Terminal MSY	Gillnet	0.70	0.0
H3	Mixed-maturation MSY	Troll	0.45	1.0
H4	Mixed-maturation MSY	Gillnet	0.50	1.0
H5	Terminal MMCWE	Troll	0.42 5	0.0
H6	Terminal MMCWE	Gillnet	0.44	0.0

442 Global harvest rates (hg) in scenarios 1, 2, 3, and 4 are estimates of the MSY harvest rate. Global
 443 harvest rates in scenarios 5 and 6 are estimates of the harvest rate in terminal fisheries that
 444 produce approximately the same total catch weight (mixed-maturation-MSY-catch-weight-
 445 equivalent/ MMCWE) as the corresponding mixed-stock MSY fishery (scenarios H3 and H4,
 446 respectively).

447
 448 Since we model harvest as occurring immediately before unharvested fish spawn, annual natural
 449 mortality during the final year of life of mature fish implicitly includes natural mortality incurred
 450 during spawning migration that occurs after passing the fishery. We consider this to be a
 451 reasonable simplification and discuss it further in the Discussion.

452
 453 **Fishery scenario H1. Terminal MSY troll fishery harvest on mature adults**

454 Harvest scenario H1 simulates a terminal fishery harvesting mature adults equal to or greater
 455 than 610 mm (~24 inches) fork length at a global harvest rate (hg) that achieves maximum

456 sustainable yield (MSY) in total weight of the catch. This excluded harvest of most age 2 mature
457 males (mean fork length 450 mm (Table 1, Fig 2) plus 3 standard deviations for CV length =
458 $0.09 * \text{mean}$: 572 mm. This established a baseline against which to compare MM fishery scenarios
459 involving harvest of mature and immature Chinook.

460 We chose 24 inches (610 mm) as the minimum fork length, as this is the size limit for the tribal
461 treaty troll fishery off the northwest Washington Coast [63]. We feel it provides a reasonable,
462 and likely conservative, estimate of the minimum fork length of Chinook vulnerable to capture
463 by troll gear in the early years of mixed stock coastal troll fisheries to which our model
464 population would have been vulnerable.

465

466 **Fishery scenario H2. Terminal MSY gillnet fishery harvest on mature adults**

467 Harvest scenario H2 is the gillnet counterpart to scenario H1. H2 simulates a terminal fishery
468 harvesting mature adults at the global harvest rate (hg) within the length interval [783 mm, 1158
469 mm], and at $h_a = 0.1 * h_g$ at lengths below 783 mm and $h_a = 0.4 * h_g$ at lengths above 1158 mm.

470 The MSY harvest rate is estimated by trial and error by simulating the harvest scenario at several
471 different values of hg at intervals of 0.05, starting at 0.60 as for scenario H1. For further details,
472 see the section **parameterization of gillnet scenarios** below and Supplementary Files S1, A9,
473 and S2, B8.

474

475 **Fishery scenario H3. Mixed maturation MSY troll fishery**

476 Harvest scenario H3 simulates a mixed maturation troll fishery on mature and immature Chinook
477 with a minimum fork length of 610 mm (vulnerability of age 3 and older = 1.0). Individuals aged
478 3 to 6 of both sexes greater than 610 mm FL were fully vulnerable to the gear regardless of
479 maturation state. This would result in only a small proportion of age 3 immatures and matures
480 not being vulnerable to the fishery, essentially simulating a troll fishery with a minimum size
481 limit of 610 mm FL. We also assumed that the 610 mm cut-off was perfect (knife-edge), in the
482 sense that there was no by-catch of sub-legal fish. Thus, in effect, we model fisheries with gears
483 that are perfectly selective for fish equal to or greater than the minimum size limit. The global
484 harvest rate was set by trial and error to determine the rate that achieved the MSY harvest when
485 age 3 to 5 immatures \geq 610 mm FL are equally as vulnerable to the gear as mature (age 3 to 6)
486 individuals.

487

488 **Fishery scenario H4. Mixed maturation MSY gillnet fishery**

489 Similar to scenario H3, this scenario searched for a value of hg that achieved the greatest total
490 catch weight in a gillnet fishery in which both mature and immature Chinook were vulnerable to
491 a gillnet as parameterized in scenario H2.

492

493 **Fishery scenario H5. Terminal mixed maturation catch weight equivalent** 494 **(MMCWE) troll fishery**

495 This scenario searched for a global harvest rate (hg) that achieved a total catch weight
496 approximately equal to that of the mixed maturation MSY troll fishery (H3), but in a terminal

497 fishery in which only matures are harvested. This consideration provides the harvest rate that
498 would be required of a terminal fishery replacing a MM fishery, but achieving the same average
499 annual total catch weight. This scenario is identical to scenario H1 except that the global harvest
500 rate was set by trial and error to achieve approximately the same total annual catch weight as
501 scenario H3, (“catch-equivalent MSY harvest rate”).

502

503 **Fishery scenario H6. Terminal mixed-maturation - catch weight equivalent**
504 **(MMCWE) gillnet fishery**

505 Similar to scenario H5 but for a terminal gillnet fishery, this scenario searched for a global
506 harvest rate (hg) that closely approximated the total MSY catch weight achieved in the MM
507 gillnet scenario H4.

508

509 **Parameterization of gillnet fishery scenarios.**

510 Gillnets generally harvest individuals with fork lengths between a lower and upper size limit, at
511 or near the global harvest rate. Individuals with lengths below the lower and above the upper
512 limits are harvested at rates below the global rate due to lower vulnerabilities to the gillnet mesh
513 (lower selectivities). In addition, gillnets generally impose different selectivities on lengths
514 within the interval of greatest vulnerability, with the greatest selectivity (catchability) on
515 intermediate lengths. Catchability generally drops abruptly below the lower length limit and
516 more gradually above the upper limit. Below the lower length threshold catchability declines
517 abruptly as smaller fish can swim through the mesh and are entangled less frequently than fish

518 above the upper threshold. Above the upper length threshold, catchability gradually levels off
519 above zero, because larger fish can still be caught from entanglement of the fins or operculum.
520 Supplementary File S1, A9, Fig B shows a gillnet selectivity curve for the standard 8-inch mesh
521 commonly used for Chinook. This curve was based on a Pearson function applied to an extensive
522 data set for Yukon River Chinook salmon analyzed by [62].

523 We modeled gillnet catchability with an approach that is a compromise between using an explicit
524 function like Pearson that assumes a selectivity of 0.0, and the lower and upper length threshold
525 within which selectivity is 1.0 (e.g., [34]). Based upon the selectivity curve of our
526 parameterization of the Pearson function of [62], we chose the interval [783, 1158 mm FL] as the
527 length interval in which vulnerability was equal to 1.0. Selectivity on lengths below 783 FL was
528 set to 0.10, and selectivity on lengths greater than 1158 were set to 0.40. (See Supplementary
529 Files S1, A9 and S2, B8 for further details).

530

531 **Results**

532 We describe and compare the results of the troll and gillnet harvest scenarios under no
533 environmental variation for each of the three types of harvest scenarios.

534 To consider environmental variation, we repeated the above harvest scenarios (H1 to H6) adding
535 bivariate normal random variation to the daily growth (GR) and annual survival (S) rates of
536 smolts and post-smolts age 1 to 5 (as described in Supplement File S1, A8). None of these
537 additional harvest scenarios produced results that differed substantially from the 6 primary

538 scenarios in regard to the magnitude or direction of the differences between mixed maturation
539 and terminal harvests. Consequently, we do not report them.

540 We provide graphical summaries that highlight specific impacts of each scenario on population
541 life history, and summarize the results of each harvest scenario. Data tables of the primary results
542 are provided in Supplementary File S4 and S5 Table.

543

544 **Comparisons of mixed maturation to terminal harvest scenarios**

545

546 There are clear differences between the terminal and MM scenarios for both gear types in regard
547 to the average weight of the catch, the age composition of the returning adult and spawner
548 populations, (Figs 3 and 4) and in the mean age composition of the catch and spawner
549 populations (Figs 5 and 6). In each case, MM fisheries shift the age composition of both sexes
550 toward younger ages and smaller average catch weights (Fig 3).

551

552

553 **Fig 3. Mean number of total spawner and harvested numbers and weights, and average**
554 **weights, for all 6 harvest scenarios for the harvest and post-harvest periods (simulation**
555 **years 101 – 125 and 126 – 150, respectively). X axis labels: H1: Terminal troll; H2:**
556 **Terminal gillnet; H3: Mixed maturation troll; H4: Mixed maturation gillnet; H5: Terminal**
557 **mixed maturation catch equivalent troll; H6: Terminal mixed maturation catch equivalent**
558 **gillnet. We do not show standard errors as they are very low for all groups, ranging from a**

559 **maximum of 0.068 for terminal harvest scenario H1 and a minimum of 0.002 for pre-**
560 **terminal spawner weight.**

561
562 **Fig 4. Time series of number of spawners by age and sex for simulation years 75 to 150 for**
563 **all 6 harvest scenarios. Harvest period shaded in grey.**

564
565 **Fig 5. Average spawner weights for each harvest scenario. Harvest period shaded in grey.**

566
567 **Fig 6. Average age of spawners and harvested Chinook for each sex for simulation years**
568 **75 to 150 for all six harvest scenarios.**

569
570 In addition, the total weight of the catch at MSY in MM fisheries is 30% to 35% lower than in
571 terminal MSY fisheries for both gear types (Fig 3). MM fisheries of both gear types significantly
572 decrease the proportions of the 2 oldest age classes relative to the terminal fishery (Figs 4 and 7;
573 Supplement File S4, Table C). MM fisheries also decrease the average weight of the spawning
574 population (Fig 5), and thereby impair the ability of the harvested population to recover in the
575 direction of the pre-fishery age composition compared to the terminal scenarios (Figs 4 and 5;
576 Supplement Files S4, Table D). This is primarily due to the legacy of the harvest of immature
577 individuals in the MM fisheries.

578

579

580 **Fig 7. Age-specific proportions of total egg deposition vs. age proportions of spawners by**
581 **harvest scenario.**

582

583 Importantly, over the 25-year harvest period the 2 terminal MSY scenarios (H1 and H2) achieve
584 considerably greater total and average harvest weights than the MM MSY scenarios (Figs 3 and
585 8; Supplement File S4, Table A).

586

587 **Fig 8. Total weight of harvest for all 25 years for each sex in all six harvest scenarios.**

588

589 With respect to the sustainability of the fishery regimes, the terminal catch-equivalent MM
590 fisheries (H5 and H6) achieve the target total catch weights of the MM MSY scenarios with
591 fewer and larger fish than the corresponding MM MSY fisheries. Additionally, they do so with a
592 spawning population that has a larger average size, weight, and age than the mixed-stock
593 fisheries (Figs 3, 5 and 6).

594

595 **Troll scenarios versus gillnet scenarios**

596 There are biologically meaningful differences in average spawner and catch weights between the
597 2 gear types in each of the three types of fishery scenarios. In the terminal MSY troll fishery
598 scenarios (H1), the average weight of spawners during the harvest period is one-half lb smaller
599 than the pre-harvest average (17.8 versus 18.3). In the terminal MSY gillnet scenario (H2), the

600 average weight of spawners during the harvest period is a full five lb smaller than the pre-harvest
601 average (13.3 versus 18.3; Figs 3 and 5). Comparing between fisheries, the average size of
602 harvested fish in the terminal MSY gillnet fishery is more than 2 lb greater than in the
603 corresponding troll fishery (21.0 lb versus 18.7 lb; Figs 3 and 5).

604 In the mixed-maturation MSY scenarios (H3 and H4), both total and average catch weights of
605 each gear type are significantly below their terminal fishery counterparts (Fig 3). However, there
606 are some interesting differences between the 2 gear types. In the mixed-maturation troll scenario,
607 the total number of fish caught is greater than in the gillnet scenario (728 versus 564; Figs 3 and
608 9), but the average weight of the catch is smaller (12.0 versus 14.5 lb; Fig 3). This is due to the
609 greater selectivity of the gillnet for larger, older fish than the troll scenario, which captures more
610 younger-age, immature fish. Correspondingly, there are more spawners in the gillnet scenario
611 (603 versus 403), but average spawner weights are similar (14.5 versus 14.3, respectively; Fig
612 3). This is due to the troll fishery catching more fish across the size range, including more
613 immatures, than the gillnet (432 weighing an average of 9.5 lb versus 226 weighing an average
614 of 5.3 lb, respectively (Fig 9)). This leaves fewer spawners on average than the gillnet fishery
615 (Fig 4). In both cases, the average spawner weights are 4 lb smaller than the pre-harvest average.

616

617 **Fig 9. Total number and weight of Chinook of each sex harvested in the mixed maturation**
618 **troll and gillnet fishery scenarios.**

619

620 In the MMCWE fishery scenarios (H5 and H6), the terminal troll scenario achieves an average
621 spawner weight of 18.5 lb, compared to the pre-harvest average of 18.3, and an average catch

622 weight of 18.5 lb, which is similar to the average catch weight of the terminal MSY troll
623 scenario. Total number of spawners is nearly 300 more than in the terminal MSY fishery and
624 more than 200 than the MM troll scenario. The gillnet scenario achieves an average weight of
625 spawners of 16.3 lb, and an average catch weight of 21.3 lb, and 100 more total spawners (750)
626 than the troll scenario (Fig 3; Supplement File S4, Table A).

627 The mean age of spawners in the MMCWE troll scenario is slightly, though not significantly,
628 greater than in the terminal MSY troll scenario and the mean spawner weights in each period are
629 equal to or slightly greater than the pre-harvest means (Fig 3). In the MMCWE gillnet scenario,
630 the mean ages in the harvest and post-harvest periods are lower, but close to the values in the
631 terminal MSY troll scenario (Fig 6), while the mean weight of spawners in these two periods are
632 1 to 2 lb smaller than in the two terminal troll scenarios (Fig 3; Supplement File S4, Table D).

633

634 **Harvest impacts to egg deposition**

635 Harvest impacts are also reflected in the total and age-specific egg deposition and in the
636 proportional contribution of female spawners of each age. For all 6 harvest scenarios, we provide
637 summary data for the proportion of total egg deposition contributed by female spawners of each
638 age (3 to 6) relative to the proportion of each female age in the total female spawner population.
639 Fig 10 shows the total egg deposition for simulation years 75 to 150 for all six harvest simulation
640 scenarios. data is provided in tabular form in Supplementary File S4, Tables E and F.

641

642

643 **Fig 10. Age-specific total spawner egg deposition by harvest scenario for simulation years**
644 **75 to 150.**

645

646 The reference terminal harvest scenarios (H1 and H2) reveal clear differences in the impact on
647 the age structure of the spawning population between the troll and gillnet. The age composition
648 in the terminal troll scenario is noticeably less skewed toward younger ages (3 and 4) relative to
649 the pre-harvest period, and compared to the terminal gillnet scenario (Fig 10; Supplement File
650 S4, Table C).

651 An illustrative comparison of the impact of each scenario on the structure of the spawning
652 population is the proportion of age 3-to-6-year-old spawners and the proportion of total egg
653 deposition contributed by each. In the gillnet scenario (H2), the proportion of age 3 female
654 spawners increases and the proportion of age 4, 5, and 6 female spawners decreases relative to
655 the pre-harvest period. This change is mirrored by the proportion of total egg deposition
656 contributed by age 4 and 5 spawners, but less so in the case of age 6 spawners (Fig 10, middle
657 panel; Supplement File S4, Table C). During the pre-harvest period, age three females comprise
658 15% to 25% of the spawning population but contribute less than 18 percent of the total egg
659 deposition. During the harvest period, the proportion of age three females in the spawning
660 population rises above 40% and contribute 30% to 40% of the total egg deposition. Both
661 numerically and in terms of contribution to total egg deposition, the gillnet harvest renders the
662 population during the harvest period more dependent on age 3 spawners, which likely have lower
663 overall fitness measured as recruits-per-spawner than the 3 older ages. During the post-harvest
664 recovery period, age 5 spawners increase significantly in both proportions relative to the pre-

665 harvest period, age 3 and 4 spawners recover to near their pre-harvest levels, but age 6 spawners
666 fall below pre-harvest levels and thus fail to rebuild during the 25-year period.

667 In contrast, there is little significant change in either proportion of the 4 age classes in the
668 terminal troll scenario (H1). Thus, harvest across the entire size range (fork length) of mature
669 adults vulnerable to the troll gear has little impact on either the proportion of each age class in
670 the total spawning population, or in the proportional contribution to egg deposition relative to the
671 pre-harvest period. Consequently, there is little disruption of spawning age structure, and less
672 correction during the 25-year recovery period.

673 In the mixed maturation fishery scenarios, the situations are similar between the 2 gear types (H3
674 and H4) (Fig 10; Supplement File S4, Table C). Both scenarios result in a marked reduction in
675 the proportion of age 5 and 6 female spawners and corresponding increases in the proportion of
676 ages 3 and 4 female spawners, relative to the pre-harvest proportions. Pre-harvest, ages 5 and 6
677 combined make up 51% of total spawners and ages 3 and 4 combined 49%. In the mixed
678 maturation troll harvest period, ages 5 and 6 combined represent 40% and ages 3 and 4 60% of
679 total spawners. In the mixed maturation gillnet harvest period, ages 5 and 6 represent 37% and
680 ages 3 and 4 63% of total spawners (Fig 10; Supplement File S4, Table C). Both gear types
681 effect similar reductions in the proportional contribution to total egg deposition of age 6
682 spawners, similar increases in the proportional contribution of age 3 spawners, and little
683 alternation in the proportional contributions of ages 4 and 5 spawners (Fig 10). There is little
684 difference between the 2 scenarios during the post-harvest recovery period. In both scenarios,
685 age 6 females lag behind the pre-harvest proportions. The 3 younger age classes recover to near
686 pre-harvest period levels, though there are some slight differences between the 2 gear types.

687 Age composition of the spawning population in the 2 terminal catch weight equivalent harvest
688 scenarios (H5 and H6) shows considerably less alternation from the pre-harvest age structure,
689 than the corresponding mixed-maturation scenarios. However, the MMCWE gillnet scenario
690 produces an increase in the proportion of age 3 spawners that does not occur in the
691 corresponding troll scenario. The troll scenario (H5) retains the pre-harvest average proportions
692 of ages 5 and 6 in the total spawning population (0.522 versus 0.518. The average proportions of
693 age 5 and 6 spawners in the MMCWE gillnet scenario is 0.452 (Fig 10; Supplement File S4,
694 Table C), an improvement over the average in the mixed maturation scenario (H4) of 0.372, but
695 still below the pre -fishery average. However, both scenarios permit a recovery to at (troll) or
696 near (gillnet) the pre-fishery spawner age proportions over the 25-year post-harvest period
697 (Supplement File S4, Table C).

698

699 To provide further perspective for evaluating the impacts of the harvest scenarios on age-specific
700 spawner contributions to population growth, we calculated the reproductive values of female
701 spawners (ages 3 to 6) for a representative average deterministic population projection matrix.
702 For interested readers further details are provided in Supplement File S1, section A6.

703

704 **Discussion**

705 **Size- versus age-overfishing**

706 Our results show that in mixed maturation fisheries (where mature and immature individuals
707 attain lengths that render them equally vulnerable to the fishing gear), mortality in MSY harvests
708 imposes biological effects that are likely to compromise a population's resilience and adversely
709 affect potential yield. These effects are primarily demographic in the short-term extending one to
710 several generations, the period of time over which we conducted our simulations. Biological
711 effects occur from shifting the population's size structure toward smaller lengths at maturity (i.e.,
712 size-overfishing) and, consequently, a younger adult age structure (Figs 3, 4, 5, 6, 10;
713 Supplement File S4, Table C). These shifts occur independent of and in addition to, any potential
714 genetic effect due to selection on growth or maturation rates. The shift toward a younger age
715 structure is, therefore, an indirect effect of size selection. Note that the shift to smaller sizes is
716 not a result of selection on size-at-age, since our model does not allow the genotype-specific
717 maturation probabilities to evolve in response to selection on age or size. Rather, the shift to
718 smaller size is simply the result of selection on the fitness of growth rates and lengths-at-maturity
719 that result from the size selection of the fishing regime; it is fundamentally a demographic effect.

720 Thus, our model results in this respect are conservative. We expect that if selection on the
721 genotype-specific maturation probabilities (daily growth rate and maturation weight/length) were
722 incorporated into our model (via no or a reduced degree of diversified bet-hedging), selection
723 toward smaller sizes and hence younger ages, would increase the shift in the directions observed.

724 For example, if heritabilities for growth rate and size-at-maturity were higher, such that age x
725 parents had a very high (e.g., >0.75) probability of producing offspring with growth rates and
726 size-at-maturity identical to their own, and if size-assortative mating were much stronger than
727 our current parameterization, older-aged/larger-size adults would have a very low (perhaps zero)
728 probability of producing offspring with higher growth rates and smaller size-/younger age-at-

729 maturity. Younger/smaller-size adults would have similarly low probabilities of producing
730 offspring with lower growth rate and larger size- older age-at-maturity. Under exploitation rates
731 as high as (or likely even less than) those observed in our terminal and mixed maturation MSY
732 scenarios, there would be a high probability of losing larger, older adults altogether from the
733 population due to strong selection for faster growth rates and smaller size-/younger age-at-
734 maturity.

735
736 By incorporating diversification bet-hedging in our parameterization of the genetics of
737 maturation (a form of genetic and environmental canalization that prioritizes geometric mean
738 fitness rather than arithmetic mean fitness [46-50]) our model population retains the ability to
739 produce all growth rates and maturation sizes and ages of the pre-harvest population under a
740 range of realistic exploitation rates. However, given our focus on time periods relevant to
741 management, (25 years or 5 to 6 generations), we chose not to incorporate the added complexity
742 of allowing selection to operate on growth rates and/or maturation lengths. In any case, our
743 results strongly suggest that incorporating evolution of the genetics controlling maturation would
744 not affect the generality of our results regarding the benefits of terminal fisheries and the
745 detrimental impact of mixed-maturation fisheries.

746
747 The demographic impacts that occur under mixed maturation harvest also have suboptimal
748 effects on the total numbers and weight of the catch (Fig 8; Supplementary File S4, Table A). In
749 the MM troll scenario (H3) where immature and mature fish 610 mm FL and larger are equally
750 vulnerable to the global harvest rate, immature Chinook comprise 59% of the total numbers

751 caught, and 47% of the total weight of the catch (Fig 9). In the MM gillnet scenario where
752 immature and mature fish are also equally vulnerable to the global harvest rate, but the gear is
753 disproportionately selective for larger, older fish, immature Chinook comprise 40% of the total
754 number caught and 15% of the total weight of the catch (Fig 9). Importantly, we did not include
755 release mortality on sublegal catch or drop-off mortality on legal and sublegal size fish in the
756 mixed maturation scenarios, (phenomena that are common in marine, particularly troll,
757 fisheries), again emphasizing the conservative nature of our results.

758

759 As noted in the Results, the average weight of spawners in both mixed maturation scenarios are
760 reduced by roughly 4 lb from the pre-harvest average (Figs 3 and 5), the proportions of the 2
761 oldest spawner ages are reduced by more than 10% (Fig 7; Supplement File S4, Table C), and
762 the mean age of spawners is reduced by nearly half a year from the pre-harvest average (Fig
763 6).

764

765 **Demographic effects of the two gear types on population structure**

766 We found large differences in the effects of harvest on the size and age structure of the adult
767 population between the 2 gear types in both mixed maturation and terminal fishery scenarios.

768 These were due to the cutoff lengths for the selectivities of gillnet fisheries that we chose on the
769 basis of Bromaghin's analysis of the selectivity of the 8-inch mesh typically used for Chinook.

770 In troll scenarios, individuals at or above the minimum size threshold tend to be harvested close
771 to their proportions in the total population vulnerable to harvest. Gillnets, by contrast, harvest

772 larger, older individuals in proportions greater than their proportions in the total vulnerable
773 population. Thus, individuals in ages 4 to 6 were harvested to a greater extent than ages 2 and 3,
774 which were only harvested incidentally. This was due to two features of our parameterization.
775 First, our upper limit of 1158 mm FL was close to the largest length of the oldest (age 6) length
776 class, so there were few individuals subject to the lower selectivity on lengths greater than 1158.
777 Second, our lower limit of 783 mm meant that all age 2 individuals and most age 3 individuals
778 were subject to the lower harvest rate (Supplementary file S1, Fig B). Thus, fish smaller than this
779 lower limit consisted mostly of ages 2 and 3.

780 A related feature of the terminal troll harvest scenarios (H1 and H5) in comparison to the 2
781 mixed maturation (H3 and H4) and the 2 terminal gillnet scenarios (H2 and H6), is a negligible
782 alteration of the mean age of the spawning population relative to the mean age at the unfished
783 stochastic equilibrium (Fig 3; Supplement File S4, Table D). This is due to 2 features of these
784 scenarios: first, the minimum length limit (610 mm) that we chose for the troll scenarios results
785 in over 95% of all mature females and males age 3 and older being fully vulnerable to the fishing
786 gear. Second, all vulnerable individuals are equally and randomly vulnerable to the global
787 harvest rate and are therefore harvested (on average) in direct proportion to their age/length-
788 interval-specific abundance, which tends to preserve the initial proportions between ages 3 and 6.
789 This leaves mature age 2 males largely unaffected by harvest mortality which results in a small
790 increase in the proportion of age 2 males in the adult population. It has only a small effect on the
791 overall age proportions.

792 A particularly valuable comparison is between the primary mixed maturation troll harvest
793 scenario (H3) and the terminal fishery counterpart (H5) that adjusts the global harvest rate (hg)
794 downward from the un-restricted MSY rate to the MM Catch Weight Equivalent rate. This

795 achieves approximately the same total catch weight as the mixed maturation troll fishery. This
796 total catch weight (~8700) is more than 3500 lb smaller than the terminal MSY harvest of 12295
797 lb (Fig 8). This (H5) terminal harvest scenario catches fewer individuals than the MM fishery
798 (467 versus 728, but since all individuals harvested are mature, the average weight of the fish is
799 significantly larger than the mixed maturation catch (18.5 versus 12.0 lb; Fig 3; Supplementary
800 File S4, Table A). The larger weight of individuals caught in the terminal scenario likely
801 increases their economic value above that of the mixed-stock scenario because larger Chinook
802 may realize a higher price per pound (cf. [37]).

803

804 **Differences in total egg deposition between harvest scenarios**

805

806 For the troll scenarios, the lowest average fecundities occur in the mixed maturation scenario
807 (H3) where the average is 200 eggs per female lower than for either the pre-fishery or the post-
808 fishery averages. For the gillnet scenarios, both the terminal MSY and the mixed maturation
809 MSY scenarios (H2, H4) are more than 350 to 500 eggs per female lower than the pre-fishery
810 averages. Fig 7 shows a related change in the proportion of the average total egg deposition
811 contributed by the two youngest female ages (3 and 4), which increases from an average of 40%
812 in the pre-harvest period to 50% and 52%, respectively in scenarios H3 and H4. This illustrates
813 that the MM harvest scenarios shift the spawner age structure toward younger average ages and
814 renders the population more dependent on egg deposition from the younger, less fecund
815 spawners. In addition, the terminal MSY gillnet scenario (H2) increases the proportion of total

816 egg deposition by age 3 and 4 spawners to 54% due to the strong size selectivity of the gear
817 (Supplement File S4, Table C).

818

819 **Model assumptions of note**

820

821 **Spawner age and egg size**

822 For both modeling convenience and lack of available data, we assumed that all eggs were the
823 same size and had the same probability of surviving to emergence, and that all emergent parr
824 were of the same size regardless of female age or size, and hence were equal in overall fitness
825 with respect to density dependent survival to the smolt stage. In reality, larger female Chinook
826 deposit larger, better provisioned, eggs that likely possess greater fitness than smaller eggs. As a
827 consequence, the comparisons between the MM fishery scenarios (H3 and H4) and the 4
828 terminal fishery scenarios may slightly exaggerate the impact of mixed maturation fisheries on
829 population productivity and resilience to the extent that older age spawners are deprived the
830 marginal fitness advantage that may accrue to larger, better provisioned eggs than smaller,
831 younger age females. This is a feature that can be remedied in case-specific applications where
832 population-specific egg-size and/or energy content data are available. However, we believe this
833 effect to be relatively minor compared to the overall change in population structure effected by
834 MM fisheries and thus does not distort the generality of our results.

835

836 **Parameterization of daily growth and density-independent survival rates**

837 Although we lack good data on the actual growth rates associated with maturation at each age, as
838 parameterized in the McGurk growth-mortality equations (Supplementary File S1, A5, equations
839 5.1 and 5.2), the parameterizations that we chose (Supplementary File S2, Table L) produce
840 reasonable and realistic mean lengths for each of the maturation ages (Fig 2) and realistic age-
841 specific density-independent marine survival rates (Supplementary File S2, Table M). Further,
842 by modeling harvest as length-based, our assumption that older maturing individuals grow more
843 slowly than individuals maturing at younger ages, is more realistic than models that assume that
844 all individuals of a given age in mixed-stock fishery have the same lengths.

845

846 **Fisheries related incidental mortality**

847 An important lacuna in our harvest modeling was ignoring fisheries related incidental mortality
848 (FRIM). FRIM includes retained landings of sub-legal-size fish, post-release mortality of
849 released landed sub-legal, and drop-off mortality of legal and sublegal fish that encounter the
850 gear and die through predation or injury as a consequence. FRIM can be (and normally is) a
851 significant source of fishing mortality in mixed maturation fisheries. We intentionally chose to
852 ignore FRIM in our simulations in order to focus clearly on the impacts to legal size fish. Thus,
853 our results for the 2 MM fishery scenarios are likely an under-estimate of the impact of these
854 fisheries on immature fish. This further highlights the conservative nature of our harvest
855 analyses.

856

857 **Vulnerability of immature Chinook to harvest gear**

858 We assumed that all immature Chinook were equally vulnerable to fishing gear as mature
859 individuals of the same size (fork length). This would require all such immatures to rear in areas
860 where matures are located and where fishing occurs. While likely true for many Pacific Salmon
861 Treaty marine Chinook fisheries in our area of interest, there may be times and areas where this
862 isn't the case. To the extent to which this is not the case the impact of indirect age-overfishing
863 will be smaller than shown in our model results. Our model, therefore, highlights the most
864 extreme case. To the extent this departs from a specific real-world situation, our results will
865 overestimate the effect of indirect age overfishing. Even in such a case, the harvest of immatures
866 in harvest areas with mature fish will have the kind of detrimental impact on total catch weight,
867 total spawner weight and egg deposition, and age-specific proportions of the catch and spawning
868 population that we show, though the magnitude will be reduced to some degree.

869

870 **Conclusion**

871 Our individual-based model of ocean-type Chinook salmon provides for robust evaluations of the
872 likely impacts of different harvest regimes and gear types on the structure and productivity of
873 Pacific coast Chinook populations. It also illuminates the strengths and weaknesses of different
874 harvest regimes for returning benefits to fishers. The results of our modeling exercise provide a
875 succinct analysis of the primary differences between terminal and marine MM fishery regimes
876 on Chinook life-history, productivity, and return to harvesters (measured by catch number and
877 catch weight).

878 We find that, on balance, terminal fisheries provide greater harvest benefits to fishers than MM
879 fisheries. Additionally, they provide greater protection for the productivity and resilience of the
880 harvested populations. Although we assumed a common egg size independent of female age and
881 size, our results highlight the importance of the greater fecundity of older, larger females to the
882 productivity of Chinook salmon populations, and provide evidence of the importance of
883 monitoring Chinook populations for total egg deposition and the age composition of spawners,
884 rather than (or in addition to) total number of spawners. These results should be of value to
885 scientists and managers concerned with the long-term sustainability of harvestable wild Chinook
886 populations and with the rebuilding of depleted and at-risk populations.

887 Future planned work examining existing Chinook populations and development of a model
888 applicable to stream-type Chinook, will further our understanding of how recent and past harvest
889 practices have affected wild Chinook populations along the coast of the eastern North Pacific.
890 The development of appropriately targeted monitoring and assessment projects are also needed
891 to improve understanding of the status of wild Chinook populations at regional and population-
892 specific scales.

893

894 **Supporting Information**

895 **S1 File. Chinook survivability parameters and equations. (DOCX)**

896 **S2 File. Chinook growth parameters. (DOCX)**

897 **S3 File. Characteristics of the equilibrium spawner abundance of the IBDEM Chinook**
898 **model. (DOCX)**

899 **S4 File. Tables of harvest simulation results. (DOCX)**

900 **S5 Table. Summary of a representative 1000 year simulation. (XLSX)**

901 **Acknowledgments**

902 We thank Marco Castellani for generously sharing all of the code for the IBSEM model [38] and
903 for answering questions regarding some aspects of the coding of the model. We thank Jeffrey
904 Hard (Conservation Biology Division, Northwest Fisheries Science Center, National Marine
905 Fisheries Service, retired) for reviewing the coding of the maturation genetics in an earlier
906 version of the model and for providing advice and answering questions regarding the expected
907 magnitude of the heritability of maturation. We are grateful to Marty Kardos of the Conservation
908 Biology Division, Northwest Fisheries Science Center and Robin Waples of the Northwest
909 Fisheries Science Center (retired) for providing helpful comments on a draft of the current paper,
910 particularly our approach to coding the quantitative genetics. These all greatly improved the
911 organization of the paper. This does not, however, imply any endorsement of our approach and
912 results by these reviewers or NMFS.

913

914 **References**

- 915 1. Van Hyning JM. 1968. Factors affecting the abundance of fall Chinook salmon in the
916 Columbia River. Submitted in defense of Ph.D Thesis, Oregon State University.
917 <https://ir.library.oregonstate.edu/downloads/vt150n520>

- 918 2. Ricker WE. 1980. Causes of the decrease in age and size of Chinook salmon
919 (*Oncorhynchus tshawytscha*). *Can. Tech. Rep. of Fish. & Aq. Sci.* no. 944.
- 920 3. Ricker WE. 1981. Changes in the average size and average age of Pacific salmon. *Can.*
921 *J. of Fish & Aquat. Sci.*38: 1636-1656.
- 922 4. Lewis B, Grant WS, Brenner RE, Hamazaki T. 2015. Changes in size and age of Chinook
923 salmon (*Oncorhynchus tshawytscha*) returning to Alaska. *PLoS ONE* 10(6): e0130184.
924 doi:10.1371/journal.pone.0130184
- 925 5. Jeffrey KM, Cote IM, Irvine IR, Reynolds JD. 2016. Changes in body size of Canadian
926 Pacific salmon over six decades. *Can. J. Fish. Aq. Sci.* dx.doi.org/10.1139/cjfas-2015-
927 0600.
- 928 6. Ohlberger J, Ward EJ, Schindler DE, Lewis B. 2018. Demographic changes in Chinook
929 salmon across the Northeast Pacific Ocean. *Fish & Fisheries* 19: 533 - 546.
- 930 7. Munch S, Reynolds JD, Vick GK, Palkovacs EP. 2020. Recent declines in salmon body
931 size impact ecosystems and fisheries. *Nature Comm.* [doi.org/10.1038/s41467-020-17726-](https://doi.org/10.1038/s41467-020-17726-z)
932 [z](https://doi.org/10.1038/s41467-020-17726-z).
- 933 8. Oke KB, Cunningham CJ, Westley PAH, Baskett ML, Carlson SM, Clark J, et al. 2020.
934 *Nature Communications* 11:4155 | <https://doi.org/10.1038/s41467-020-17726-z> .
- 935 9. Xu Y, Decker AS, Parken CK, Ritchie LM, Patterson DA, Fu C. 2020. Climate effects on
936 size-at-age and growth rate of Chinook salmon (*Oncorhynchus tshawytscha*) in the Fraser
937 river, Canada. *Fish. Oceanog.* 29: 381 – 395.
- 938 10. Freshwater C, Parken CK, Tucker S, Velez-Espino A, King J. 2022. Nonstationary
939 patterns in demographic traits covary with Chinook salmon marine distributions.

- 940 Canadian Journal of Fisheries and Aquatic Sciences 79: 1860–1878.
941 [dx.doi.org/10.1139/cjfas-2021-0312](https://doi.org/10.1139/cjfas-2021-0312).
- 942 11. Quinn, TP, Scheurell MD, Losee JP, Hanada D. 2022. Multidecadal Trends in Body Size
943 of Puget Sound Chinook Salmon: Analysis of Data from the Tengu Derby, a Culturally
944 Unique Fishery. *Marine and Coastal Fisheries: Dynamics, Management, and Ecosystem*
945 *Science* 14:e10205
- 946 12. Malick MJ, Losee JP, Marston G, Agha M, Berejikian BA, Beckman BR, Cooper M.
947 2023. Fecundity trends of Chinook salmon in the Pacific Northwest. *Fish and Fisheries*
948 24:454–465.
- 949 13. Ruggerone GT, Irvine JR. 2018. Numbers and Biomass of Natural- and Hatchery-Origin
950 Pink Salmon, Chum Salmon, and Sockeye Salmon in the North Pacific Ocean, 1925–
951 2015. *Marine and Coastal Fisheries: Dynamics, Management, and Ecosystem Science*
952 10:152–168, 2018.
- 953 14. Peterman RM, Holt CA, Rutherford MR. 2012. The need for international cooperation to
954 reduce competition among salmon for a common pool of prey resources in the North
955 Pacific Ocean. *North Pacific Anadromous Fish Commission Technical Report* 8:99–101.
- 956 15. Ruggerone GT, Springer AM, van Vliet GB, Connors B, Irvine JR, Shaul LD, et al. 2023.
957 From diatoms to killer whales: impacts of pink salmon on North Pacific ecosystems.
958 *Marine Ecology Progress Series* 719: 1–40, 2023 <https://doi.org/10.3354/meps14402>.
- 959 16. Hard JJ. 2004. Evolution of Chinook salmon life histories under size-selective harvest.
960 Chapter 11 in *Evolution Illuminated* A.P. Hendry and S.C. Stearns, *eds.* Oxford
961 University Press 2004.

- 962 17. Kuparinen A, Merila J. 2007. Detecting and managing fisheries induced evolution.
963 *Trends in Ecol. & Evol.* 22(12): 652 – 659.
- 964 18. Hard JJ, Gross MR, Heino M, Hilborn MR, Kope RG, Law R, Reynolds JD. 2008.
965 Evolutionary consequences of fishing and their implications for salmon. *Evol. App.* 388 –
966 408.
- 967 19. Losee J, Kendall NW, Dufault AM. 2019. Changing salmon: An analysis of body mass,
968 abundance, survival, and productivity trends across 45 years in Puget Sound. *Fish and*
969 *Fisheries* 1-18. DOI: 10.1111/faf.12385
- 970 20. Czorlich Y, Aykanat T, Erkinaro J, Orell JP, Primmer CR. 2022. Rapid evolution in
971 salmon life history induced by direct and indirect effects of fishing. *Science*: eabg5980.
- 972 21. Hard JJ, Eldridge WH, Naish KA. 2009. Genetic Consequences of Size-Selective
973 Fishing: Implications for Viability of Chinook Salmon in the Arctic-Yukon-Kuskokwim
974 Region of Alaska *American Fisheries Society Symposium* 70:759–780.
- 975 22. Kendall NW, Dieckmann U, Heino UM, Punt AE, Quinn TP. 2014. Evolution of age and
976 length at maturation of Alaskan salmon under size-selective harvest. *Evol. App.* 313 –
977 322.
- 978 23. Healey MC. 1991. Life history of Chinook salmon (*Oncorhynchus tshawytscha*) in Groot
979 & Margolis (eds.) Pacific Salmon Life Histories, University of British Columbia Press.
- 980 24. Quinn TP. 2005. The Behavior and Ecology of Pacific Salmon & Trout. American
981 Fisheries Society in association with the University of Washington Press.

- 982 25. Mathews S. 2019. An analysis of Chinook salmon harvest management
983 [https://soundcatch.org/wp-content/uploads/2019/01/Analysis-of-Chinook-Salmon-](https://soundcatch.org/wp-content/uploads/2019/01/Analysis-of-Chinook-Salmon-Management-by-Stephen-Mathews.pdf)
984 [Management-by-Stephen-Mathews.pdf](https://soundcatch.org/wp-content/uploads/2019/01/Analysis-of-Chinook-Salmon-Management-by-Stephen-Mathews.pdf)
- 985 26. Conover DO, Munch SB. 2002. Sustaining fishery yields over evolutionary time scales.
986 *Science* 297: 94 – 96.
- 987 27. Ernande B, Dieckmann U, Heino M. 2004. Adaptive changes in harvested populations:
988 plasticity and evolution of age and size at maturation. *Proceedings of the Royal Society of*
989 *London. Series B: Biological Sciences* 271, no. 1537: 415-423.
- 990 28. de Roos AM, Boukal DS, Persson L. 2006. Evolutionary regime shifts in age and size at
991 maturation of exploited fish stocks. *Proc Biol Sci.* 273(1596):1873-1880.
992 doi:10.1098/rspb.2006.3518
- 993 29. Jørgensen C, Enberg K, Dunlop ES, Arlinghaus R, Boukal DS, Brander K, et al. 2007.
994 Managing evolving fish stocks. *Science* 318:1247–1248.
- 995 30. Swain DP, Sinclair AF, Hanson JM. 2007. Evolutionary response to size-selective
996 mortality in an exploited fish population. *Proc. R. Soc. B* 2007 274, 1015-1022.
- 997 31. Alos J, Palmer M, Catalan IA, Alonso-Fernandez A, Basterretxea G, Jordi A, et al. 2014.
998 Selective exploitation of spatially structured coastal fish populations by recreational
999 anglers may lead to evolutionary downsizing of adults. *Mar. Ecol. Prog. Ser.* 503:219–
1000 233.
- 1001 32. Uusi-Heikkilä S, Whiteley AR, Kuparinen A, Matsumura S, Venturelli PA, Wolter C, et
1002 al. 2015. The evolutionary legacy of size-selective harvesting extends from genes to
1003 populations. *Evol. App.* 597 – 620. doi:10.1111/eva.12268

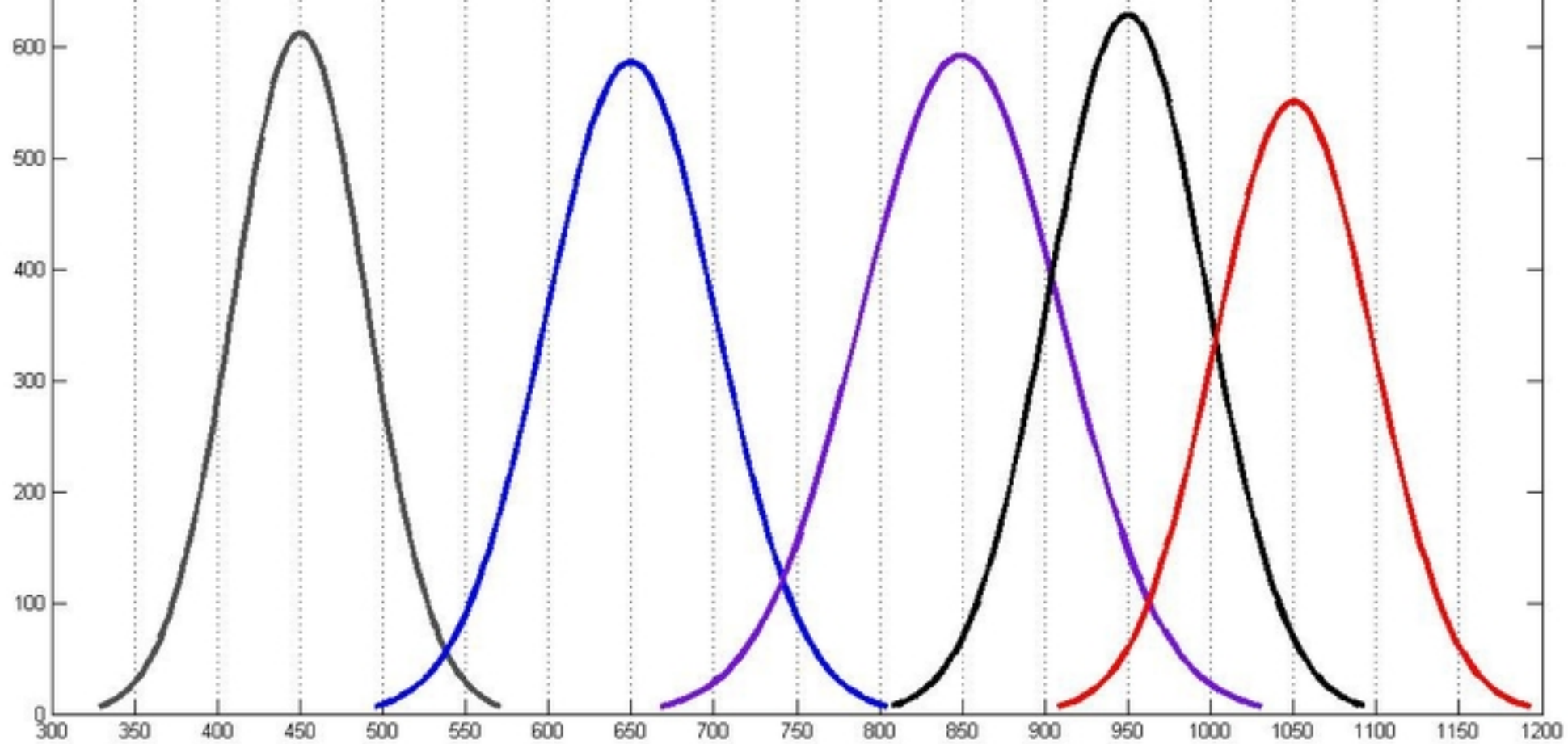
- 1004 33. Roff DA. 1992. The Evolution of Life Histories. Chapman and Hall. London.
- 1005 34. Eldridge WH, Hard JJ, Naish KA. 2010. Simulating fishery-induced evolution in
1006 Chinook salmon: the role of gear, location, and genetic correlation among traits. *Ecol.*
1007 *App.* 20(7): 1936 – 1948.
- 1008 35. Riddell B, Bradford M, Carmichael R, Hankin D, Peterman R, Wertheimer A. 2013.
1009 Assessment of Status and Factors for Decline of Southern BC Chinook Salmon:
1010 Independent Panel’s Report. Prepared with the assistance of D.R. Marmorek and A.W.
1011 Hall, ESSA
- 1012 36. Healey MC, Heard WR. 1984. Inter- and intra-population variation in the fecundity of
1013 Chinook salmon (*Oncorhynchus tshawytscha*) and its relevance to life history theory.
1014 *Can. J. Fish. Aquat. Sci.* 41: 474-483.
- 1015 37. Zimmerman F, Heino H, Steinshamm SI. 2011. Does size matter? A bioeconomic
1016 perspective on optimal harvesting when price is size-dependent. *Can. J. Fish. & Aquat.*
1017 *Sci.* 68: 1651 – 1659.
- 1018 38. Dunlop ES, Heino M, Dieckmann U. 2009. Eco-genetic modeling of contemporary life-
1019 history evolution. *Ecol. App.* 19(7): 1815 – 1834.
- 1020 39. Castellani M, Heino M, Gilbey J, Araki H, Svåsand T, Glover KA. 2015. IBSEM: An
1021 Individual-Based Atlantic Salmon Population Model. *PLoS ONE* 10(9): e0138444.
1022 doi:10.1371/journal.pone.0138444
- 1023 40. Zillig KW, Lusardi RA, Cocherell DE, Fangué NA. 2022. Interpopulation variation in
1024 thermal physiology among seasonal runs of Chinook salmon. *Can. J. Fish. & Aquat. Sci.*
1025 80: 1–13 (2023) | [dx.doi.org/10.1139/cjfas-2022-0133](https://doi.org/10.1139/cjfas-2022-0133).

- 1026 41. Bromaghin JF, Nielson RM, Hard JJ. 2011. A model of Chinook salmon population
1027 dynamics incorporating size-selective exploitation and inheritance of polygenic
1028 correlated traits. *Nat. Res. Modeling* 24(1): 1 – 47.
- 1029 42. Godfrey H. 1968. Age and physical characteristics of maturing Chinook salmon from the
1030 Nass, Skeena, and Fraser rivers in 1964, 1965, and 1966. Fisheries Research Board of
1031 Canada Manuscript Report Series no. 967.
- 1032 43. Beatty RE. 1992. Master of Science Thesis, Oregon State University. Changes in Size
1033 and Age at Maturity of Columbia River Upriver Bright Fall Chinook Salmon
1034 (*Oncorhynchus tshawytscha*): Implications for Stock Fitness, Commercial Value, and
1035 Management.
- 1036 44. Piou C, Prevost E. 2012. A demo-genetic individual-based model for Atlantic salmon
1037 populations: Model structure, parameterization and sensitivity *Ecologic. Model.* 231: 37 –
1038 52.
- 1039 45. McGurk MD. 1996. Allometry of marine mortality of Pacific salmon. *Fish. Bull.* 94: 77 –
1040 88.
- 1041 46. Castellani M, Heino M, Gilbey J, Araki H, Svasand T, Glover KA. 2018. Modeling
1042 fitness changes in wild Atlantic salmon populations faced by spawning intrusion of
1043 domesticated escapees. *Evolutionary Applications*; 11:1010 – 1025.
- 1044 47. Goodman D. 1984. Risk spreading as an adaptive strategy in iteroparus life histories.
1045 *Theoretical Population Biology* 25: 1 – 20.

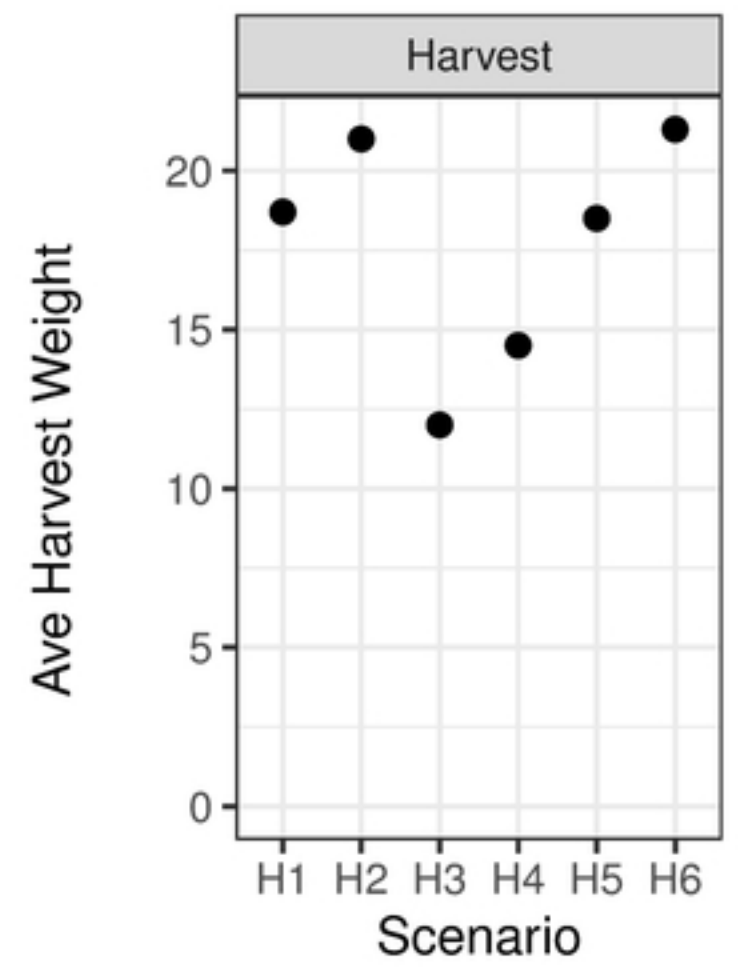
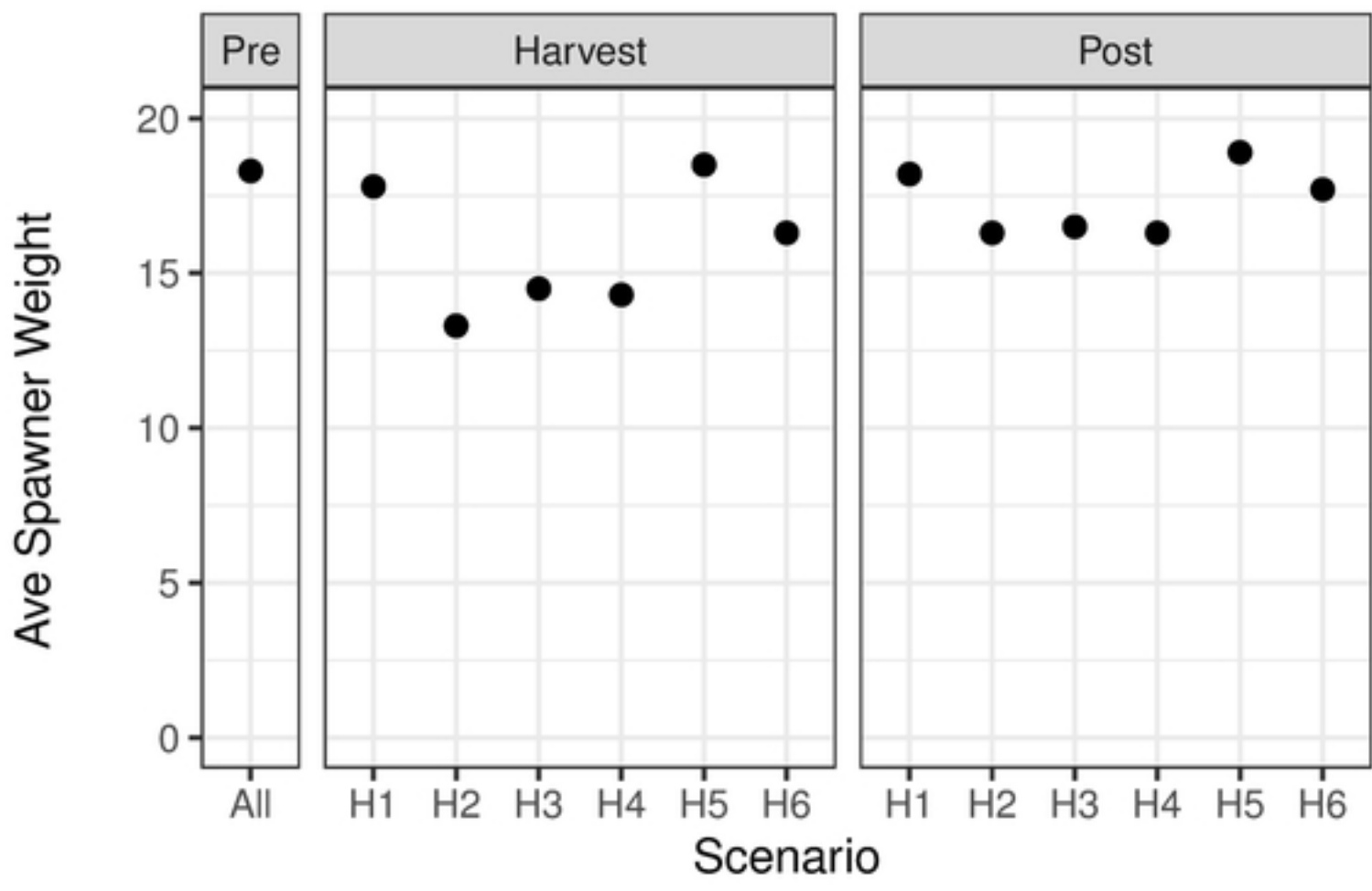
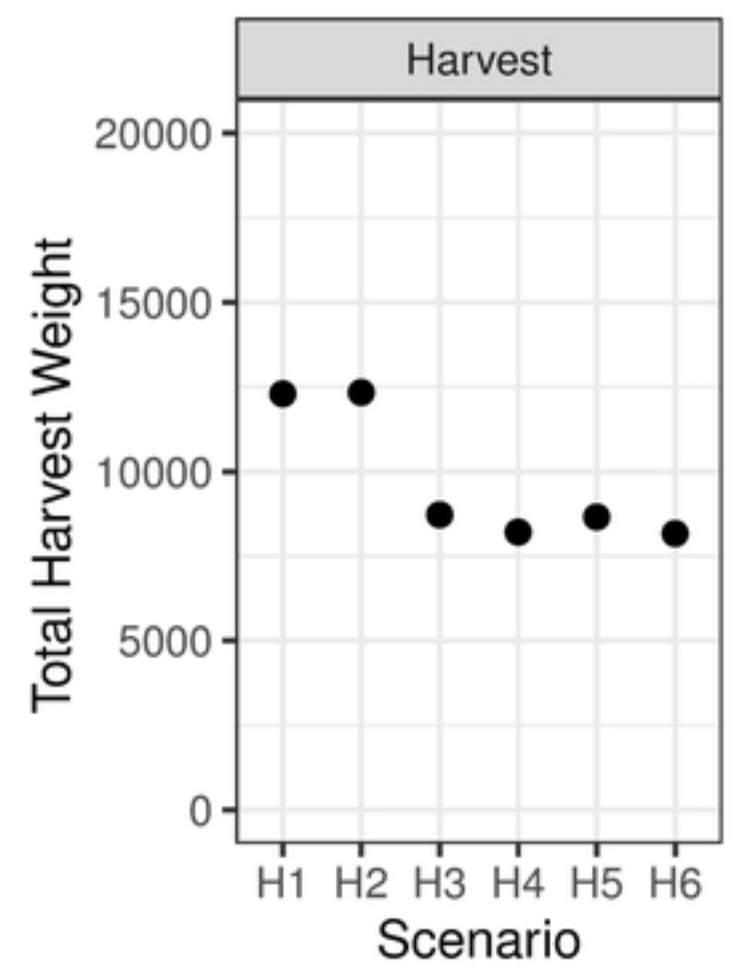
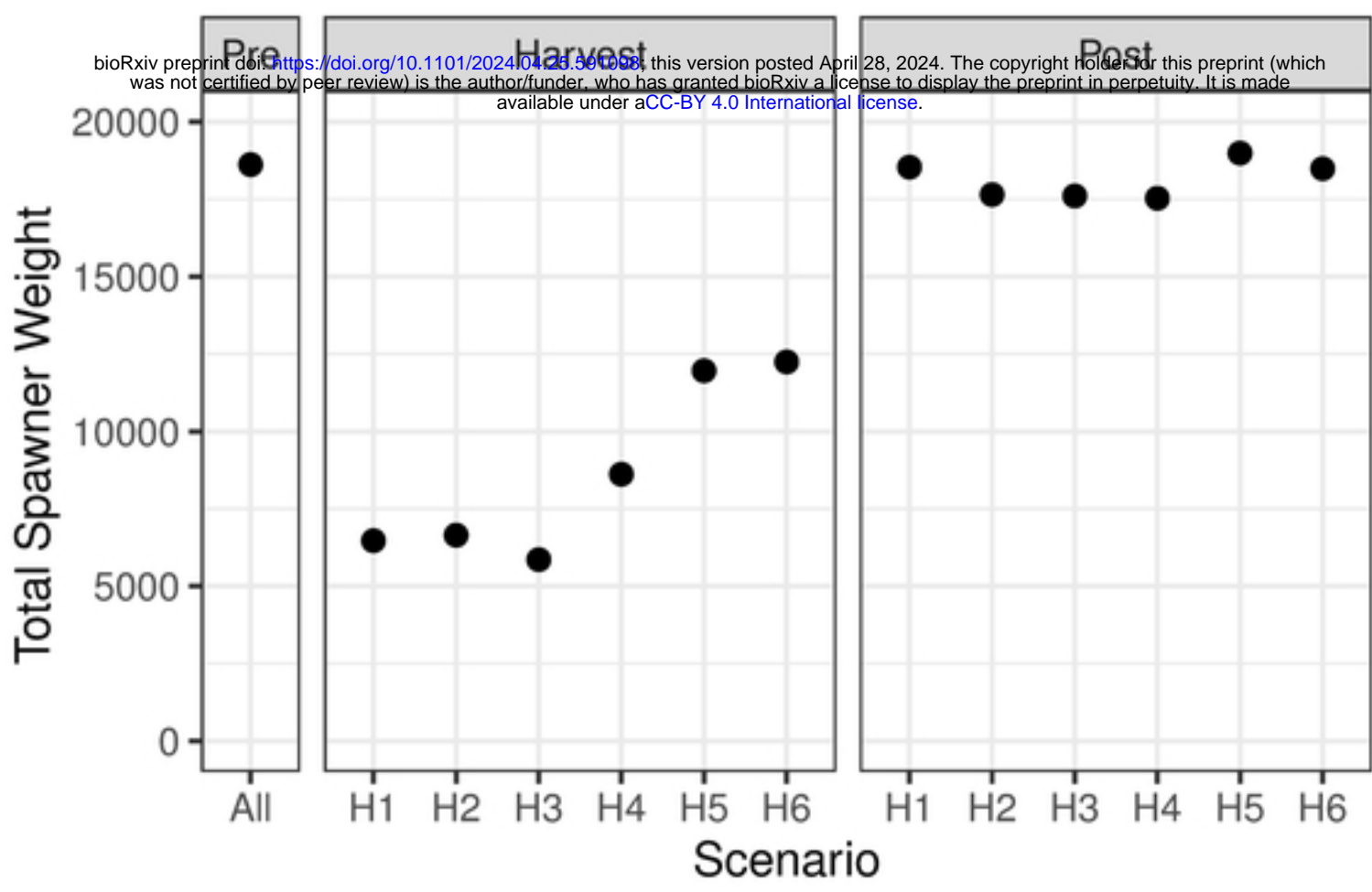
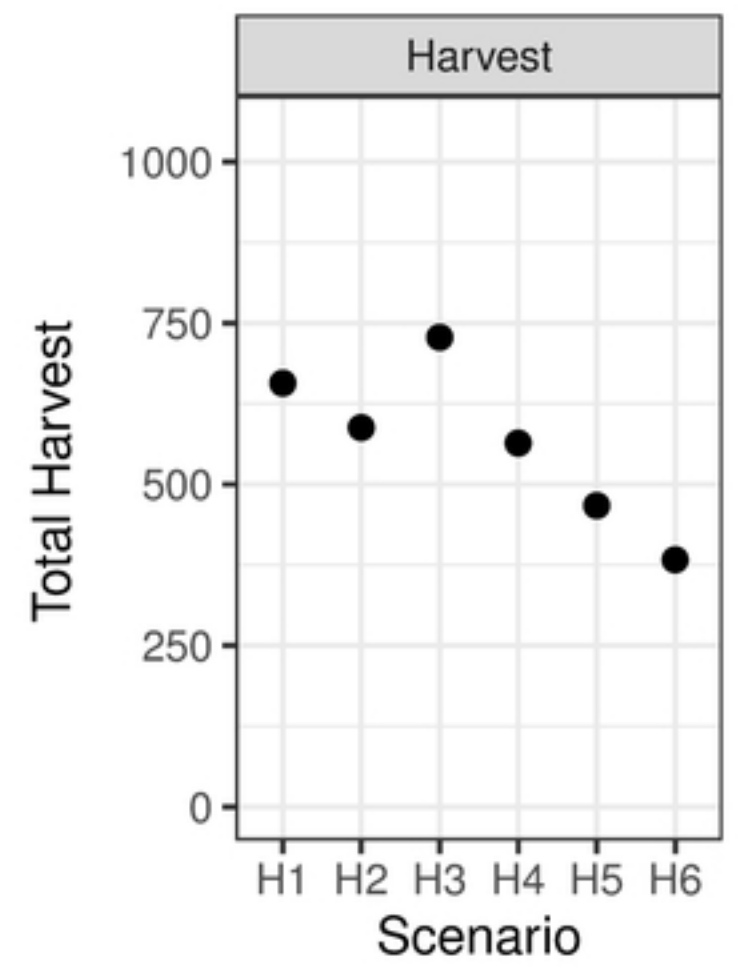
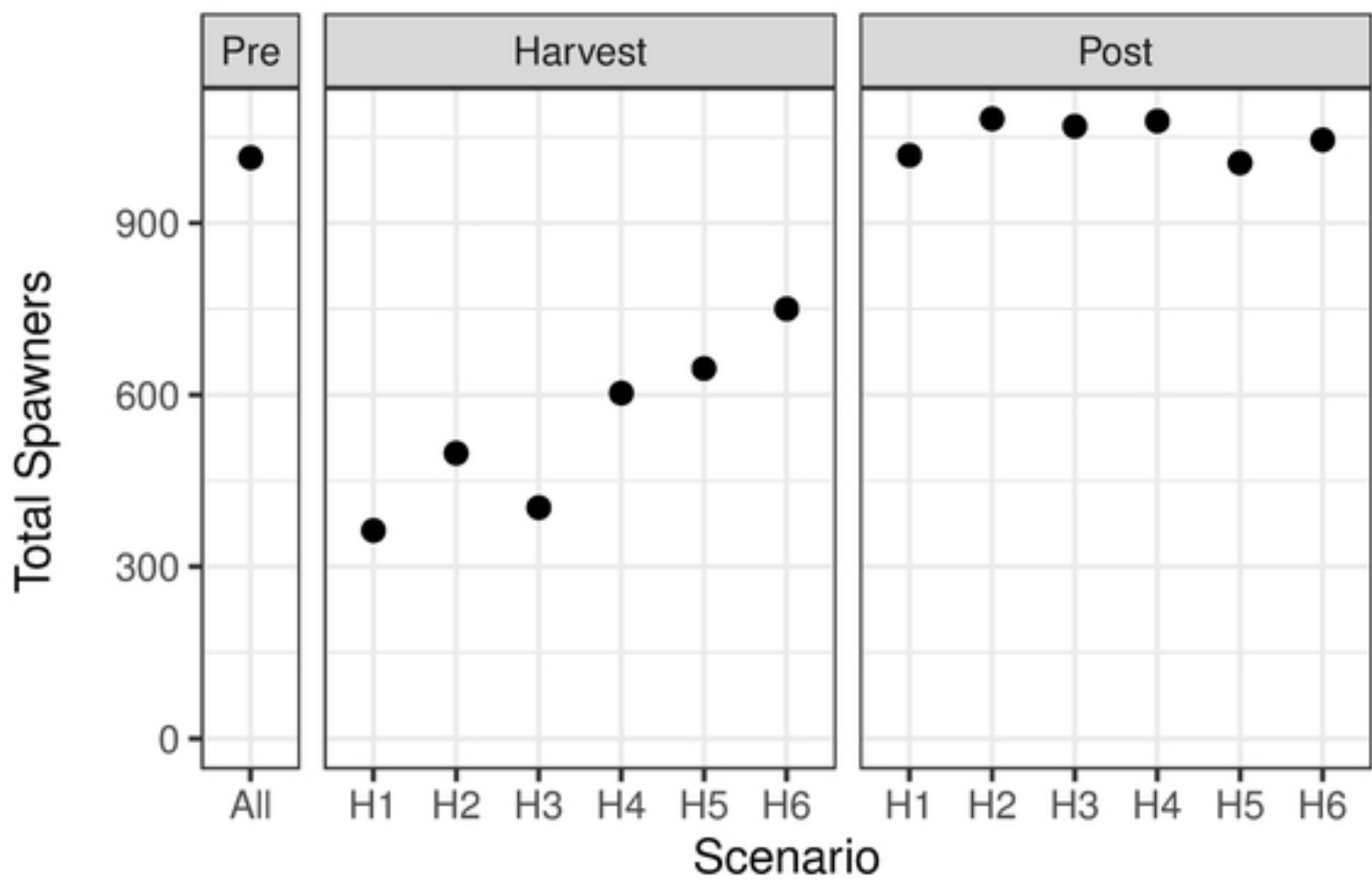
- 1046 48. Simons AM. 2009. Fluctuating natural selection accounts for the evolution of
1047 diversification bet-hedging. *Proceedings of the Royal Society of London B*. 276: 1987 –
1048 1992.
- 1049 49. Simons AM. 2011. Modes of response to environmental change and the elusive empirical
1050 evidence for bet hedging. *Proceedings of the Royal Society of London B*. 278: 1601 –
1051 1609.
- 1052 50. Scheiner SM. 2014. Bet-hedging as a complex interaction among developmental
1053 instability, environmental heterogeneity, dispersal, and life-history strategy. *Ecology and*
1054 *Evolution* 505 – 515.
- 1055 51. Haaland TR, Wright J, Ratikainen II. 2021. Individual reversible plasticity as a genotype-
1056 level bet-hedging strategy. *Journal of Evolutionary Biology* 34:1022 – 1033.
- 1057 52. Stearns SC, Kawecki TJ. 1994. Fitness sensitivity and the canalization of life-history
1058 traits. *Evolution* 48(5): 1438 – 1450.
- 1059 53. McCarthy ID, Houlihan DF, Carter CG. 1994. Individual variation in protein turnover
1060 and growth efficiency and rainbow trout, *Oncorhynchus mykiss* (Walbaum). *Proceedings*
1061 *of the Royal Society London* 257: 141 – 147.
- 1062 54. Houlihan D, McCarthy I, Owen S. 1996. Protein metabolism in fish: comparative
1063 turnover rates. <https://fishphysiology.org/wp-content/uploads/2014/02/Houlihan1.pdf>
- 1064 55. Morgan IJ, McCarthy ID, Metcalfe NB. 2000. Life-history strategies and protein
1065 metabolism in overwintering juvenile atlantic salmon: growth is enhanced in early
1066 migrants through lower protein turnover. *Journal of Fish Biology* 56: 637 – 647.

- 1067 56. Willmore KE, Hallgrímsson B. 2005. Within individual variation: developmental noise
1068 versus developmental stability. Chapter 10 in Variation: a central concept in biology. B.
1069 Hallgrímsson and B. K. Hall, editors, Elsevier, Academic Press
- 1070 57. Peterman RM, Beamesderfer R, Bue B. 2016. Review of methods for forecasting
1071 Chinook salmon abundance: Report to the Pacific Salmon Commission. PSC Tech. Rep.
1072 No. 35: 165 p.
- 1073 58. Mousseau TA, Roff DA 1987. Natural selection and the heritability of fitness
1074 components. *Heredity* 59: 181 – 197.
- 1075 59. Postma 2014. Chapter 2 in Quantitative Genetics in the Wild, Charmantier, A., D. Garant
1076 and L.E.B. Kruuk, eds. OUP Oxford.
- 1077 60. Papaix J, Cubaynes S, Buoro M, Charmantier A, Perret P, Gimenez O. 2010. Combining
1078 capture-recapture data and pedigree information to assess heritability of demographic
1079 parameters in the wild. *J. Evolutionary Bio.* 23: 2176-2184.
- 1080 61. Orr HA. 1998. The population genetics of adaptation: the distribution of factors fixed
1081 during adaptive evolution. *Evolution* 52(4): 935 – 949.
- 1082 62. Bromaghin JF. 2005. A versatile net selectivity model, with application to Pacific salmon
1083 and freshwater species of the Yukon River, Alaska. *Fisheries Research* 74: 157 – 168.
- 1084 63. PFMC. 2020. Pacific Fishery Management Council. 2020. *Preseason Report III: Council*
1085 *Adopted Management Measures and Environmental Assessment Part 3 for 2020 Ocean*
1086 *Salmon Fishery Regulations: RIN 0648-BJ48*. (Document prepared for the Council and
1087 its advisory entities.) Pacific Fishery Management Council, 7700 NE Ambassador Place,
1088 Suite 101, Portland, Oregon 97220-1384.



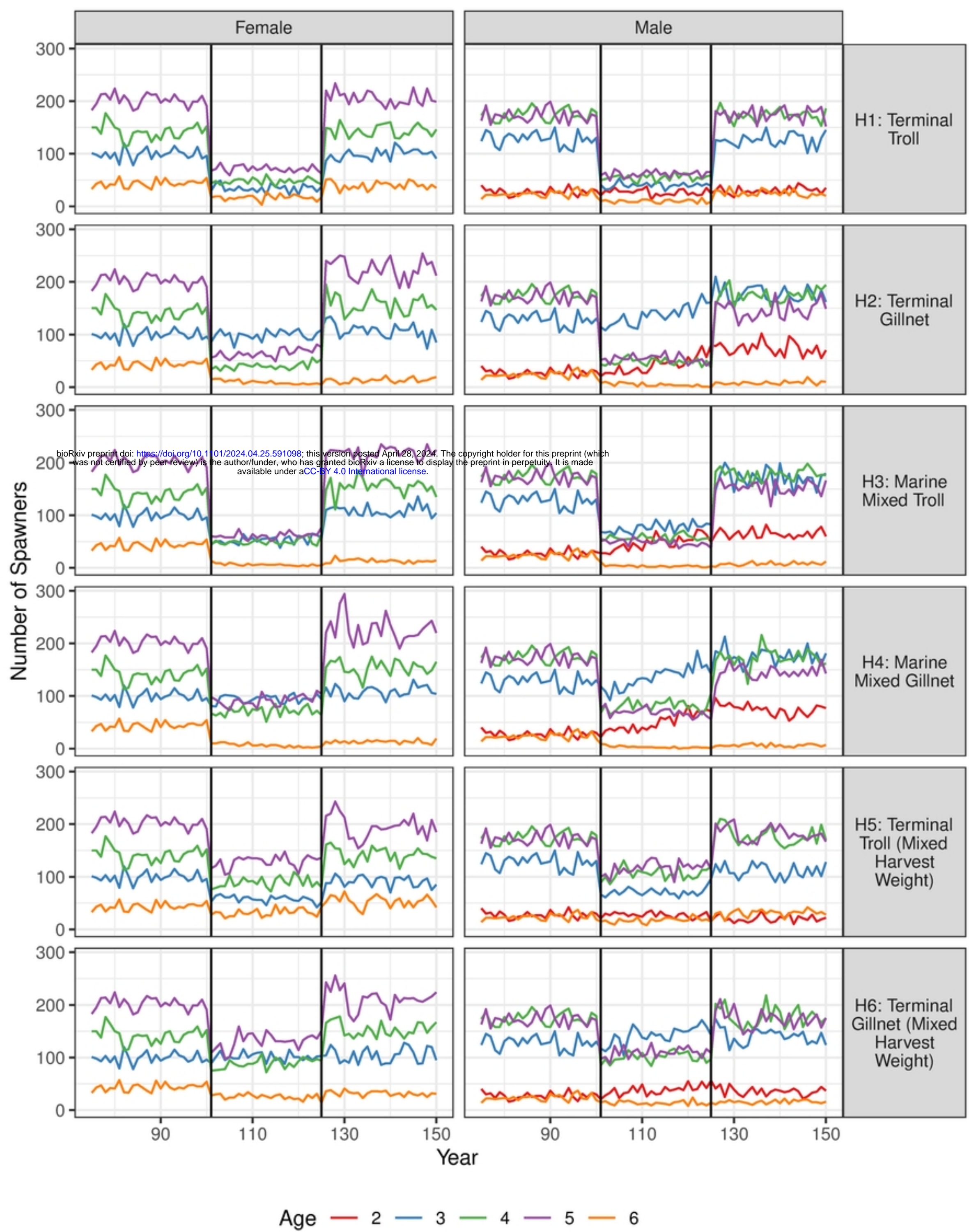


figure

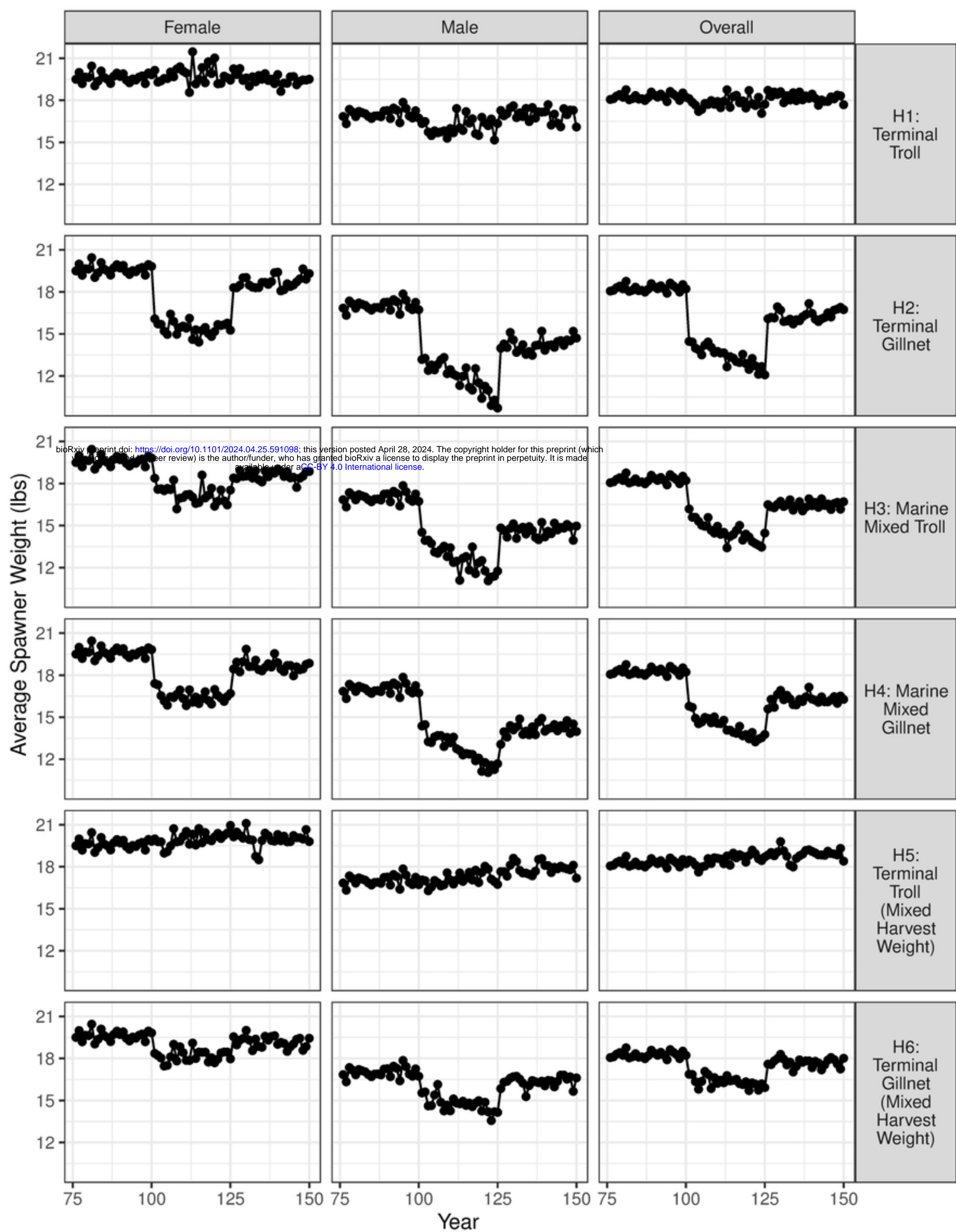


bioRxiv preprint doi: <https://doi.org/10.1101/2024.04.28.591008>; this version posted April 28, 2024. The copyright holder for this preprint (which was not certified by peer review) is the author/funder, who has granted bioRxiv a license to display the preprint in perpetuity. It is made available under aCC-BY 4.0 International license.

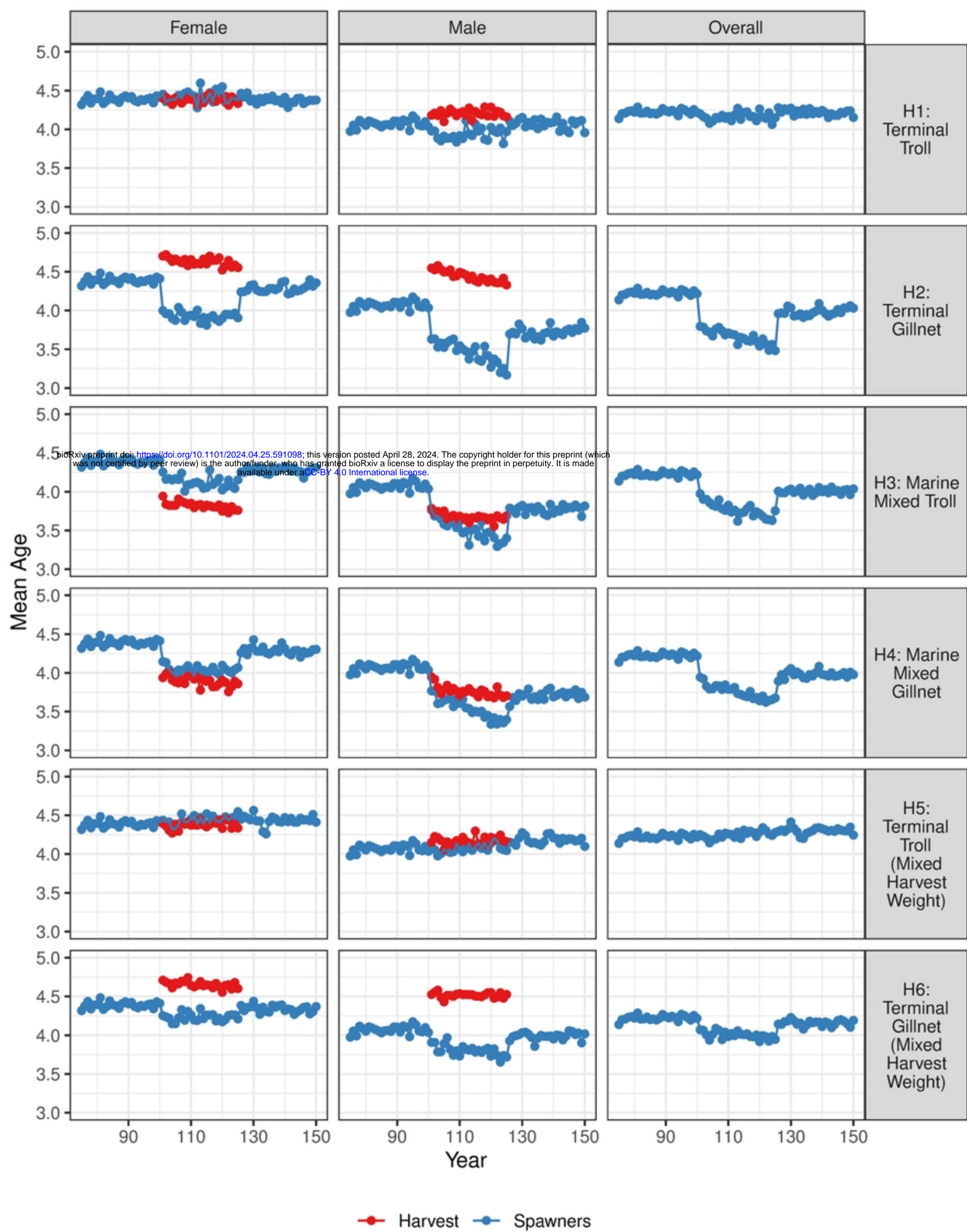
figure



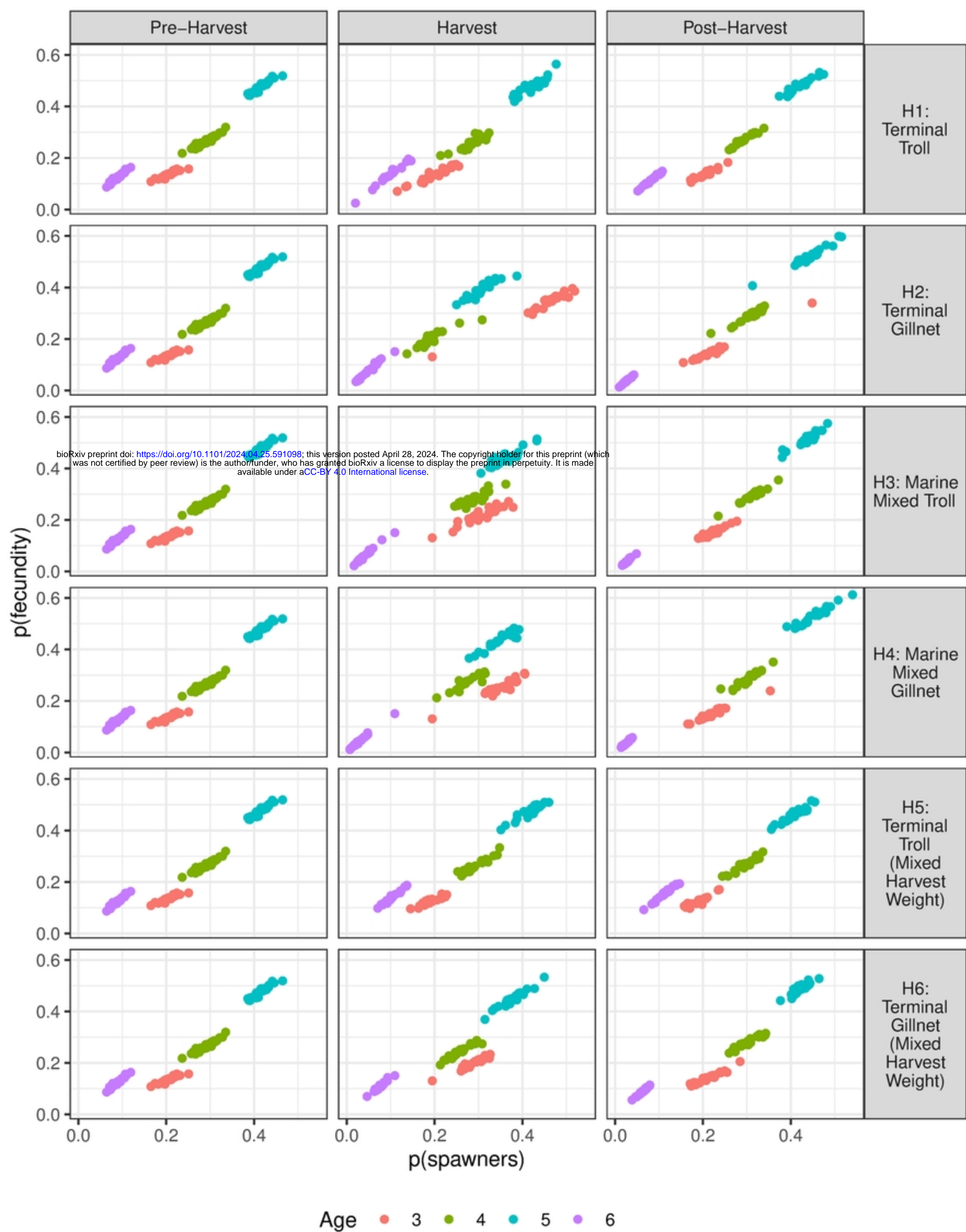
figure



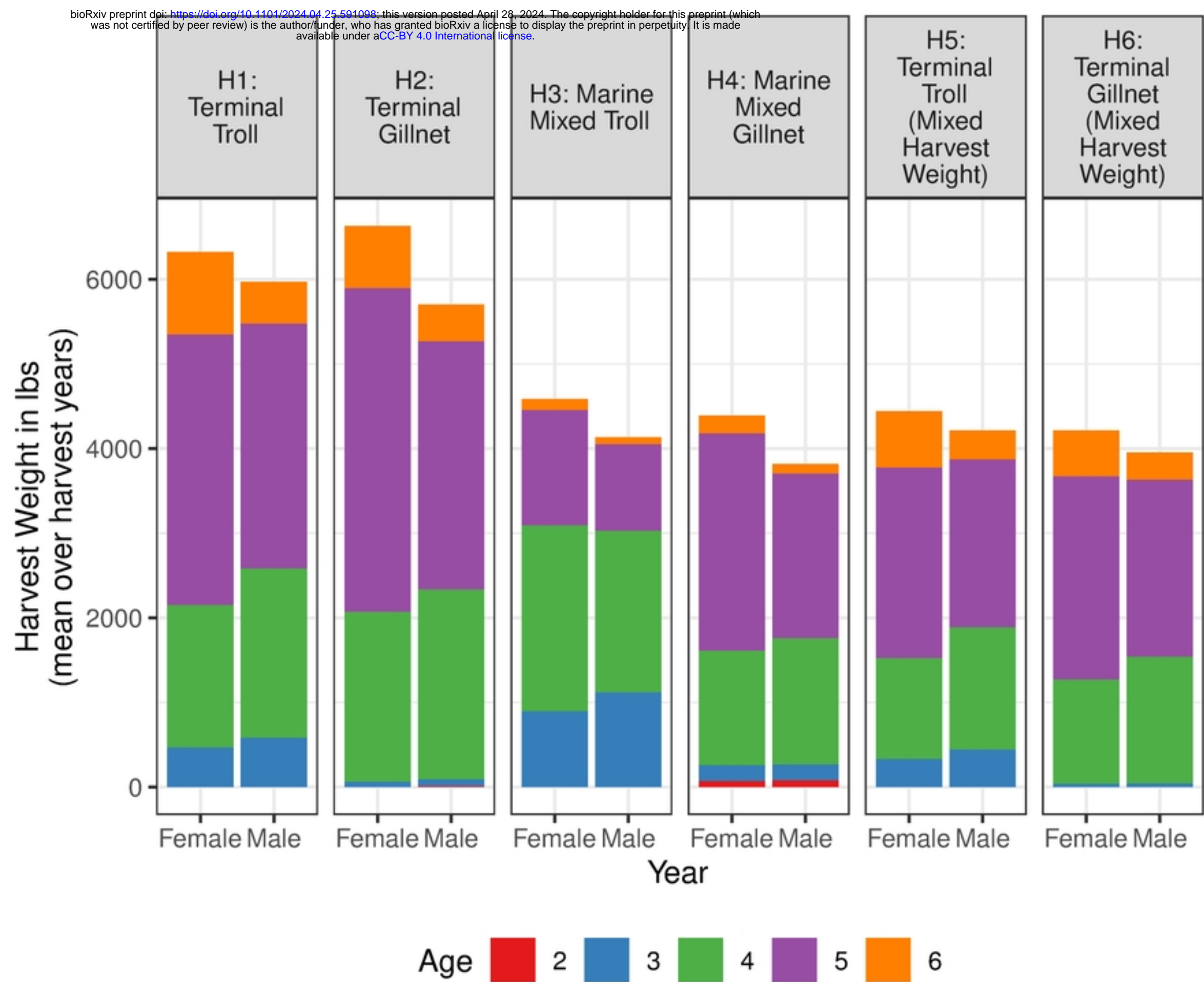
figure



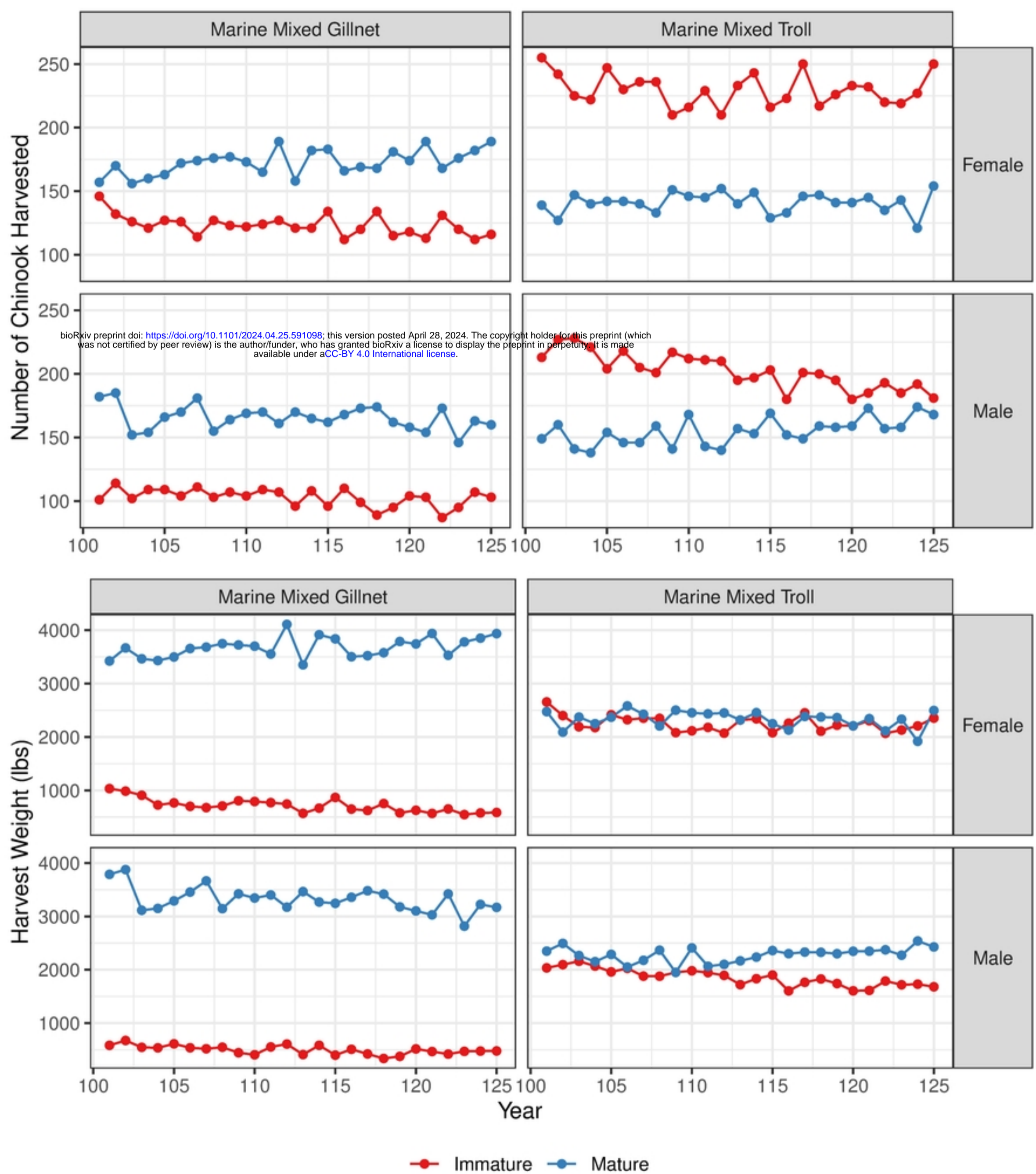
figure



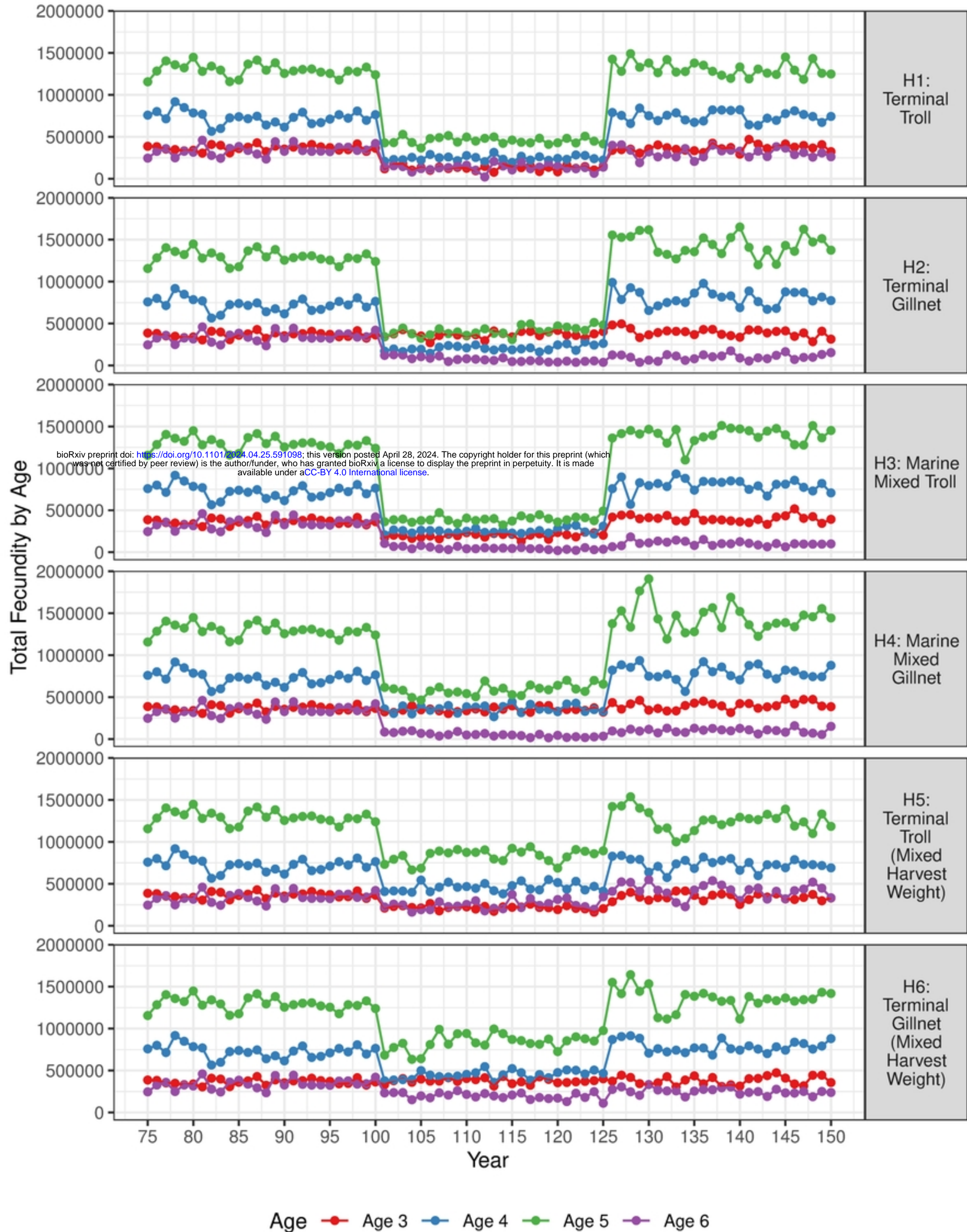
figure



figure



figure






figure

Received: 18 March 2024 | Revised: 6 May 2024 | Accepted: 24 May 2024

DOI: 10.1002/nafm.11019

ARTICLE

A new, standardized international Pacific Rim baseline for genetic stock identification (GSI) of Chinook Salmon

Donald M. Van Doornik¹  | Paul Moran² | Eric B. Rondeau³ | Krista M. Nichols² | Shawn R. Narum⁴ | Matthew R. Campbell⁵ | Anthony J. Clemento^{6,7} | John S. Hargrove⁸  | Jon E. Hess⁹  | Rebekah L. Horn⁴ | Lisa W. Seeb¹⁰ | Jeff J. Stephenson⁴ | Garrett J. McKinney¹¹

¹National Oceanic and Atmospheric Administration, National Marine Fisheries Service, Northwest Fisheries Science Center, Conservation Biology Division, Manchester, Washington, USA

²National Oceanic and Atmospheric Administration, National Marine Fisheries Service, Northwest Fisheries Science Center, Conservation Biology Division, Seattle, Washington, USA

³Fisheries and Oceans Canada, Pacific Biological Station, Nanaimo, British Columbia, Canada

⁴Columbia River Inter-Tribal Fish Commission, Hagerman Genetics Laboratory, Hagerman, Idaho, USA

⁵Idaho Department of Fish and Game, Eagle, Idaho, USA

⁶Institute of Marine Sciences' Fisheries Collaborative Program, University of California, Santa Cruz, Santa Cruz, California, USA

⁷National Oceanic and Atmospheric Administration, National Marine Fisheries Service, Southwest Fisheries Science Center, Fisheries Ecology Division, Santa Cruz, California, USA

⁸Pacific States Marine Fisheries Commission, Eagle, Idaho, USA

⁹Columbia River Inter-Tribal Fish Commission, Portland, Oregon, USA

¹⁰School of Aquatic and Fishery Sciences, University of Washington, Seattle, Washington, USA

¹¹Washington Department of Fish and Wildlife, Olympia, Washington, USA

Correspondence

Donald M. Van Doornik

Email: don.vandoornik@noaa.gov

Abstract

Objective: Genetic stock identification (GSI) can be an effective tool for fisheries management, but development of reference baselines for species with broad geographic distributions can be challenging. Mixed-stock fisheries for Chinook Salmon *Oncorhynchus tshawytscha* have utilized GSI analyses for decades with various genetic baselines, but these have largely become outdated with advances in technology that enable more efficient genotyping. Thus, our goals were to (1) create nested baselines of genotypic data for Chinook Salmon throughout their entire natural range using existing data from multiple sources and (2) evaluate the utility of those nested baselines to conduct accurate hierarchical GSI of mixture proportions or the stock identification of individual fish.

Methods: In this study, we compiled a large genetic baseline of single-nucleotide polymorphism (SNP) markers for 389 populations that encompass the entire geographic range of Chinook Salmon. We used cross validation and realistic mixture simulations to test the accuracy of the baseline in generating GSI estimates.

This is an open access article under the terms of the [Creative Commons Attribution](https://creativecommons.org/licenses/by/4.0/) License, which permits use, distribution and reproduction in any medium, provided the original work is properly cited.

© 2024 His Majesty the King in Right of Canada. Pacific States Marine Fisheries Commission and The Author(s). *North American Journal of Fisheries Management* published by Wiley Periodicals LLC on behalf of American Fisheries Society. Reproduced with the permission of the Minister of Fisheries and Oceans Canada. This article has been contributed to by U.S. Government employees and their work is in the public domain in the USA.

North American Journal of Fisheries Management. 2024;44:857–869.

wileyonlinelibrary.com/journal/nafm | 857



Result: We demonstrated that a multi-tiered assignment approach can provide high accuracy at both tier 1 (broad-scale, with three coastwide reporting groups; 97.8% mean accuracy) and tier 2 (fine-scale regional reporting groups; up to 97.7% mean accuracy) levels. Realistic mixture simulations showed that this multi-tiered approach can provide highly effective GSI results for several common mixed-stock fisheries applications in the Pacific Ocean.

Conclusion: This new SNP baseline and the multi-tiered assignment approach provide the most comprehensive rangewide GSI baseline for Chinook Salmon over any previous application and enable highly accurate estimates for GSI purposes.

KEYWORDS

Chinook Salmon, genetic stock identification, single-nucleotide polymorphisms

INTRODUCTION

Fisheries research and management often rely on the ability to identify the stock composition of aggregations of individuals in mixed-stock scenarios (e.g., high-seas, nearshore, or estuarine fisheries). A central tenet of modern fishery management is to allow for exploitation and impacts on healthy, abundant stocks but to protect sensitive populations, especially those afforded special protection under the U.S. Endangered Species Act, the Canadian Species at Risk Act, or the Convention on International Trade in Endangered Species of Wild Fauna and Flora. Stock identification of Pacific salmonids has been done primarily with coded wire tags (Bernard and Clark 1996), but as technology has evolved and conservation issues have become more acute, genetic stock identification (GSI) has also become widely implemented in stock management (Beacham et al. 2021, 2022b; Chang et al. 2021; McKinney et al. 2022). Genetic stock identification exploits genetic differences that exist among populations and lineages to identify and estimate proportions of each distinct group for specific fisheries and monitoring applications. In GSI analyses, fish of unknown origin are genotyped and then compared to a reference baseline of genotypic data collected from individuals of known origin. From that comparison, the unknown individuals are assigned to their most likely group of origin. The baseline data are comprised of multilocus genotypes of individual fish collected from representative populations that might contribute to the mixed-stock fishery. Populations are organized into genetic stocks or reporting groups, which are aggregated by factors such as genetic similarity, geographic location, or other management criteria. Genetic stock identification is most accurate when there is substantial genetic differentiation among the reporting groups (Clemento et al. 2014), and it can be used to estimate the stock proportions of a mixture or to estimate the stock of origin for individual fish.

Impact statement

A Chinook Salmon genetic stock identification baseline encompassing the species' entire range has broad applications in fishery management and harvest allocation as well as in basic research.

Genetic stock identification in diverse mixed-stock fisheries requires an extensive baseline representing all stocks that are likely to be encountered in the mixture of unknown fish. However, collecting those data is expensive and time consuming. The ability to combine regional data collected by multiple laboratories greatly facilitates baseline construction. This was done in the past, for several species of Pacific salmon *Oncorhynchus* spp., when microsatellite DNA loci were the genetic markers (loci) of choice (Seeb et al. 2007; Van Doornik et al. 2008; Stephenson et al. 2009). However, the process of combining data from multiple sources can be time consuming, as the data must be standardized to assure that all laboratories are collecting equivalent data (Moran et al. 2006). In addition, not all laboratories use the same genetic markers, as not all loci are informative for GSI across the entire range of a species. This has led agencies to collect data and assemble entire baselines for regional use, but those data are limited for broader application because distinct stocks from other regions are generally underrepresented or completely absent from local and regional baselines. This has become especially true with the present-day use of single-nucleotide polymorphism (SNP) loci, which have now become the genetic markers of choice for salmonid GSI given that SNP sequencing allows for the efficient genotyping of hundreds of loci simultaneously (Campbell et al. 2015).

In general, GSI estimates are more accurate when baselines include greater numbers of individuals and

loci and when baselines have a greater representation of populations within each reporting group (McKinney et al. 2020; Hargrove et al. 2023). However, there has not been an effort to create an interagency, standardized, rangewide GSI baseline of SNP data for Chinook Salmon *O. tshawytscha* despite initial efforts to transition from microsatellite to SNP baselines (e.g., Narum et al. 2008; Beacham et al. 2012). The Chinook Salmon is a highly valued species for commercial, recreational, and indigenous fisheries throughout its range. Several agencies have constructed GSI SNP baselines for Chinook Salmon, but they all vary in geographic coverage and in the SNP loci used (Templin et al. 2011; Warheit et al. 2013; Clemento et al. 2014; Larson et al. 2014; Hess et al. 2016; Meek et al. 2016; Barclay et al. 2019; Beacham et al. 2021).

Given the disparity in overlap among regional SNP baselines, we applied GSI in a two-tiered, hierarchical format to assemble and utilize multiple regional baselines. Hsu and Habicht (2024) developed a hierarchical model that assigns individuals to origin in a multi-step hierarchical framework, accounting for errors over levels of the hierarchy. A hierarchical approach first assigns (or fractionally allocates) an individual to a broadscale reporting group in a rangewide baseline, balancing the inclusion of the numbers of informative SNPs with the inclusion of individuals from representative stocks in broadly defined reporting groups. A second assignment is then made to a finer-scale reporting group by using one of several regional baselines depending upon the reporting group to which the fish was assigned during the first-tier analysis. Because the number of loci in common among sources is low, the first-tier baseline has fewer loci and fewer reporting groups but spans the entire natural range of Chinook Salmon. This tier of reporting groups represents very large geographical areas, which have well-documented genetic differentiation among them. The second tier of the hierarchical analysis utilizes region-specific baselines that contain more loci, more populations, and a greater number of finer-scale reporting groups within each region. This approach maximizes the use of available data and estimates the origin of fish accurately regardless of where they were caught or the stock from which they originated.

Thus, our goals were to (1) create nested baselines of genotypic data for Chinook Salmon throughout their entire natural range by using existing data from multiple sources and (2) evaluate the utility of those nested baselines for conducting accurate hierarchical GSI of mixture proportions or for the stock identification of individual fish.

METHODS

Baseline assembly

We compiled SNP data that were provided by the genetics laboratories of several different agencies (Table S1 available in the Supplement in the online version of this article). A small amount of the data was unpublished, whereas most of the data has appeared in previously published Chinook Salmon GSI baselines (Templin et al. 2011; Clemento et al. 2014; Larson et al. 2014; Hess et al. 2016; Barclay et al. 2019; McKinney et al. 2020; Beacham et al. 2021). We then determined which loci from those baselines overlapped with one another and with a panel of 299 SNP loci that are routinely used when genotyping Chinook Salmon (Table S2; Hess et al. 2016). Genotypes for these loci are determined by use of a probe-based assay, with different laboratories utilizing different genotyping platforms. Reported primer sequences for each data set were used to verify the identity of SNPs among laboratories and to standardize allele designations.

To create the tier 1 baseline, we included populations that spanned the entire range of Chinook Salmon from the Kamchatka Peninsula, Russia, to the Central Valley in California, United States. These populations were initially grouped together into three reporting groups from which we would expect very accurate GSI estimates (>95% accuracy) given the level of divergence that has been previously reported at this scale (Hecht et al. 2015): all populations north of the Columbia River (Northern), all populations within the Columbia River (Columbia), and all populations south of the Columbia River (Southern; Table S1). Previous genetic population structure SNP analyses have found that Chinook Salmon populations from the Columbia River are very distinct from other Chinook Salmon populations (Templin et al. 2011; Clemento et al. 2014; Beacham et al. 2021). This finding, along with the fact that the Columbia River is a significant source of Chinook Salmon and represents a major management group, led us to create our tier 1 groupings around the Columbia River. We found that having three tier 1 reporting groups provided a good balance between separating major genetic groups, which ensures highly accurate tier 1 assignments while minimizing the need to create a greater number of tier 2 baselines. For both the tier 1 and tier 2 baselines, we only included (1) populations with at least 20 individuals sampled and (2) individuals that had been genotyped successfully for at least 80% of the loci used in each baseline.

Each of the tier 2 baselines represented a smaller geographic area than the tier 1 baseline. Populations were grouped together into two different configurations of reporting groups. The first tier 2 configuration contained the

finest-scale reporting groups as outlined in the Genetic Analysis of Pacific Salmonids (GAPS) microsatellite baseline (Seeb et al. 2007). That baseline represents the most comprehensive and detailed GSI baseline of Chinook Salmon genetic data previously constructed, although it lacks the inclusion of any populations north and west of Southeast Alaska. For populations from those areas, we created reporting groups based upon previous studies (Templin et al. 2011; Beacham et al. 2021). We chose to consider this configuration not only because of its fine-scale reporting groups, but also because continuity in GSI assignments could be maintained for long-term projects that previously used the GAPS microsatellite baseline but have recently switched to SNPs.

The second reporting group configuration was driven by the data, optimizing the reporting groups in such a way that every reporting group had a minimum accuracy of 90%, as determined from leave-one-out simulations (see below). This was achieved by starting with the GAPS reporting groups and then combining geographically and genetically proximate groups with the largest number of misassignments among them that otherwise reduced accuracy to less than 90%.

Baseline testing

Leave-one-out cross validation was our primary means of evaluating the different configurations for both tier 1 and tier 2 baselines. A leave-one-out simulation is performed by removing one individual from the baseline, recalculating the baseline allele frequencies, and then assigning that individual to a reporting group as if its origin were unknown. This is repeated for every individual in the baseline, and the individual results are summed. Assignment accuracy to each reporting group (or population) can then be evaluated based upon how many individuals correctly assign to their reporting group of origin. This approach has been demonstrated as a robust way to evaluate a baseline because it provides unbiased estimates of GSI accuracy (Anderson et al. 2008). Leave-one-out simulations were conducted using the “self-assign” function in the R package rubias (Moran and Anderson 2019). Leave-one-out simulations provide a measure of the accuracy that can be expected when assigning individual fish to their region of origin.

To test our ability to make accurate estimates of “real-world” scenarios using these baselines, we simulated several different mixtures by removing multiple individuals from the baseline and treating them as a mixture, essentially doing a “leave-multiples-out” simulation. Whereas leave-one-out simulations are applicable to making assignments of individual fish to their region of origin, our real-world simulations tested the ability of the baseline to estimate stock proportions from a mixture

sample. We randomly removed individuals from specific reporting groups (no more than 20% of the total number of individuals in any single reporting group), in specific proportions, to create mixtures that represented real-world scenarios. To create these scenarios, we sought to duplicate the reporting group proportions as closely as we could for five different ocean-caught mixtures that have been reported in published studies. The five mixtures were sampled in the Bering Sea (Larson et al. 2013), off the coast of Southeast Alaska (Van Doornik et al. 2019), in the northern Georgia Strait (Beacham et al. 2021), off the Washington and Oregon coasts (Teel et al. 2015), and off the coast of California (Clemento et al. 2014). We estimated mixture proportions for the simulated mixtures and then compared the results to the true proportions. We configured our reporting groups to match those of the source publication, which mostly matched the GAPS reporting group configuration. Estimated mixture proportions were generated using the R package Ms.GSI (Hsu and Habicht 2024), which is a multistage algorithm that is specifically designed to make GSI assignments (both individual assignments and mixture proportions) using a two-tiered hierarchical approach. This method accounts for uncertainty in the tier 1 assignment before conducting the tier 2 assignment. For each simulated mixture, we ran five independent chains, each with 5000 iterations, the first 2500 of which were discarded as burn-in. Each mixture was simulated 10 times, and the results were then averaged.

RESULTS

Baseline description

We compiled a baseline consisting of 43,041 Chinook Salmon samples from 389 populations throughout the species' natural range (Figures 1–3; Table S1). These populations had 49 SNP loci in common, which we then used for our tier 1 baseline (Table S2). Substantially greater numbers of loci that were shared among sources could be used for our tier 2 baselines. For tier 2 regional baselines, the Northern, Columbia, and Southern baselines included 98, 178, and 88 loci, respectively (Table S2). All populations appearing in tier 1 were also in one of the tier 2 baselines, but not all populations in tier 2 were necessarily present in tier 1.

Leave-one-out simulations

At the tier 1 level, the leave-one-out assignments had a mean accuracy of 97.8%. The accuracy at the tier 2 level

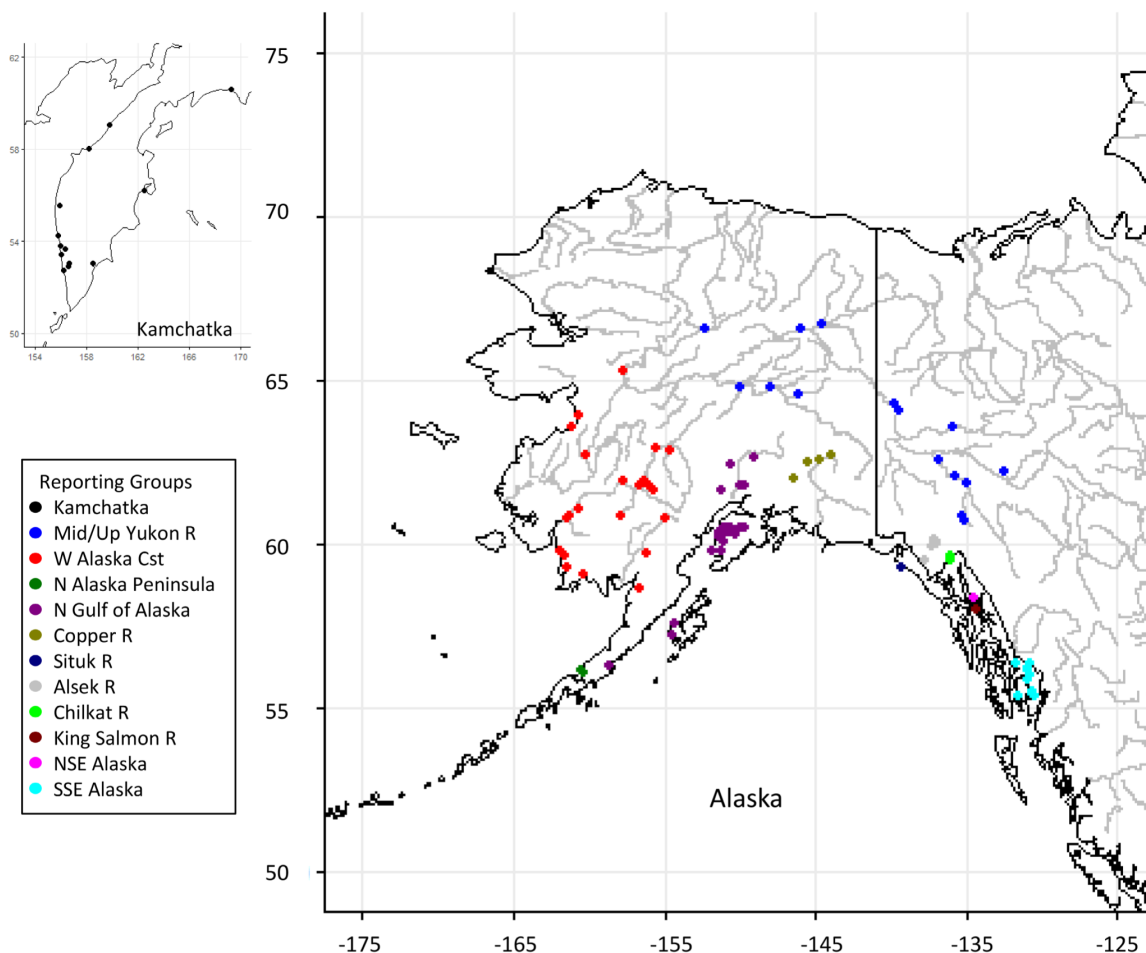


FIGURE 1 Map of sample locations for Chinook Salmon populations in Russia and Alaska. Cst, coast; R, River; Up, Upper.

varied depending upon the reporting group configuration (Figures 4 and 5). When we used the GAPS reporting group configuration (Seeb et al. 2007), the mean accuracy rate was 90.5%, with all but 5 of the 49 reporting groups having accuracy rates greater than 80% (Figure 4). We also created an optimized set of reporting groups such that each reporting group had an accuracy greater than 90% (mean = 97.6%; Figure 5). This configuration maintained many but not all of the conservation and management units of interest. For example, when using this configuration, we lost the ability to discriminate (1) Southeast Alaska fish from northern/central British Columbia fish or (2) mid/upper Columbia River fish from Snake River fish.

Simulated mixtures

The simulated mixtures that we created also indicated that we can expect accurate estimates from these baselines

(Figure 6). Each of the simulated mixtures returned very accurate estimates for almost every reporting group. For the only instances in which the true value was not contained within our estimated 95% confidence intervals (the lower/mid-Columbia River fall group and the Snake River fall group in the Southeast Alaska mixture), the true values were less than 5%. All of the major contributing groups in each mixture were within the 95% confidence intervals of our estimates.

DISCUSSION

We successfully consolidated and standardized a new rangewide genetics reference baseline for Chinook Salmon in the North Pacific Ocean. Because of the multi-laboratory, international scale of this endeavor, not all populations included the same suite of genetic markers. We demonstrated here that the hierarchical, multistage

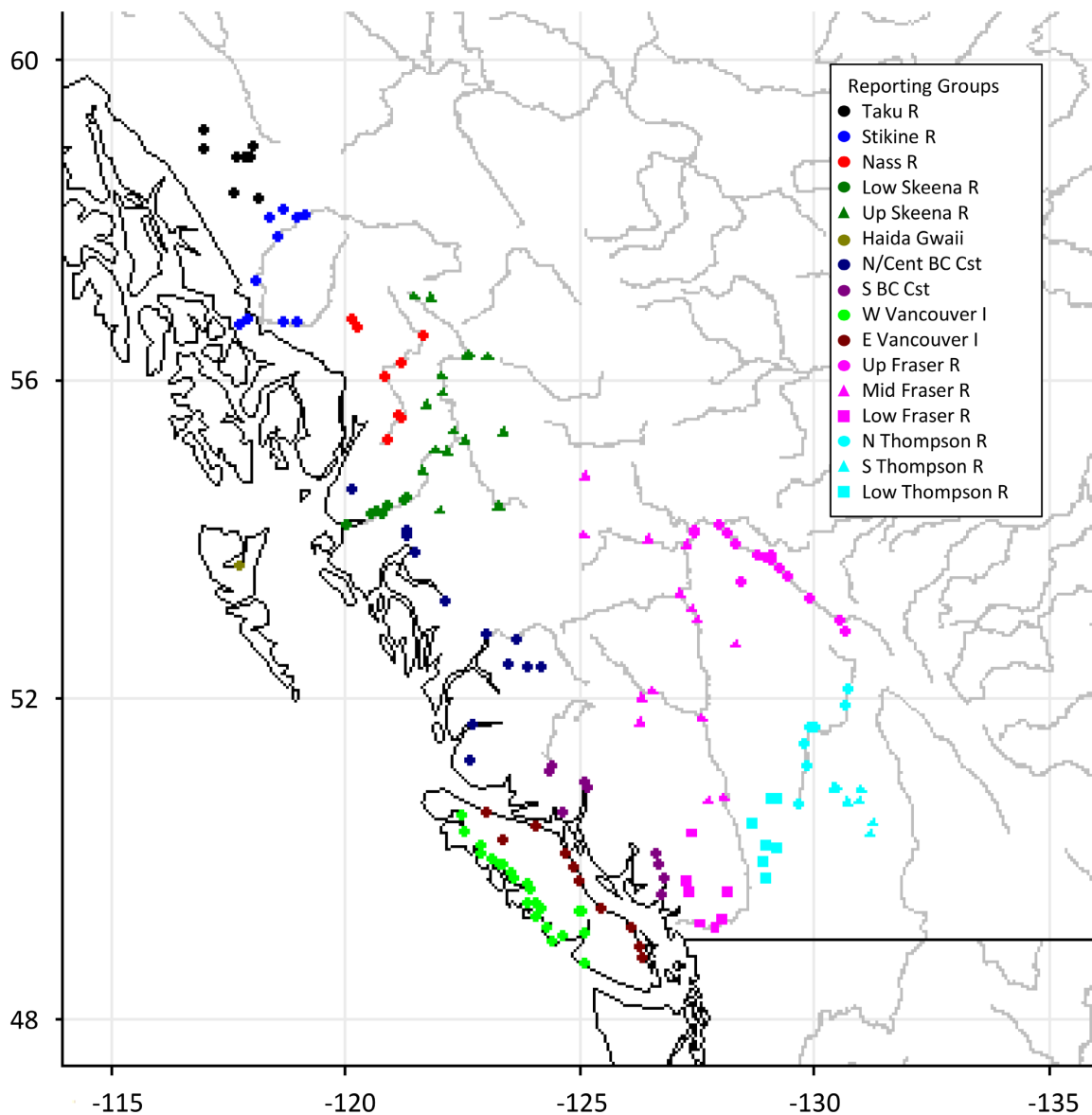


FIGURE 2 Map of sample locations for Chinook Salmon populations in British Columbia. BC, British Columbia; Cent, Central; Cst, coast; I, Island; Low, Lower; R, River; Up, Upper.

mixture modeling and individual assignment method that Hsu and Habicht (2024) applied to northern populations are also suited to more diverse genetic mixtures in southern fisheries. Some harvest fisheries and incidental bycatch of Chinook Salmon on the central and southern west coast of North America take fish from southern British Columbia to the Central Valley of California (Sabal et al. 2023). Moreover, some Alaskan and British Columbian fisheries take fish from U.S. West Coast populations (Winther 2018; Shedd 2019; Beacham et al. 2022a). With Chinook Salmon, it is important to use a baseline

that spans their entire range because fish can be collected thousands of kilometers away from their natal rivers (Larson et al. 2013; Van Doornik et al. 2019). The current analysis shows that this hierarchical method will benefit management and conservation in many of the fisheries that take Chinook Salmon from diverse geographical locations, which are likely represented by different baseline loci.

Our leave-one-out results, which were explored through three distinct reporting group configurations, revealed the delicate balance between accuracy and resolution for

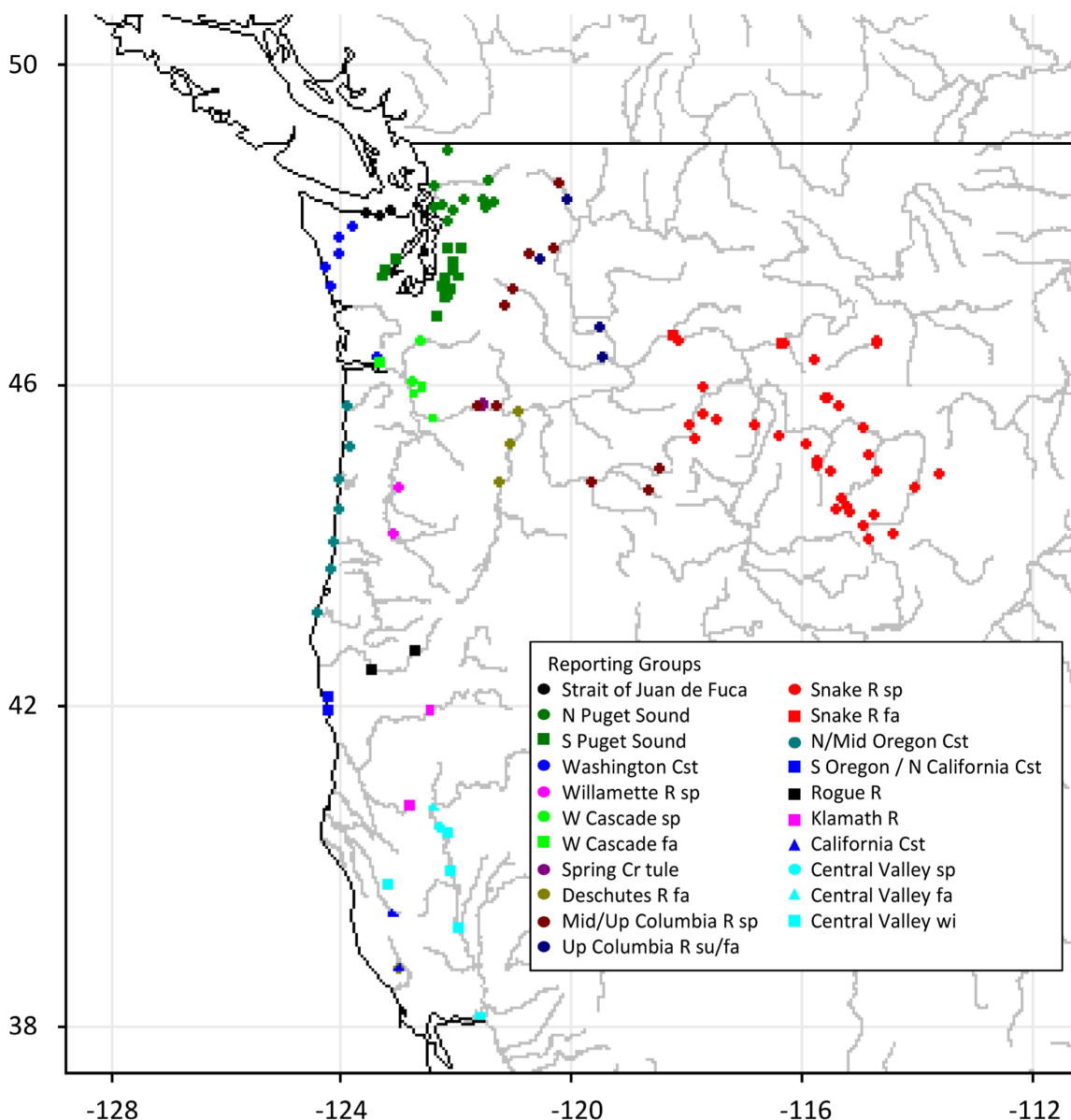


FIGURE 3 Map of sample locations for Chinook Salmon populations in Washington, Oregon, and California. Cr, Creek; Cst, coast; fa, fall run; R, River; sp, spring run; su, summer run; Up, Upper; wi, winter run.

GSI applications and pinpointed the areas of greatest and lowest genetic differentiation among populations. The variety in reporting group configurations allows for the selection of resolution or accuracy levels based on specific study or management goals. For example, the optimized configuration might not be ideal for certain management needs, especially in regions where reporting groups span extensive geographic areas (e.g., northern/central British Columbia coast/Southeast Alaska) and where the

level of accuracy that we achieved was inadequate. The 98 loci that we employed in our tier 2 Northern baseline were likely insufficient to provide resolution among the desired reporting groups in this area. Employing a tier 2 baseline with more loci could offer superior resolution in this case, as has been done in British Columbia (Beacham et al. 2021). In areas like the mid and upper Columbia River and the Snake River, historical stock transfers have eroded genetic distinctiveness among these groups

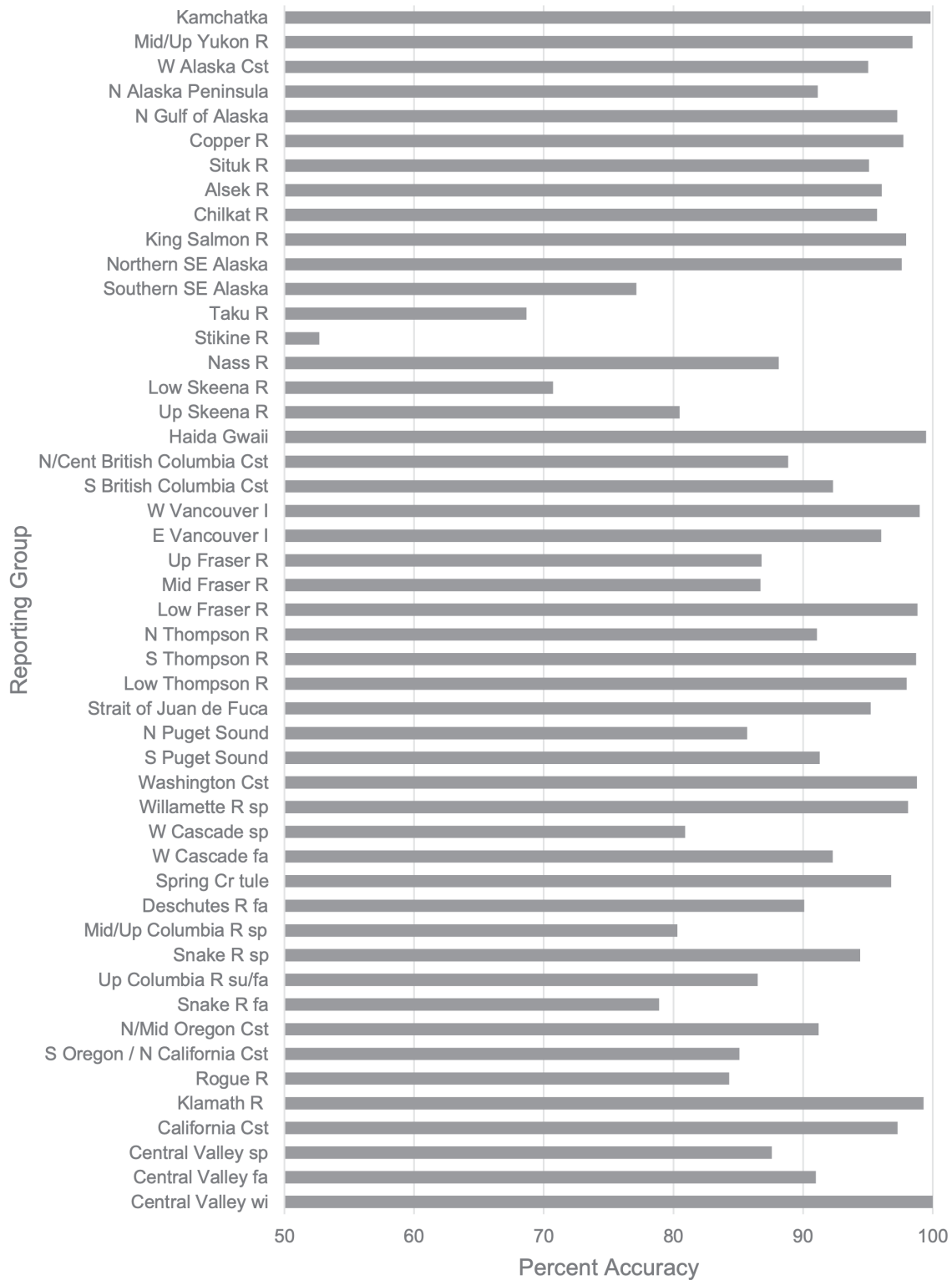


FIGURE 4 Accuracy of leave-one-out simulations for the Genetic Analysis of Pacific Salmonids reporting group configuration. Cent, Central; Cr, Creek; Cst, coast; fa, fall run; I, Island; Low = Lower; R, River; sp, spring run; su, summer run; Up, Upper; wi, winter run.

15488675, 2024, 4, Downloaded from https://afspubs.onlinelibrary.wiley.com/doi/10.1002/nafm.11019. By American Fisheries Society, Wiley Online Library on [04/09/2024]. See the Terms and Conditions (https://onlinelibrary.wiley.com/terms-and-conditions) on Wiley Online Library for rules of use; OA articles are governed by the applicable Creative Commons License

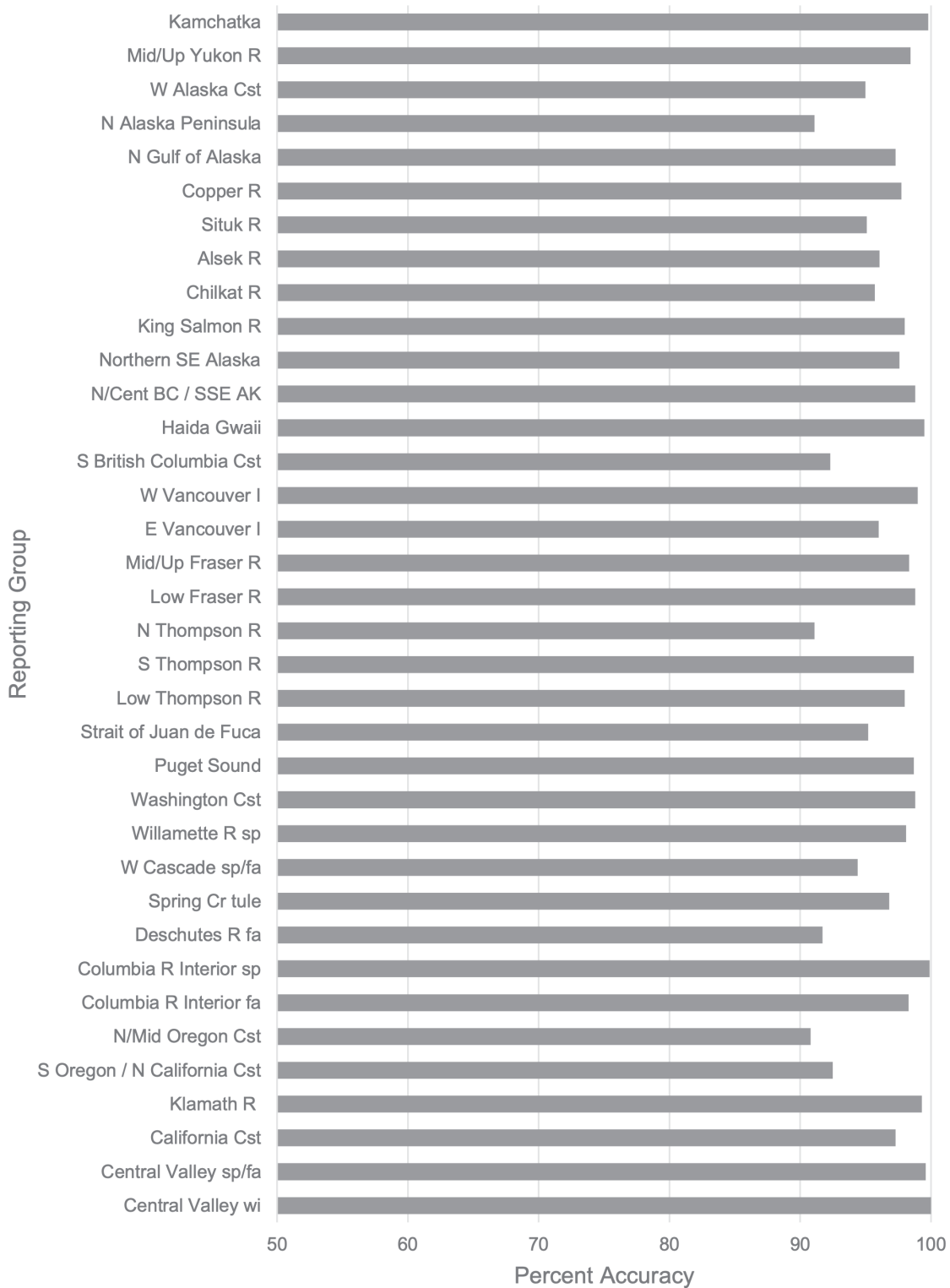


FIGURE 5 Accuracy of leave-one-out simulations for the optimized Chinook Salmon reporting group configuration. AK, Alaska; BC, British Columbia; Cent, Central; Cr, Creek; Cst, coast; fa, fall run; I, Island; Low=Lower; R, River; sp, spring run; Up, Upper; wi, winter run.

15488675, 2024, 4, Downloaded from https://afspubs.onlinelibrary.wiley.com/doi/10.1002/nafm.11019. By American Fisheries Society, Wiley Online Library on [04/09/2024]. See the Terms and Conditions (https://onlinelibrary.wiley.com/terms-and-conditions) on Wiley Online Library for rules of use; OA articles are governed by the applicable Creative Commons License

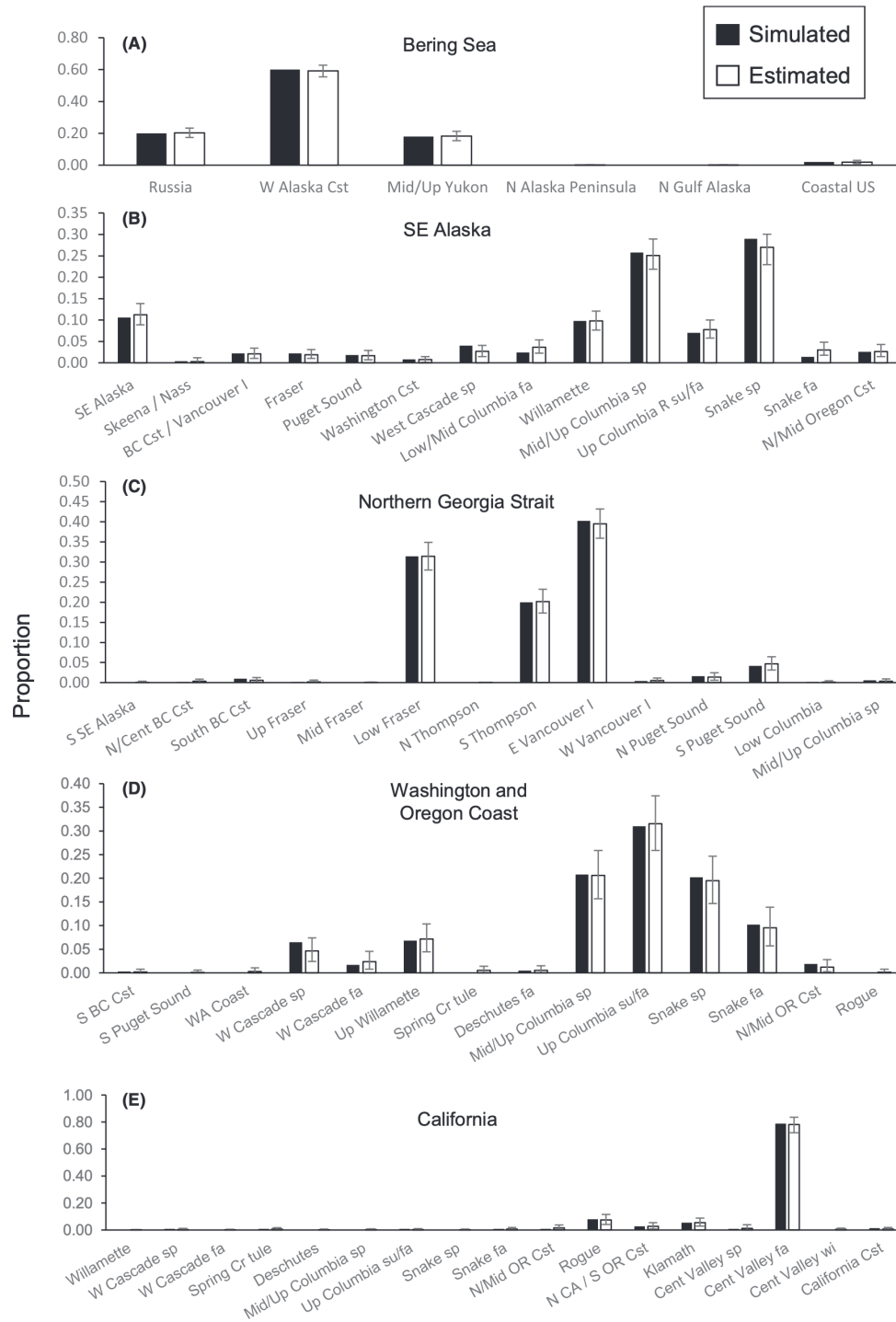


FIGURE 6 Mixture proportion estimates (with 95% confidence intervals) for simulated real-world fishery mixtures of Chinook Salmon. Simulated proportions were similar to the mixture proportions reported by Larson et al. (2013) for the (A) Bering Sea mixture; Van Doornik et al. (2019) for the (B) Southeast Alaska mixture; Beacham et al. (2021) for the (C) northern Georgia Strait mixture; Teel et al. (2015) for the (D) Washington and Oregon coast mixture; and Clemento et al. (2014) for the (E) California mixture. BC, British Columbia; CA, California; Cent, Central; Cr, Creek; Cst, coast; fa, fall run; I, Island; Low = Lower; OR, Oregon; R, River; sp, spring run; su, summer run; Up, Upper; WA, Washington; wi, winter run.

15488675, 2024, 4, Downloaded from https://afspubs.onlinelibrary.wiley.com/doi/10.1002/nafm.11019. By American Fisheries Society, Wiley Online Library on [04/09/2024]. See the Terms and Conditions (https://onlinelibrary.wiley.com/terms-and-conditions) on Wiley Online Library for rules of use; OA articles are governed by the applicable Creative Commons License

(Myers et al. 1998; Narum et al. 2010), but they are still managed separately. In this instance, the combination of parentage-based tagging (PBT) with GSI can significantly improve the accuracy of hatchery-origin fish assignment (Hargrove et al. 2021). Currently, Chinook Salmon management in British Columbia (Beacham et al. 2022a) and the Columbia River (Hargrove et al. 2021; Hess et al. 2024) benefits from the use of PBT baselines.

The results of our real-world simulated mixtures demonstrated the utility of these baselines throughout many Chinook Salmon management areas. Although leave-one-out simulations are highly informative for estimating assignment accuracy, GSI simulations comprised of mixtures that one would expect to encounter in real management situations provided a better indication of the performance that can be expected in practical applications with the baselines. By using geographically diverse fisheries with very different stock compositions, we demonstrated the broad utility of this multi-tier baseline. We expect that this new community resource will find application in fishery management and harvest allocation as well as in basic research on subjects such as stock-specific estuarine habitat use (Weitkamp et al. 2022), migration patterns (Teel et al. 2015), and marine mammal trophic ecology (Hanson et al. 2021).

The tier 1 baseline that we constructed holds great value for the wider fisheries management community. Without previous coordination among the agencies that conduct salmonid GSI, SNP baselines have been created by individual agencies focusing on their own specific locations and priorities (e.g., Templin et al. 2011; Clemento et al. 2014; Hess et al. 2016; Meek et al. 2016; Barclay et al. 2019; Beacham et al. 2021). None of these baselines comprehensively encompasses the entire range of Chinook Salmon, which could lead to misidentification when fish that are present in a mixture come from outside of those baseline regions. By implementing the multistage techniques outlined in this work and by Hsu and Habicht (2024), agencies can continue to utilize their established loci and baselines as the second-stage reference while incorporating our tier 1 baseline in the first stage—provided they are genotyping most (if not all) of the 49 loci contained within tier 1. This approach assures that occasional fish coming from unexpected regions are identified correctly. Although we divided the tier 1 baseline into three reporting groups, other researchers have the flexibility to create more or fewer divisions as they see fit for their specific needs.

Eventually, the expectation is that Pacific salmon genetics laboratories will converge on a common set of more than 300 molecular markers. This set could include some combination of SNPs and microhaplotypes, which are combinations of phased SNPs that yield multistate characters (Moran et al. 1997), providing an

exponential increase in power for GSI and mixture analysis (McKinney et al. 2017). These panels of markers will include neutral and putatively adaptive SNPs and haplotypes (Willis et al. 2021) as well as markers that are optimized for parentage analysis (Steele et al. 2019). However, convergence on common marker panels has been slow. We believe that our internationally standardized baseline will serve as a valuable resource until a more comprehensive reference data set becomes available for mixed-stock fishery analysis.

ACKNOWLEDGMENTS

We thank the countless agency, department, First Nations, and Native American tribal biologists whose efforts on the ground collecting genetic samples made this work possible. The present work was supported in part by National Oceanic and Atmospheric Administration Temporary Funds through the Cooperative Research Program 2021–2022. We also thank Mike Ford, Sara Gilk-Baumer, Bobby Hsu, and Kyle Shedd for their reviews of previous drafts of the manuscript. The inclusion of data provided by the Alaska Department of Fish and Game does not necessarily indicate that agency's endorsement or agreement with the statements, findings, conclusions, and recommendations presented in this article.

CONFLICT OF INTEREST STATEMENT

The authors declare that there is no conflict of interest.

DATA AVAILABILITY STATEMENT

Files formatted for use in Ms.GSI or rubias are available in Dryad (<https://doi.org/10.5061/dryad.dz08kps5b>). In addition, genotypes and metadata are available at [FishGen.net](https://fishgen.net) (data set identification number 20240340).


ETHICS STATEMENT

This research meets the American Fisheries Society's *Ethical Guidelines for Publication of Fisheries Research* (<https://fisheries.org/books-journals/writing-tools/authorship-guidelines/>).

ORCID

Donald M. Van Doornik  <https://orcid.org/0009-0007-3541-8836>

John S. Hargrove  <https://orcid.org/0000-0002-8643-7822>

Jon E. Hess  <https://orcid.org/0000-0002-3643-202X>

REFERENCES

- Anderson, E. C., Waples, R. S., & Kalinowski, S. T. (2008). An improved method for predicting the accuracy of genetic stock identification. *Canadian Journal of Fisheries and Aquatic Sciences*, 65(7), 1475–1486. <https://doi.org/10.1139/F08-049>

- Barclay, A. W., Evenson, D. F., & Habicht, C. (2019). *New genetic baseline for upper Cook Inlet Chinook Salmon allows for the identification of more stocks in mixed stock fisheries: 413 loci and 67 populations* (Fishery Manuscript Series No. 19-06). Alaska Department of Fish and Game. <https://www.adfg.alaska.gov/FedAidPDFs/FMS19-06.pdf>
- Beacham, T. D., Jonsen, K., Sutherland, B., Ramshaw, B., & Rondeau, E. B. (2022a). Parentage-based tagging and genetic stock identification applied to assessment of mixed-stock fisheries and hatchery broodstocks for Chinook Salmon in British Columbia, Canada. *Fisheries Research*, 253, Article 106369. <https://doi.org/10.1016/j.fishres.2022.106369>
- Beacham, T. D., Jonsen, K., Sutherland, B. J. G., Lynch, C., & Rondeau, E. B. (2022b). Assessment of mixed-stock fisheries and hatchery broodstocks for Coho Salmon in British Columbia, Canada via parentage-based tagging and genetic stock identification. *Fisheries Research*, 245, Article 106136. <https://doi.org/10.1016/j.fishres.2021.106136>
- Beacham, T. D., Jonsen, K., & Wallace, C. (2012). A comparison of stock and individual identification for Chinook Salmon in British Columbia provided by microsatellites and single-nucleotide polymorphisms. *Marine and Coastal Fisheries: Dynamics, Management, and Ecosystem Science*, 4(1), 1–22. <https://doi.org/10.1080/19425120.2011.649391>
- Beacham, T. D., Wallace, C., Jonsen, K., Sutherland, B. G., Gummer, C., & Rondeau, E. B. (2021). Estimation of conservation unit and population contribution to Chinook Salmon mixed-stock fisheries in British Columbia, Canada, using direct DNA sequencing for single nucleotide polymorphisms. *Canadian Journal of Fisheries and Aquatic Sciences*, 78(10), 1422–1434. <https://doi.org/10.1139/cjfas-2020-0462>
- Bernard, D. R., & Clark, J. E. (1996). Estimating salmon harvest with coded-wire tags. *Canadian Journal of Fisheries and Aquatic Sciences*, 53(10), 2323–2332. <https://doi.org/10.1139/f96-182>
- Campbell, N., Harmon, S., & Narum, S. R. (2015). Genotyping in thousands by sequencing (GT-seq): A low cost, high-throughput, targeted SNP genotyping method. *Molecular Ecology Resources*, 15, 855–867. <https://doi.org/10.1111/1755-0998.12357>
- Chang, S. L., Ward, H. G. M., & Russello, M. A. (2021). Genotyping-in-thousands by sequencing panel development and application to inform kokanee salmon (*Oncorhynchus nerka*) fisheries management at multiple scales. *PLOS ONE*, 16(12), Article e0261966. <https://doi.org/10.1371/journal.pone.0261966>
- Clemento, A. J., Crandall, E. D., & Garza, J. C. (2014). Evaluation of a single nucleotide polymorphism baseline for genetic stock identification of Chinook Salmon (*Oncorhynchus tshawytscha*) in the California Current large marine ecosystem. *U.S. National Marine Fisheries Service Fishery Bulletin*, 112(2–3), 112–130. <https://doi.org/10.7755/FB.112.2-3.2>
- Hanson, M. B., Emmons, C. K., Ford, M. J., Everett, M., Parsons, K., Park, L. K., Hempelmann, J., Van Doornik, D. M., Schorr, G. S., Jacobsen, J. K., Sears, M. F., Sears, M. S., Sneva, J. G., Baird, R. W., & Barre, L. (2021). Endangered predators and endangered prey: Seasonal diet of southern resident killer whales. *PLOS ONE*, 16(3), Article e0247031. <https://doi.org/10.1371/journal.pone.0247031>
- Hargrove, J. S., Camacho, C. A., Schrader, W. C., Powell, J. H., Delomas, T. A., Hess, J. E., Narum, S. R., & Campbell, M. R. (2021). Parentage-based tagging improves escapement estimates for ESA-listed adult Chinook Salmon and steelhead in the Snake River basin. *Canadian Journal of Fisheries and Aquatic Sciences*, 78(4), 349–360. <https://doi.org/10.1139/cjfas-2020-0152>
- Hargrove, J. S., Delomas, T. A., Powell, J. H., Hess, J. E., Narum, S. R., & Campbell, M. R. (2023). Efficient population representation with more genetic markers increases performance of a steelhead (*Oncorhynchus mykiss*) genetic stock identification baseline. *Evolutionary Applications*, 17, Article e13610. <https://doi.org/10.1111/eva.13610>
- Hecht, B. C., Matala, A. P., Hess, J. E., & Narum, S. R. (2015). Environmental adaptation in Chinook Salmon (*Oncorhynchus tshawytscha*) throughout their North American range. *Molecular Ecology*, 24(22), 5573–5595. <https://doi.org/10.1111/mec.13409>
- Hess, J. E., Campbell, N. R., Matala, A. P., Hasselman, D. J., & Narum, S. R. (2016). *Genetic assessment of Columbia River stocks, 4/1/2014 - 3/31/2015* (Annual Report, Project 2008-907-00). Bonneville Power Administration. <https://critfc.org/wp-content/uploads/2021/08/16-03.pdf>
- Hess, J. E., Deacy, B. M., Rub, M. W., Van Doornik, D. M., Whiteaker, J. M., Fryer, J. K., & Narum, S. R. (2024). Visual and genetic stock identification of a test fishery to forecast Columbia River spring Chinook Salmon stocks two weeks into the future. *Evolutionary Applications*, 17, Article e13667. <https://doi.org/10.1111/eva.13667>
- Hsu, B., & Habicht, C. (2024). Harnessing the power of regional baselines for broad-scale genetic stock identification: A multistage, integrated, and cost-effective approach. *Evolutionary Applications*, 17, Article e13621. <https://doi.org/10.1111/eva.13621>
- Larson, W. A., Seeb, J. E., Pascal, C. E., Templin, W. D., & Seeb, L. W. (2014). Single-nucleotide polymorphisms (SNPs) identified through genotyping-by-sequencing improve genetic stock identification of Chinook Salmon (*Oncorhynchus tshawytscha*) from western Alaska. *Canadian Journal of Fisheries and Aquatic Sciences*, 71(5), 698–708. <https://doi.org/10.1139/cjfas-2013-0502>
- Larson, W. A., Utter, F. M., Myers, K. W., Templin, W. D., Seeb, J. E., Guthrie, C. M., Bugaev, A. V., & Seeb, L. W. (2013). Single-nucleotide polymorphisms reveal distribution and migration of Chinook Salmon (*Oncorhynchus tshawytscha*) in the Bering Sea and North Pacific Ocean. *Canadian Journal of Fisheries and Aquatic Sciences*, 70(1), 128–141. <https://doi.org/10.1139/cjfas-2012-0233>
- McKinney, G. J., Barry, P. D., Pascal, C., Seeb, J. E., Seeb, L. W., & McPhee, M. V. (2022). A new genotyping-in-thousands-by-sequencing single nucleotide polymorphism panel for mixed-stock analysis of Chum Salmon from coastal western Alaska. *North American Journal of Fisheries Management*, 42(5), 1134–1143. <https://doi.org/10.1002/nafm.10805>
- McKinney, G. J., Pascal, C. E., Templin, W. D., Gilk-Baumer, S. E., Dann, T. H., Seeb, L. W., & Seeb, J. E. (2020). Dense SNP panels resolve closely related Chinook Salmon populations. *Canadian Journal of Fisheries and Aquatic Sciences*, 77(3), 451–461. <https://doi.org/10.1139/cjfas-2019-0067>
- Meek, M. H., Baerwald, M. R., Stephens, M. R., Goodbla, A., Miller, M. R., Tomalty, K. M. H., & May, B. (2016). Sequencing improves our ability to study threatened migratory species: Genetic population assignment in California's Central Valley Chinook Salmon. *Ecology and Evolution*, 6, 7706–7716. <https://doi.org/10.1002/ece3.2493>
- Moran, B. M., & Anderson, E. C. (2019). Bayesian inference from the conditional genetic stock identification model. *Canadian*

- Journal of Fisheries and Aquatic Sciences*, 76(4), 551–560. <https://doi.org/10.1139/cjfas-2018-0016>
- Moran, P., Dightman, D. A., Waples, R. S., & Park, L. K. (1997). PCR-RFLP analysis reveals substantial population-level variation in the introns of Pacific salmon (*Oncorhynchus* spp.). *Molecular Marine Biology and Biotechnology*, 6(4), 315–327.
- Moran, P., Teel, D. J., LaHood, E. S., Drake, J., & Kalinowski, S. (2006). Standardising multi-laboratory microsatellite data in Pacific salmon: An historical view of the future. *Ecology of Freshwater Fish*, 15, 597–605. <https://doi.org/10.1111/j.1600-0633.2006.00201.x>
- Myers, J. M., Kope, R. G., Bryant, G. J., Teel, D., Lierheimer, L. J., Wainwright, T. C., Grant, W. S., Waknitz, F. W., Neely, K., Lindley, S. T., & Waples, R. S. (1998). *Status review of Chinook Salmon from Washington, Idaho, Oregon, and California* (Technical Memorandum NMFS-NWFSC-35). National Oceanic and Atmospheric Administration.
- Narum, S. R., Banks, M., Beacham, T. D., Bellinger, M. R., Campbell, M. R., Dekoning, J., Elz, A., Guthrie, C. M., Kozfkay, C., Miller, K. M., Moran, P., Phillips, R., Seeb, L. W., Smith, C. T., Warheit, K., Young, S. F., & Garza, J. C. (2008). Differentiating salmon populations at broad and fine geographical scales with microsatellites and single nucleotide polymorphisms. *Molecular Ecology*, 17(15), 3464–3477. <https://doi.org/10.1111/j.1365-294X.2008.03851.x>
- Narum, S. R., Hess, J. E., & Matala, A. P. (2010). Examining genetic lineages of Chinook Salmon in the Columbia River basin. *Transactions of the American Fisheries Society*, 139(5), 1465–1477. <https://doi.org/10.1577/T09-150.1>
- Sabal, M. C., Richerson, K., Moran, P., Levi, T., Tuttle, V. J., & Banks, M. (2023). Warm oceans exacerbate Chinook Salmon bycatch in the Pacific Hake fishery driven by thermal and diel depth-use behaviours. *Fish and Fisheries*, 24(6), 910–923. <https://doi.org/10.1111/faf.12775>
- Seeb, L. W., Antonovich, A., Banks, A. A., Beacham, T. D., Bellinger, A. R., Blankenship, S. M., Campbell, A. R., Decovich, N. A., Garza, J. C., Guthrie, C. M., Lundrigan, T. A., Moran, P., Narum, S. R., Stephenson, J. J., Supernault, K. J., Teel, D. J., Templin, W. D., Wenburg, J. K., Young, S. E., & Smith, C. T. (2007). Development of a standardized DNA database for Chinook Salmon. *Fisheries*, 32(11), 540–552. [https://doi.org/10.1577/1548-8446\(2007\)32\[540:DOASDD\]2.0.CO;2](https://doi.org/10.1577/1548-8446(2007)32[540:DOASDD]2.0.CO;2)
- Shedd, K. (2019). *Origins of Chinook Salmon harvested in Southeast Alaska fisheries, 2019* (Report N19-I09A). Pacific Salmon Commission.
- Steele, C. A., Hess, M., Narum, S., & Campbell, M. (2019). Parentage-based tagging: Reviewing the implementation of a new tool for an old problem. *Fisheries*, 44(9), 412–422. <https://doi.org/10.1002/fsh.10260>
- Stephenson, J. J., Campbell, M. R., Hess, J. E., Kozfkay, C., Matala, A. P., McPhee, M. V., Moran, P., Narum, S. R., Paquin, M. M., Schlei, O., Small, M. P., Van Doornik, D. M., & Wenburg, J. K. (2009). A centralized model for creating shared, standardized, microsatellite data that simplifies inter-laboratory collaboration. *Conservation Genetics*, 10(4), 1145–1149. <https://doi.org/10.1007/s10592-008-9729-4>
- Teel, D. J., Burke, B. J., Kuligowski, D. R., Morgan, C. A., & Van Doornik, D. M. (2015). Genetic identification of Chinook Salmon: Stock-specific distributions of juveniles along the Washington and Oregon coasts. *Marine and Coastal Fisheries: Dynamics, Management, and Ecosystem Science*, 7(1), 274–300. <https://doi.org/10.1080/19425120.2015.1045961>
- Templin, W. D., Seeb, J. E., Jasper, J. R., Barclay, A. W., & Seeb, L. W. (2011). Genetic differentiation of Alaska Chinook Salmon: The missing link for migratory studies. *Molecular Ecology Resources*, 11, 226–246. <https://doi.org/10.1111/j.1755-0998.2010.02968.x>
- Van Doornik, D. M., Banks, M., Garza, J. C., Gilbert, L., Kassler, T., LaHood, E., Lewis, C., Moran, P., Theriault, V., Warheit, K., & Wenburg, J. (2008). *Allele ladder-based standardization of existing Coho Salmon microsatellite data and implementation in the GAPS database* (Project SF-2008-I-4). Pacific Salmon Commission Southern Boundary Restoration & Enhancement Fund. <https://swfsc-publications.fisheries.noaa.gov/publications/CR/2008/2008VanDoornik.pdf>
- Van Doornik, D. M., Beckman, B. R., Moss, J. H., Strasburger, W. W., & Teel, D. T. (2019). Stock specific relative abundance of Columbia River juvenile Chinook Salmon off the Southeast Alaska coast. *Deep Sea Research Part II: Topical Studies in Oceanography*, 165, 322–328. <https://doi.org/10.1016/j.dsr2.2019.05.008>
- Warheit, K. I., Seeb, L., Templin, W. D., & Seeb, J. E. (2013). *Moving GSI into the next decade: SNP coordination for Pacific Salmon Treaty fisheries* (Report N10-8). Pacific Salmon Commission.
- Weitkamp, L. A., Beckman, B. R., Van Doornik, D. M., Munguia, A., Hunsicker, M., & Journey, M. (2022). Life in the fast lane: Feeding and growth of juvenile steelhead and Chinook Salmon in main-stem habitats of the Columbia River estuary. *Transactions of the American Fisheries Society*, 151(5), 587–610. <https://doi.org/10.1002/tafs.10376>
- Willis, S. C., Hess, J. E., Fryer, J. K., Whiteaker, J. M., & Narum, S. R. (2021). Genomic region associated with run timing has similar haplotypes and phenotypic effects across three lineages of Chinook Salmon. *Evolutionary Applications*, 14(9), 2273–2285. <https://doi.org/10.1111/eva.13290>
- Winther, I. (2018). *Genetic stock identification of Chinook Salmon caught in northern British Columbia troll fisheries, 2018* (Report N18-VHP10). Pacific Salmon Commission.

SUPPORTING INFORMATION

Additional supporting information can be found online in the Supporting Information section at the end of this article.

Evidence of prevalent heat stress in Yukon River Chinook salmon

Vanessa R. von Biela, Lizabeth Bowen, Stephen D. McCormick, Michael P. Carey, Daniel S. Donnelly, Shannon Waters, Amy M. Regish, Sarah M. Laske, Randy J. Brown, Sean Larson, Stanley Zuray, and Christian E. Zimmerman

Abstract: Migrating adult Pacific salmon (*Oncorhynchus* spp.) are sensitive to warm water (>18 °C), with a range of consequences from decreased spawning success to early mortality. We examined the proportion of Yukon River Chinook salmon (*O. tshawytscha*) exhibiting evidence of heat stress to assess the potential that high temperatures contribute to freshwater adult mortality in a northern Pacific salmon population. Water temperatures greater than 18 °C have occurred almost annually in the Yukon River and correspond with low population abundance since the 1990s. Using gene transcription products and heat shock protein 70 biomarkers validated by field experiment, we identified heat stress in half of Chinook salmon examined (54%, $n = 477$) across three mainstem locations and three tributaries in 2016–2017. Biomarkers tracked wide variation in water temperature (14–23 °C) within a tributary. The proportion of salmon with heat stress differed between years at four of the six locations, with more prevalent heat stress in the warmer year. This work demonstrates that warming water temperatures are currently affecting northern populations of Pacific salmon.

Résumé : Les saumons du Pacifique (*Oncorhynchus* spp.) en migration sont sensibles à l'eau chaude (>18 °C), les conséquences pouvant aller d'une diminution du succès du frai à une mortalité précoce. Nous avons examiné la proportion de saumons chinooks (*O. tshawytscha*) du fleuve Yukon qui présentent des indices de stress thermique afin d'évaluer la possibilité que des températures élevées jouent un rôle dans la mortalité en eau douce des adultes dans une population septentrionale de saumons de Pacifique. Des températures de l'eau supérieures à 18 °C se sont produites presque chaque année dans le fleuve Yukon et correspondent à de faibles abondances de la population depuis les années 1990. En utilisant des biomarqueurs de produits de transcription génique et de la protéine de choc thermique 70 validés par une expérience de terrain, nous avons relevé un stress thermique chez la moitié des saumons chinooks examinés (54 %, $n = 477$) dans trois sites du cours principal et dans trois affluents, en 2016–2017. Les biomarqueurs témoignent de grandes variations de la température de l'eau (14–23 °C) au sein d'un affluent. La proportion des saumons présentant un stress thermique diffère entre les deux années dans quatre des six sites, la prévalence du stress thermique étant plus grande durant l'année plus chaude. Ces travaux démontrent que la hausse des températures de l'eau a actuellement une incidence sur les populations septentrionales de saumons du Pacifique. [Traduit par la Rédaction]

Introduction

Air temperatures in the Arctic have warmed by more than 2 °C since the late 19th century, disproportionately higher than the 0.8 °C rise globally during the same time period (Post et al. 2019). Recently, the rate of Arctic warming has accelerated, with 0.75 °C of the 2 °C increase occurring in just the last decade (Post et al. 2019). Indeed, the five warmest years on record globally have all occurred since 2015 (NOAA and NASA 2020), and in Alaska four of the five warmest years have occurred since 2014. The negative effects of warming on Arctic specialist species have been widely anticipated and increasingly well-documented (reviewed in Post et al. 2019). A less obvious result of disproportionate and accelerating warmth at high latitudes could be negative effects on more generalist, broadly distributed Northern Hemisphere fish and

wildlife species encountering unsuitable temperatures at their northern range extent. Pacific salmon (*Oncorhynchus* spp.) are an ideal taxon for examining the possibility that fish and wildlife species are already encountering unsuitable habitats at their northern range extents. There is a long history of Pacific salmon thriving at northern latitudes with a wide range of climatic conditions (Finney et al. 2000). They occur over a broad geographic distribution, and the negative effects of heat stress in the southern parts of their range have been well-documented (Crozier et al. 2008; Hinch et al. 2012). Heat stress is a cellular and physiological stress response that can cause mortality and results from warming beyond suitable temperatures. High water temperatures may cause mortality through several mechanisms, including increased virulence of pathogens (McCullough 1999; Kocan et al. 2009;

Received 8 June 2020. Accepted 15 August 2020.

V.R. von Biela, M.P. Carey, D.S. Donnelly, S.M. Laske, and C.E. Zimmerman. US Geological Survey, Alaska Science Center, Anchorage, Alaska, USA. L. Bowen and S. Waters. US Geological Survey, Western Ecological Research Center, University of California, Davis, California, USA.

S.D. McCormick. US Geological Survey, Leetown Science Center, Conte Anadromous Fish Research Laboratory, Turners Falls, Massachusetts, USA; Department of Biology, University of Massachusetts, Amherst, Massachusetts, USA.

A.M. Regish. US Geological Survey, Leetown Science Center, Conte Anadromous Fish Research Laboratory, Turners Falls, Massachusetts, USA.

R.J. Brown. US Fish and Wildlife Service, Fairbanks, Alaska, USA.

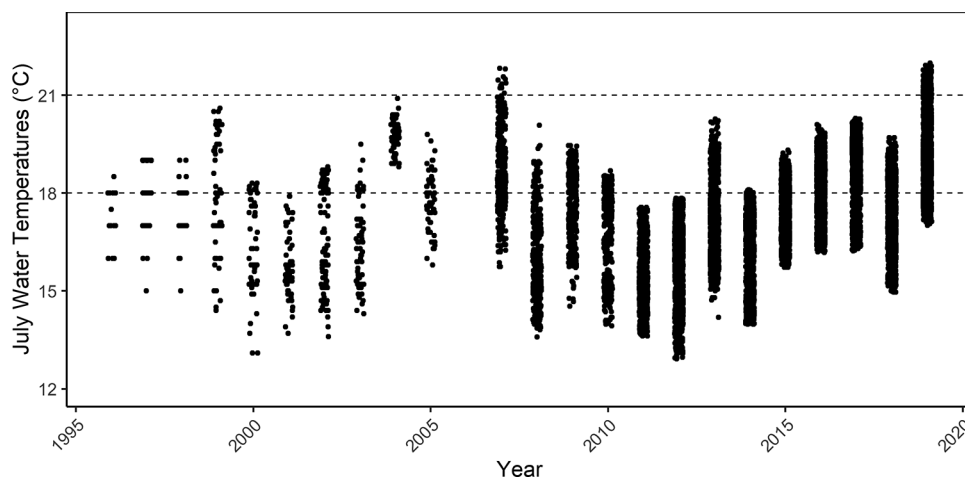
S. Larson. Alaska Department of Fish and Game, Anchorage, Alaska, USA.

S. Zuray. Rapids Research Center, Tanana, Alaska, USA.

Corresponding author: Vanessa R. von Biela (email: vvonbiela@usgs.gov).

Copyright remains with the author(s) or their institution(s). This work is licensed under a [Creative Commons Attribution 4.0 International License](https://creativecommons.org/licenses/by/4.0/) (CC BY 4.0), which permits unrestricted use, distribution, and reproduction in any medium, provided the original author(s) and source are credited.

Fig. 1. Water temperatures recorded by the Alaska Department of Fish and Game during the seasonal peak of temperature in July near Pilot Station, Alaska, 1996–2019. Data include all measurements made from both river banks. Averages were not calculated, as measurement frequency varies across years from one or no measurements made each day by hand (2005 and prior) to consistent and frequent measurements at 4 h (2007–2011) or hourly (2012–2019) intervals daily. Dashed lines indicate the two experimental temperatures, 18 and 21 °C, shown in this experiment to induce a low and high level of heat stress, respectively. Data available at https://www.adfg.alaska.gov/CF_R3/external/sites/aykdbms_website/Default.aspx.



Miller et al. 2011), steep increases in metabolic rate that outstrip energy resources (Rand et al. 2006), and an oxygen demand that exceeds the heart's capacity to deliver oxygen (Farrell et al. 2008; Eliason et al. 2013). We hypothesized that water temperatures are already warm enough to induce heat stress in migrating adults near the northern range extent of Pacific salmon in Alaska's subarctic Yukon River.

The Yukon River is a subarctic, seasonally ice-covered, transboundary river originating in Canada. It flows through the US state of Alaska and terminates in the Bering Sea. The watershed area (~850 000 km²) is the fifth largest in North America and supports important Pacific salmon fisheries (Revenge et al. 1998; Brabets et al. 2000). Despite the high latitude (~62°N to 67°N) and ice-covered winters, summer water temperatures have consistently exceeded typical thresholds associated with stress and elevated mortality in migrating adult Pacific salmon (>18 °C) at lower latitudes (~44°N to 50°N; McCullough 1999; Wagner et al. 2005; Crossin et al. 2008; Kefer et al. 2008; Mathes et al. 2010; Strange 2010; Hinch et al. 2012; Bowerman et al. 2016). Indeed, water temperature in the Yukon River during spawning migration met or exceeded 18 °C in 85% of years, 19 °C in 70% of years, and 20 °C in 40% of years ($n = 23$ years: 1996–2019, except no data in 2006) at Pilot Station, Alaska (Fig. 1). Surprisingly, the peak summer water temperatures for the Yukon River are generally similar to that of the Fraser River (Hinch et al. 2012), despite the Fraser River being ~3000 km further south. Fraser River sockeye salmon (*Oncorhynchus nerka*) have been used as a model system for assessing heat stress and related mortality that can exceed 90% in the warmest cases (reviewed by Hinch et al. 2012). Even water temperature of 18 °C can double adult sockeye salmon mortality rates compared with cooler temperatures if the exposure is prolonged (i.e., weeks; Crossin et al. 2008). Mortality of migrating and spawning adults due to heat stress can undermine escapement-based management practices and exacerbate population declines if a large component of the individuals counted do not successfully reproduce.

Chinook salmon (*Oncorhynchus tshawytscha*) have been a management focus in the Yukon River and broader Arctic–Yukon–Kuskokwim (AYK) region of Alaska and Canada since a population decline occurred in the late 1990s and failed to recover (Kruger and Zimmerman 2009; ADF&G 2013; AYK-SSI 2013). The causes of the initial population decline and failure to recover are unclear (Kruger and Zimmerman 2009; ADF&G 2013; AYK-SSI 2013). Low Chinook salmon numbers are a hardship for virtually all residents

in the region given their key role in the local economies, food security, and culture (ADF&G 2013). In contrast with other regions with declining salmon populations across North America, freshwater and marine habitats are largely intact in the AYK region with little development and sparse human populations (Brabets et al. 2000). Evidence of heat stress in Yukon River salmon is limited to anecdotal observations of listless behavior during warm water periods (generally >20 °C) and the Pacific salmon mortality event that occurred across Alaska in 2019, where carcasses of various species were observed along migration corridors with eggs retained (i.e., en route mortality) (various observations from LEONetwork.org and media stories; Westley 2020).

Cellular and physiological biomarkers of heat stress precede obvious behavioral changes, which provide an early warning of heat stress that is often predictive of death (Miller et al. 2011; Jeffries et al. 2012). Changes in gene transcription (mRNA) and protein expression of heat shock proteins are natural biomarkers of cellular stress that may provide information for assessing the prevalence of heat stress in wild populations (Iwama et al. 1998; Basu et al. 2002; Deane and Woo 2011; Jeffries et al. 2012). Many genes and proteins are highly conserved among taxa and allow for comparisons across a wide array of species (Welch 1993; Feder and Hofmann 1999; Basu et al. 2002). These techniques require experimental validation studies to demonstrate the response of specific genes or proteins to high temperatures and establish the specific signatures that reflect heat stress. Validations with model laboratory species and more southern wild populations have supported the use of these biomarkers to identify heat stress in salmonids (Feder and Hofmann 1999; Basu et al. 2002; Iwama 2004; Crossin et al. 2008; Chadwick and McCormick 2017).

Here, we conducted an experimental temperature manipulation with a subset of wild Yukon River Chinook salmon to validate heat stress biomarkers and subsequently estimated the proportion of adult Chinook salmon with heat stress biomarkers across six collection locations in the Yukon River watershed that were sampled in 2 years (2016 and 2017) with different water temperatures. While differences in water temperatures were small between the 2 years, water temperatures in July of both years were predominantly >18 °C and in a range where the Pacific salmon heat stress response is known to be extremely sensitive. We classified each Chinook salmon as heat-stressed or not using thresholds of muscle gene transcription levels and heat shock protein 70 (HSP70) abundance developed from the experiment. Gene tran-

Table 1. Genes examined with their description, associated pathway, and references.

Full name	Short name	Function	Reference
Heat shock protein 27	<i>HSP27</i>	Heat stress chaperone	Basu et al. 2002
Heat shock protein 70	<i>HSP70</i>	Heat stress chaperone	Iwama et al. 1999; Tsan and Gao 2004
Heat shock protein 90	<i>HSP90</i>	Heat stress chaperone	Iwama et al. 1999; Tsan and Gao 2004
Leptin	<i>leptin</i>	Metabolism: lipid liberation and storage	Copeland et al. 2011
Th2-specific transcription factor	<i>Gata3</i>	Immune system: initiates Th2 response in the presence of parasites	Wang et al. 2010
Th1-specific interferon alpha, type I	<i>IFNa</i>	Immune system: cytokines for viruses; Th1	Robertsen 2018)
Orthomyxovirus resistance gene 1	<i>MX1</i>	Immune system: antiviral activity	Verrier et al. 2011
Th1-specific Tbox transcription factor	<i>tbx21</i>	Immune system: initiates Th1 response in the presence of intracellular pathogens	Wang et al. 2010
Aryl hydrocarbon receptor	<i>AHR</i>	Immune system: inflammation and Th differentiation Detox: oxidative metabolism regulator	Quintana et al. 2008; Veldhoen et al. 2010
Hydrocarbon-inducible cytochrome P4501A	<i>CYP1A</i>	Detox: oxidative metabolism enzyme	Erdoğan et al. 2011
Cyp1A superoxide dismutase	<i>SOD</i>	Detox: anti-oxidant enzymes	Roberts et al. 2006
Metallothionein A	<i>MT-A</i>	Detox: oxidative metabolism enzyme	Erdoğan et al. 2011; Vignesh and Deepe 2017

Note: Associated pathways indicate the function each gene is most associated with and is not comprehensive of all known roles.

scription levels were measured for a panel of 12 genes associated with heat shock (*HSP27*, *HSP70*, *HSP90*), oxidative stress and detoxification (*AHR*, *CYP1A*, *SOD*, *MT-A*), immune system function (*AHR*, *tbx21*, *Gata3*, *MX1*, *IFNa*), and metabolism (*leptin*) (Table 1). The gene transcription and protein biomarkers were examined jointly because they provide different snapshots of the heat stress response, as gene transcription precedes protein translation, and the combination of the two biomarkers may also help differentiate between moderate and severe heat stress (Lund et al. 2002; Lewis et al. 2016).

Methods

Temperature manipulation experiment

A temperature manipulation experiment was conducted in the lower Yukon River, adjacent to the Alaska Department of Fish and Game's (ADF&G) test fishery site (61.94716°N, 162.84161°W) at the beginning of the spawning migration in June, when ambient water temperatures were cooler to ensure that individuals had not already experienced temperatures near or above heated treatment conditions. Pilot Station is a mixed stock, and population fishery and genetics (single nucleotide polymorphisms) estimates the contributions of three major groups during the experiment (mid-June 2018) were approximately 10% US lower Yukon, 40% US middle Yukon, and 50% Canada (West and Prince 2019), such that the experimental results are unlikely to be specific to a particular stock or population. Genetic stock assignments are not available for individual Chinook salmon. Across the Yukon River basin, 183 separate Chinook salmon spawning areas are known, with 32 areas being major producers, suggesting the potential for a high number of genetic populations (Brown et al. 2017).

Sample size was determined in consultation with ADF&G managers and was limited given the low population size of Yukon River Chinook salmon. Briefly, up to three individual Chinook salmon were acquired daily from the ADF&G test fishery across 9 consecutive days ($n = 27$) and randomly assigned to one of three tanks: control (~15 °C), 18 °C, or 21 °C. The treatment temperatures were selected because they already occur with some frequency in the mainstem Yukon River as well as some tributaries and headwater streams (Zuray 2010; Carlson and Edwards 2017; Conitz 2018; Koch et al. 2020) (Fig. 1) and spanned the temperature range associated with heat stress, decreased migration performance, and increased mortality based on review of literature (McCullough 1999; Goniea et al. 2006; Farrell et al. 2008; Keefer et al. 2008; Martins et al. 2012). Water temperatures of 18 and 21 °C are likely near the thresholds for detecting heat stress and the upper temperature limit, respectively, for migrating Chinook

salmon (McCullough 1999). Animals were cared for in accordance with the Guide for the Care and Use of Laboratory Animals (NAS 2011). This work was approved by the USGS Alaska Science Center Animal Care & Use Committee (ACUC 2018-04) and under a permit from the ADF&G (SF2018-132).

Treatment tanks were 587 L polyethylene stock tanks with a liquid propane fueled heater to raise temperature, electric aquarium heaters to maintain temperature, circulation pumps to prevent thermal stratification, aerators to supplement dissolved oxygen, and temperature loggers to record water temperature every 5 min. Each experimental run lasted ~6 h with 1 or 2 h of heating (18 and 21 °C, respectively) and a minimum of 4 h at the treatment temperature. Prior experiments indicate that 4 h is sufficient to elicit gene transcription and protein responses to heat stress (Buckley et al. 2006). The rate of temperature rise to treatment temperatures was 3.71 ± 1.31 °C (mean \pm SD), with a mean hold temperature of 18.0 °C in the low heat stress treatment (range = 17.3–18.6 °C) and 20.9 °C in the high heat stress treatment (range = 19.8–22.0 °C). Individuals in the control group were held at a near consistent ambient water temperature until the completion of the heat treatments each day. Details of the heating and control system used for these experiments can be found in Donnelly et al. (2020).

All fish were sacrificed immediately following the 4 h period at the target temperature by cranial stunning. All individuals in the control and 18 °C groups survived the trial, but one individual that began the 18 °C trial failed to acclimate to the tank and was released. Fifty-six percent ($n = 9$) of those in the 21 °C treatment group survived and provided samples for this study. Mortality in the 21 °C treatment is not surprising given that 21 °C has been suggested as the upper thermal limit for migrating Chinook salmon (McCullough 1999). Experimental mortality is discussed in greater detail in Donnelly et al. (2020). Individuals that survived the 21 °C treatment were not especially lethargic or moribund and were similar in appearance and behavior to fish in other treatments. Twenty-two individuals were used in the experimental results, with nine in the control group, eight in the 18 °C treatment group, and five in the 21 °C treatment group. Samples consisted of three muscle biopsy plugs taken from the white dorsal muscle above the lateral line and posterior to the operculum. Muscle tissue was chosen because it can be sampled nonlethally in adult salmonids with minimal training by those already staffing monitoring sites. All samples were immediately placed in microcentrifuge tubes and then into a liquid nitrogen dry shipper. All tissue samples were stored at –70 °C or below until laboratory

Table 2. Chinook salmon quantitative real-time polymerase chain reaction primers.

Gene	Primer name	FP1	Primer name	RP1 rc	Expected amplicon (bp)
<i>HSP90</i>	Onts HSP90 F1	atgatcgggcagttcggtg	Onts HSP90 R1rc	agtgtaactttgacagtga	140
<i>HSP70</i>	Onts HSP70 F1	gcaccctctctccagca	Onts HSP70 R1rc	ggtaccgcggaacaggta	124
<i>CYP1A</i>	Onts CYP1A F1	agacagtcgccaggctc	Onts CYP1A R1rc	agccttgcggtgctgaag	115
<i>AHR</i>	Onts AHR F	gctccagatgtggtcaagt	Onts AHR R	gagtttgcaggcgaga	122
<i>HSP27</i>	Onts HSP27 F	ctgacgctgagaaggtga	Onts HSP27 R	tagggcttggtctgctg	135
<i>MT-A</i>	Onts MT-A F	atcttgaactgcggtgg	Onts MT-A R	gacagcagtcgcagcaac	253
<i>SOD</i>	Onts SOD F3	gagacaacaccaacggctg	Onts SOD R3rc	gctcctgcagtcacgtgc	120
<i>IFNg2</i>	Onts IFNg2 F3	tataagatctccaaggaccag	Onts IFNg2 R2rc	ccagaaccacactcatcaac	100
<i>MX1</i>	Onts MX1 F1	ctgatgtggagaagaaaattcg	Onts MX1 R1rc	gcaggctgatgagtgtag	128
<i>Gata3</i>	Onts GATA F2	caagcgacgactgtctgca	Onts GATA R3rc	gaccgcaagcgttacacac	118
<i>tbx21</i>	Onts TBX21 F	agtgaaggaggatggttctgag	Onts TBX21 R	ggtgatgtctgcgttctgatag	111
<i>IFNa</i>	Onts IFNa F	cctgccatgaacctgagaaga	Onts IFNa R	tttctgatgagctccatgc	107
<i>leptin</i>	Onts Lep F1	cttccatagtggagaccatg	Onts Lep R1rc	ggcagcgtgatcatccag	131
<i>rpL8</i>	Onts rpL8 F	ttggtaatgttctgcctgtg	Onts rpL8 R	gggtgtgggatgactg	129
<i>EF1a</i>	Onts EF1a F1	gcgtggtatcaccattgaca	Onts EF1a R2rc	ctgagaggtaccagtgatca	120

work was conducted to assess the gene transcription and protein abundance.

Experimental laboratory analyses

Genes are denoted in italic font (e.g., *HSP70*) and proteins are denoted in plain font followed by the word “protein” (e.g., HSP70 protein) for clarity throughout. The particular genes selected for this study are relatively well-studied, with heat shock genes selected for their specific response to elevated water temperatures and the remaining genes selected for their broad response to a variety of stressors (references in Table 1). Gene transcription was measured using quantitative real-time polymerase chain reaction (qPCR) assays of mRNA at the US Geological Survey Western Ecological Research Center in Davis, California, USA. Total RNA was extracted from ground muscle tissue using the RNeasy Lipid Tissue Mini Kit (Qiagen; www.qiagen.com). To remove contaminating genomic (g)DNA, extracted total RNA was treated with 10 U·μL⁻¹ of RNase-free DNase I (DNase, Amersham Pharmacia Biotech Inc.) at room temperature (20–30 °C) for 15 min. The extracted RNA was stored in a –80 °C freezer until analyzed.

A standard cDNA synthesis was performed on 2 μg of RNA template from each salmon. Reaction conditions included four units reverse transcriptase (Omniscript, Qiagen, Valencia, California), 1 μmol·L⁻¹ random hexamers, 0.5 mmol·L⁻¹ each dNTP, and 10 units RNase inhibitor, in reverse transcription (RT) buffer (Qiagen, Valencia, California). Reactions were incubated for 60 min at 37 °C, followed by an enzyme inactivation step of 5 min at 93 °C, and then stored at –20 °C until further analysis.

Briefly, 1 μL of cDNA was added to a mix containing 12.5 μL of QuantiTect Fast SYBR Green Master Mix (5 mmol·L⁻¹ Mg²⁺; Qiagen, Valencia, California), 0.5 μL each of forward and reverse sequence-specific primers (Table 2), and 10.5 μL of RNase-free water; total reaction mixture was 25 μL. The primers for *HSP27*, *HSP70*, and *HSP90* are specific to the inducible forms of these genes. The reaction mixture cDNA samples for each gene of interest and reference genes were loaded into MicroAmp Fast Optical 96 well reaction plates in duplicate and sealed with optical sealing tape (Applied Biosystems, Foster City, California). Reaction mixtures containing water, but no cDNA, were used as negative controls.

Amplifications were conducted on a QuantStudio 3 Real-time Thermal Cycler (Applied Biosystems, Foster City, California), using the QuantStudio 3 software. Reaction conditions were as follows: an initial hold stage of 95 °C for 20 s, 40 cycles of 95 °C for 1 s, and 60 °C for 20 s. The melt curve was 95 °C for 1 s, 60 °C for 20 s, and 0.3 °C·s⁻¹ temperature increase, and then 95 °C for 1 s.

We analyzed qPCR data using normalized values calculated as the threshold cycle (C_T) of the reference gene subtracted from the C_T of the gene of interest, where C_T is the amplification cycle that

allows for detection (Bustin 2002). Because samples with inherently higher numbers of transcripts require fewer amplification cycles for detection, lower normalized values indicate that more transcripts are present. A change in normalized value of 2 is approximately equivalent to a fourfold change in the amount of the transcript.

HSP70 protein abundance of the inducible form was analyzed at the US Geological Survey S.O. Conte Anadromous Fish Research Laboratory, Turners Falls, Massachusetts, USA. Muscle from the dermal punch was separated from subdermal fat and skin and weighed to the nearest milligram. All tissues were thawed and homogenized with a Kontes Pestle Pellet handheld homogenizer (Thermo Fisher Scientific, Hampton, New Hampshire, USA) in 10 volumes of SEID (150 mmol·L⁻¹ sucrose, 10 mmol·L⁻¹ EDTA (ethylenediaminetetraacetic acid), and 50 mmol·L⁻¹ imidazole, pH 7.3 plus 0.1% deoxycholic acid). Homogenates were centrifuged at 3000g for 7 min at 4 °C. A portion of the resulting supernatant was immediately diluted with an equal volume of 2× Laemmli buffer, heated for 15 min at 65 °C, and stored at –80 °C. A small volume of supernatant was used to determine total protein concentration in quadruplicate using the Pierce BCA Protein Assay kit (Thermo Fisher Scientific, Hampton, New Hampshire, USA). Thawed samples were run on a 7.5% SDS–PAGE gel along with Precision Plus protein standards at 5 μg in a reference lane (Bio-Rad Laboratories, Hercules, California, USA). Dilution titration for tissue homogenates was completed to establish the range of linearity. A total of 10 μg of muscle protein was loaded per sample. Two lanes were reserved on each gel for a standard consistent tissue preparation as reference to control for blot-to-blot variation and to allow for comparison across all treatments and locations. Following electrophoresis, proteins were transferred to Immobilon polyvinylidene difluoride (PVDF) transfer membrane (Millipore, Bedford, Massachusetts, USA) at 30 V overnight in 25 mmol·L⁻¹ Tris, 192 mmol·L⁻¹ glycine buffer, pH 8.3. Equal loading was verified by reversible total protein staining with ponceau S. Samples with unequal loading or alternate banding patterns were removed from analysis. PVDF membranes were blocked with 5% nonfat dry milk in PBST (phosphate buffered saline plus 0.1% Triton X-100) for 1 h at room temperature, rinsed in PBST, and exposed to primary polyclonal antibody specific for the inducible form of salmonid HSP70 (AS05061; Agrisera, Vannas, Sweden) at 1:25 000 dilution in PBST with 5% nonfat dry milk for 1 h at room temperature. After rinsing in PBST, blots were exposed to goat anti-rabbit IgG conjugated to horseradish peroxidase diluted 1:10 000 in PBST and 5% nonfat dry milk for 1 h at room temperature. Blots were washed in PBST and incubated for 1 min in a 1:1 mixture of enhanced chemiluminescent (ECL) solution A (396 μmol·L⁻¹ coumaric acid,

Table 3. Sample size (*n*) and length (mean mid-eye to fork length \pm standard deviation in mm) for field sampled Chinook salmon at sites in the Yukon River and tributaries in 2016 and 2017 along with the dates when sample collections occurred.

Location	Year	Sampling date	<i>n</i>	Length (mm)
Mainstem Yukon River				
Emmonak	2016	10–18 June	45	801 \pm 113
	2017	8–21 June	38	773 \pm 80.5
Rapids	2016	6–7 July	39	622 \pm 111
	2017	5–7 July	30	681 \pm 111
Eagle	2016	11 July – 2 August	40	790 \pm 79.1
	2017	16 July – 9 August	33	789 \pm 71.5
Tributaries				
East Fork Andreafsky River	2016	30 June – 14 July	46	708 \pm 89.0
	2017	23 June – 5 July	40	648 \pm 126
Gisasa River	2016	4–18 July	38	665 \pm 97.6
	2017	3–20 July	39	668 \pm 105
Chena River	2016	13–18 July	51	676 \pm 81.1
	2017	18 July	38	775 \pm 66

Note: Sample size reflects the number of individuals for which data were obtained for gene transcription and HSP70 protein analyses.

2.5 $\mu\text{mol}\cdot\text{L}^{-1}$ luminol, 100 $\text{mmol}\cdot\text{L}^{-1}$ Tris, pH 8.5) and ECL B (0.018% H_2O_2 , 100 $\text{mmol}\cdot\text{L}^{-1}$ Tris, pH 8.5), and then digitally imaged and quantified (Syngene PXi, GeneTools, Frederick, Maryland, USA). All blots were normalized to the internal standard consistent tissue preparation and are represented as a ratio to the mean standard value that we refer to as HSP70 relative abundance.

Statistical analyses of controlled experiment

Heat stress was inferred through differences between fish held in the control and elevated temperature treatments that allow for high classification accuracy (correct classification > 75%) for both the gene transcript levels and HSP70 protein abundance. Following separate statistical analyses for the two biomarkers, heat stress classifications based on gene transcription and HSP70 protein were considered jointly, with indications of heat stress in both biomarkers interpreted as more severe stress (Lund et al. 2002; Lewis et al. 2016).

A linear discriminate analysis (LDA) was used to identify the combination of muscle gene transcript levels that best classified individuals among the control and two elevated temperature treatments. LDA was chosen as the data reduction technique, as it explicitly attempts to model the difference among a priori groups. Specifically, the “lda” function in the MASS package of R (Venables and Ripley 2002) was implemented to identify a linear combination of the mRNA transcript values from genes that results in maximum separation between the centers of the groups while minimizing variation within the groups.

Data for all genes were examined to assess statistical assumptions of normal distribution and multicollinearity. The muscle mRNA transcript data for *leptin* were removed because concurrent investigations of similar data in Yukon River Chinook salmon that were not part of the experiment revealed a violation of normal distribution due to a high frequency of individuals without detectable levels of *leptin* and the need for any model developed from the experimental results to be applicable to the broader population of Chinook salmon. *MT-A* was also removed from the analysis due to strong positive correlations ($r > 0.60$) with both *HSP27* and *IFNa* that were not dependent on a single influential point (i.e., outlier).

Given the small experiment sample size, a sequential reduction in the number of genes in the LDA was preformed to limit the number of genes used in the model and reduce overfitting. The sequential reduction was based upon gene transcript data that were centered and scaled prior to analysis so that coefficients reflected the influence of each gene in the model. The least influential gene with the coefficient closest to zero (mean of LD1 and LD2 coefficients weighted by the variation attributed to each LD)

was dropped from the analysis sequentially until the classification rate fell below the desired threshold of 75%. The model that used the fewest number of genes and still maintained a classification rate of >75% was considered the preferred model. HSP70 protein abundance was plotted and visually examined for the location of a threshold that best separated fish among treatments. The mean HSP70 abundance was compared among treatments using a one-way analysis of variance (ANOVA).

Application of experimentally derived heat stress thresholds

Muscle biopsy samples were collected from 477 live Chinook salmon during their spawning migration in the Yukon River watershed during summers of 2016 and 2017 (Table 3). The timing of sample collection varied by sites to generally align with the peak of spawning migration at each location. Collection locations were annual management assessment projects or subsistence fishing efforts that varied in capture methods. Chinook salmon were sampled in Alaska at three locations on the mainstem Yukon River and three tributaries. Mainstem sites sample a mix of populations, while tributary locations presumably sample a single population. Genetic stock identification is not routine at all collection sites, nor are genetic assignments available for individual fish or designed to identify the spawning population (West and Prince 2019). This work was approved by the USGS Alaska Science Center Animal Care & Use Committee (ACUC 2017-08) and under permits from the ADF&G (SF2016-186 and SF2017-167).

Mainstem Yukon River locations were near the mouth at Emmonak (ADF&G test fishery gillnets), subsistence fish wheels in the middle portion of the mainstem Yukon River (Rapids Fish Wheel operated by Stan Zuray and others), and just before the Canadian border at Eagle (ADF&G test fishery gillnets). Individuals captured at the Rapids Fish Wheel are predominantly Canadian stocks, as there are only two major spawning areas in the US beyond there, and all individuals captured at Eagle are Canadian stocks (Eiler et al. 2014; Brown et al. 2017). Upstream migration in the main stem occurs primarily in June and July. Tributary collections occurred at weirs in the East Fork Andreafsky and Gisasa rivers (US Fish and Wildlife Service) and electrofishing in the Chena and Salcha rivers (ADF&G). Fish collected in the Chena and Salcha rivers were grouped together for analysis because both are components of the Tanana River with similar migration routes and temperature histories. Sampling at all tributary locations occurred primarily in July. In all cases, muscle biopsies were taken within minutes of capture, including at the Rapids Fish Wheel where individuals were sampled directly from the capture basket and not the live-well holding box. This approach assumes that

capture, short handling time (minutes), and differences in capture methods described here have no effect on the cellular stress biomarkers used because they require hours for response (Lund et al. 2003; Buckley et al. 2006). To date, there is no evidence that physical stressors and confinement can induce heat shock proteins in fish, nor does cortisol (which does respond rapidly to stressors) have direct effects on heat shock proteins (Deane and Woo 2011). Moreover, the experimentally derived heat stress classifications are developed by contrasting control fish with heated fish. Thus, heat stress classifications are primarily related to the water temperature while minimizing the potential effects of capture and confinement that are more likely in tissue samples collected hours after capture and confinement.

All laboratory analyses of gene transcription and HSP70 protein were conducted in an identical fashion as above for the experimental fish. The preferred LDA model for classifying experimental fish to their respective treatments was then applied to gene transcript data from the field-sampled fish to classify each individual as grouping with control fish that were not heat-stressed, 18 °C treated fish, or 21 °C treated fish. Only the experiment data were used to estimate the model coefficients. Because the gene transcript C_T values of the field-sampled fish likely differed in their gene-specific means and standard deviations from the experiment fish, the classifications of field-sampled fish were based on coefficients from a model that was refit with transcript data that was not centered and scaled from experimental fish.

Assessment of experimentally derived models to identify heat stress in field-sampled fish

A subset of field-sampled fish ($n = 477$), just those from the East Fork Andreafsky site collected in 2016 and 2017 ($n = 86$), were used to assess the experimentally derived thresholds to identify heat stress. At this location, individuals have spent enough time in fresh water (~200 river kilometres (rkm) over several days at a minimum) to encounter warm water but have not traveled so far that a reasonable assessment of their temperature history is difficult. At sites further upstream in the Yukon River watershed, spans stretching hundreds of river kilometres lack water temperature data and preclude a reasonable assessment of temperatures previously encountered. Moreover, the individuals captured at this location experienced a wide range of temperatures, including seasonal increases that rose to >23 °C in 2016. The East Fork Andreafsky is one of only two major spawning populations that are downstream from the experimental location and therefore could not have contributed to the sample used in the experiment.

The relationships between results from each individual's heat stress biomarkers were compared with the 3-day maximum water temperature at the capture location (maximum temperature on the day of and 2 days prior to capture based upon US Fish and Wildlife Service water temperature data collected at East Fork Andreafsky River weir every 15 min). The 3-day maximum temperature from the capture location is a reasonable metric for recent temperature history given that the capture location on the East Fork Andreafsky River is just 43 rkm from the mainstem Yukon River. While lower Yukon River Chinook salmon could travel that distance in about 1–1.5 days (Eiler et al. 2015), warm water temperatures are known to decrease migration speeds by ~50% in Columbia River Chinook salmon (Goniae et al. 2006) and may result in a travel time closer to 3 days if speed reductions with warming temperatures are comparable. To assess the strength of gene transcription data to identify heat stress caused by warm temperatures, the 3-day maximum temperature was compared with the LD1 value calculated for each fish captured in the Andreafsky River using linear regression. LD1 values were predicted from each individual's gene transcription data using coefficients estimated during the experiment. LD1 captured the majority (70%) of the variability in the gene transcription data used to assigned individuals among the control and experimental treatments (see Re-

sults). Similarly, we plotted the HSP70 protein abundance relative to the 3-day maximum temperature. Next, we tested whether the presence of elevated HSP70 abundance was related to the 3-day maximum temperature using logistic regression (values greater than threshold set to 1 and values less than or equal to threshold set to 0).

Heat stress proportions and water temperatures across the Yukon River watershed

Each field-sampled fish was classified as heat-stressed or not based on gene transcription levels and HSP70 protein abundance. An individual was classified as stressed if the LDA equation developed from experiment fish classified the individual with Chinook salmon treated at 18 or 21 °C or if their HSP70 protein abundance exceeded 0.14, the experimental derived threshold. The proportion of individuals with evidence of heat stress in either biomarker was calculated for each location and year. The proportion of individuals with evidence of heat stress were compared between years at each site using a z test for independent proportions.

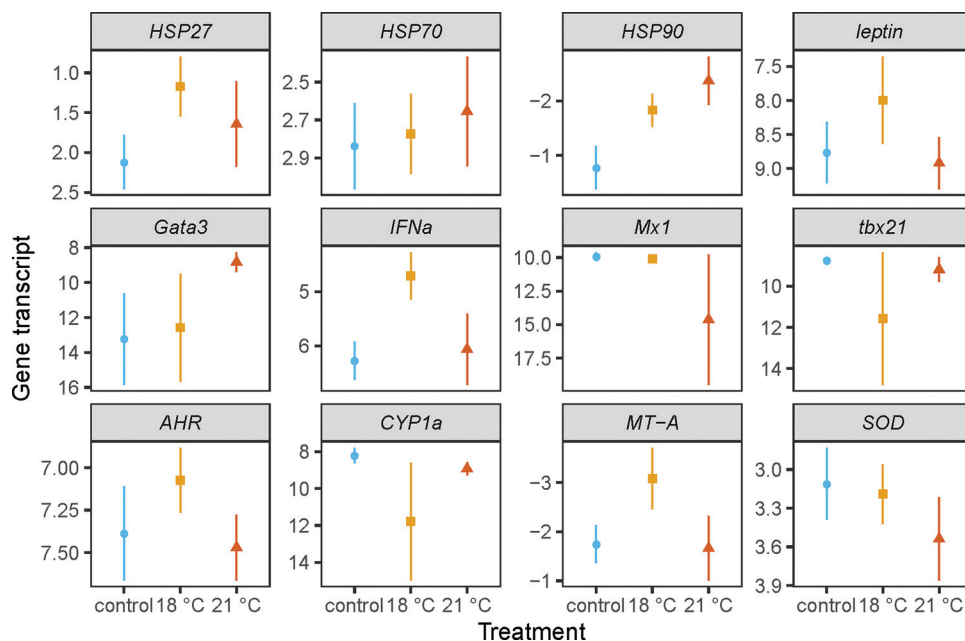
Water temperature data were available from the mainstem Yukon River and the three tributaries where Chinook salmon were captured in 2016 and 2017. Mainstem Yukon River water temperatures were measured hourly by ADF&G in the lower river near Pilot Station on the left and right sides of the river using HOBO Pro v2 data logger. In the East Fork Andreafsky and Gisasa rivers, water temperatures were measured every 15 and 20 min, respectively, by US Fish and Wildlife Service at the weirs using HOBO Pro v2 data loggers. In the Chena River, water temperatures were measured every 15 min by the US Geological Survey at the gage station near Two Rivers, Alaska (station number 15493000). Monthly mean water temperatures were compared in each river between years using a Welch's t test for unequal variances for qualitative comparison with interannual differences in the heat stress proportions. All data and metadata associated with this study is publicly available in von Biela and Donnelly (2020) and von Biela et al. (2020).

Results

Temperature manipulation experiment

Heat stress was inferred through differences in gene transcription of individuals in both the 18 and 21 °C treatment groups compared with the control group. The mean and standard error for all normalized qPCR data that reflected gene transcript levels from each experimental treatment were calculated to visualize input data used in the LDA (Fig. 2). The LDA produced two linear combinations of the continuous predictor variables, LD1 and LD2, and established a threshold that classified individuals based on their location in the ordination of LD1 and LD2. Data from the ten genes that met statistical assumptions (HSP27, HSP70, HSP90, *Gata3*, *tbx21*, *MX1*, *IFNa*, *AHR*, *SOD*, and *CYP1A*) classified individuals by treatment with 82% accuracy, with LD1 accounting for 61% and LD2 accounting for 39% of the variability. Sequential model reduction to include fewer genes resulted in a preferred model with six genes (HSP70, HSP90, *Gata3*, *IFNa*, *AHR*, and *SOD*) with a classification rate among the three treatments of 77% (Fig. 3A). Misclassification of individuals by the preferred model always involved the intermediate 18 °C treatment. No individuals from the control were classified with the 21 °C fish or vice versa. Among individuals in the control group, classification was accurate in 88% of individuals, with one misclassification to the 18 °C treatment. Similarly, 80% of individuals from the 21 °C treatment were correctly classified, and only a single fish was misclassified to the 18 °C treatment. Classification rate was lowest among fish from the 18 °C treatment at 63%, with one individual grouped with the control and two individuals grouped with the 21 °C treatment. If the classifications are summarized as more simplistic control or heat-

Fig. 2. The mean and standard error of normalized qPCR values for 12 genes in muscle tissue of Chinook salmon from individuals held in three different temperatures: control (blue circles, river ambient, ~15 °C), 18 °C (orange squares), or 21 °C (red triangles). Because lower normalized gene transcript values represent more transcripts present, the y axis is displayed in reverse order. A change in normalized value of two is approximately equivalent to a fourfold change in the amount of the transcript. [Colour online.]



treated (18 and 21 °C combined), 91% of individuals are correctly classified by the LDA.

The LDA based upon centered and scaled gene transcript data resulted in the following coefficients, with LD1 accounting for 70% of the variability across the six genes and LD2 account for the remaining 30%:

$$(1) \quad LD1 = 0.83HSP70 + 1.97HSP90 + 0.88Gata3 - 2.06IFNa - 0.04AHR - 1.96SOD$$

$$(2) \quad LD2 = -1.06HSP70 - 0.07HSP90 - 0.07Gata3 - 7.04IFNa + 3.08AHR - 1.54SOD$$

Higher normalized qPCR values used in the analysis indicate less mRNA transcript. For example, positive coefficients of LD1 indicate a higher normalized value from qPCR moving from left to right along the LD1 axis, but less mRNA transcript. The first linear discriminate axis, LD1, of the six-gene model accounted for 70% of the variation in the genes examined and primarily separated individuals from the 21 °C treatment group from both the 18 °C treatment and control groups (Fig. 3). The positive coefficients and relative position of fish from the treatments in Fig. 3 indicated that 21 °C treatment group had more transcript for the genes *HSP70*, *HSP90*, and *Gata3* and less transcript for *IFNa* and *SOD* compared with control and 18 °C groups. The second linear discriminate axis, LD2, accounted for the remaining 30% of the variation in the gene transcript data and primarily separated fish between the 18 °C treatment and control groups (Fig. 3). Coefficients indicated that fish from the 18 °C treatment group had more transcript from *HSP70*, *IFNa*, and *SOD* (i.e., negative coefficients indicate a lower normalized qPCR value and more gene transcript, moving upward along the LD2 axis in Fig. 3), but less *AHR* compared with the control group. Coefficients for the genes *HSP90* and *Gata3* were near zero for LD2 and indicated little influence in distinguishing between the 18 °C treatment and control groups.

The reduced six-gene model was refit with data that was not centered and scaled for application to Chinook salmon collected

across the Yukon River watershed that were not part of the experiment. The formulae for LD1 and LD2 fitted by the analysis were

$$(3) \quad LD1 = 0.67HSP70 + 1.08HSP90 + 0.13Gata3 - 0.36IFNa - 0.02AHR - 1.27SOD$$

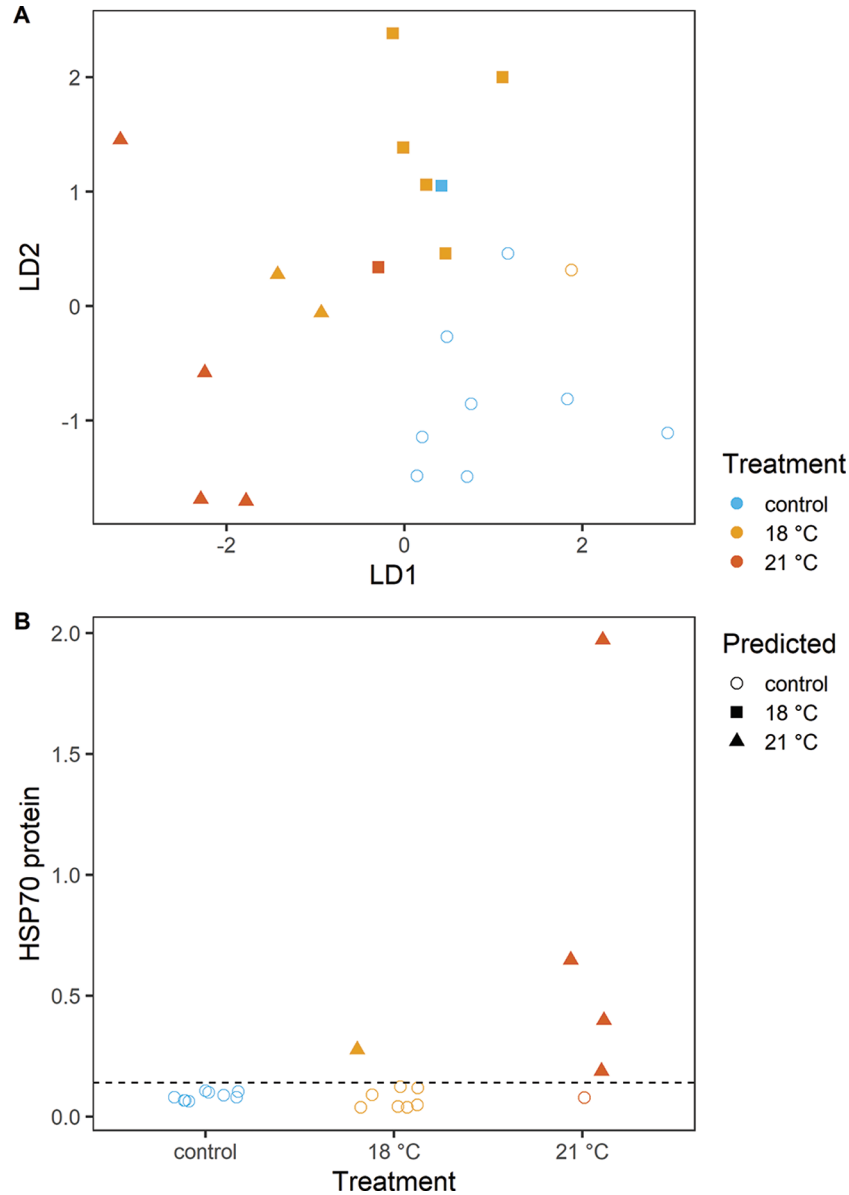
$$(4) \quad LD2 = -0.87HSP70 - 0.04HSP90 - 0.01Gata3 - 1.23IFNa + 1.09AHR - 1.00SOD$$

HSP70 protein abundance distinguished fish in the 21 °C treatment group and was higher compared with both the 18 °C treatment and control groups in muscle (ANOVA; $F = 4.95$, $P = 0.02$; Fig. 3B). The threshold that separated *HSP70* protein values between control and 21 °C fish with the fewest misclassifications was 0.14 (Fig. 3B). The threshold for *HSP70* protein from muscle tissue resulted in correct classifications for 93% of individuals overall, with 100% correct classifications of fish in the control group and 80% correct classification of fish in the 21 °C fish treatment group. Only the 21 °C treatment group elicited a detectable response in both gene transcription and the *HSP70* protein.

Assessment of experimentally derived model to identify heat stress

Among Chinook salmon captured in the East Fork Andreafsky River, the 3-day maximum water temperature was related to the LD1 value of gene transcript data calculated based on coefficients that were fit using only fish from the experiment (eq. 3; linear regression, $y = -0.92x + 17.6$, $t = -9.46$, $df = 84$, $r^2 = 0.510$, $P < 0.001$; Fig. 4A). When the continuous LD1 variable is used to classify the heat stress status of each Andreafsky River fish, an abrupt shift is observed between 20 and 22 °C, where individuals switch from being primarily categorized as unstressed (e.g., similar to experimental control group) to all individuals categorized as high heat stress fish (e.g., similar to the 21 °C treatment group; Fig. 4A). Water temperature was also related to the presence of elevated *HSP70* protein abundance (logistic regression, deviance = -55.7, $df = 1$, $P < 0.001$; Fig. 4B). Each degree of increase in temperature

Fig. 3. Results from a linear discriminate analysis (A) used to reduce mRNA abundance of six genes (*HSP70*, *HSP90*, *Gata3*, *IFNa*, *AHR*, and *SOD*) to two linear discriminate axes (LD1 and LD2) and HSP70 protein abundance (B) in muscle tissue of Chinook salmon from individuals held in three different experimental temperatures: control (blue, river ambient, ~15 °C), 18 °C (orange), or 21 °C (red). Shapes indicate the model prediction for each individual with either the control (open circles), 18 °C (filled squares), or 21 °C (filled triangles) treatment group. The dashed line in panel B is the proposed threshold for elevated HSP70 protein that distinguishes heat stress, and points in this panel are spread out (i.e., jittered) so that data are more visible.



resulted in a 4.3-fold increase in the odds of elevated HSP70 (log-odds ratio = 1.46). The 3-day maximum water temperature associated with a 50% probability of elevated HSP70 protein was 17.8 °C.

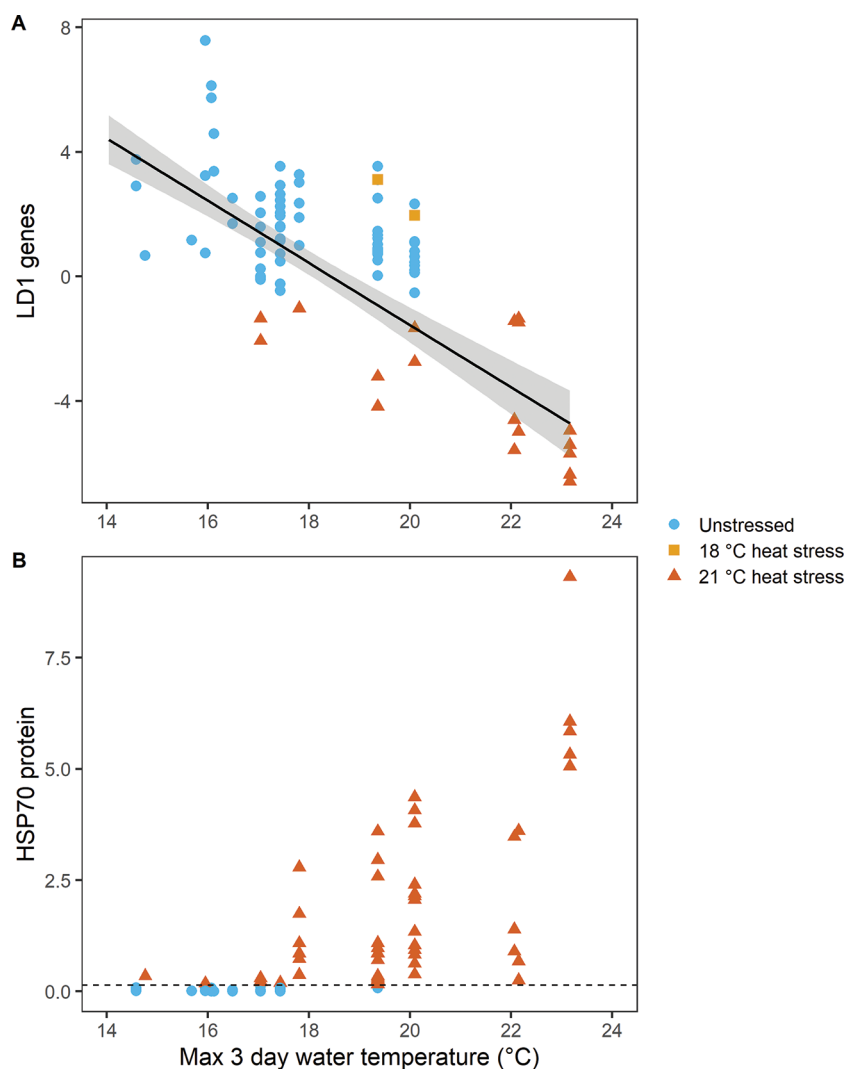
Heat stress proportions and water temperatures across the Yukon River watershed

Gene transcription and HSP70 protein abundance results (Fig. 5) were available for 477 Chinook salmon captured in the Yukon River and three spawning tributaries (Table 3). Across all capture locations and both study years, heat stress was identified using gene transcription and protein biomarkers in more than half of Chinook salmon examined (54%, n = 477). The overall evidence of heat stress was summed across individuals for which heat stress was only indicated by gene transcription (15%), only indicated by HSP70 protein (20%), or indicated by both biomarkers (19%).

The proportion of Chinook salmon with evidence of heat stress was higher in 2017 than in 2016 at the three locations further upstream: Rapids Fish Wheel (18% in 2016 versus 97% in 2017, z = 4.45, P < 0.001), the Chena River (45% in 2016 versus 64% in 2017, z = 3.12, P = 0.002), and Eagle (38% in 2016 versus 64% in 2017, z = 2.12, P = 0.028; Fig. 6). Among individuals captured at the East Fork Andreafsky River, heat stress was more common in 2016 (98% in 2016 versus 18% in 2017, z = -4.90, P < 0.001; Fig. 6). The proportion of fish with heat stress was similar between years for fish captured at Emmonak (31% in 2016 versus 34% in 2017, z = 0.30, P = 0.764) and in the Gisasa River (66% in 2016 versus 77% in 2017, z = 1.08, P = 0.282).

Water temperatures in the mainstem Yukon River were warm during both years, although not extremely so in the context of the

Fig. 4. The LD1 gene (A) and HSP70 protein abundance (B) plotted against the maximum 3-day water temperature for Chinook salmon captured at the East Fork Andreafsky River weir during spawning migrations in 2016 and 2017 ($n = 86$). LD1 gene is calculated based on gene transcript data for each individual fish and gene-specific model coefficients fit based on experiment results (preferred model). Symbol color and shape reflects the heat stress classifications based on predictions fit with experiment data. Field-sampled individuals categorized as unstressed were similar to experimental control fish (blue circles), and individuals classified with heat stress were distinguished between heat stress similar to 18 °C experiment group (orange squares, LD1 genes only) or the 21 °C experiment group (red triangles). [Colour online.]



last decade (Fig. 1). Mainstem mean water temperatures at Pilot Station were similar between the 2 years in June (Table 4; t test, $t = 0.65$, $df = 2701$, $P = 0.517$) and August (t test, $t = 0.40$, $df = 1612$, $P = 0.693$), but differed in July (t test, $t = -13.6$, $df = 2964$, $P < 0.001$), with July 2017 being warmer than July 2016 (Table 4). Water temperatures were also warmer in 2017 than 2016 in the Gisasa River during July (t test, $t = -32.8$, $df = 2213$, $P < 0.001$) and Chena River during June (t test, $t = -12.4$, $df = 4952$, $P < 0.001$), July (t test, $t = -53.6$, $df = 4553$, $P < 0.001$), and August (t test, $t = -38.9$, $df = 3749$, $P < 0.001$). In contrast, water temperatures at the East Fork Andreafsky River weir were warmer in 2016 during the second half of June (data only available for 15 to 30 June; t test, $t = 32.4$, $df = 2553$, $P < 0.001$) and July (t test, $t = 21.5$, $df = 4334$, $P < 0.001$).

Discussion

This study provides evidence that heat stress is prevalent in migrating adult Chinook salmon near their northern range extent in the Yukon River. Given the established links between heat stress and increased mortality, warm water temperatures may already contribute to population-level consequences for Yukon

River Chinook salmon and the failure to recover from declines that began more than two decades ago. Because water temperature data are limited prior to population declines in the late 1990s, the possibility that warming temperatures contributed to the initial decline is difficult to assess. Our experiment identified gene transcription and HSP70 protein response consistent with heat stress at two water temperatures (18 and 21 °C) that regularly occur during the spawning migration. The experimental fish response was used to train biomarker classification models that subsequently identified field-captured individuals as heat-stressed or not and allowed heat stress to be summarized as a proportion. More than half of the field-captured Chinook salmon had evidence of heat stress in at least one biomarker. The proportion of heat-stressed fish varied between years at most locations, with higher heat stress proportions estimated in the warmer year. Between the two biomarkers, the HSP70 protein is a more straightforward, cost-effective tool for identifying and monitoring heat stress in future studies, and gene transcription results provided a deeper understanding of how warm temperatures disrupt processes in the body and helped

Fig. 5. Boxplots of LD1 genes (A) and HSP70 protein abundance (B) for spawning Chinook salmon captures across the Yukon River watershed in either 2016 (navy, lower boxplot for each location) or 2017 (purple, upper boxplot for each location) in relation to results from an experimental temperature manipulation (green). Dashed lines reflect the threshold for identifying heat stress. Heat stress is indicated by values lower than the LD1 threshold and higher than the HSP70 protein threshold. In each boxplot, the horizontal line is the median, the upper and lower ends of the box are the first and third quartiles, and the whiskers extend to the highest and lowest values that are within the 1.5x interquartile range. Outliers are not shown.

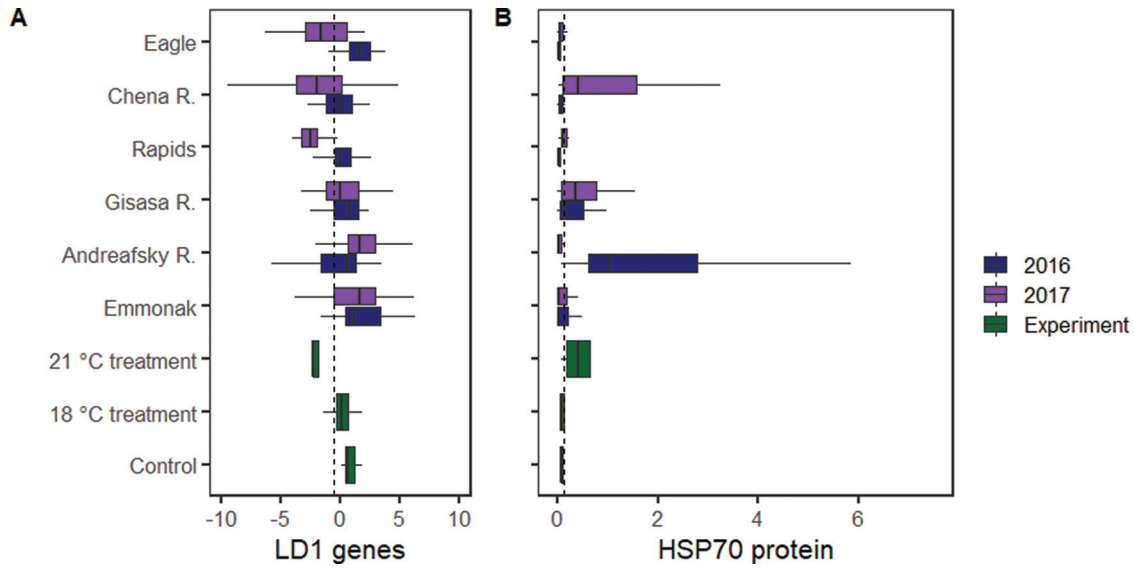


Fig. 6. A map depicting the percentage of Chinook salmon in each capture location (black circles) and year with evidence of heat stress. Paired stacked bar charts reflect the heat stress classifications from gene transcript and HSP70 protein for fish captured in summer 2016 (left) and 2017 (right). Fill reflects the proportion of individuals in each of the four heat stress categories: hatched green = no evidence of heat stress in either gene transcription or HSP70 protein; gold = heat stress identified only in gene transcription; red = heat stress identified in gene transcription and elevated HSP70 protein; and dotted purple = heat stress identified only by elevated HSP70 protein). Numbers near each bar are the sum across the three categories that identified heat stress presence. The white star is the location of the temperature experiment near Pilot Station, Alaska, USA. An asterisk (*) prior to the capture location name denotes a significant difference ($P < 0.05$) in the heat stress proportion between capture years. Map created in ArcMap 10.7 (Esri, Redlands, California, USA) with selected rivers from the National Hydrography Dataset (US Geological Survey 2015) and shorelines from Wessel and Smith (1996).

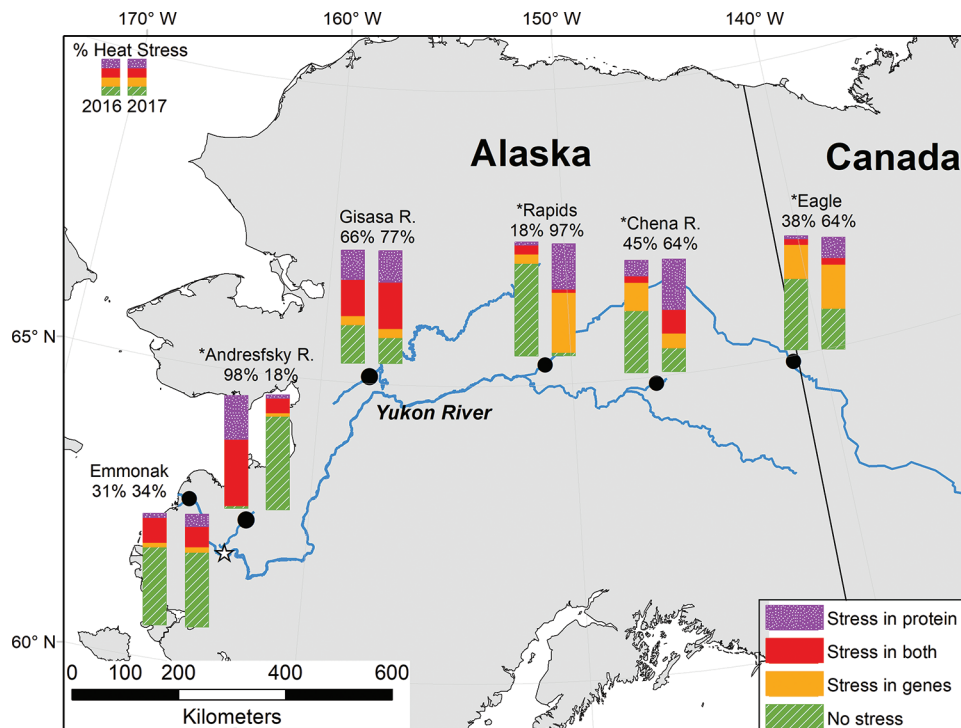


Table 4. Mean (\pm standard deviation) and maximum monthly water temperatures ($^{\circ}$ C) for the mainstem Yukon River and sampled tributaries in June, July, and August of 2016 and 2017.

River	Year	June		July		August	
		Mean	Max.	Mean	Max.	Mean	Max.
Yukon River	2016	15.3 \pm 1.4	19.6	18.3 \pm 0.9	20.1	16.1 \pm 0.4	17.6
	2017	15.3 \pm 1.8	18.2	18.7 \pm 1.0*	20.3	16.1 \pm 1.8	18.7
East Fork Andreafsky River	2016	16.2 \pm 2.3*	22.2	17.2 \pm 2.3*	23.2	—	—
	2017	14.0 \pm 1.5	21.7	15.9 \pm 1.8	20.5	—	—
Gisasa River	2016	—	—	15.2 \pm 2.0	20.5	—	—
	2017	—	—	17.1 \pm 1.5*	21.2	—	—
Chena River	2016	8.67 \pm 1.5	12.2	8.28 \pm 1.6	13.1	7.66 \pm 0.7	9.3
	2017	9.22 \pm 1.7*	13.1	10.5 \pm 1.3*	13.6	9.05 \pm 1.8*	13.7

Note: Water temperature data for the East Fork Andreafsky River in June are incomplete and begin on 15 June. No data are available in June for the Gisasa River or August for the East Fork Andreafsky or Gisasa rivers. Water temperature records are only collected at the East Fork Andreafsky and Gisasa rivers when staff are present at weirs to monitor Pacific salmon escapement.

*Denotes the warmer water temperature in interannual monthly comparisons at each river ($P < 0.05$).

identify potential mechanisms linking heat stress to mortality (also see Bowen et al. 2020).

Temperature manipulation experiment

Gene transcript biomarkers successfully identified a cellular response to 18 and 21 $^{\circ}$ C, while the HSP70 protein response only distinguished fish in the 21 $^{\circ}$ C treatment group. The differences in mRNA and protein response identified here largely agree with previous studies of Pacific salmon in southern regions of their range, namely the upregulation of heat shock genes and proteins and differential immune system response (Evans et al. 2011; Miller et al. 2011, 2014; Jeffries et al. 2014). This study is the first to identify a cellular stress response to elevated temperature from a high-latitude Pacific salmon population.

An increase in the transcription and protein abundance of heat shock proteins is the hallmark of the heat shock response (Lindquist 1986). Thus, it was no surprise that HSP70 and HSP90 were influential in distinguishing heat stress in muscle tissue or that the HSP70 protein alone was able to correctly classify individuals to the 21 $^{\circ}$ C treatment in all cases. The transcription and protein abundance of heat shock proteins exhibit a ubiquitous increase in response to elevated water temperature in past studies regardless of tissue type (Palmisano et al. 2000; Basu et al. 2002; Iwama 2004; Buckley et al. 2006; Evans et al. 2011). A differential response between the heat shock protein genes was evident between the 18 and 21 $^{\circ}$ C treatment groups, with both HSP70 and HSP90 contributing to classification of the 21 $^{\circ}$ C group; HSP90 responded more strongly based upon the magnitude of the coefficients in the model. In contrast, the 18 $^{\circ}$ C treatment group was distinguished by elevated HSP70 in the LDA model with little influence of HSP90.

Immune system genes were differentially expressed in the muscle tissue of 18 and 21 $^{\circ}$ C treatment groups compared with control fish. Immune system responses to heat stress have often been documented in Pacific salmon and include examples from gill and cardiac tissue (McCullough et al. 2009; Evans et al. 2011; Miller et al. 2011; Jeffries et al. 2012; Anttila et al. 2014). The immune response in muscle tissue has been less frequently studied in fish, but muscle is known to be immunologically active (Valenzuela et al. 2017) and is a common site of disease and infection in Pacific salmon (Meyers et al. 2019). Immune system genes retained in the final model were related to two pathways of T helper (Th) cells, Th1 immune response (*IFN α*) and Th2 immune response (*Gata3*) (citations in Table 1). Within our results, an influence of the Th1 immune gene *IFN α* was consistent with upregulation at 18 $^{\circ}$ C but downregulation at 21 $^{\circ}$ C. The Th2 immune gene *Gata3* was upregulated at 21 $^{\circ}$ C, but no clear influence was present at 18 $^{\circ}$ C. The upregulation of Th1 immune response seen in the 18 $^{\circ}$ C treatment is typical of acute stressors and reflects an appropriate immune defense, while the Th2 response seen in the 21 $^{\circ}$ C treatment is

typical of a chronic response and immune suppression that can be detrimental (Tort 2011). Still, data reflected the changes in just two of many genes that are part of the immune system and did not provide a full picture of the immune system response. Concurrent results from an analysis of the entire transcriptome for individuals included in this experiment offers more insight to the complexity of the immune system response to warming temperatures (Bowen et al. 2020).

Immune system genes may respond to temperature if warming increases activity of latent pathogens in the body of the fish (Crossin et al. 2008; Miller et al. 2011, 2014). Many pathogens occur at chronic low levels in fish under normal circumstances and are poised to respond when conditions are more suitable (Arkoosh et al. 2004; Miller et al. 2014). Although there are likely many pathogens present, the most studied pathogen in Yukon River Chinook salmon is the parasite *Ichthyophonus hoferi* that causes inflammation in several tissues including muscle (Kocan et al. 2004; AYK-SSI 2013). Disease progression for fish infected with *I. hoferi* is known to be faster in warmer water (Kocan et al. 2004), but it is not clear whether the short (\sim 6 h) duration of this experiment would allow enough time for the response of a latent pathogen. Without an independent assessment of pathogen load or even a synoptic examination of pathogens in Yukon River Chinook salmon, interpreting the cause of differential responses among immune system genes following exposure to heat is speculative. Still, the response of the immune system and immune genes is a consistent feature in heat-stressed salmon (McCullough et al. 2009; Evans et al. 2011; Miller et al. 2011; Jeffries et al. 2012; Anttila et al. 2014) and warrants further study about the potential for pathogens to exacerbate stress and mortality with warming in Alaska Pacific salmon.

Warming was associated with differential expression of a gene closely linked with contaminants (*AHR* and *SOD*; Wheelock et al. 2005; Arellano-Aguilar et al. 2009; Erdoğan et al. 2011; Uno et al. 2012). *AHR* transcripts were lower in the 18 $^{\circ}$ C treatment, while *SOD* transcripts declined with warming and contributed to distinguishing fish from both the 18 and 21 $^{\circ}$ C treatments. Decreased expression of genes related to detoxification of xenobiotics has been associated with heat stress (Veldhoen et al. 2010; Lapointe et al. 2011; Tomalty et al. 2015), as well as hypoxia (Rahman and Thomas 2012) and pathogens (Reynaud et al. 2008). Although the mechanisms involved are unclear, decreased expression of genes involved in detoxification may simply indicate a reallocation of resources to the more substantial stressor.

Assessment of experimentally derived models to identify heat stress

The experimentally derived models for gene transcription and the HSP70 protein used to identify heat stress performed well in an independent assessment using Chinook salmon captured in a

lower Yukon River tributary, the East Fork Andreafsky River. Salmon captured when water temperatures had recently exceeded 21 °C were all identified by the model as being similar to fish treated with 21 °C based on gene transcription response (represented by LD1, Fig. 4A). Moreover, differences in gene transcription were related to recent maximum water temperature across the whole range of observed temperature values. Elevated HSP70 protein was also strongly related to water temperature (Fig. 4B), with an inflection point separating unstressed and heat stress individuals near 18 °C, the presumed heat stress threshold for migrating adult Pacific salmon based on our literature review (see Introduction).

Very few individuals in the East Fork Andreafsky River had gene transcription results similar to fish treated with 18 °C despite water temperature data suggesting that several individuals recently experienced water temperatures between 18 and 21 °C (Fig. 4A). In the experiment, a lower level of heat stress could be detected in the gene transcript response but not the HSP70 protein response; the opposite appeared to be true in the assessment of Andreafsky fish. A HSP70 protein response identified heat stress for nearly all individuals captured when water temperatures had recently exceeded 18 °C (98%, $n = 40$) in the tributary. It appears that prolonged exposure to temperatures near 18 °C (or increased time since exposure) may have resulted in an HSP70 protein response in field-sampled Chinook salmon, which was not apparent in the acute experiment. This hypothesis is supported by laboratory studies that indicate that HSP70 protein abundance first appears after 2 h of exposure to elevated temperature and peaks and stays elevated for 24–72 h (Lund et al. 2003). This possibility is also supported by evidence of increased HSP70 mRNA levels in individuals treated with 18 °C that would presumably have resulted in more HSP70 protein in time. The gene transcription signature that defined our 18 °C treated individuals, captured by LD2, may be relatively fleeting. Indeed, a gene transcription response similar to that of individuals treated with 18 °C was rarely (5%, $n = 477$) observed in field-sampled Chinook salmon across all locations in the Yukon River watershed.

Heat stress prevalence

Heat stress was prevalent (>50% of individuals) at all locations in at least one of the two study years, except near the river mouth at Emmonak (Figs. 5 and 6). Lower and consistent rates of heat stress for individuals passing through Emmonak agree with the cooler water temperatures that occur early in the migration during June. Heat stress was prevalent in 2017 at all three upper watershed locations (Rapids, Chena River, and Eagle), but not 2016, in agreement with warmer temperatures in the mainstem Yukon River (Fig. 6). Within the East Fork Andreafsky River, a lower Yukon River tributary, an opposite interannual difference was observed consistent with the local water temperatures in the tributary. The lack of coherence in water temperature interannual variation among rivers is likely related to differences in the hydrology and atmospheric conditions across the distinct regions of the watershed (Brabets and Walvoord 2009). The East Fork Andreafsky River differs from the rest of the watershed in terms of its lower elevation and gradient (Olsen et al. 2010) and closer proximity to the Bering Sea, which results in more of a maritime climate as compared with middle and upper river tributaries (Brabets et al. 2000).

Results for Chinook salmon captured in the Chena River may be among the most surprising and informative given that water temperatures are often cool in the Chena, Salcha, and greater Tanana rivers watershed owing to a higher influence of cold groundwater and glacier melt (Brabets et al. 2000; Walvoord and Striegl 2007). It appears that prolonged (weeks) exposure to warmer water temperatures in the mainstem Yukon River during the spawning migration was still detectable when individuals were captured in the Chena River's cooler water further upstream. Chinook salmon captured in the Chena River have spent ~24 days in the mainstem

Yukon River (~1100 km) and ~11 days in the cooler Tanana and Chena rivers (~500 km) assuming a migration speed of 45.8 km·day⁻¹ for Chena River Chinook salmon (Eiler et al. 2015). Note that individuals may spend more or less time in each of these rivers given that migration speeds are known to decline with warm temperature (Gonia et al. 2006) and as migration progresses (Eiler et al. 2015).

Similarity in results among fish captured from the three sites (Rapids, Chena River, and Eagle) further upstream in the Yukon River watershed suggests that long stretches of shared migration corridors may synchronize the influence of heat stress among populations. Synchrony in any attribute of Pacific salmon across populations has usually been interpreted as a reflection of their shared conditions during ocean residency (e.g., ocean temperature, feeding conditions), as the natal freshwater habitats of each population can have dramatic differences in environmental conditions (Hare et al. 1999; Mueter et al. 2002). Synchrony as a result of shared migration corridors is rarely considered because this phase is short relative to the life-span of the fish, many attributes are set prior to river entry (e.g., body length), and not all watersheds have a long, shared migration route like the Yukon River.

In addition to thermal stress, heat stress biomarkers can be induced by a variety of environmental factors (Deane and Woo 2011), including social stressors and lack of food (Currie et al. 2010). In our studies, the wide variation in heat stress rates between study years within locations provided additional confidence that heat stress classifications were robust to changes in gene transcription and HSP70 protein during the spawning migration that are associated freshwater entry, sexual maturation, and senescence (Evans et al. 2011; Miller et al. 2011; Carey et al. 2019). Our sampling focused on collections that occurred in migration corridors and used only live fish sampled within minutes of capture. The thresholds developed here for identifying heat stress are likely inappropriate for Chinook salmon captured on spawning grounds or collected as carcasses. Among the locations included in this study, the applicability of these thresholds is most uncertain for individuals collected near Emmonak. This location is the closest to the river mouth where fish undergo a major physiological shift from salt water to fresh water that may result in shifts to gene transcription and HSP70 protein abundance (Evans et al. 2011). Indeed, any detection of heat stress at this location is suspect because water temperatures were cool (generally <15 °C) at the time of collection, and there was no reason to suspect previous exposure to warm water temperatures at this time of year. Moreover, gene transcription and HSP70 protein values are just above the threshold for heat stress detection (Fig. 5).

The Gisasa River was the only location where heat stress was prevalent in both study years, and no interannual difference in heat stress proportion was detected despite warmer temperatures in 2017. The high heat stress proportions in both years may simply reflect that Chinook salmon reach the Gisasa River weir at the seasonal peak of water temperatures in mid-July. The largest observed Pacific salmon mortality event within the Yukon River watershed during the 2019 heatwave was also located within the same portion of the Yukon watershed (Koyukuk River) in mid-July with chum salmon (*Oncorhynchus keta*) that have similar migration timing (Westley 2020). The only other site with a strong overlap in sample collections and peak water temperatures was in the much cooler Chena River, where individuals likely move into cooler tributary waters prior to the seasonal maximum temperature in the mainstem Yukon River in mid-July.

Here, we did not have the data necessary to consider the effects of population on the response of heat stress biomarkers. Previous studies have indicated that populations with a long-term history of warmer water temperatures have physiological adaptations that moderately increase thermal tolerance and performance (Eliason et al. 2011). The potential for similar population-specific adaptations to spawning migration temperatures appears unlikely within the Yukon River Chinook salmon because nearly all

Yukon River Chinook salmon populations encounter warm water during their upstream migrations. Thus, the variability in water temperature experience among populations might be too weak to elicit or detect variability in thermal tolerance in Yukon River Chinook salmon. Still, we cannot rule out the effects of variability in water temperatures of spawning and rearing habitats on thermal tolerances among populations.

Conclusions

The evidence presented here was consistent with routine, prevalent heat stress for Chinook salmon near their northern range extent in the Yukon River. Three major findings support this conclusion. First, the experiment and field results from the East Fork Andreafsky River agreed with the general presumption that water temperatures near 18 °C approximate the threshold of heat stress. Second, water temperatures routinely exceeded this threshold during the spawning migration each July over the last two decades. Third, gene transcription and HSP70 protein levels identified prevalent heat stress during field sampling in 2016 and 2017, years when outward signs of heat stress were nearly nonexistent. The cellular stress response used to identify heat stress in this study is an adaptive response that can protect cellular function for just a limited amount of time in a relatively narrow temperature range. To this point, heat stress often predicts en route and prespawn mortality or reduced reproductive success because warm temperatures often exceed the protection afforded by the cellular stress response (Evans et al. 2011; Miller et al. 2011; Jeffries et al. 2012). In light of the findings presented here, the unusual mortality of Pacific salmon species along migration routes during the record-breaking warmth and low water level of 2019 (e.g., Westley 2020) is not surprising. The mortality observations provide additional evidence that water temperatures are already high enough to cause mortality among Pacific salmon populations near their northern range extent. The apparent absence of carcasses in previous years does not infer a lack of mortality because carcasses initially sink at death and are rarely observable in large turbid rivers (Farrell et al. 2008) like the Yukon River. Indeed, the low water levels may be a key reason that carcasses were observed in 2019 and not previous years with warm water temperatures.

This work has immediate implications for management considerations and research priorities, particularly in the context of projections that universally forecast continued warming (Post et al. 2019). This study is the first to confirm that freshwater temperatures are stressful to Pacific salmon migrating in a northern river. Results here raise concerns that unaccounted mortality may result in an overestimation of Pacific salmon spawning success in warm water years. Spawning abundances are the primary data used to assess management success in escapement-based management. In fact, the productivity (log recruits per spawner) of Chinook salmon populations across several southcentral Alaska watersheds was recently shown to decline steeply when spawning water temperatures exceed 18 °C, the same water temperature threshold identified for heat stress in this study (Jones et al. 2020). More research is needed that links water temperature, heat stress, and mortality in northern rivers to assess the sensitivity of population dynamics to environmental conditions during the spawning migration. Useful studies for assessing the severity and scale of this threat include expanding water temperature and heat stress monitoring to additional northern watersheds, simple surveys of egg retention on spawning grounds (e.g., prespawn mortality), large-scale tagging studies to estimate en route mortality rates, and physiological experiments to identify lethal temperature and dissolved oxygen thresholds (e.g., aerobic scope).

Acknowledgements

The USGS Ecosystems Mission Area and the Arctic–Yukon–Kuskokwim Sustainable Salmon Initiative (award No. 1611) provided funding for this study. We thank the ADF&G Pilot Station

2018 Sonar Crew, especially L. Dreese, for their assistance in the field, subsistence fishers in the Rapids area for allowing sampling at their fish wheels, the Pilot Station Tribal Council for assistance with logistics, A. Tesch for providing space at the William Jack Hernandez Sport Fish Hatchery to test the experimental apparatus, D. Hall for his help in processing muscle samples for HSP70 analysis, J. Spaeder and K. Gillis of Bering Sea Fisherman's Association who provided thoughtful discussion of these findings, and E. Eliason and two anonymous reviewers for comments that improved the manuscript. Any use of trade names or products is for descriptive purposes only and does not imply endorsement of the US Government.

References


- ADF&G. 2013. Chinook salmon stock assessment and research plan, 2013. In Alaska Department of Fish and Game, Special Publication No. 13-01, Anchorage, Alaska.
- Anttila, K., Eliason, E.J., Kaukinen, K.H., Miller, K.M., and Farrell, A.P. 2014. Facing warm temperatures during migration: Cardiac mRNA responses of two adult *Oncorhynchus nerka* populations to warming and swimming challenges. *J. Fish Biol.* **84**(5): 1439–1456. doi:10.1111/jfb.12367. PMID:24684400.
- Arellano-Aguilar, O., Montoya, R.M., and Garcia, C.M. 2009. Endogenous functions and expression of cytochrome P450 enzymes in teleost fish: a review. *Rev. Fish. Sci.* **17**(4): 541–556. doi:10.1080/10641260903243487.
- Arkoosh, M.R., Clemons, E., Kagle, A.N., Stafford, C., Glass, A.C., Jacobson, K., et al. 2004. Survey of pathogens in juvenile salmon *Oncorhynchus* spp. migrating through Pacific Northwest estuaries. *J. Aquat. Anim. Health*, **16**(4): 186–196. doi:10.1577/H03-071.1.
- AYK-SSI. 2013. Arctic–Yukon–Kuskokwim Chinook Salmon research action plan: evidence of decline of Chinook salmon populations and recommendations for future research. In Arctic–Yukon–Kuskokwim Sustainable Salmon Initiative, Anchorage, Alaska.
- Basu, N., Todgham, A.E., Ackerman, P.A., Bibeau, M.R., Nakano, K., Schulte, P.M., and Iwama, G.K. 2002. Heat shock protein genes and their functional significance in fish. *Gene*, **295**: 173–183. doi:10.1016/S0378-1119(02)00687-X. PMID:12354651.
- Bowen, L., von Biela, V.R., McCormick, S.D., Regish, A.M., Waters, S., Durbin-Johnson, B., et al. 2020. Transcriptomic response to elevated water temperatures in adult migrating Yukon River Chinook salmon (*Oncorhynchus tshawytscha*). *Conserv. Physiol.* **8**(1): coaa084. doi:10.1093/conphys/coaa084.
- Bowerman, T., Keefer, M.L., and Caudill, C.C. 2016. Pacific salmon prespawn mortality: patterns, methods, and study design considerations. *Fisheries*, **41**(12): 738–749. doi:10.1080/03632415.2016.1245993.
- Brabets, T.P., Walvoord, M.A. 2009. Trends in streamflow in the Yukon River Basin from 1944 to 2005 and the influence of the Pacific Decadal Oscillation. *J. Hydrol.* **371**(1–4): 108–119. doi:10.1016/j.jhydrol.2009.03.018.
- Brabets, T.P., Wang, B., and Meade, R.H. 2000. Environmental and hydrologic overview of the Yukon River basin, Alaska and Canada. In US Geological Survey, Water Resources Investigations Report 99–4204.
- Brown, R.J., von Finster, A., Henszey, R.J., and Eiler, J.H. 2017. Catalog of Chinook Salmon spawning areas in Yukon River basin in Canada and United States. *J. Fish Wildl. Manage.* **8**(2): 558–587. doi:10.3996/052017-JFWM-045.
- Buckley, B.A., Gracey, A.Y., and Somero, G.N. 2006. The cellular response to heat stress in the goby *Gillichthys mirabilis*: a cDNA microarray and protein-level analysis. *J. Exp. Biol.* **209**: 2660–2677. doi:10.1242/jeb.02292. PMID:16809457.
- Bustin, S.A. 2002. Quantification of mRNA using real-time reverse transcription PCR (RT-PCR): trends and problems. *J. Mol. Endocrinol.* **29**(1): 23–39. doi:10.1677/jme.0.0290023. PMID:12200227.
- Carlson, J.G., and Edwards, O.N. 2017. Abundance and run timing of adult Pacific salmon in the East Fork Andreafsky River, Yukon Delta National Wildlife Refuge, Alaska, 2016. US Fish and Wildlife Service, Alaska Fisheries Data Series 2017-5.
- Carey, M.P., Keith, K.D., Schelske, M., Lean, C., McCormick, S.D., Regish, A., and Zimmerman, C.E. 2019. Energy depletion and stress levels in sockeye salmon migrating at the northern edge of their distribution. *Trans. Am. Fish. Soc.* **148**(4): 785–797. doi:10.1002/tafs.10172.
- Chadwick, J.G., and McCormick, S.D. 2017. Upper thermal limits of growth in brook trout and their relationship to stress physiology. *J. Exp. Biol.* **220**(21): 3976–3987. doi:10.1242/jeb.161224. PMID:29093190.
- Conitz, J.M. 2018. Abundance and run timing of adult Pacific salmon in the East Fork Andreafsky River, Yukon Delta National Wildlife Refuge, Alaska, 2017. Alaska Fish. Data Ser. 2018-8: 22.
- Copeland, D.L., Duff, R.J., Liu, Q., Prokop, J., and Londraville, R.L. 2011. Leptin in teleost fishes: an argument for comparative study. *Front. Physiol.* **2**: Article 26. doi:10.3389/fphys.2011.00026. PMID:21716655.
- Crossin, G.T., Hinch, S.G., Cooke, S.J., Welch, D.W., Patterson, D.A., Jones, S.R.M., et al. 2008. Exposure to high temperature influences the behaviour, physiology, and survival of sockeye salmon during spawning migration. *Can. J. Zool.* **86**(2): 127–140. doi:10.1139/Z07-122.
- Crozier, L.G., Hendry, A.P., Lawson, P.W., Quinn, T.P., Mantua, N.J., Battin, J.,

- et al. 2008. Potential responses to climate change in organisms with complex life histories: evolution and plasticity in Pacific salmon. *Evol. Appl.* **1**: 252–270. doi:10.1111/j.1752-4571.2008.00033.x. PMID:25567630.
- Currie, S., LeBlanc, S., Watters, M.A., and Gilmour, K.M. 2010. Agonistic encounters and cellular angst: Social interactions induce heat shock proteins in juvenile salmonid fish. *Proc. R. Soc. B Biol. Sci.* **277**(1683): 905–913. doi:10.1098/rspb.2009.1562. PMID:19923129.
- Deane, E.E., and Woo, N.Y.S. 2011. Advances and perspectives on the regulation and expression of piscine heat shock proteins. *Rev. Fish Biol. Fish.* **21**(2): 153–185. doi:10.1007/s11160-010-9164-8.
- Donnelly, D.S., Von Biela, V.R., McCormick, S.D., Laske, S.M., Carey, M.P., Waters, S., et al. 2020. A manipulative thermal challenge protocol for adult salmonids in remote field settings. *Conserv. Physiol.* **8**(1): coaa074. doi:10.1093/conphys/coaa074.
- Eiler, J.H., Masuda, M.M., Spencer, T.R., Driscoll, R.J., and Schreck, C.B. 2014. Distribution, stock composition and timing, and tagging response of wild chinook salmon returning to a large, free-flowing river basin. *Trans. Am. Fish. Soc.* **143**(6): 1476–1507. doi:10.1080/00028487.2014.959997.
- Eiler, J.H., Evans, A.N., and Schreck, C.B. 2015. Migratory patterns of wild Chinook salmon *Oncorhynchus tshawytscha* returning to a large, free-flowing river basin. *PLoS ONE*, **10**(4): e0123127. doi:10.1371/journal.pone.0123127.
- Eliason, E.J., Clark, T.D., Hague, M.J., Hanson, L.M., Gallagher, Z.S., Jeffries, K.M., et al. 2011. Differences in thermal tolerance among sockeye salmon populations. *Science*, **332**(6025): 109–112. doi:10.1126/science.1199158. PMID:21454790.
- Eliason, E.J., Clark, T.D., Hinch, S.G., and Farrell, A.P. 2013. Cardiorespiratory collapse at high temperature in swimming adult sockeye salmon. *Conserv. Physiol.* **1**(1): cot008. doi:10.1093/conphys/cot008.
- Erdogan, O., Ceyhan, S.B., Ekinci, D., and Aksakal, E. 2011. Impact of deltamethrin exposure on mRNA expression levels of metallothionein A, B and cytochrome P450 1A in rainbow trout muscles. *Gene*, **484**(1–2): 13–17. doi:10.1016/j.gene.2011.05.026. PMID:21658436.
- Evans, T.G., Hammill, E., Kaukinen, K., Schulze, A.D., Patterson, D.A., English, K.K., et al. 2011. Transcriptomics of environmental acclimatization and survival in wild adult Pacific sockeye salmon (*Oncorhynchus nerka*) during spawning migration. *Mol. Ecol.* **20**: 4472–4489. doi:10.1111/j.1365-294X.2011.05276.x. PMID:21951593.
- Farrell, A., Hinch, S.G., Cooke, S.J., Patterson, D.A., Crossin, G.T., Lapointe, M., and Mathes, M.T. 2008. Pacific salmon in hot water: applying aerobic scope models and biotelemetry to predict the success of spawning migrations. *Physiol. Biochem. Zool.* **81**(6): 697–709. doi:10.1086/592057. PMID:18922081.
- Feder, M.E., and Hofmann, G.E. 1999. Heat-shock proteins, molecular chaperones, and the stress response: evolutionary biology and ecological physiology. *Annu. Rev. Physiol.* **61**: 243–282. doi:10.1146/annurev.physiol.61.1.243. PMID:10099689.
- Finney, B.P., Gregory-Eaves, I., Sweetman, J., Douglas, M.S.V., and Smol, J.P. 2000. Impacts of climatic change and fishing on Pacific salmon abundance over the past 300 years. *Science*, **290**(5492): 795–799. doi:10.1126/science.290.5492.795. PMID:11052941.
- Gonia, T.M., Keefer, M.L., Bjornn, T.C., Peery, C.A., Bennett, D.H., and Stuehrenberg, L.C. 2006. Behavioral thermoregulation and slowed migration by adult fall Chinook salmon in response to high Columbia River water temperatures. *Trans. Am. Fish. Soc.* **135**: 408–419. doi:10.1577/T04-113.1.
- Hare, B.S.R., Mantua, N.J., and Francis, R.C. 1999. Inverse production regimes: Alaska and west coast Pacific salmon. *Fisheries*, **24**(1): 6–14. doi:10.1577/1548-8446(1999)024<0006:IPR>2.0.CO;2.
- Hinch, S.G., Cooke, S.J., Farrell, A.P., Miller, K.M., Lapointe, M., and Patterson, D.A. 2012. Dead fish swimming: A review of research on the early migration and high premature mortality in adult Fraser River sockeye salmon *Oncorhynchus nerka*. *J. Fish Biol.* **81**: 576–599. doi:10.1111/j.1095-8649.2012.03360.x. PMID:22803725.
- Iwama, G.K. 2004. Are hsp suitable for indicating stressed states in fish? *J. Exp. Biol.* **207**(1): 15–19. doi:10.1242/jeb.00707. PMID:14638828.
- Iwama, G.K., Thomas, P.T., Forsyth, R.B., and Vijayan, M.M. 1998. Heat shock protein expression in fish. *Rev. Fish Biol. Fish.* **8**: 35–56. doi:10.1023/A:1008812500650.
- Iwama, G.K., Vijayan, M.M., Forsyth, R.B., and Ackerman, P.A. 1999. Heat shock proteins and physiological stress in fish. *Am. Zool.* **39**(6): 901–909. doi:10.1093/icb/39.6.901.
- Jeffries, K.M., Hinch, S.G., Sierocinski, T., Clark, T.D., Eliason, E.J., Donaldson, M.R., et al. 2012. Consequences of high temperatures and premature mortality on the transcriptome and blood physiology of wild adult sockeye salmon (*Oncorhynchus nerka*). *Ecol. Evol.* **2**(7): 1747–1764. doi:10.1002/ece3.274. PMID:22957178.
- Jeffries, K.M., Hinch, S.G., Sierocinski, T., Pavlidis, P., and Miller, K.M. 2014. Transcriptomic responses to high water temperature in two species of Pacific salmon. *Evol. Appl.* **7**: 286–300. doi:10.1111/eva.12119. PMID:24567748.
- Jones, L.A., Schoen, E.R., Shaftel, R., Cunningham, C.J., Manger, S., Rinella, D.J., and St. Saviour, A. 2020. Watershed-scale climate influences productivity of Chinook salmon populations across southcentral Alaska. *Global Change Biol.* **26**: 4919–4936. doi:10.1111/gcb.15155.
- Keefer, M.L., Peery, C.A., and Heinrich, M.J. 2008. Temperature-mediated en route migration mortality and travel rates of endangered Snake River sockeye salmon. *Ecol. Freshw. Fish.* **17**: 136–145. doi:10.1111/j.1600-0633.2007.00267.x.
- Kocan, R.M., Hershberger, P.K., and Winton, J. 2004. Ichthyophthiasis: an emerging disease of Chinook salmon (*Oncorhynchus tshawytscha*) in the Yukon River. *J. Aquat. Anim. Health*, **16**: 58–72. doi:10.1577/H03-068.1.
- Kocan, R., Hershberger, P., Sanders, G., and Winton, J. 2009. Effects of temperature on disease progression and swimming stamina in *Ichthyophonus*-infected rainbow trout, *Oncorhynchus mykiss* Walbaum. *J. Fish Dis.* **32**: 835–843. doi:10.1111/j.1365-2761.2009.01059.x. PMID:19570061.
- Koch, J.C., Records, M.K., Striegl, R., and Walvoord, M.A. 2020. Water Level, temperature, and discharge of headwater streams in the Yukon River basin, Alaska, 2016 and 2017. US Geological Survey data release. doi:10.5066/P9NOHTRB.
- Kruger, C., and Zimmerman, C.E. 2009. Pacific salmon: ecology and management of Western Alaska's populations. American Fisheries Society, Bethesda, Md.
- Lapointe, D., Pierron, F., and Couture, P. 2011. Individual and combined effects of heat stress and aqueous or dietary copper exposure in fathead minnows (*Pimephales promelas*). *Aquat. Toxicol.* **104**(1–2): 80–85. doi:10.1016/j.aquatox.2011.02.022. PMID:21543052.
- Lewis, M., Götting, M., Anttila, K., Kanerva, M., Prokkola, J.M., Seppänen, E., et al. 2016. Different relationship between hsp70 mRNA and hsp70 levels in the heat shock response of two salmonids with dissimilar temperature preference. *Front. Physiol.* **7**: 1–12. doi:10.3389/fphys.2016.00511. PMID:26858649.
- Lindquist, S. 1986. The heat shock response. *Annu. Rev. Biochem.* **55**: 1151–1191. doi:10.1146/annurev.bi.55.070186.005443. PMID:2427013.
- Lund, S.G., Caissie, D., Cunjak, R.A., Vijayan, M.M., and Tufts, B.L. 2002. The effects of environmental heat stress on heat-shock mRNA and protein expression in Miramichi Atlantic salmon (*Salmo salar*) parr. *Can. J. Fish. Aquat. Sci.* **59**(9): 1553–1562. doi:10.1139/f02-117.
- Lund, S.G., Lund, M.E.A., and Tufts, B.L. 2003. Red blood cell Hsp 70 mRNA and protein as bio-indicators of temperature stress in the brook trout (*Salvelinus fontinalis*). *Can. J. Fish. Aquat. Sci.* **60**(4): 460–470. doi:10.1139/f03-039.
- Martins, E.G., Hinch, S.G., Cooke, S.J., and Patterson, D.A. 2012. Climate effects on growth, phenology, and survival of sockeye salmon (*Oncorhynchus nerka*): a synthesis of the current state of knowledge and future research directions. *Rev. Fish Biol. Fish.* **22**(4): 887–914. doi:10.1007/s11160-012-9271-9.
- Mathes, M.T., Hinch, S.G., Cooke, S.J., Crossin, G.T., Patterson, D.A., Lotto, A.G., and Farrell, A.P. 2010. Effect of water temperature, timing, physiological condition, and lake thermal refugia on migrating adult Weaver Creek sockeye salmon (*Oncorhynchus nerka*). *Can. J. Fish. Aquat. Sci.* **67**(1): 70–84. doi:10.1139/F09-158.
- McCullough, D.A. 1999. A review and synthesis of effects of alterations to the water temperature regime on freshwater life stages of Salmonids, with special reference to Chinook salmon. *Reg. 10 Water Resour. Assess. Rep. No. 910-R-99-010*.
- McCullough, D.A., Bartholow, J.M., Jager, H.I., Beschta, R.L., Cheslak, E.F., Deas, M.L., et al. 2009. Research in thermal biology: burning questions for coldwater stream fishes. *Rev. Fish. Sci.* **17**: 90–115. doi:10.1080/10641260802590152.
- Meyers, T., Burton, T., Bentz, C., Ferguson, J., Stewart, D., and Starkey, N. 2019. Diseases of wild and cultured fishes in Alaska. Alaska Department of Fish and Game, Fish Pathology Laboratories.
- Miller, K.M., Li, S., Kaukinen, K.H., Ginther, N., Hammill, E., Curtis, J.M.R., et al. 2011. Genomic signatures predict migration and spawning failure in wild Canadian salmon. *Science*, **331**: 214–217. doi:10.1126/science.1196901.
- Miller, K.M., Teffer, A., Tucker, S., Li, S., Schulze, A.D., Trudel, M., et al. 2014. Infectious disease, shifting climates, and opportunistic predators: cumulative factors potentially impacting wild salmon declines. *Evol. Appl.* **7**(7): 812–855. doi:10.1111/eva.12164. PMID:25469162.
- Mueter, F.J., Peterman, R.M., and Pyper, B.J. 2002. Opposite effects of ocean temperature on survival rates of 120 stocks of Pacific salmon (*Oncorhynchus* spp.) in northern and southern areas. *Can. J. Fish. Aquat. Sci.* **59**(3): 456–463. doi:10.1139/F02-020.
- NAS. 2011. Guide for the care and use of laboratory animals. 8th ed. National Academy of Sciences, Washington, D.C.
- NOAA, and NASA. 2020. 2019 was 2nd hottest year on record for Earth say NOAA, NASA [online]. Available from <https://www.noaa.gov/news/2019-was-2nd-hottest-year-on-record-for-earth-say-noaa-nasa>.
- Olsen, J.B., Beacham, T.D., Wetklo, M., Seeb, L.W., Smith, C.T., Flannery, B.G., and Wenburg, J.K. 2010. The influence of hydrology and waterway distance on population structure of Chinook salmon *Oncorhynchus tshawytscha* in a large river. *J. Fish Biol.* **76**(5): 1128–1148. doi:10.1111/j.1095-8649.2010.02554.x. PMID:20409166.
- Palmisano, A., Winton, J., and Dickhoff, W. 2000. Tissue-specific induction of Hsp90 mRNA and Plasma cortisol response in chinook salmon following heat shock, seawater challenge, and handling challenge. *Mar. Biotechnol.* **2**(4): 329–338. doi:10.1007/s101260000005. PMID:10960122.
- Post, E., Alley, R.B., Christensen, T.R., Macias-Fauria, M., Forbes, B.C., Gooseff, M.N., et al. 2019. The polar regions in a 2°C warmer world. *Sci. Adv.* **5**: eaaw9883. doi:10.1126/sciadv.aaw9883. PMID:31840060.
- Quintana, F.J., Basso, A.S., Iglesias, A.H., Korn, T., Farez, M.F., Bettelli, E., et al. 2008. Control of Treg and TH17 cell differentiation by the aryl hydrocarbon receptor. *Nature*, **453**(7191): 65–71. doi:10.1038/nature06880. PMID:18362915.
- Rahman, M.S., and Thomas, P. 2012. Effects of hypoxia exposure on hepatic cytochrome P450 1A (CYP1A) expression in Atlantic croaker: Molecular mechanisms of CYP1A down-regulation. *PLoS ONE*, **7**(7): e40825. doi:10.1371/journal.pone.0040825. PMID:22815834.

- Rand, P.S., Hinch, S.G., Morrison, J., Foreman, M.G.G., MacNutt, M.J., Macdonald, J.S., et al. 2006. Effects of river discharge, temperature, and future climates on energetics and mortality of adult migrating Fraser River Sockeye Salmon. *Trans. Am. Fish. Soc.* **135**(3): 655–667. doi:10.1577/T05-023.1
- Revena, C., Murray, S., Abramovitz, J., and Hammond, A. 1998. Watersheds of the world: ecological value and vulnerability. World Resources Institute, Washington, D.C.
- Reynaud, S., Raveton, M., and Ravanel, P. 2008. Interactions between immune and biotransformation systems in fish: A review. *Aquat. Toxicol.* **87**: 139–145.
- Roberts, A.P., Oris, J.T., and Stubblefield, W.A. 2006. Gene expression in caged juvenile coho salmon (*Oncorhynchus kisutch*) exposed to the waters of Prince William Sound, Alaska. *Mar. Pollut. Bull.* **52**(11): 1527–1532. doi:10.1016/j.marpolbul.2006.05.016. PMID:16854435.
- Robertson, B. 2018. The role of type I interferons in innate and adaptive immunity against viruses in Atlantic salmon. *Dev. Comp. Immunol.* **80**: 41–52. doi:10.1016/j.dci.2017.02.005. PMID:28196779.
- Strange, J.S. 2010. Upper thermal limits to migration in adult Chinook Salmon: evidence from the Klamath River Basin. *Trans. Am. Fish. Soc.* **139**(4): 1091–1108. doi:10.1577/T09-171.1.
- Tomalty, K.M.H., Meek, M.H., Stephens, M.R., Rincón, G., Fangue, N.A., May, B.P., and Baerwald, M.R. 2015. Transcriptional response to acute thermal exposure in juvenile Chinook salmon determined by RNAseq. *G3: Genes, Genomes, Genet.* **5**(7): 1335–1349. doi:10.1534/g3.115.017699.
- Tort, L. 2011. Stress and immune modulation in fish. *Dev. Comp. Immunol.* **35**(12): 1366–1375. doi:10.1016/j.dci.2011.07.002.
- Tsan, M.F., and Gao, B. 2004. Heat shock protein and innate immunity. *Cell. Mol. Immunol.* **1**(4): 274–279. PMID:16225770.
- Uno, T., Ishizuka, M., and Itakura, T. 2012. Cytochrome P450 (CYP) in fish. *Environ. Toxicol. Pharmacol.* **34**(1): 1–13. doi:10.1016/j.etap.2012.02.004. PMID:22418068.
- US Geological Survey. 2015. National Hydrography Dataset (ver. USGS National Hydrography Dataset (NHD) Best Resolution for HU4-1909 20151218 HU-4 Sub-region FileGDB 10.1 [published 20151218]) [online]. Available from <https://www.usgs.gov/core-science-systems/ngp/national-hydrography/access-national-hydrography-products>.
- Valenzuela, C.A., Zuloaga, R., Poblete-Morales, M., Vera-Tobar, T., Mercado, L., Avendaño-Herrera, R., et al. 2017. Fish skeletal muscle tissue is an important focus of immune reactions during pathogen infection. *Dev. Comp. Immunol.* **73**: 1–9. doi:10.1016/j.dci.2017.03.004. PMID:28279806.
- Veldhoen, N., Ikonomou, M.G., Dubetz, C., MacPherson, N., Sampson, T., Kelly, B.C., and Helbing, C.C. 2010. Gene expression profiling and environmental contaminant assessment of migrating Pacific salmon in the Fraser River watershed of British Columbia. *Aquat. Toxicol.* **97**(3): 212–225. doi:10.1016/j.aquatox.2009.09.009. PMID:19811841.
- Venables, W., and Ripley, B. 2002. Modern applied statistics with S. 4th ed. Springer, New York.
- Verrier, E.R., Langevin, C., Benmansour, A., and Boudinot, P. 2011. Early antiviral response and virus-induced genes in fish. *Dev. Comp. Immunol.* **35**(12): 1204–1214. doi:10.1016/j.dci.2011.03.012. PMID:21414349.
- Vignesh, K.S., and Deepe, G.S. 2017. Metallothioneins: emerging modulators in immunity and infection. *Int. J. Mol. Sci.* **18**(10): 2197. doi:10.3390/ijms18102197. PMID:29065550.
- von Biela, V.R., and Donnelly, D.S. 2020. Water temperature and dissolved oxygen measured during a manipulative thermal challenge experiment for adult salmonids, Yukon River, Alaska, 2018. US Geological Survey data release. doi:10.5066/P9ECW77M.
- von Biela, V.R., McCormick, S.D., Bowen, L., Regish, A., and Waters, S. 2020. Gene transcription and heat shock protein 70 abundance results from migrating adult Chinook salmon, Yukon watershed, 2016–2017. US Geological Survey data release. doi:10.5066/P9Y0I2H2.
- Wagner, G.N., Hinch, S.G., Kuchel, L.J., Lotto, A., Jones, S.R.M., Patterson, D.A., et al. 2005. Metabolic rates and swimming performance of adult Fraser River sockeye salmon (*Oncorhynchus nerka*) after a controlled infection with *Parvicapsula minibicornis*. *Can. J. Fish. Aquat. Sci.* **62**(9): 2124–2133. doi:10.1139/f05-126.
- Walvoord, M.A., and Striegl, R.G. 2007. Increased groundwater to stream discharge from permafrost thawing in the Yukon River basin: potential impacts on lateral export of carbon and nitrogen. **34**. doi:10.1029/2007GL030216.
- Wang, T., Holland, J.W., Martin, S.A.M., and Secombes, C.J. 2010. Sequence and expression analysis of two T helper master transcription factors, T-bet and GATA3, in rainbow trout *Oncorhynchus mykiss* and analysis of their expression during bacterial and parasitic infection. *Fish Shellfish Immunol.* **29**(5): 705–715. doi:10.1016/j.fsi.2010.06.016. PMID:20633655.
- Welch, W.J. 1993. How cells respond to stress. *Sci. Am.* **268**(5): 56–64. doi:10.1038/scientificamerican0593-56. PMID:8097593.
- Wessel, P., and Smith, W.H.F. 1996. A global, self-consistent, hierarchical, high-resolution shoreline database. *J. Geophys. Res.* **101**(B4): 8741–8743. doi:10.1029/96JB00104.
- West, F., and Prince, D. 2019. Genetic stock identification of Pilot Station Chinook salmon, 2018. Alaska Department of Fish and Game, Division of Commercial Fisheries, Regional Information Report 3A19-09, Anchorage, Alaska.
- Westley, P.A.H. 2020. Documentation of *en route* mortality of summer chum salmon in the Koyukuk River, Alaska and its potential linkage to the heat-wave of 2019. *Ecol. Evol.* [Online ahead of print.] doi:10.1002/ece3.6751.
- Wheelock, C.E., Eder, K.J., Werner, I., Huang, H., Jones, P.D., Brammell, B.F., et al. 2005. Individual variability in esterase activity and CYP1A levels in Chinook salmon (*Oncorhynchus tshawytscha*) exposed to esfenvalerate and chlorpyrifos. *Aquat. Toxicol.* **74**(2): 172–192. doi:10.1016/j.aquatox.2005.05.009. PMID:16011852.
- Zuray, S. 2010. Rampart rapids full season video monitoring 2010. In Annual report to the Yukon River Panel, Anchorage, Alaska.

FEATURE

Premature Mortality Observations among Alaska's Pacific Salmon During Record Heat and Drought in 2019

Vanessa R. von Biela  | U.S. Geological Survey, Alaska Science Center, 4210 University Drive, Anchorage, AK, 99508. E-mail: wvonbiela@usgs.gov

Christopher J. Sergeant  | University of Montana, Flathead Lake Biological Station, Polson, MT | University of Alaska Fairbanks, Fairbanks, AK


Michael P. Carey  | U.S. Geological Survey, Alaska Science Center, Anchorage, AK

Zachary Liller | Alaska Department of Fish and Game, Anchorage, AK

Charles Russell | Alaska Department of Fish and Game, Cordova, AK

Stephanie Quinn-Davidson | Tanana Chiefs Conference, Yukon River Inter-Tribal Fish Commission, Fairbanks, AK | Alaska Venture Fund, Anchorage, AK

Peter S. Rand  | Prince William Sound Science Center, Cordova, AK

Peter A.H. Westley  | University of Alaska Fairbanks, Fairbanks, AK

Christian E. Zimmerman  | U.S. Geological Survey, Alaska Science Center, Anchorage, AK

Chinook Salmon *Oncorhynchus tshawytscha* make their way up Ship Creek in Alaska to spawn. Photo Credit: Ryan Hagerty, U.S. Fish and Wildlife Service.

Widespread mortality of Pacific salmon *Oncorhynchus* spp. returning to spawn in Alaska coincided with record-breaking air temperatures and prolonged drought in summer 2019. Extreme environmental conditions are expected to happen more frequently with rapid climate change and challenge the notion that Alaska could indefinitely provide abundant, cool freshwater habitat for Pacific salmon. A total of 110 geographically widespread opportunistic observations of premature mortality (carcasses) were collected from a variety of sources. Premature mortalities were documented for Pink Salmon *Oncorhynchus gorbuscha*, Sockeye Salmon *O. nerka*, Chum Salmon *O. keta*, Chinook Salmon *O. tshawytscha*, and Coho Salmon *O. kisutch*. Additionally, observations of Pink Salmon returning to spawn in Prince William Sound streams in 2019, obtained from systematic aerial surveys conducted annually, revealed low migration success in 87% of rain-driven streams ($n = 30$), 52% of snow-driven streams ($n = 65$), and only 18% of glacier-driven streams ($n = 11$). Salmon mortality observations were consistent with death due to heat stress resulting from high water temperatures or drought caused hypoxia and stranding. Developing a better understanding of how broad-scale climate patterns manifest at the stream scale can help us determine whether a major shift in Pacific salmon productivity is underway and inform fisheries management plans to better mitigate future risks.

INTRODUCTION

Air temperatures have warmed more rapidly at northern latitudes compared to other areas of the globe, resulting in reduced snow and ice across northern landscapes (Post et al. 2019). The consequences of these climate conditions include warming of freshwater habitats and shifts in the hydrograph in some locations (Hinzman et al. 2005; O'Reilly et al. 2015; Beamer et al. 2017; Littell et al. 2018; Pitman et al. 2020). For decades, biologists predicted that warming and drying of northern freshwaters will eventually lead to declines in coldwater fishes, including salmonids (i.e., family Salmonidae) throughout their distribution (Houghton et al. 1990; Russo et al. 2014; Schoen et al. 2017). In the summer of 2019, these concerns became tangible in Alaska when record high temperature and persistent drought conditions (ACRC 2020) coincided with observations of Pacific salmon *Oncorhynchus* spp. premature mortality in the northern portion of their range (Figure 1). The annual average air temperature was 3.4°C warmer in 2019 than the long-term average (1925–2000; National Oceanic and Atmospheric Administration: www.ncdc.noaa.gov/cag). Drought conditions lasted 79 weeks (July 2018 – January 2020; National Integrated Drought Information System: www.drought.gov) and were caused by warm air temperatures that melted snowpack earlier in the year and, in the southern half of Alaska, below normal snowpack and below normal summer rains (Fisher et al. 2019a; ACRC 2020).

Declines in multiple salmon populations throughout more southerly parts of their range in the Pacific Northwest have been associated in part with premature mortality caused by poor environmental conditions along migration corridors and on spawning grounds (Gonia et al. 2006; Strange 2012; Hinch et al. 2021). Premature mortality is the death of upstream-migrating adult Pacific salmon before spawning and encompasses the terms en route mortality along migration corridors and prespawn mortality on spawning grounds (Bowerman et al. 2016; Keefer et al. 2017; Hinch et al. 2021). Warm water temperatures, low dissolved oxygen, or low water levels can cause high rates of premature mortality, in some cases exceeding 90% of total returning adults (Strange 2012; Sergeant et al. 2017; Tillotson and Quinn 2017; Hinch et al. 2021). In Alaska, observations and studies that associated poor freshwater conditions and premature mortality do exist prior to 2019, but are more localized (Murphy 1985; Sergeant et al. 2017; Tillotson and Quinn 2017), and are presumably due to Alaska's cooler conditions and more abundant freshwaters compared to the southern portion of their range.

Our goal was to evaluate whether observed Pacific salmon premature mortalities in 2019 were due to atmospheric conditions. The first objective was to assemble opportunistic

observations of Pacific salmon premature mortalities during 2019 to describe the geographic extent and species affected. If mortalities were in response to atmospheric conditions, we anticipated widespread geographic observations of multiple affected species. The second objective was to better understand how the impact of the anomalous conditions were mediated by local habitat conditions such as the source of streamflow in rivers (i.e., rain, snow, or glacier). Available data for this objective were categorical observations of migration success acquired during routine escapement surveys of Pink Salmon *Oncorhynchus gorbuscha* returning to 134 streams in Prince William Sound (PWS) conducted by the Alaska Department of Fish and Game (Morella et al. 2021). We expected that migration success would be lowest in rain-driven systems, which tend to dry quickly during drought conditions, and highest in glacier-driven systems, which tend to provide greater amounts of stored water from snow and glaciers (Sergeant et al. 2020).

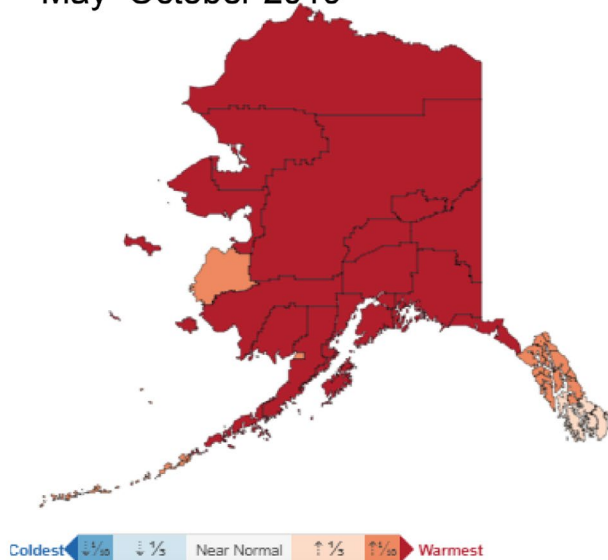
PREMATURE MORTALITY OBSERVATIONS

Methods for Premature Mortality Observations

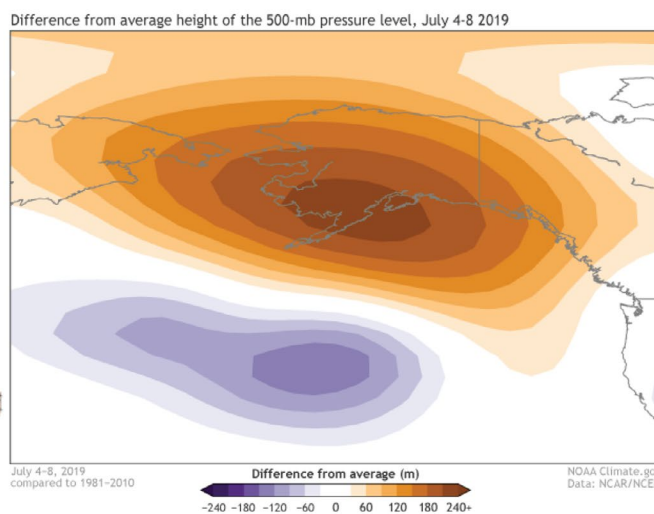
An observation was defined as one or more Pacific salmon carcasses along a migration route or an unspawned carcass (i.e., a carcass containing gametes) on a spawning ground. Carcasses along migration routes were either trapped on riverbanks, sandbars, and dried streambeds or floating in the water. Most observers (87%, $n = 110$) did not explicitly note gamete retention to classify a carcass as a premature mortality. Rather, carcass observations were presumed to reflect premature mortalities based on location and time of year. For example, a carcass found along a migration route and well downstream of a spawning habitat was considered a premature mortality. The associated data release (von Biela and Stanek 2021) specified which observations included confirmation of gamete retention from internal examination of some carcasses and which did not. Each observation was specific to a location, time period, and species such that a single observer generated multiple observations in the database when more than one species was noted.

Observations from four sources were included in the database: (1) the Local Environmental Observer Network (LEONetwork.org), initiated by the Alaska Native Tribal Health Consortium, which provides local observers with a platform to share information that helps describe the connections between climate, environment, and public health; (2) reports to the Alaska Department of Fish and Game's Arctic-Yukon-Kuskokwim Region by community members or staff; (3) social media reports and traditional media articles; and (4) directed emails from the lead author to selected individuals to assess whether a lack of observations from particular geographic areas

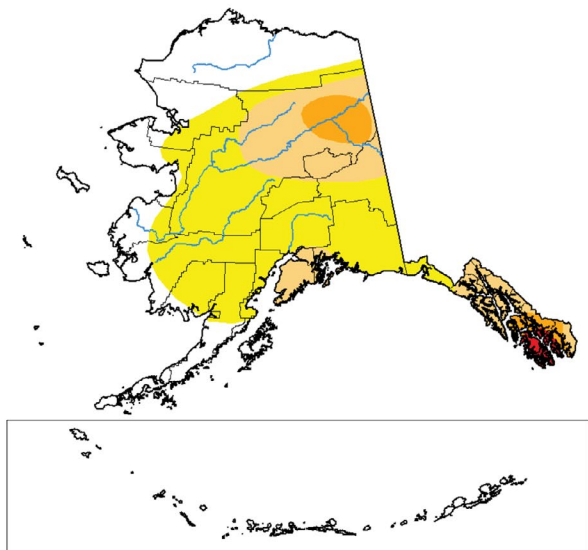
(A) Air temperature rank for May–October 2019



(B) Air pressure July 4–8, 2019



(C) Drought July 23, 2019



(D) Drought August 27, 2019

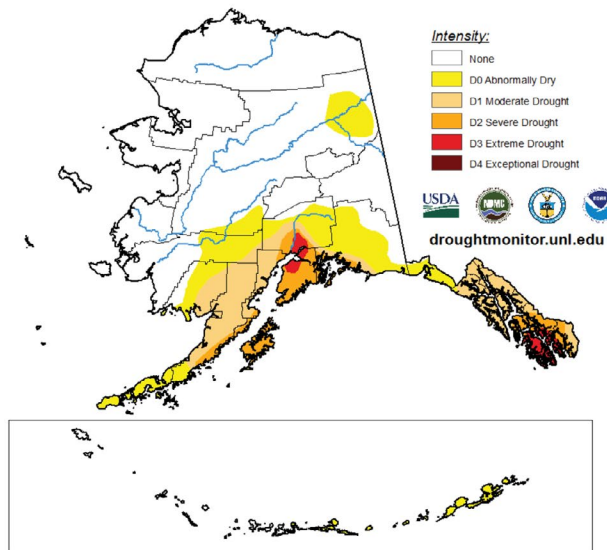


Figure 1. Maps depicting (A) 6-month air temperature rank for the Pacific salmon spawning period (May–October) in all boroughs (i.e., counties) in Alaska. (B) The high-pressure system associated with peak air temperatures in July 2019. (C) Drought extent for a representative week in July 2019. (D) Drought extent for a representative week in August 2019. For A, red indicates the warmest 6-month period on record for each borough (record length varies from 81 to 95 years). For C and D, colored shading represents drought severity, with yellow being the least severe and red the most severe. Sources: Panel A was generated using the National Oceanic and Atmospheric Administration (NOAA) National Center for Environmental Information Climate at a Glance Mapping Tool (<https://bit.ly/3ILtqwq>), Panel B is a NOAA Climate.gov image based on the National Center for Atmospheric Research/National Centers for Environmental Prediction Reanalysis data provided by the NOAA Earth System Research Laboratory Physical Sciences Division, and Panels C and D are from the U.S. Drought Monitor (<https://bit.ly/3239zaZ>).

were a true reflection of geographic scope or simply a reflection of biases or limitations inherent in the first three sources.

While the level of detail varied among observations, all observations included identification of carcasses to at least genus, month, and a location (e.g., specific river, lake, or beach). Other observation details were sometimes collected and included: additional location detail (descriptive narrative or latitude and longitude), number of carcasses observed (estimated by order of magnitude or counted),

water temperature, observer name, and a website link to the report. If latitude and longitude were not provided with an observation, they were assigned by the first author based on the narrative location description provided. Observations were grouped into one of eight geographic regions identified by colloquial names that typically refer to the large river(s) or marine waterbodies where rivers and streams flow (Figure 2). All mortality observations in the database were made in rivers, streams, and estuaries.

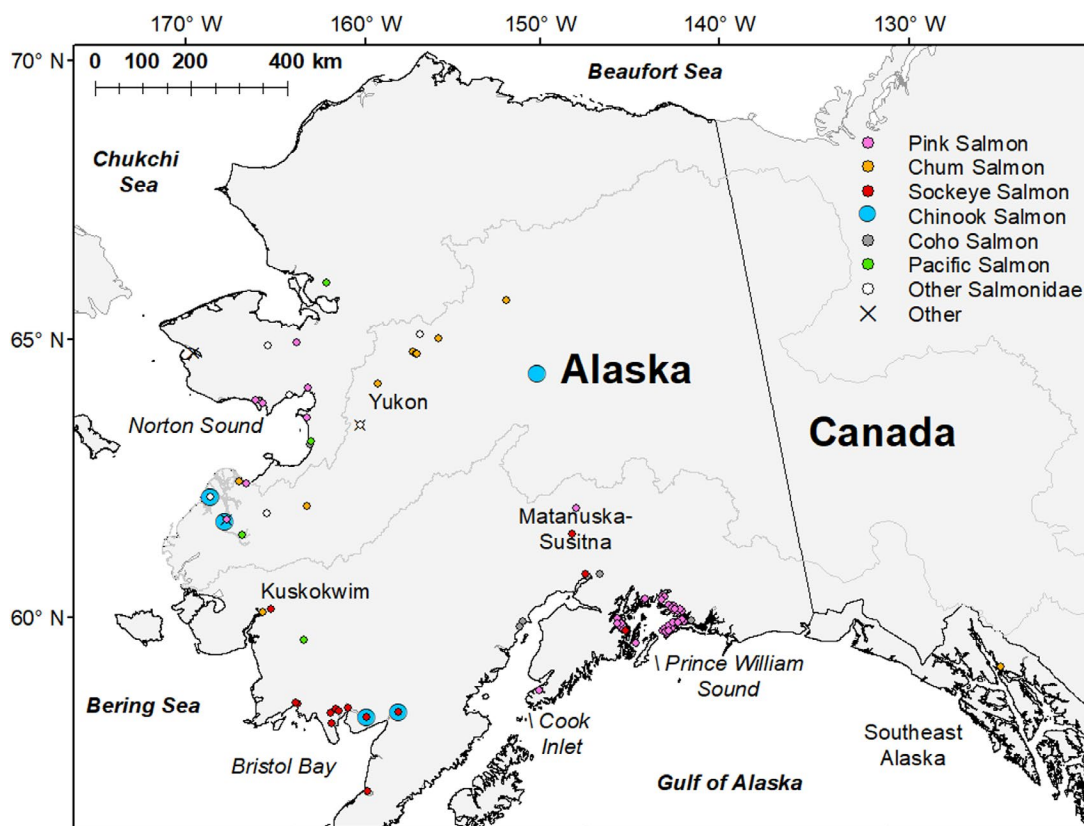


Figure 2. Premature mortality observations of Pacific salmon carcasses in Alaska during the summer and fall of 2019. Symbol color and shape denotes Pacific salmon species or alternative taxonomic groupings specified in the legend. Symbols denoting Chinook Salmon mortalities are slightly larger so that they remain visible, since these observations often occurred at locations with carcasses of another Pacific salmon species. Region names referenced in the text are shown on the map and are colloquial. Three regions are named for their large river(s): Yukon (outlined in light gray to separate it from Norton Sound to the north and Kuskokwim to the south), Kuskokwim, and Matanuska-Susitna. Four regions are named for marine waterbodies that their rivers and streams flow into: Norton Sound, Bristol Bay, Cook Inlet, and Prince William Sound, respectively. One region, the southernmost portion of Alaska, is named Southeast Alaska.

Estimates of carcass abundance reported here were used only for descriptive purposes. Carcass detection and counts of Pacific salmon are known to underestimate actual mortality (Patterson et al. 2007). Not only is it difficult for observers to get accurate counts of visible carcasses, but carcasses sink and cannot be seen in large, deep, and turbid river systems (Patterson et al. 2007) that characterize much of Alaska, and can also be removed by bears and other wildlife. Carcass count estimates were grouped into three categories: (1) abundant when $\geq 1,000$ carcasses were reported, (2) moderate when ≥ 100 and $< 1,000$ carcasses were reported, and (3) low when < 100 carcasses were reported. We categorized the infrequent observations without a carcass count as a low count.

Results for Premature Mortality Observations

We collected a total of 110 observations of Pacific salmon premature mortalities in 2019 (Figure 2). Only four observations (3.6%) were identified as “Pacific salmon” rather than a specific species. Of the remaining observations, 60 (54.6%) were for Pink Salmon, 20 (18.2%) for Chum Salmon *O. keta*, 15 (13.6%) for Sockeye Salmon *O. nerka*, 6 (5.5%) for Coho Salmon *O. kisutch*, and 5 (4.5%) for Chinook Salmon *O. tshawytscha*. Observations of mortality occurred across many regions in Alaska, including Norton Sound, Yukon,

Kuskokwim, Bristol Bay, Matanuska-Susitna, Cook Inlet, and PWS (Figure 2). Only a single observation of premature mortality was identified in Southeast Alaska, despite an effort by the authors to specifically seek out additional observations.

Most observations (89%) included an estimated carcass count. The number of carcasses for a single observation ranged from 1 to 35,000. Overall, 53 (48.2%) observations estimated abundant carcasses ($\geq 1,000$). Most observations with abundant carcasses were of Pink Salmon from PWS (47 observations) and involved drought so severe that low water or the absence of water prevented individuals from reaching spawning grounds (Figures 3, 4). The remaining instances with abundant carcasses involved Sockeye Salmon from Bristol Bay (three observations), Sockeye Salmon from Matanuska-Susitna (one observation from Larson Creek), Chum Salmon from the Yukon (Figure 5; one observation from the Koyukuk River; Westley 2020), and Coho Salmon from PWS (Figure 6). Observers often included additional details they deemed important about the biophysical settings associated with carcasses, including warm water temperature, low water level, low dissolved oxygen, and high fish density.

The remaining observations were split among moderate (≥ 100 and $< 1,000$; 24.5%) and low carcass numbers (< 100 ;



Figure 3. Image of a Pink Salmon premature mortality observation consisting of a large number of carcasses in Hogan Creek (Hogan Bay), Knight Island, Prince William Sound, Alaska, in early September 2019 during a field study conducted by the Prince William Sound Science Center. Photo credit: Brad von Wichman, Babkin Charters.

27.3%). Observations with moderate numbers of carcasses included Chum Salmon (29.6%) from Yukon, Bristol Bay, or PWS; Sockeye Salmon (29.6%) primarily from Bristol Bay; Pink Salmon (25.9%) primarily from PWS and Norton Sound; and Coho Salmon (14.8%) from Cook Inlet streams. Observations with low numbers included Chum Salmon (36.7%) primarily from the Yukon, Pink Salmon (20%) from Yukon and Norton Sound, Chinook Salmon (16.7%) from Bristol Bay, Pacific salmon not identified to species (13.3%), Sockeye Salmon (10%) from Bristol Bay and Norton Sound, and one observation of Coho Salmon in Norton Sound (3.3%). A set of 11 observations of unusual mortality for species other than Pacific salmon were also included in the database.

RELATING MIGRATION SUCCESS TO STREAMFLOW SOURCE IN PRINCE WILLIAM SOUND Methods for Relating Migration Success to Streamflow Source in Prince William Sound

In PWS, observations from a set of 134 salmon spawning index streams annually monitored by the Alaska Department of Fish and Game (ADFG; Morella et al. 2021) provided an opportunity to better understand how migration success corresponds to primary watershed runoff sources (i.e., rain, snow, or glacier ice). Index streams are surveyed systematically and have been used in the management of PWS Pink Salmon since the 1960s to monitor escapement across the ~1,000 streams that produce Pink Salmon. Aerial surveys occur approximately weekly during the spawning migration



Figure 4. Image of a Pink Salmon premature mortality observation in St. Matthews Creek, Prince William Sound, Alaska, 2019. This image was taken in a tidally influenced area following a high tide event that allowed Pink Salmon to enter the lower river, but did not provide enough time or water for spawning or further upstream migration. This picture is representative of observations in several Prince William Sound streams during 2019. Photo credit: Charles Russell.



Figure 5. Image of representative male (top) and female (bottom) summer Chum Salmon carcasses from an observation that included more than 1,000 carcasses in July 2019 on the Koyukuk River, Yukon watershed, Alaska (Westley 2020). Testes and eggs were determined to be underdeveloped, which confirmed that mortalities were premature and en route and was consistent with observation location on a migration corridor and not a spawning ground. Several carcasses had signs of fungal growth consistent with bacterial *columnaris* infection. Photo credit: Stephanie Quinn-Davidson.

months of July and August. A single biologist (C. Russell, ADFG) categorized migration success in each index stream as high, medium, or low during routine aerial overflights to index salmon abundance in 2019. Categories were based on comparisons of Pink Salmon counts associated with three locations for each stream: marine bay staging waters, the stream mouth, and the spawning area. Streams with high migration success were those where abundance in marine bay staging waters was similar to that in the stream mouth and spawning area. Streams with medium migration success had noticeably fewer individuals reach the spawning area compared to the abundance in marine bay staging waters, while those categorized with low migration success had far fewer Pink Salmon reach the spawning area. This analysis complemented direct mortality observations by using aerial survey information to characterize migration success, not only carcass observations included in the observation database.

We used a Fisher's exact test to test the hypothesis that migration success in individual streams during drought was associated with the primary runoff source in the watershed. From the original set of 134 surveyed salmon spawning index streams, we identified primary runoff sources for 106 streams by matching latitude-longitude survey positions to watershed polygons of an existing streamflow classification for the Gulf of Alaska coast (Sergeant et al. 2020). Index streams with drainage areas $<5 \text{ km}^2$ could not be classified and were removed from the analysis ($n = 28$). Rain source streams have hydrographs with maximum discharge in fall or winter; snow source streams have maximum discharge in spring or summer with a secondary maximum in fall; and glacier source streams have maximum discharge in summer without a secondary maximum in fall. Specific snow source classifications are based on differences in timing and amplitude of discharge maximums. Snow-II and Snow-IV source streams differ from Snow-I and Snow-III source streams in having larger watersheds and higher maximum discharges due to greater glacier areas (2–4% vs. 0–1%).



Figure 6. Image of a Coho Salmon premature mortality observation in Ibeck Creek, Cordova Prince William Sound, Alaska, 2019. Photo credit: Jeremy Botz, Alaska Department of Fish and Game.

Because glaciers are an important and dynamic driver of streamflow patterns in PWS (Sergeant et al. 2020), we used logistic regression analysis to predict the probability of either reduced or high migration success. To represent a binary migration success outcome, we grouped low and medium migration success into a “reduced” migration success category with a binary response of 1 and assigned high migration success a binary response of 0. Responses were compared to the proportion of glacier(s) present in each watershed (*glm* function in R statistical software [Vienna] with binomial error). Glacier ice spatial extent (area) in each watershed was estimated using the Randolph Glacier Inventory, version 3.2 (Pfeffer et al. 2014).

Results for Relating Migration Success to Streamflow Source in Prince William Sound

Migration success of Pink Salmon returning to PWS streams was significantly associated with a stream's primary runoff source (Fisher's exact test; $P = 0.0005$). Low migration success was observed in 87% of Rain-I streams ($n = 30$), 75% of Snow-I streams ($n = 8$), 41% of Snow-II streams ($n = 41$), 89% of Snow-III Streams ($n = 9$), and 43% of Snow-IV streams ($n = 7$). In contrast, most Pink Salmon runs returning to Glacier-I streams had high migration success (82% of streams; $n = 11$; Figure 7). The proportional glacier coverage in a watershed was a significant predictor of binary migration success (high vs. reduced; $P < 0.001$). The inflection point of the logistic regression, where the probability of reduced migration success = 0.5, occurred at 18% glacier coverage (Figure 8). Across the 28 watersheds with some proportion of glacier ice coverage, 64% of Pink Salmon runs to streams with $<18\%$ coverage ($n = 14$) were observed to have reduced migration success, while only 21% of Pink Salmon runs returning to streams with $>18\%$ coverage ($n = 14$) had reduced migration success. Most (97%) Pink Salmon runs returning to streams with no glacier

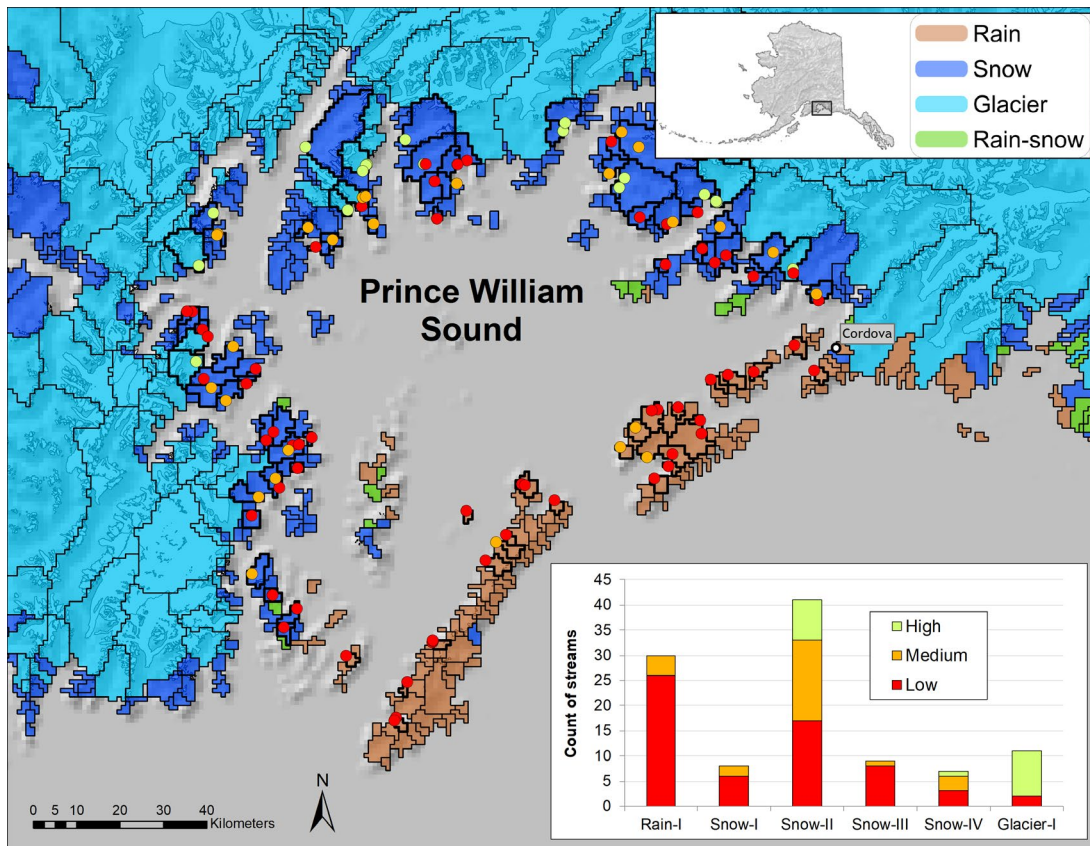


Figure 7. Observed summer 2019 migration success of Pink Salmon returning to streams in Prince William Sound (PWS), regularly surveyed for spawning salmon by the Alaska Department of Fish and Game. Colored circles indicate migration success, where green = high, orange = medium, and red = low. Polygons with black outlines represent individual watersheds with coastal outlets draining into PWS (thin line = not surveyed; thick line = surveyed). Polygon colors correspond to the primary runoff source. Bar chart represents counts of streams by streamflow class (as defined by Sergeant et al. 2020) that correspond with the three migration success categories.

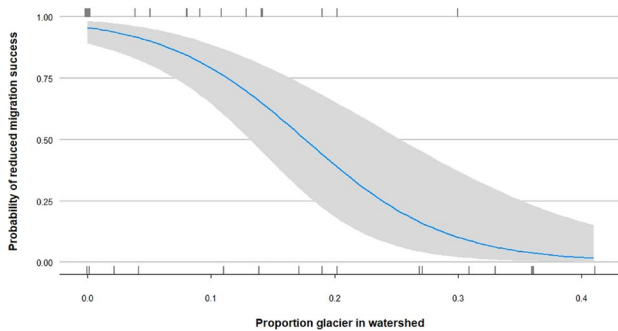


Figure 8. Probability of reduced spawning success (high vs. low or medium) for Pink Salmon returning to different Prince William Sound streams relative to the glacier proportion in a watershed. Gray shading represents a 95% confidence band. Gray tick marks at top and bottom of the horizontal axis indicates actual observations.

ice coverage (i.e., 0%) in the watershed experienced reduced migration success.

DISCUSSION

The first-documented widespread Pacific salmon mortality event in Alaska was related to a convergence of persistent climate extremes consistent with long-term

climate warming: high temperatures, high pressure ridges, and drought. Opportunities for a cooling marine influence were reduced because marine waters were abnormally warm, as evidenced by the northeastern Pacific marine heatwave of 2019 and low September sea ice extent (ACRC 2020; Amaya et al. 2020). Mortality observations extended from Norton Sound in northwest Alaska through PWS in south-central Alaska (~1 million km²), and included all five Pacific salmon species present. This geographic extent aligns with the area of record-breaking air temperatures and drought (Figure 1). The notable exception was Southeast Alaska, which experienced warm temperatures and drought, but had just one mortality observation. Conditions may have been more manageable for Pacific salmon returning to Southeast Alaska streams because the warm air temperature anomalies were more moderate and summer rainfall totals were higher on an absolute basis compared to other regions of Alaska (ACRC 2020).

In PWS, migration success of Pink Salmon runs was reduced (low and medium migration success categories) in nearly every rain- and snow-driven stream (Figure 7). Low water and dry stream channels associated with drought conditions seemed to be the primary barrier to migrating Pink Salmon. Drought also impacted some glacially influenced streams, including most streams with less than 18% glacial coverage in their watersheds. Reduced migration success was pervasive in rain-driven streams, common in snow-driven

Pacific salmon premature mortality and spawning success in 2019

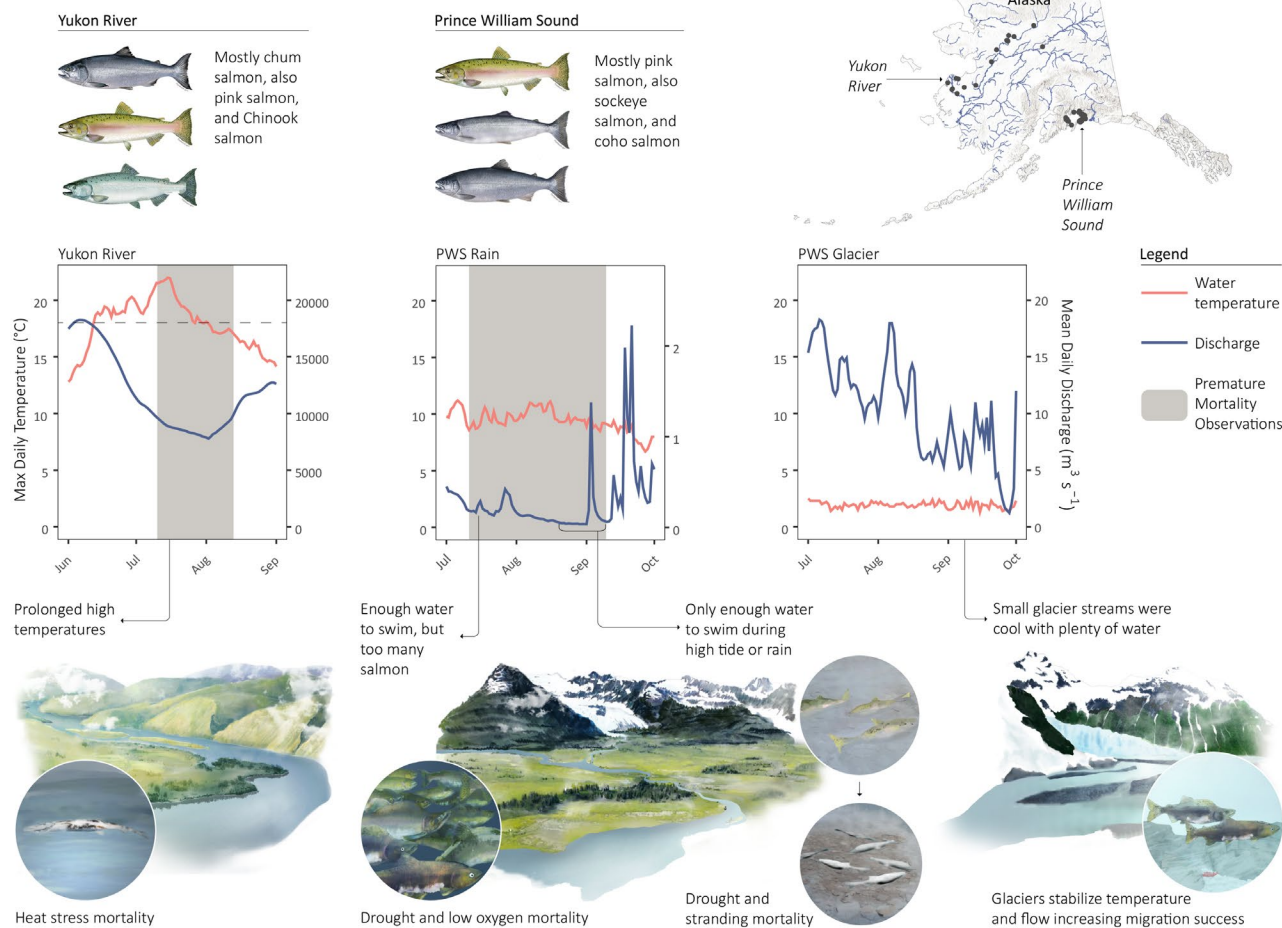


Figure 9. A conceptual model contrasting different conditions associated with Pacific salmon premature mortality in Alaska during record heat and drought in 2019, with conditions associated with typical levels of spawning success. Map (top right) shows selected mortality observations in Yukon and Prince William Sound (PWS) regions from Figure 2. Pictures of Pacific salmon species included in mortality observations from the Yukon region (top left) and PWS region (top center). Plot panels show maximum (max) daily water temperature (red line) and mean daily discharge (blue line; axes have different scales), contrasting physical conditions in three different streams during spawning migration (gray shading is mortality observation timing; no observations in right panel). Illustrations along the bottom depict Pacific salmon spawning outcomes under three different conditions. Left panel shows how prolonged, high water temperatures causes heat stress mortality of Pacific salmon when the upper thermal limit reached the Yukon River (water temperatures from Alaska Department of Fish and Game and discharge data from U.S. Geological Survey [USGS] gage station 15565447, Pilot Station; dashed line is 18°C water temperature threshold associated with heat stress from von Biela et al. 2020). Center panel shows representative PWS rain-driven stream where thousands of Pink Salmon carcasses were observed (water temperature and discharge data from USGS gage station 15215900, Glacier River, Cordova, glaciers actually outside this watershed). Also depicted are two ways in which drought causes hypoxia mortalities: (1) low and declining discharge reduced dissolved oxygen and increased crowding; (2) near zero discharge in August and early September inhibited upstream migration; thus, Pink Salmon entering intertidal regions on high tides or during an early September rain event were stranded at low tide or when the rain ended. Right panel shows representative PWS glacier-driven stream where Pink Salmon achieved high migration and spawning success in 2019 (water temperature and discharge from USGS gage station 15236900, Wolverine Creek, Whittier; gage located well above spawning areas, where water temperatures were not as cold). Figure design and illustration by Cecil Howell.

streams, and rare in glacier-driven streams. Our results support the perspective that understanding the local stream- or population-scale response to broad-scale climate forcing requires consideration of physical watershed characteristics as well as population-specific traits such as escapement abundance and run timing.

The propensity for spawning Pacific salmon to be influenced by water temperature and streamflow is well known

(Rand et al. 2006; Quinn 2018; Dahlke et al. 2020). A recent meta-analysis revealed that across nearly 700 fish species, spawning adults had a narrower thermal tolerance with a cooler maximum temperature limit as compared to juveniles and nonspawning adults (Dahlke et al. 2020). The most likely cause for temperature sensitivity in spawning adults appears to be a reduced cardiorespiratory (aerobic) capacity associated with the energetic demands of gamete production (Dahlke

et al. 2020). Cardiorespiratory capacity has been specifically identified as a limitation for spawning Pacific salmon in warm temperatures (Eliason et al. 2011) and is thought to explain the high rates of mortality with warm water temperatures in Fraser River Sockeye Salmon, as well as disproportionate negative effects on females, because they must produce energy-dense eggs (Quinn 2018; Hinch et al. 2021). Particularly difficult years for spawning salmon are occasionally apparent and provide examples where extreme atmospheric conditions resulted in particularly high mortality. For example, Pacific salmon spawning migrations in the U.S. Pacific Northwest during 2015 faced a similar set of environmental anomalies as Alaska in 2019, including record-breaking warm temperatures, low streamflows associated with drought, and the 2014–2016 Pacific marine heatwave (Crozier et al. 2020). This resulted in almost complete premature mortality among Snake River Sockeye Salmon and unusually high premature mortality among Snake River Chinook Salmon (Crozier et al. 2020).

Observations reported here are part of an emerging picture that biological tipping points are being reached for Alaska's Pacific salmon, where warming switches from beneficial to detrimental in some locations, years, and life stages. In western Alaska, evidence of heat stress was detected in about half of spawning Yukon River Chinook Salmon sampled during 2016 and 2017, when migration water temperatures exceed 18°C (von Biela et al. 2020). Jones et al. (2020), in a south-central Alaska study, also documented the negative effects of water temperatures above 18°C on annual measures of Chinook Salmon production. Unfortunately, protracted periods (weeks to a month) of summer water temperatures above 18°C are anticipated to be more common in south-central Alaska (e.g., Matanuska-Susitna and Cook Inlet regions) over the next 50 years (Shaftel et al. 2020). The opportunistic observations we collected reinforce concerns raised in these studies and identify additional Pacific salmon populations where detrimental effects from warming may also be emerging.

Premature Mortality Observations

The large number of premature mortality observations, involvement of multiple Pacific salmon species, and wide geographic distribution of the observations are consistent with a response to large-scale atmospheric conditions in 2019. While carcass detections grossly underestimate the true levels of premature mortality, Patterson et al. (2007) noted that anecdotal carcass reports provide some of the earliest indicators of en route losses as mortality observations often occur in runs where negative discrepancies between en route escapement projections and final spawner escapement estimates are later identified. In fact, other data from 2019 also indicated unusually high levels of premature mortality in the Yukon region where carcasses were observed. High en route mortality for Yukon Chinook salmon was consistent with a large and negative discrepancy between the prediction of Canadian-bound fish estimated from the lower river monitoring station in Pilot Station, Alaska, and estimates at the Canadian border, which resulted in a Canadian fishery closure (JTC 2020). Similarly, summer Chum Salmon abundance in the Koyukuk River portion of the Yukon was well below average at both the Gisasa River and Henshaw Creek weirs, which were located upriver from areas where many carcasses were observed (Brenner et al. 2020).

Several factors preclude us from drawing conclusions about the number of premature mortality observations associated with

each species, since observations were opportunistic and did not come from a designed study. For example, carcass detection was likely higher for more abundant species, clearer streams, shallower streams, warmer streams, and more frequented locations (Patterson et al. 2007). Indeed, all of these observation biases are present for observations of Pink Salmon, the most frequently reported species. Pink Salmon are far more abundant than the other species in Alaska (Brenner et al. 2020); there was a high degree of survey effort by the ADFG, and most PWS streams surveyed were clear and shallow since peak drought conditions occurred during the time spawning surveys were conducted.

Relating Migration Success to Streamflow Source in Prince William Sound

Conditions in the PWS region prior to and during the 2019 Pink Salmon spawning migration were unusual, and migration success varied widely (Figure 7). While April snowpack conditions were normal at higher elevations, snow melted early at lower elevations (Fisher et al. 2019a). For example, there was no snow in the Lowe River and Valdez in April, when normally snow depth would be 0.82 m and 0.71 m, respectively (Fisher et al. 2019a). Air temperature anomalies were warm in March and April, which melted snow at lower elevations, and warm from June through August, along with low precipitation (Fisher et al. 2019b).

Most regions of PWS include examples of Pink Salmon runs with high, medium, and low migration success, with high and low migration success streams often occurring in adjacent watersheds. Southern PWS's large islands (Montague, Hinchinbrook, and Hawkins) were the exception, with Pink Salmon migration success universally reduced to low and medium levels. Different streamflow sources among watersheds reliably predicted Pink Salmon migration success. Pink Salmon runs to rain- and snow-driven streams were vulnerable to the drought, with rain-driven systems being most vulnerable. Glacier-driven streams were generally buffered from the drought because glacier melt water provided a more reliable source of streamflow. Southern PWS's large islands have minimal glacier coverage and nearly all their watersheds are rain-driven, which explains why migration success was universally reduced there. Our results align with predicted climate change impacts, particularly increasing temperatures and drought severity in Arctic and subarctic watersheds that reduce the snowpack available for enhancing streamflow during summer and fall (Nilsson et al. 2015; Littell et al. 2018).

In PWS streams, Rain-I and Snow-II watersheds accounted for the largest number of streams with reduced migration success. Throughout the coastal Gulf of Alaska, these two watershed types account for 27% of the 4,140 watersheds that have been classified (Sergeant et al. 2020), suggesting that stream response to drought conditions could have been more widespread across southern Alaska. Snow-driven watersheds in this area are anticipated to continue shifting toward snow–rain transitional hydrographs through the end of the 21st century (Littell et al. 2018). Based on the results presented here, that streamflow transition would also confer a higher likelihood of reduced salmon migration success during summer drought conditions. While our analysis indicated that watersheds with glacier coverage greater than 18% appear to be somewhat buffered from low summer flows, modeling in southern coastal Alaska predicts the magnitude of summer flow will decrease as glacier volumes continue to diminish (Beamer et al. 2017; Pitman et al. 2020). In current times, short-term glacier melt can also be so rapid that it causes anomalously high flows

that impede migration (Valentin et al. 2018). Indeed, high flows in PWS's glacierized Copper River appeared to impede the migration of radio-tagged Sockeye Salmon near Wood Canyon in 2019 and resulted in a high rate (>50%) of en route mortality for the component of the run migrating during mid-season (P. S. Rand, unpublished data).

In glaciated southern coastal Alaska (Cook Inlet through Southeast Alaska), two primary mechanisms have been described in which drought leads to adult salmon mortality despite generally cool (<15°C) freshwater temperatures: (1) exposure to lethally low dissolved oxygen levels due to reduced reaeration rates from lower water turbulence at low discharges and increased respiration due to high salmon density (Sergeant et al. 2017; Tillotson and Quinn 2017), and (2) stranding in channels that dry up as the tide ebbs (Murphy 1985; P. S. Rand, personal observations).

Prior to 2019, observations of drought-related mortality occurred in just a few streams during a particular year and tended to involve a few thousand carcasses or fewer (C. Russell, personal observations). Two exceptions were 1991 and 2004, when drought and related mortalities were widespread within PWS (ADFG records reviewed by Russell). However, 2019 conditions differed from those in 1991 and 2004 because marine water temperatures were also warm and reached at least 18°C in July (R. Campbell, Prince William Sound Science Center; unpublished data from central PWS). Some Pink Salmon appeared to respond to warm marine water temperatures by entering cooler streams (<13°C; P.S. Rand, unpublished data collected above the high tide line in PWS streams) earlier than normal (e.g., July instead of August). The intensity of die-offs in some PWS Pink Salmon streams may also be exacerbated by high rates of straying of hatchery-origin fish into natural streams, which, by increasing fish density and dissolved oxygen demand prior to spawning, can lead to density-dependent hypoxia. Hogan Creek, where a significant die-off event was observed, is comprised mostly of hatchery-origin Pink Salmon (>50% during 2013–2015; Knudsen et al. 2021), and had markedly higher fish densities, leading to a greater risk of premature mortality among natural-origin fish than would otherwise be the case.

Synthesis

Our three plots of water temperature and discharge (Figure 9) show the wide range of freshwater temperatures and flows under warm air temperature and drought conditions that occurred in Alaska during 2019, and also led us to identify three main causes of premature mortality when examined in conjunction with observations of carcasses: heat stress due to high water temperatures, hypoxia due to drought, and stranding due to drought. This did not occur in PWS's glacier-driven streams, where glacier runoff continued to provide a cold and stable water source. Elsewhere in Alaska, it is likely that glacial runoff, as well as cool groundwater sources, provided similar successful outcomes for migrating and spawning of Pacific salmon.

The strongest support for high water temperature as a cause of premature mortality came from the Yukon region salmon carcass observations in conjunction with available temperature and discharge data (Figure 9; ADFG temperature data and U.S. Geological survey [USGS] discharge data at station 15565447 from Pilot Station, Alaska). Other studies have also identified a heat stress response in several species of Pacific salmon in water near 18°C and mortalities in water ranging from 21°C to 25°C (McCullough 1999; Strange 2010; Donnelly et al. 2020; von Biela et al. 2020). For Yukon River Chinook Salmon, von Biela et al. (2020) reported heat stress during 2016 and 2017,

when water temperatures were less extreme than in 2019 (von Biela et al. 2020). In 2019, the Yukon River had a maximum daily water temperature >18°C for 44 consecutive days (June 13 – July 26) and >21°C for 9 consecutive days (July 9–17). Pacific salmon mortality observation dates were well correlated with dates when water temperatures associated with mortality were reached (>21°C). Mortality observations in the Yukon region were first reported on July 10, just 1 d after the first daily maximum water temperature was >21°C, while the latest mortality observations were made in early August, just after maximum daily water temperatures fell to <18°C. Other factors may have also contributed to mortalities, including hypoxia, reduced streamflow from drought, and pathogens.

The strongest support for drought as a cause of premature mortality was in PWS Pink Salmon carcass observations in conjunction with aerial survey estimates of migration success and stream discharge information. Stream discharge levels dropped through July, but high densities of Pink Salmon still had enough water to move into streams. This combination of less water and many salmon likely caused hypoxic conditions that led to mortality observations in July (Figure 9). By August, water levels were often too low for upstream movement, and arriving Pink Salmon appeared to congregate in cooler (<13°C) and deeper PWS marine waters, where they were occasionally visible during aerial surveys in areas of cold water upwelling. This pattern persisted for several weeks and delayed the typical timing of upstream migration. By the middle of August, Pink Salmon attempted to migrate upstream during diurnal high tides, only to be either stranded in dewatered channels near stream mouths or trapped in tide pools during subsequent low tides (Figures 4, 9). Eventually, a rain event in early September provided a narrow window of opportunity for Pink Salmon to migrate upstream, and some were able to successfully complete their migration to spawning areas. The subsequent drop in water levels after the rain ended was associated with new mortality observations (Figure 9).

In contrast, high migration success was generally associated with runs into small glacier-driven PWS streams that were buffered or responded differently to the atmospheric effects of warm temperatures and drought. A water monitoring station just below Wolverine Glacier in western PWS demonstrated that glacier melt continued to provide cold, stable water temperatures near 2°C and discharges well above zero (Figure 9; data from USGS gage station 15236900 on Wolverine Creek near Whitter, Alaska; upstream of spawning grounds).

Despite the drought, return of PWS Pink Salmon from the 2019 brood in 2021 was above average for wild stocks (ADFG preliminary data for 2021 season). Both adaptive management decisions and biological compensatory responses potentially facilitated PWS Pink Salmon recruitment success despite an uncertain 2021 forecast (Brenner et al. 2021). After detecting premature mortality early in the 2019 fishing season, managers limited harvest at critical times to provide more opportunity for fish to successfully migrate and spawn during drought conditions (Russell, unpublished data). This provides an example of how proactive management can adapt to benefit fish populations experiencing unusual environmental conditions. However, major drivers of salmon population dynamics, like compensatory processes (e.g., density dependence and competitive interactions) and favorable ocean conditions, almost certainly contributed to improved recruitment and led to a relatively strong return in 2021. Among other species with premature mortality observations, generations

times are longer and outcomes from the 2019 brood are not yet known.

Extreme heat and drought events are often viewed as windows into the future (Russo et al. 2014; Crozier et al. 2020). Observations from 2019 may prove to be one early warning of widespread shifts in Alaska's Pacific salmon production, given some recent studies on future water temperature and salmon production. First, watersheds with near optimal water temperatures over the past several decades are projected to warm beyond lethal limits of Pacific salmon within the next 50 years (Shaftel et al. 2020). Second, there is already evidence of declining population productivity with increasing water temperature in southcentral Alaska's warmest watersheds (Jones et al. 2020). Third, there is some evidence that warming will increase Pacific salmon production in rivers and streams that have been historically below thermal preferences (e.g., Schoen et al. 2017; Jones et al. 2020). Fourth, there is evidence that an increasing number of Pacific salmon will encounter challenging environmental conditions in marine as well as freshwater habitats as climate warming proceeds. Marine conditions are known to influence Pacific salmon production with warmer oceans previously linked to higher production in Alaska (Mueter et al. 2002), but more recent evidence hinting that extremely warm ocean conditions are problematic (Carey et al. 2021). More frequent extreme warm ocean conditions are anticipated (e.g., Pacific marine heatwaves in 2014–2016 and 2019; Amaya et al. 2020). This is particularly concerning because it would likely lower productivity more than if stressful conditions were limited to either marine or freshwaters.

Federal and state agencies, tribal organizations, nonprofit organizations, and citizen scientists are already working to maintain and increase the capacity to monitor water temperature, streamflow, and fish populations across Alaska's expansive and remote landscape. Mortality observations can continue to be reported via the LEO Network (LEONetwork.org). These efforts are an important step to better detect and prepare for long-term fisheries change and inform habitat conservation efforts at local and regional scales. However, systematic sampling of en route and prespawn mortality is extremely limited in Alaska and not easily implemented in most of Alaska's remote salmon spawning habitat that lack road access. Instead, researchers may need to validate new biomarkers or models that predict premature mortality from environmental conditions with the goal of developing alternative tools for monitoring premature mortality. Increased opportunities for data sharing and organized repositories (e.g., waterdata.usgs.gov and the anticipated AKTEMP water temperature repository from the Alaska Center for Conservation Science) can improve the utility of all these data sources, and will help fishery scientists and managers determine whether a major shift in Pacific salmon productivity is underway. A shift in the abundance of Pacific salmon would be a significant disruption for communities that depend on salmon to sustain their culture, food security, and local economy.

ACKNOWLEDGMENTS

We thank the dozens of citizens and scientists who generously shared their observations of unusual fish mortality across Alaska during 2019. Please see the associated data release for acknowledgments of each observer associated with their specific observations. We also thank Michael

Brubaker, Erica Lujan, and the Alaska Native Tribal Health Consortium for their efforts in developing and maintaining the LEO Network. Erik Schoen, Bill Templin, Jack Erickson, and Matthew Nemeth provided helpful reviews of the initial version of this article. Nate Mantua, Matthew Keefer, and an anonymous reviewer provided constructive comments that improved the article during journal review. Any use of trade, firm, or product names is for descriptive purposes only and does not imply endorsement by the U.S. Government. There is no conflict of interest declared in this article.

ORCID

Vanessa R. von Biela  <https://orcid.org/0000-0002-7139-5981>

Christopher J. Sergeant  <https://orcid.org/0000-0002-3363-3213>

Michael P. Carey  <https://orcid.org/0000-0002-3327-8995>

Peter S. Rand  <https://orcid.org/0000-0003-0166-2201>

Peter A.H. Westley  <https://orcid.org/0000-0003-4190-7314>

Christian E. Zimmerman  <https://orcid.org/0000-0002-3646-0688>

REFERENCES

- ACRC (Alaska Climate Research Center). 2020. 2019 Alaska climate review. The Alaska Climate Research Center, Fairbanks.
- Amaya, D. J., A. J. Miller, S. P. Xie, and Y. Kosaka. 2020. Physical drivers of the summer 2019 north Pacific marine heatwave. *Nature Communications* 11:1–9.
- Beamer, J. P., D. F. Hill, D. McGrath, A. Arendt, and C. Kienholz. 2017. Hydrologic impacts of changes in climate and glacier extent in the Gulf of Alaska watershed. *Water Resources Research* 53:7502–7520.
- von Biela, V. R., L. Bowen, S. D. McCormick, M. P. Carey, D. S. Donnelly, S. Waters, A. M. Regish, S. M. Laske, R. J. Brown, S. Larson, S. Zuray, and C. E. Zimmerman. 2020. Evidence of prevalent heat stress in Yukon River Chinook Salmon. *Canadian Journal of Fisheries and Aquatic Sciences* 77:1878–1892.
- von Biela, V. R., and A. Stanek. 2021. Observations documenting premature mortality among Alaska's Pacific salmon in 2019. U.S. Geological Survey data release Available: <https://bit.ly/3AcnDfr> (January 2022).
- Bowerman, T., M. L. Keefer, and C. C. Caudill. 2016. Pacific salmon pre-spawn mortality: patterns, methods, and study design considerations. *Fisheries* 41:738–749.
- Brenner, R. E., S. J. Larsen, A. R. Munro, and A. M. Carroll, editors. 2020. Run forecasts and harvest projections for 2020 Alaska Salmon Fisheries and Review of the 2019 season. Alaska Department of Fish and Game, Divisions of Sport Fish and Commercial Fisheries, Special Publication 20-06, Anchorage.
- Brenner, R. E., S. L. Larsen, A. R. Munro, and A. M. Carroll, editors. 2021. Run forecasts and harvest projections for 2021 Alaska salmon fisheries and review of the 2020 season. Alaska Department of Fish and Game, Divisions of Sport Fish and Commercial Fisheries, Special Publication 21-07, Anchorage.
- Carey, M. P., V. R. von Biela, A. Dunker, K. D. Keith, M. Schelske, C. Lean, and C. E. Zimmerman. 2021. Egg retention of high-latitude Sockeye Salmon (*Oncorhynchus nerka*) in the Pilgrim River, Alaska, during the Pacific marine heatwave of 2014–2016. *Polar Biology* 44:1643–1654.
- Crozier, L. G., J. E. Siegel, L. E. Wiesebron, E. M. Trujillo, B. J. Burke, B. P. Sandford, and D. L. Widener. 2020. Snake River Sockeye and Chinook Salmon in a changing climate: implications for upstream migration survival during recent extreme and future climates. *PLOS One* 15:9:e0238886.
- Dahlke, F. T., S. Wohrlab, M. Butzin, and H.-O. Pörtner. 2020. Thermal bottlenecks in the life cycle define climate vulnerability of fish. *Science* 369:65–70.
- Donnelly, D. S., V. R. Von Biela, S. D. McCormick, S. M. Laske, M. P. Carey, S. Waters, L. Bowen, R. J. Brown, S. Larson, and C. E. Zimmerman. 2020. A manipulative thermal challenge protocol for adult salmonids in remote field settings. *Conservation Physiology* 8:coaa074.

- Eliason, E. J., T. D. Clark, M. J. Hague, L. M. Hanson, Z. S. Gallagher, K. M. Jeffries, M. K. Gale, D. A. Patterson, S. G. Hinch, and A. P. Farrell. 2011. Differences in thermal tolerance among Sockeye Salmon populations. *Science* 332:109–112.
- Fisher, D., T. DeMarco, and D. Kenney. 2019a. Alaska Snow Survey Report May 1, 2019. U.S. Department of Agriculture, Natural Resources Conservation Service, Palmer, Alaska.
- Fisher, D., T. DeMarco, and D. Kenney. 2019b. Alaska Snow Survey Report April 1, 2019. U.S. Department of Agriculture, Natural Resources Conservation Service, Palmer, Alaska.
- Goniaea, T. M., M. L. Keefer, T. C. Bjornn, C. A. Peery, D. H. Bennett, and L. C. Stuehnenberg. 2006. Behavioral thermoregulation and slowed migration by adult fall Chinook Salmon in response to high Columbia River water temperatures. *Transactions of the American Fisheries Society* 135:408–419.
- Hinch, S. G., N. N. Bett, E. J. Eliason, A. P. Farrell, S. J. Cooke, and D. A. Patterson. 2021. Exceptionally high mortality of adult female salmon: a large-scale pattern and a conservation concern. *Canadian Journal of Fisheries and Aquatic Sciences* 78:639–654.
- Hinzman, L. D., N. D. Bettez, W. R. Bolton, F. S. Chapin, M. B. Dyrurgorov, C. L. Fastie, B. Griffith, R. D. Hollister, A. Hope, H. P. Huntington, A. M. Jensen, G. J. Jia, T. Jorgenson, D. L. Kane, D. R. Klein, G. Kofinas, A. H. Lynch, A. H. Lloyd, A. D. McGuire, F. E. Nelson, W. C. Oechel, T. E. Osterkamp, C. H. Racine, V. E. Romanovsky, R. S. Stone, D. A. Stow, M. Sturm, C. E. Tweedie, G. L. Vourlitis, M. D. Walker, D. A. Walker, P. J. Webber, J. M. Welker, K. S. Winker, and K. Yoshikawa. 2005. Evidence and implications of recent climate change in Northern Alaska and other Arctic regions. *Climatic Change* 72:251–298.
- Houghton, P. J., G. Jenkins, and J. Ephraums, editors. 1990. *Climate change: the IPCC scientific assessment*. Cambridge University Press, New York.
- Jones, L. A., E. R. Schoen, R. Shaftel, C. J. Cunningham, S. Mauger, D. J. Rinella, and A. St. Saviour. 2020. Watershed-scale climate influences productivity of Chinook Salmon populations across southcentral Alaska. *Global Change Biology* 26:4919–4936.
- Keefer, M. L., M. A. Jepson, G. P. Naughton, T. J. Blubaugh, T. S. Clabough, and C. C. Caudill. 2017. Condition-dependent en route migration mortality of adult Chinook Salmon in the Willamette river main stem. *North American Journal of Fisheries Management* 37:370–379.
- Littell, J. S., S. A. McAfee, and G. D. Hayward. 2018. Alaska snowpack response to climate change: statewide snowfall equivalent and snowpack water scenarios. *Water* 10(5):668.
- McCullough, D. A. 1999. A review and synthesis of effects of alterations to the water temperature regime on freshwater life stages of Salmonids, with special reference to Chinook Salmon. U.S. Environmental Protection Agency Region 10 Water Resources Assessment Report No. 910-R-99-010, Seattle.
- Morella, J., C. W. Russell, J. Botz, and S. B. Haught. 2021. 2019 Prince William Sound area finfish management report. Alaska Department of Fish and Game, Fishery Management Report No. 21-19, Anchorage.
- Mueter, F. J., R. M. Peterman, and B. J. Pypser. 2002. Opposite effects of ocean temperature on survival rates of 120 stocks of Pacific salmon (*Oncorhynchus* spp.) in northern and southern areas. *Canadian Journal of Fisheries and Aquatic Sciences* 59:456–463.
- Murphy, M. L. 1985. Die-offs of pre-spawn adult Pink Salmon and Chum Salmon in southeastern Alaska. *North American Journal of Fisheries Management* 5:302–308.
- Nilsson, C., L. E. Polvi, and L. Lind. 2015. Extreme events in streams and rivers in arctic and subarctic regions in an uncertain future. *Freshwater Biology* 60:2535–2546.
- O'Reilly, C. M., S. Sharma, D. K. Gray, S. E. Hampton, J. S. Read, R. J. Rowley, P. Schneider, J. D. Lenters, P. B. McIntyre, B. M. Kraemer, G. A. Weyhenmeyer, D. Straille, B. Dong, R. Adrian, M. G. Allan, O. Anneville, L. Arvola, J. Austin, J. L. Bailey, J. S. Baron, J. D. Brookes, E. de Eyto, M. T. Dokulil, D. P. Hamilton, K. Havens, A. L. Hetherington, S. N. Higgins, S. Hook, L. R. Izmesteva, K. D. Joehnk, K. Kangur, P. Kasprzak, M. Kumagai, E. Kuusisto, G. Leshkevich, D. M. Livingstone, S. MacIntyre, L. May, J. M. Melack, D. C. Mueller-Navarra, M. Naumenko, P. Noges, T. Noges, R. P. North, P.-D. Plisnier, A. Rigosi, A. Rimmer, M. Rogora, L. G. Rudstam, J. A. Rusak, N. Salmaso, N. R. Samal, D. E. Schindler, S. G. Schladow, M. Schmid, S. R. Schmidt, E. Silow, M. E. Soyly, K. Teubner, P. Verburg, A. Voutilainen, A. Watkinson, C. E. Williamson, and G. Zhang. 2015. Rapid and highly variable warming of lake surface waters around the globe. *Geophysical Research Letters* 42:10,773–10,781.
- Patterson, D. A., K. M. Skibo, D. P. Barnes, J. A. Hills, and J. S. MacDonald. 2007. The influence of water temperature on time to surface for adult Sockeye Salmon carcasses and the limitations in estimating salmon carcasses in the Fraser River, British Columbia. *North American Journal of Fisheries Management* 27:878–884.
- Pfeffer, W. T., A. A. Arendt, A. Bliss, T. Bolch, J. G. Cogley, A. S. Gardner, J. O. Hagen, R. Hock, G. Kaser, C. Kienholz, E. S. Miles, G. Moholdt, N. Mölg, F. Paul, V. Radić, P. Rastner, B. H. Raup, J. Rich, M. J. Sharp, L. M. Andreassen, S. Bajracharya, N. E. Barrand, M. J. Beedle, E. Berthier, R. Bhambri, I. Brown, D. O. Burgess, E. W. Burgess, F. Cawkwell, T. Chinn, L. Copland, N. J. Cullen, B. Davies, H. De Angelis, A. G. Fountain, H. Frey, B. A. Giffen, N. F. Glasser, S. D. Gurney, W. Hagg, D. K. Hall, U. K. Haritashya, G. Hartmann, S. Herreid, I. Howat, H. Jiskoot, T. E. Khromova, A. Klein, J. Kohler, M. König, D. Kriegel, S. Kutuzov, I. Lavrentiev, R. Le Bris, X. Li, W. F. Manley, C. Mayer, B. Menounos, A. Mercer, P. Mool, A. Negrete, G. Nosenko, C. Nuth, A. Osmonov, R. Pettersson, A. Racoviteanu, R. Ranzì, M. A. Sarikaya, C. Schneider, O. Sigurdsson, P. Sirguey, C. R. Stokes, R. Wheate, G. J. Wolken, L. Z. Wu, and F. R. Wyatt. 2014. The Randolph glacier inventory: a globally complete inventory of glaciers. *Journal of Glaciology* 60:537–552.
- Pitman, K. J., J. W. Moore, M. R. Sloat, A. H. Beaudreau, A. L. Bidlack, R. E. Brenner, E. W. Hood, G. R. Pess, N. J. Mantua, A. M. Milner, V. Radić, G. H. Reeves, D. E. Schindler, and D. C. Whited. 2020. Glacier retreat and Pacific salmon. *BioScience* 70:220–236.
- Post, E., R. B. Alley, T. R. Christensen, M. Macias-fauria, B. C. Forbes, M. N. Gooseff, A. Iler, J. T. Kerby, K. L. Lairde, M. E. Mann, J. Olofsson, J. C. Stroeve, F. Ulmer, R. A. Virginia, and M. Wang. 2019. The polar regions in a 2°C warmer world. *Science Advances* 5:eaaw9883.
- Quinn, T. P. 2018. *The behavior and ecology of Pacific salmon and trout*, second edition. University of Washington Press, Seattle.
- Rand, P. S., S. G. Hinch, J. Morrison, M. G. G. Foreman, M. J. MacNutt, J. S. Macdonald, M. C. Healey, A. P. Farrell, and D. A. Higgs. 2006. Effects of river discharge, temperature, and future climates on energetics and mortality of adult migrating Fraser River Sockeye Salmon. *Transactions of the American Fisheries Society* 135:655–667.
- Russo, S., A. Dosio, R. G. Graversen, J. Sillmann, H. Carrao, M. B. Dunbar, A. Singleton, P. Montagna, P. Barbola, and J. V. Vogt. 2014. Magnitude of extreme heat waves in present climate and their projection in a warming world. *Journal of Geophysical Research: Atmospheres* 119:12,500–12,512.
- Schoen, E. R., M. S. Wipfli, E. J. Trammell, D. J. Rinella, A. L. Floyd, J. Grunblatt, M. D. McCarthy, B. E. Meyer, J. M. Morton, J. E. Powell, A. Prakash, M. N. Reimer, S. L. Stuefer, H. Toniolo, B. M. Wells, and F. D. W. Witmer. 2017. Future of Pacific salmon in the face of environmental change: lessons from one of the world's remaining productive Salmon regions. *Fisheries* 42:538–553.
- Sergeant, C. J., J. R. Bellmore, C. McConnell, and J. W. Moore. 2017. High salmon density and low discharge create periodic hypoxia in coastal rivers. *Ecosphere* 8:e01846.
- Sergeant, C. J., J. A. Falke, R. A. Bellmore, J. R. Bellmore, and R. L. Crumley. 2020. A classification of streamflow patterns across the coastal Gulf of Alaska. *Water Resources Research* 56:1–17.
- Shaftel, R., S. Mauger, J. Falke, D. Rinella, J. Davis, and L. Jones. 2020. Thermal diversity of salmon streams in the Matanuska-Susitna Basin, Alaska. *Journal of the American Water Resources Association* 56:630–646.
- Strange, J. S. 2010. Upper thermal limits to migration in adult Chinook Salmon: evidence from the Klamath River Basin. *Transactions of the American Fisheries Society* 139:1091–1108.
- Strange, J. S. 2012. Migration strategies of adult Chinook Salmon runs in response to diverse environmental conditions in the Klamath River Basin. *Transactions of the American Fisheries Society* 141:1622–1636.
- Tillotson, M. D., and T. P. Quinn. 2017. Climate and conspecific density trigger pre-spawning mortality in Sockeye Salmon (*Oncorhynchus nerka*). *Fisheries Research* 188:138–148. Elsevier B.V.
- Valentin, M. M., T. S. Hogue, and L. E. Hay. 2018. Hydrologic regime changes in a high-latitude glacierized watershed under future climate conditions. *Water* 77:1878–1892.
- Westley, P. A. H. 2020. Documentation of en route mortality of summer Chum Salmon in the Koyukuk River, Alaska and its potential linkage to the heatwave of 2019. *Ecology and Evolution* 10:10296–10304. **AFS**



NOAA Technical Memorandum NMFS-AFSC-446

Genetic Stock Composition Analysis of Chinook Salmon (*Oncorhynchus tshawytscha*) Bycatch Samples from the 2020 Bering Sea Pollock Trawl Fisheries

C. M. Guthrie III, Hv. T. Nguyen, C. L. D'Amelio,
K. Karpan, P. D. Barry, and W. A. Larson

August 2022

U.S. DEPARTMENT OF COMMERCE

National Oceanic and Atmospheric
Administration
National Marine Fisheries Service
Alaska Fisheries Science Center

The National Marine Fisheries Service's Alaska Fisheries Science Center uses the NOAA Technical Memorandum series to issue informal scientific and technical publications when complete formal review and editorial processing are not appropriate or feasible. Documents within this series reflect sound professional work and may be referenced in the formal scientific and technical literature.

The NMFS-AFSC Technical Memorandum series of the Alaska Fisheries Science Center continues the NMFS-F/NWC series established in 1970 by the Northwest Fisheries Center. The NMFS-NWFSC series is currently used by the Northwest Fisheries Science Center.

This document should be cited as follows:

Guthrie, C. M. III, Hv. T. Nguyen, C. L. D'Amelio, K. Karpan, P. D. Barry, and W. A. Larson. 2022. Genetic stock composition analysis of Chinook salmon (*Oncorhynchus tshawytscha*) bycatch samples from the 2020 Bering Sea pollock trawl fisheries . U.S. Dep. Commer., NOAA Tech. Memo. NMFS-AFSC-446, 35 p.

This document is available online at:

Document available: <https://repository.library.noaa.gov>

Reference in this document to trade names does not imply endorsement by the National Marine Fisheries Service, NOAA.



NOAA
FISHERIES

Genetic Stock Composition Analysis of Chinook Salmon (*Oncorhynchus tshawytscha*) Bycatch Samples from the 2020 Bering Sea Pollock Trawl Fisheries

Auke Bay Laboratories
Alaska Fisheries Science Center
National Marine Fisheries Service
National Oceanic and Atmospheric Administration
17109 Pt. Lena Loop Road
Juneau, AK 99801

U.S. DEPARTMENT OF COMMERCE

National Oceanic and Atmospheric Administration
National Marine Fisheries Service
Alaska Fisheries Science Center

NOAA Technical Memorandum NOAA-TM-AFSC-446

August 2022

ABSTRACT

Genetic analysis of Chinook salmon (*Oncorhynchus tshawytscha*) captured as bycatch in the 2020 Bering Sea-Aleutian Island (BSAI) trawl fishery for walleye pollock (*Gadus chalcogrammus*) was undertaken to determine the overall stock composition of the bycatch and examine variation in stock compositions across space and time. Samples were genotyped for 37 single nucleotide polymorphism (SNP) DNA markers and stock compositions were estimated using a SNP baselined developed by the Alaska Department of Fish and Game (ADF&G). Genetic samples were collected using a systematic random sampling protocol where one out of every 10 Chinook salmon encountered was sampled. Based on analysis of 2,614 Chinook salmon bycatch samples, Coastal Western Alaska was the largest contributor (52%), with smaller contributions from British Columbia (15%), North Alaska Peninsula (13%), and West Coast US (7%) The proportional contribution of Western Alaska stocks was higher than the average over the last ten years (44%) and the proportion of Middle (2%) and Upper Yukon (2%) stocks was about average (2% and 4%, respectively). In total, we estimated that 16,796 (16,032-17,561 95% CI) fish were caught from Coastal Western Alaska stocks, 670 (396-981 95% CI) were caught from the Middle Yukon and 729 (517-968 95% CI) were caught from the Upper Yukon. The number of fish caught from the Coastal Western Alaska stock was substantially higher than the 10-year average and represented the second highest catch in the last decade. In general, the contributions of southern stocks (British Columbia and West Coast US) were lower than average in 2020 declining since 2018, contributions from Western Alaska were above average, and all other stock groups were similar to their 10-year average.

CONTENTS

ABSTRACT	iii
CONTENTS	v
INTRODUCTION	1
SAMPLE DISTRIBUTION	3
GENETIC STOCK COMPOSITION PROCEDURE	6
GENETIC STOCK COMPOSITION RESULTS	8
COMPARISON WITH PREVIOUS ESTIMATES	12
AGE COMPOSITION ANALYSIS	15
Ageing Methods	15
BSAI Ages	15
SUMMARY	16
Sampling Issues	17
Stock Composition Estimates	17
Application of These Estimates	18
ACKNOWLEDGMENTS	21
CITATIONS	23
APPENDICES	27

INTRODUCTION

Pacific salmon (*Oncorhynchus* spp.) are prohibited species in the federally managed Bering Sea groundfish fisheries, which are subject to management rules (NPMFC 2017a) that are in part designed to reduce prohibited species catch, hereafter referred to as “bycatch”. It is important to understand the stock composition of Pacific salmon caught in these fisheries, which take place in areas that are known feeding habitat for multiple brood years of Chinook salmon (*Oncorhynchus tshawytscha*) from many different localities in North America and Asia (Myers et al. 2007, Davis et al. 2009). Chinook salmon are economically valuable and highly prized in commercial, subsistence, and sport fisheries. Determining the geographic origin of salmon caught in federally managed fisheries is essential to understanding the effects that fishing has on Chinook salmon stock groups, especially those with conservation concerns (NPFMC 2017a). This report provides genetic stock identification results for the Chinook salmon bycatch samples collected from the Bering Sea walleye pollock (pollock; *Gadus chalcogrammus*) trawl fishery. National Marine Fisheries Service (NMFS) geographical statistical areas (NMFS area) associated with the Bering Sea groundfish fishery (NMFS areas 509-524) and Alaska Department of Fish and Game (ADF&G) statistical areas grids¹ (Fig. 1) are used to describe the spatial distribution of the Chinook salmon bycatch and genetic samples.

Amendment 91 to the North Pacific Fishery Management Council (NPFMC) Fishery Management Plan (FMP) for groundfish of the Bering Sea Aleutian Island (BSAI) Management Area was enacted in 2010 and included retention of all salmon caught in the pollock fishery. In 2011, a systematic random sampling design recommended by Pella and Geiger (2009) was

¹ http://www.adfg.alaska.gov/static/fishing/PDFs/commercial/chart03_bs.pdf

implemented by the Alaska Fisheries Science Center's (AFSC) Fisheries Monitoring and Analysis Division's (FMA) North Pacific Groundfish and Halibut Observer Program (Observer Program) to collect genetic samples from one out of every 10 Chinook salmon encountered as bycatch in the Bering Sea pollock fishery.

In 2020, genetic samples were collected by the Observer Program from the Chinook salmon caught as bycatch in the Bering Sea pollock fishery. The number of available samples and the unbiased sampling methodology facilitated the extrapolation of the sample stock composition to the overall Chinook bycatch from the Bering Sea pollock trawl fishery in 2020. Samples were collected from both the Bering Sea "A" season which started 01/01/2020 and ended 06/09/2021, and the Bering Sea "B" season which started 6/10/2020 and ended 12/31/2020. Stock composition analyses were performed using the single nucleotide polymorphism (SNP) baseline provided by ADF&G (Templin et al. 2011), the same baseline that was used previously to estimate stock composition of samples from the 2005-2019 Chinook salmon bycatch (NMFS 2009; Guyon et al. 2010a,b; Guthrie et al. 2012-2021; Larson et al. 2013).

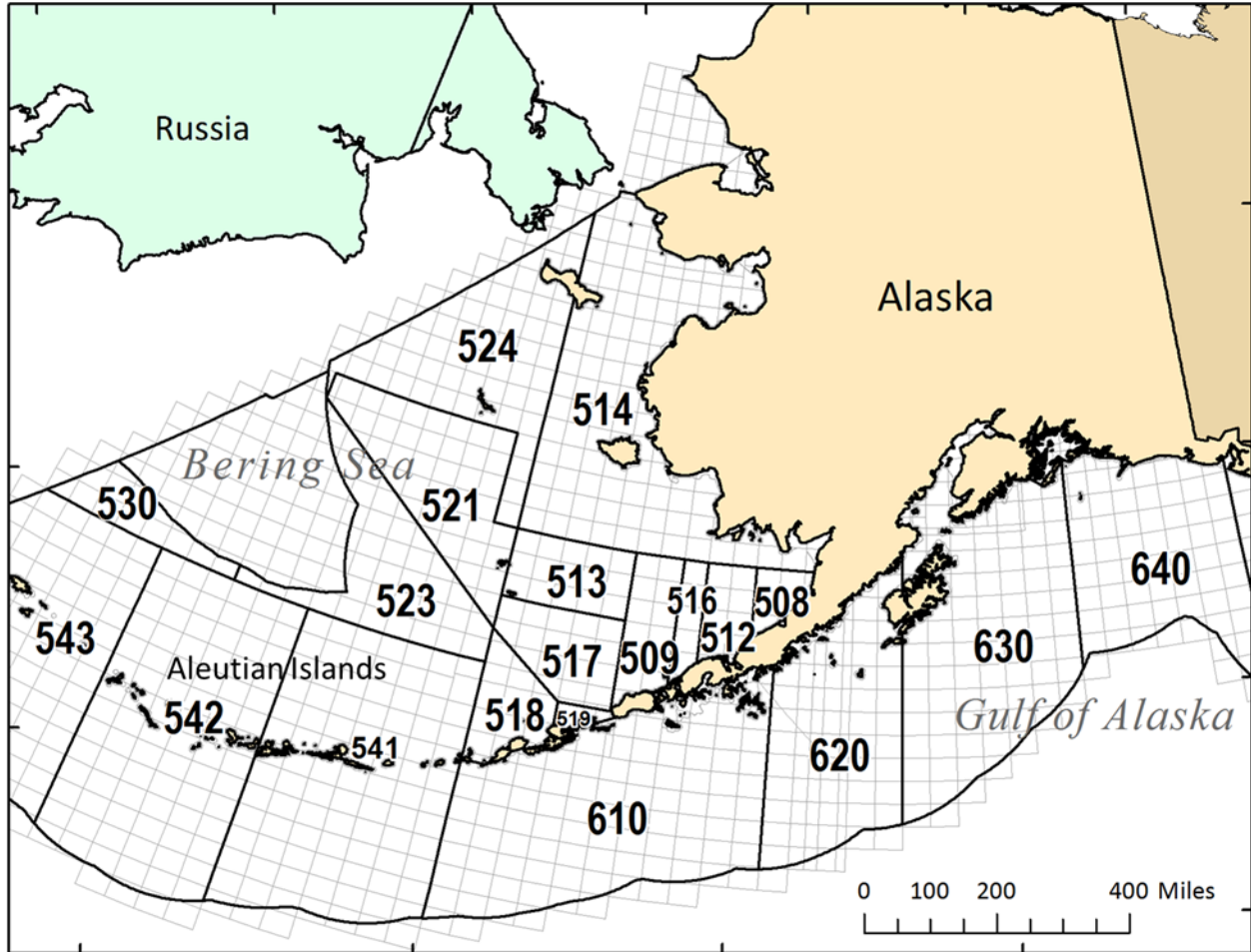


Figure 1. -- NMFS (outlined in black) and ADF&G (outlined in light gray) statistical areas associated with the Bering Sea and Gulf of Alaska groundfish fisheries.

SAMPLE DISTRIBUTION

Samples were collected from Chinook salmon bycatch by the Observer Program for analysis at AFSC's Auke Bay Laboratories (ABL). Axillary process tissues and 3-4 scales were stored in coin envelopes which were labeled, frozen, and shipped to ABL for analysis. Scales were collected as an additional source for ageing and a backup for genetic analysis.

In 2020, an estimated 32,294 Chinook salmon were taken in the bycatch of BSAI pollock trawl fisheries (NMFS 2021). The Chinook salmon bycatch estimate is 6% below the historical average (34,589) between 1991 and 2019, and far below the highest overall Chinook bycatch in

2007 when an estimated 122,195 fish were taken (Fig. 2). Of the total 2020 bycatch, 18,369 were from the trawl “A” season and 13,925 were from the “B” season. For the genetic analysis, the “B” season started on 6/01/20 (Statistical Week 23) because all but one of the “A” season samples were collected by 4/18/20. This difference is reflected in Appendix 2.

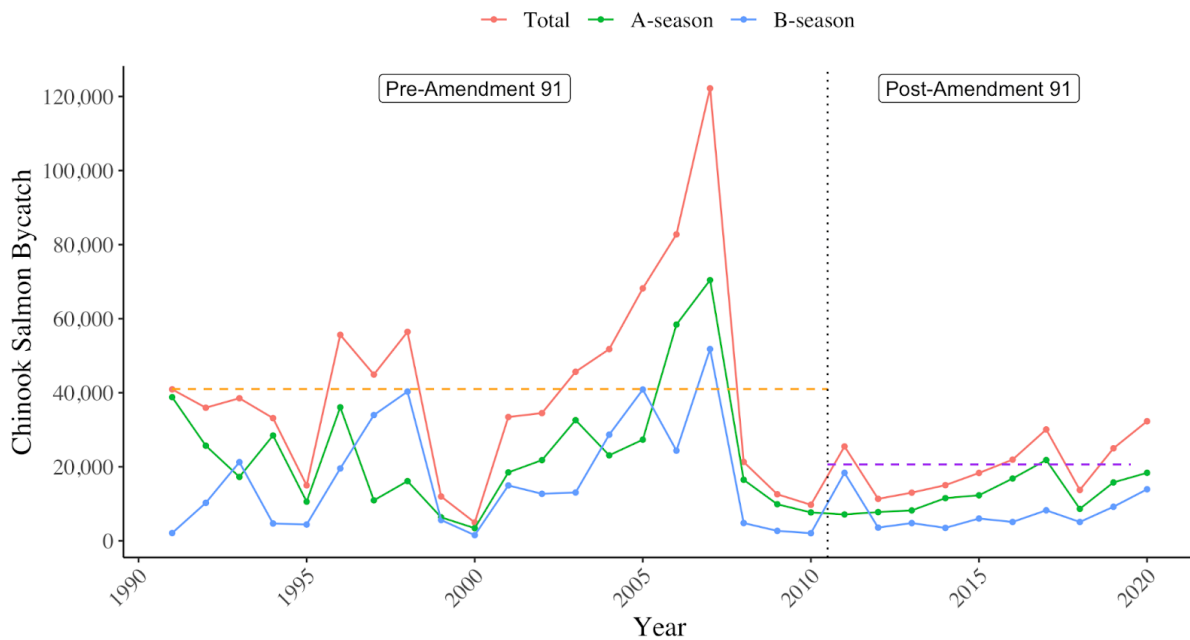


Figure 2. -- Annual “A” and “B” season estimates for the Chinook salmon bycatch from the Bering Sea pollock trawl fishery (NMFS 2021). The yellow dashed line shows the average bycatch before Amendment 91 and the purple shows the average after.

In 2020, there were 3,241 genetic samples received from the Bering Sea Chinook salmon bycatch collected by the Observer Program; of those samples, 2,614 were successfully genotyped for an overall genotyped sampling rate of 8.1% (“A” season $N = 1,371$ fish, 7.5% sampling rate; “B” season $N = 1,243$ fish, 8.9% sampling rate).

Potential biases primarily introduced through spatial and temporal aspects of genetic sample collection from the bycatch are well documented and have the potential to affect resulting stock composition estimates (Pella and Geiger 2009). The distributions of 2020 Chinook salmon bycatch genetic samples were evaluated by comparing the collection of genetic samples with the

overall bycatch distribution (Fig. 3). The temporal distribution of samples collected and successfully genotyped was evaluated across the two fishing seasons (Fig. 3). The sample spatial distribution was compared with the total bycatch by NMFS statistical area (NMFS area) over time (Fig. 3). While there was minor over- and under-sampling, genetic samples were generally spatially and temporally representative of the total Chinook bycatch (Fig. 3), since most under- and oversampled collections are from small bycatch collections.

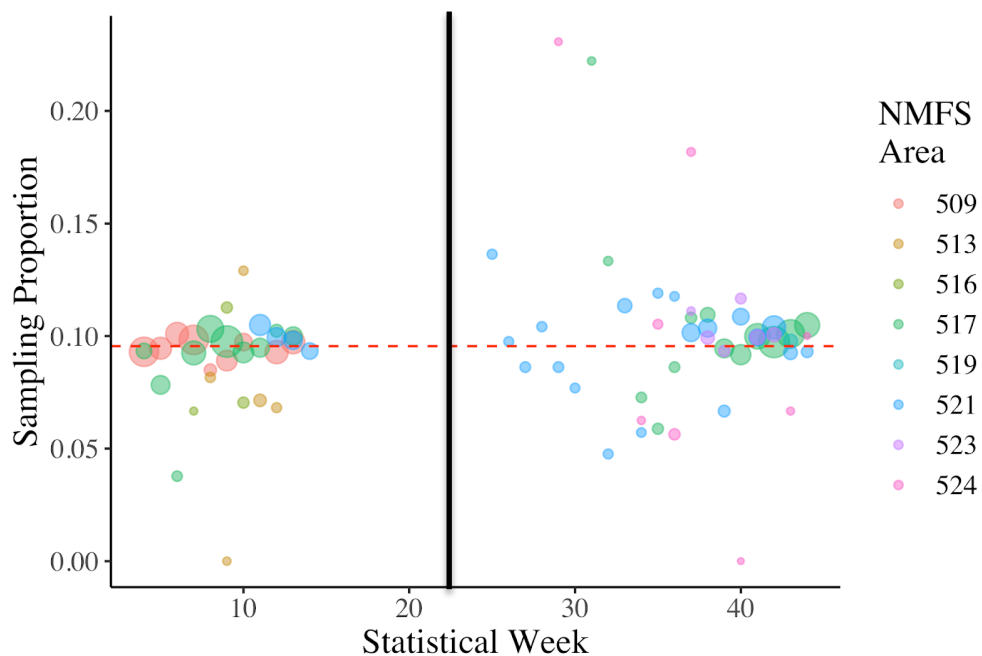


Figure 3. -- Proportion of Bering Sea Chinook salmon bycatch sampled for genetic analysis by statistical week and NMFS Statistical Areas. The size of the circles correspond to the number of bycatch fish. Weeks 4-20 correspond to the groundfish “A” season, whereas weeks 24-48 correspond to the “B” season. The black line delineates the “A” and “B” seasons. Sample sizes smaller than five not shown.

GENETIC STOCK COMPOSITION - PROCEDURE

DNA was extracted from axillary process tissues with Machery-Nagel kits (Allentown, PA) SNP genotyping was performed using Genotyping-in-Thousands by Sequencing (GTseq; Campbell et al. 2015) chemistry that uses short-read sequencing on an Illumina platform to interrogate the 37 SNP DNA markers represented in the Chinook salmon baseline (Templin et al.

2011; Appendix 4. The SNP baseline contains genetic information for 172 populations of Chinook salmon grouped into 11 geographic regions (also known as stock groups or reporting groups; Appendix 1). Proof tests performed previously have shown the baseline to be suitable for stock composition analysis using the regional reporting groups defined in Appendix 1 (Templin et al. 2011).

Sequencing libraries were prepared using the GT-seq protocol (Campbell, et al. 2015). PCR was performed on extracted DNA with primers that amplify 37 SNP loci (Templin et al. 2011). These PCR products were then indexed in a barcoding PCR, normalized using SequelPrep plates (Invitrogen) and each 96 well plate was subsequently pooled after Sequel prep normalization. Next, a double-sided bead size selection was performed using AMPure XP beads (Beckman Coulter), using ratios of beads to library of 0.5x to remove non-target larger fragments and then 1.2x to retain the desired amplicon. Libraries were sequenced on a MiSeq (Illumina) using a single 150-cycle lane run with 2×75 bp paired-end (PE) chemistry. PE reads for each individual were joined with FLASH2 (Magoč & Salzberg, 2011; <https://github.com/dstrett/FLASH2>). Merged reads were genotyped with the R package GTscore (McKinney; <https://github.com/gjmckinney/GTscore>). Individuals with low quality multilocus genotypes (< 80% of loci scored) were discarded. We re-genotype 3% of all project individuals as quality control measures.

From the 2020 Chinook salmon bycatch from the Bering Sea pollock trawl fishery, a total of 3,241 samples were analyzed of which 2,614 samples were successfully genotyped for 30 or more of the 37 SNP loci, a successful genotyping rate of 81%. The successfully genotyped samples had genetic information for an average of 36 of 37 markers from both the “A” (n = 1,371) and “B” (n = 1,243) seasons. Unfortunately, the Dutch Harbor air cargo carrier left a large

percentage of the “A” season samples in their warehouse unfrozen for over a month, which resulted in the lowered genotyping success rate for the “A” season. We were pleasantly surprised that we were able to extract as much genotypic information as we did given this logistical error.

Mixtures were created by separating sampled fish into spatial and temporal groups from observer data from the AKFIN database. Genetic stock identification was performed with the conditional genetic stock identification model in the R package *rubias* (Moran and Anderson 2019). For all estimates, the Dirichlet prior parameters for the stock proportions were defined by region to be $1/(GC_g)$, where C_g is the number of baseline populations in region g , and G is the number of regions. To ensure convergence to the posterior distribution, 11 separate MCMC chains of 70,000 iterations (burn-in of 35,000) of the non-bootstrapped model were run, with each chain starting at disparate values of stock proportions; configured such that for each chain 95% of the mixture came from a single designated reporting group (with probability equally distributed among the populations within that reporting group) and the remaining 5% equally distributed among remaining reporting groups. The convergence of chains for each reporting group estimate was assessed with the Gelman-Rubin statistic (Gelman and Rubin 1992) estimated with the `gelman.diag` function in the *coda* library (Plummer et al. 2006) within R. Once chain convergence was confirmed, inference was conducted with the conditional genetic stock identification model with bootstrapping over reporting groups (70,000 MCMC iterations, burn-in of 35,000, 100 bootstrap iterations).

GENETIC STOCK COMPOSITION - RESULTS

For “A” and “B” seasons combined, 69% of the bycatch samples were estimated to be from Alaska river systems flowing into the Bering Sea (Appendix 1, Reg. Num. numbers 2-5) with the Coastal Western Alaska region contributing the most (52%), followed by the North Alaska

Peninsula (13%). Thirty-one percent of all of the samples were from the southern (Appendix 1, Reg. Num. numbers 6, 9-11) regions, with the British Columbia (15%) region contributing the most, followed by the West Coast US (7%) and Northwest GOA (6%) regions (Appendix 2, Fig. 5).

The stock composition results indicate that 81% of the 1,371 Chinook salmon samples from the “A” season originated from Alaska river systems flowing into the Bering Sea with the largest contributions from Coastal Western Alaska region (52%) and the North Alaska Peninsula (25%). The remaining 19% were from southern regions with British Columbia (12%) contributing the most, followed by the West Coast US (3%) (Appendix 2, fig. 5). In the “B” season, 58% percent of the 1,243 “B” season samples originated from Alaska river systems flowing into the Bering Sea with the largest contribution from Coastal Western Alaska region (54%), while 32% were from southern regions; British Columbia (18%), West Coast US (11%), and Northwest GOA (9%) regions (Appendix 2, Fig. 5).

Using information from the ANSWERS tool provided by AKFIN (NMFS 2022), geographical (ADF&G statistical areas) aggregations were developed to investigate how stock compositions might vary among smaller areas of interest to the NPFMC. It should be noted that some of these strata overlap, with some samples being used in multiple analyses.

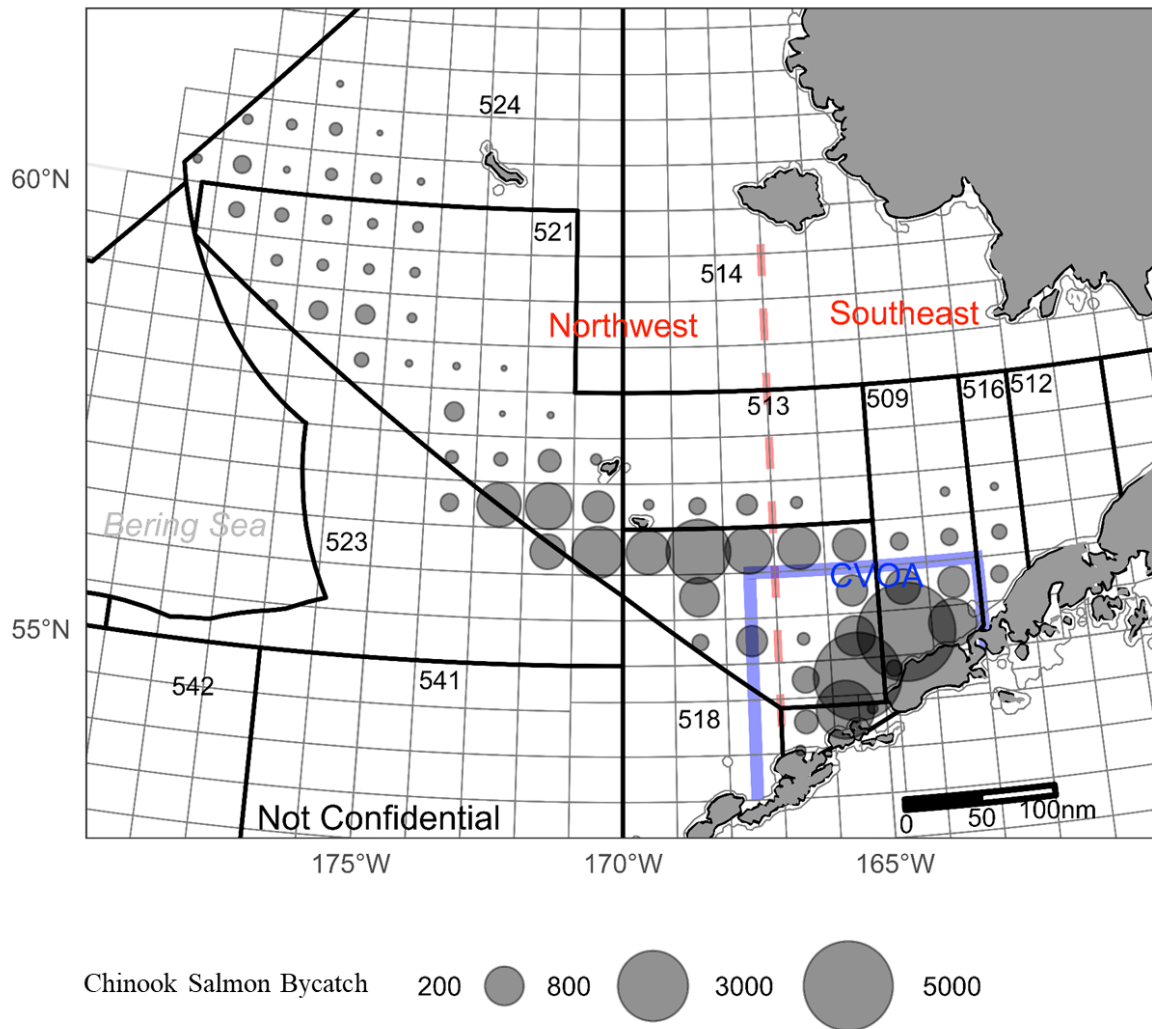


Figure 4. -- Location of sample strata used in comparative stock composition estimates from the 2020 Bering Sea Chinook salmon bycatch. Circles represent the amount of total bycatch in each stratum. The red dashed line delineates the Northwest and Southeast strata, while the solid blue line shows the boundary of the CVOA (NMFS 2021).

The “A” season estimates were developed for overlapping strata with sufficient numbers of samples (Appendix 2; Figs. 4, 5); Catcher Vessel Operation Area (CVOA) (659 samples, Figs. 4, 5), NMFS Statistical Area 509 (578 samples; Figs. 1, 5), Southeast Bering (792 samples, Figs. 4, 5), and Northwest Bering (579 samples, Figs. 4, 5). Over 73% of the Chinook salmon bycatch in the CVOA, NMFS Area 509 and Southeast Bering strata during the “A” season were from Alaska river systems flowing into the Bering Sea. For the CVOA, NMFS area 509, and

Southeast Bering Sea during the “A” season, most fish were from Coastal Western Alaska (47%, 46%, and 47%, respectively) followed by North Alaska Peninsula at (26%, 26% and 28%). The largest southern components for CVOA, NMFS Area 509 and Southeast Bering Sea during the “A” season were British Columbia (18%, 20% and 16%, respectively) and West Coast US (5%, 5% and 4%). For the Northwest Bering “A” season stratum, 88% of the bycatch was estimated to

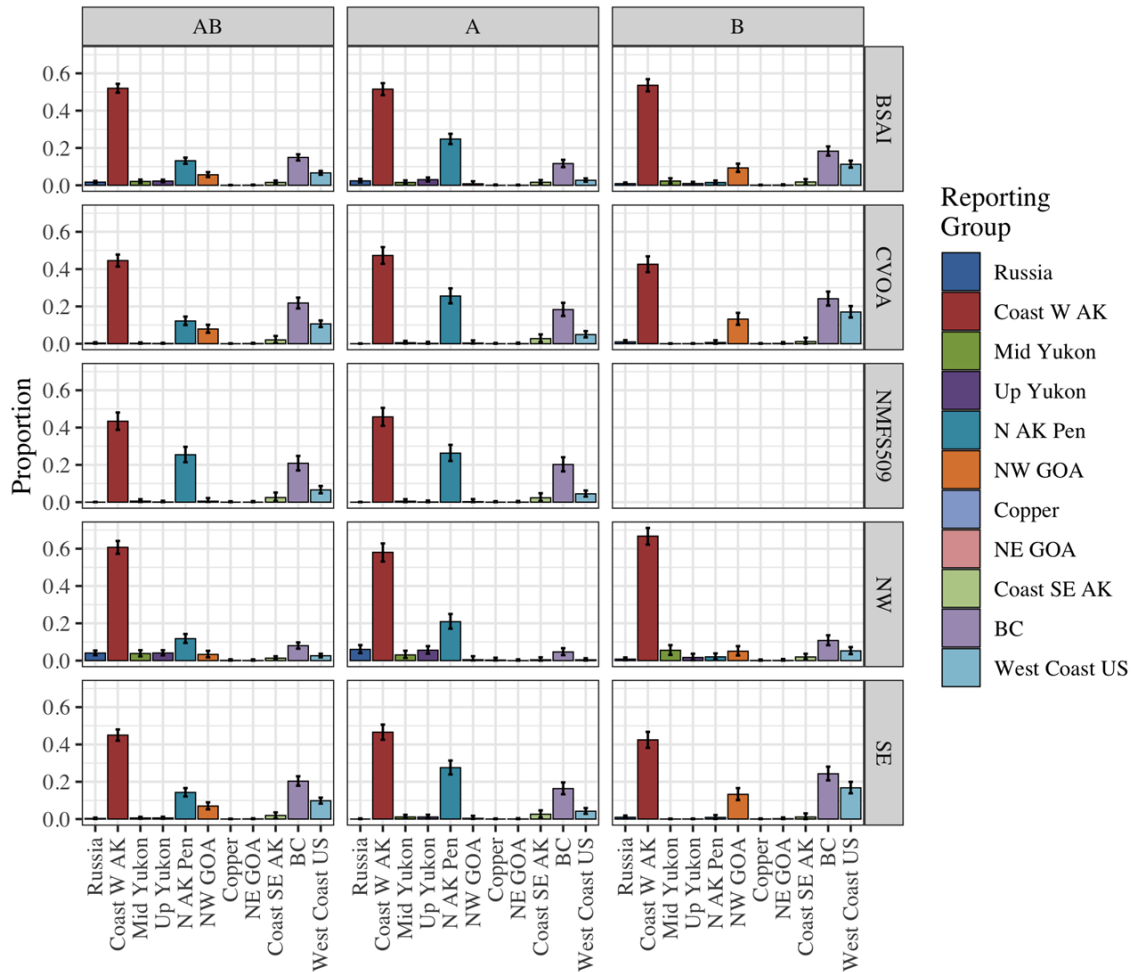


Figure 5. -- Stock composition estimates with 95% credible intervals of the 2020 BSAI Chinook salmon bycatch for overall (3,241 samples) “A” and “B” seasons; CVOA overall (1,325 samples), “A” and “B” season; NMFS area 509 overall (1,332 samples) and “A” season (bottom); Northwest Bering overall (1,150 samples), “A” and “B” seasons; and Southeast Bering overall (1,464 samples) “A and “B” seasons (NMFS 2021)

be from Alaska river systems flowing into the Bering Sea, with the largest contributions from Coastal Western Alaska (58%) followed by North Alaska Peninsula (21%), Upper Yukon (6%)

and Mid Yukon (3%). Six percent of the stock composition was estimated to be from southern regions, with most fish from British Columbia (5%).

For the “B” season, stock composition estimates were developed for CVOA (766 samples, Figs. 4, 5), Southeast Bering (672 samples, Figs. 4, 5), and Northwest Bering (372 samples, Figs. 4, 5) (NMFS 2021). For the Northwest Bering “B” season stratum, 76% of the stock composition was estimated to be from Alaska river systems flowing into the Bering Sea, which includes the largest contributor Coastal Western Alaska (67%). Twenty-three percent of the stock composition was estimated to be from southern regions, where the largest contributors were British Columbia (11%), Northwest GOA (5%) and West Coast US (5%).

Fifty-six percent of the “B” season stock composition estimates for the CVOA and Southeast Bering were from southern regions (Fig. 5, Appendix 2). The largest contributors were British Columbia (25% for CVOA, 24% for Southeast Bering), West Coast US (16% for CVOA, 17% for Southeast Bering), and Northwest GOA (13%). The major contributor from the Bering Sea was Coastal Western Alaska at 43% for CVOA and Southeast Bering. It is important to note that CVOA is a subsection of the Southeast Bering where most of the bycatch occurs.

Both the CVOA and Southeast Bering “B” season samples had a higher proportion of fish from southern regions (56%) than the “B” season overall (41%). The stock compositions were highly variable in the CVOA and Southeast Bering across the seasons. It is notable that the contribution from the West Coast US region increased from 5% to 17% for CVOA and Southeast Bering strata from the “A” and “B” seasons while the contribution from the Northern Alaska Peninsula region decreased from ~27% to almost zero in the same time frame. The Northwest GOA region increased from almost zero to 13% between the CVOA and Southeast Bering “A” and “B” seasons. The largest differences in the Northwest Bering between the “A” and “B”

seasons were the increase of Coastal Western Alaska from 58% to 67% and the decrease of North Alaska Peninsula from 21% to 2%.

COMPARISON WITH PREVIOUS ESTIMATES

About 60% of the Chinook salmon bycatch in 2020 occurred during the “A” season (Fig. 2), which is similar to most previous years since 2011. As in most previous years (with the exception of 2017), stock compositions from the analysis of the 2020 “A” season Chinook salmon bycatch showed that the majority of fish originated from river systems flowing into the Bering Sea (81%; Fig. 6). The Coastal Western Alaska region was the largest contributor in the 2020 “A” season, consistent with every year except 2017. The 2020 “B” season stock composition estimates from Coastal Western Alaska at 52% was higher than 2018 and 2019 (~30%), with Coastal Western Alaska contributions in all three of these years being substantially more than 2016 and 2017 when Coastal Western Alaska stock proportions were closer to 15% (Fig. 6, Appendix 3). Contrastingly, the higher levels of southern stock groups contributions observed from 2015 to 2018 are continuing to decrease. The estimated relative contributions from these more southern regions in the “B” season previously increased from a low of 20% in 2011 to a high of 86% in 2017, declining to 63% in 2018, and bumping up slightly to 67% in 2019, then dropping to 41% in 2020 (Fig. 6, Appendix 3).

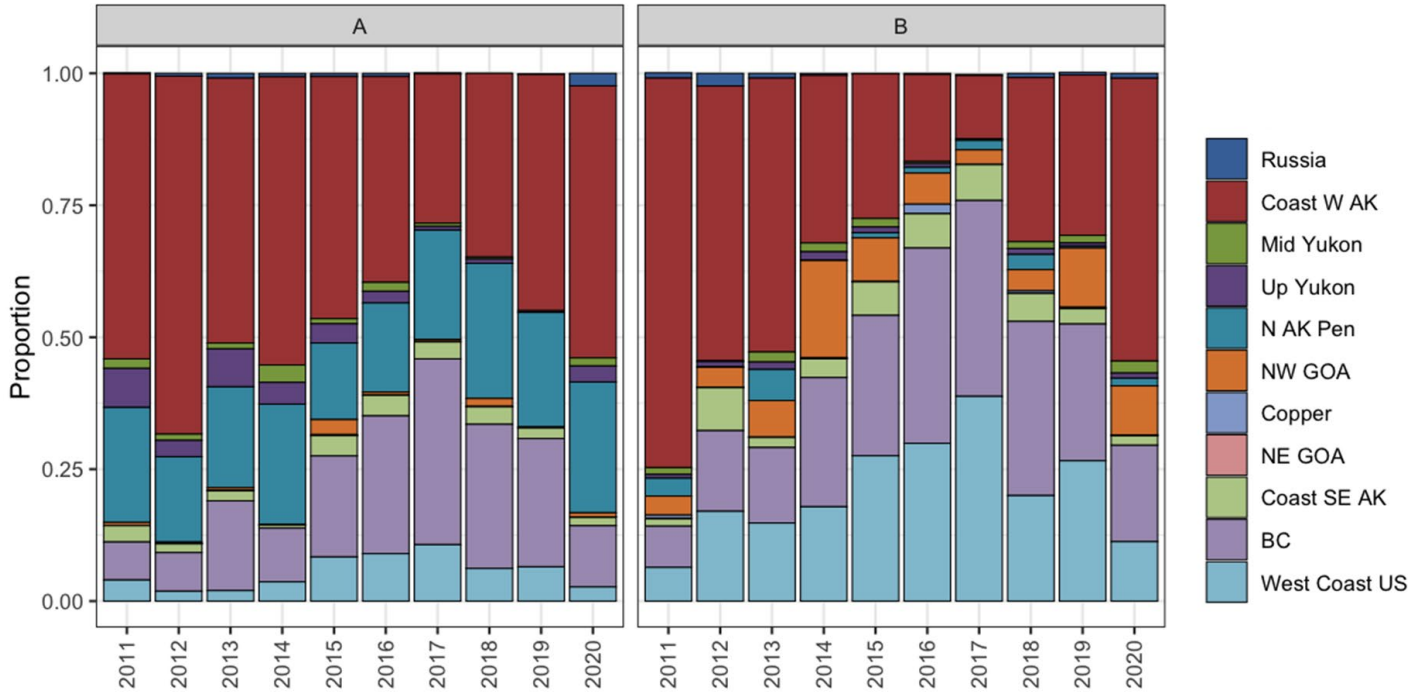


Figure 6. -- Annual “A” season (left) and “B” season (right) genetic stock composition estimates for 2011-2020 from the Bering Sea Chinook salmon bycatch.

When the stock compositions were analyzed on a yearly basis, the Coastal Western Alaska region shows variable contributions over time, but it was generally trending downward since 2011 until 2017, and since 2018 it has been trending upwards (Fig. 7). The 2020 North Alaska Peninsula region contribution of 13% was about average compared to previous years (Fig. 7). The Upper and Middle Yukon River, GOA, and Coastal Southeast Alaska contributions continued to be low in 2020, while contributions from the British Columbia and West Coast US regions have generally decreased from 2017 to 2020 (Fig. 7).

The estimated numbers of Chinook salmon caught as bycatch from Coastal Western Alaska stocks has varied from a high of 17,421 in 2011 to a low of 4,635 in 2018 (Fig. 7, Appendices 2, 3). Total catches of Coastal Western Alaska stocks were relatively stable from 2012 to 2018 and were consistently below 8,000 fish. In 2019, the catch increased slightly to near 10,000. In 2020 the catch further increased to nearly 17,000, close to the high in 2011.

Catches from the North Alaska Peninsula stock group have been relatively consistent over the last decade, ranging from ~2,500 to 5,000. Catches of southern stocks from British Columbia and the US West Coast peaked in 2017 at ~15,000 fish but generally range between 5,000 and 10,000. Catches of these two stocks in 2020 were the lowest since 2015. It is important to note these catch estimates represent the removals by region in each year but they cannot be used as is to represent any trends in the impact rates to particular regions over time because the amount of bycatch and areas fished vary. Stock-specific impacts are best estimated with adult equivalency models (Ianelli and Stram 2015).

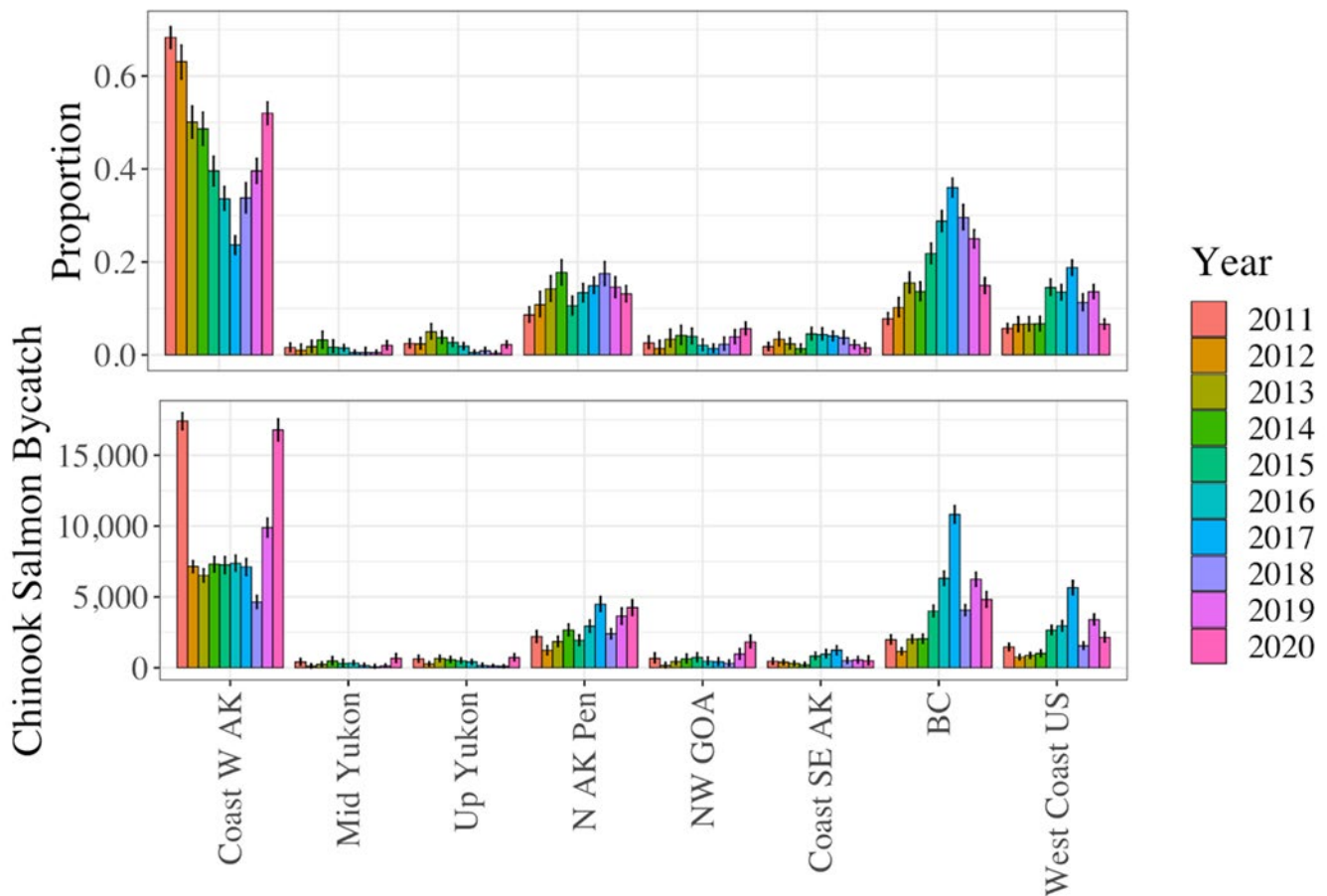


Figure 7. -- Annual (2011-2020) stock composition estimates with 95% credible intervals from the Bering Sea Chinook salmon bycatch (Top). Annual (2011-2020) bycatch estimates in numbers of fish with 95% credible intervals from the Bering Sea Chinook salmon bycatch (Bottom). Regions with low catches, Russia (Avg. N = 145) Copper (Avg. N = 22), and Northeast GOA (Avg. N = 6) were omitted.

AGE COMPOSITION ANALYSIS

Ageing Methods

Obtaining ages is important for parameterizing adult equivalency models and can also provide information on specific cohorts that can be used to better understand stock composition trends. The AFSC genetics program received paired genetic and scale samples from the Observer program. Scales were removed from sample envelopes and cleaned of dried slime and grit by moistening the scale with RO water and gently rubbing the scale between thumb and forefinger. Clean scales were then moistened and the sculptured side of the scale was mounted up on the scale gum card. Acetate impressions of each card of scales were made with a PHI PW22OH scale press. All acetate impressions were delivered to the ADF&G Mark Tag and Age Lab (MTA Lab) for age estimation. All age estimates are stored in the AKFIN database with paired observer information.

BSAI Ages

Of the 2,926 scales that were pressed, 1,782 scales were successfully read by the ADF&G MTA Lab (Fig. 8). The most common freshwater and saltwater zone error codes were inverted and wrong species. The most common freshwater age was 1 (79.2%), followed by age 0 (20.7%) whereas the most common saltwater ages were 2 (46.9%), 3 (30.9%), and 1 (14.8%). Of the three-, four-, and five-year-old fish caught in the BSAI trawl fishery, the majority were from Coastal Western Alaska (48.58%, 53.27%, and 56.03%, respectively). Middle and Upper Yukon stock groups contributed a relatively small amount, with the largest contribution of Middle Yukon stocks to the age-4 and age-5 mixtures (2.7 and 2.8%) and Upper Yukon to the age-5 and age-6 mixtures (7.7% and 6.6%). The North Alaska Peninsula stock groups comprised the largest

proportion of the oldest age class of fish, 6-year-olds (59.5%), with progressively declining contributions at younger ages. Northwest Gulf of Alaska stock groups comprised 10.9% and 4.8% of the age-3 and age-4 mixtures but contributed less than 1% to age-5 and age-6 mixtures. The southernmost stock groups (BC and West Coast US) were predominately age-3 and age-4 when captured, comprising 32.1% and 23.3%, respectively.

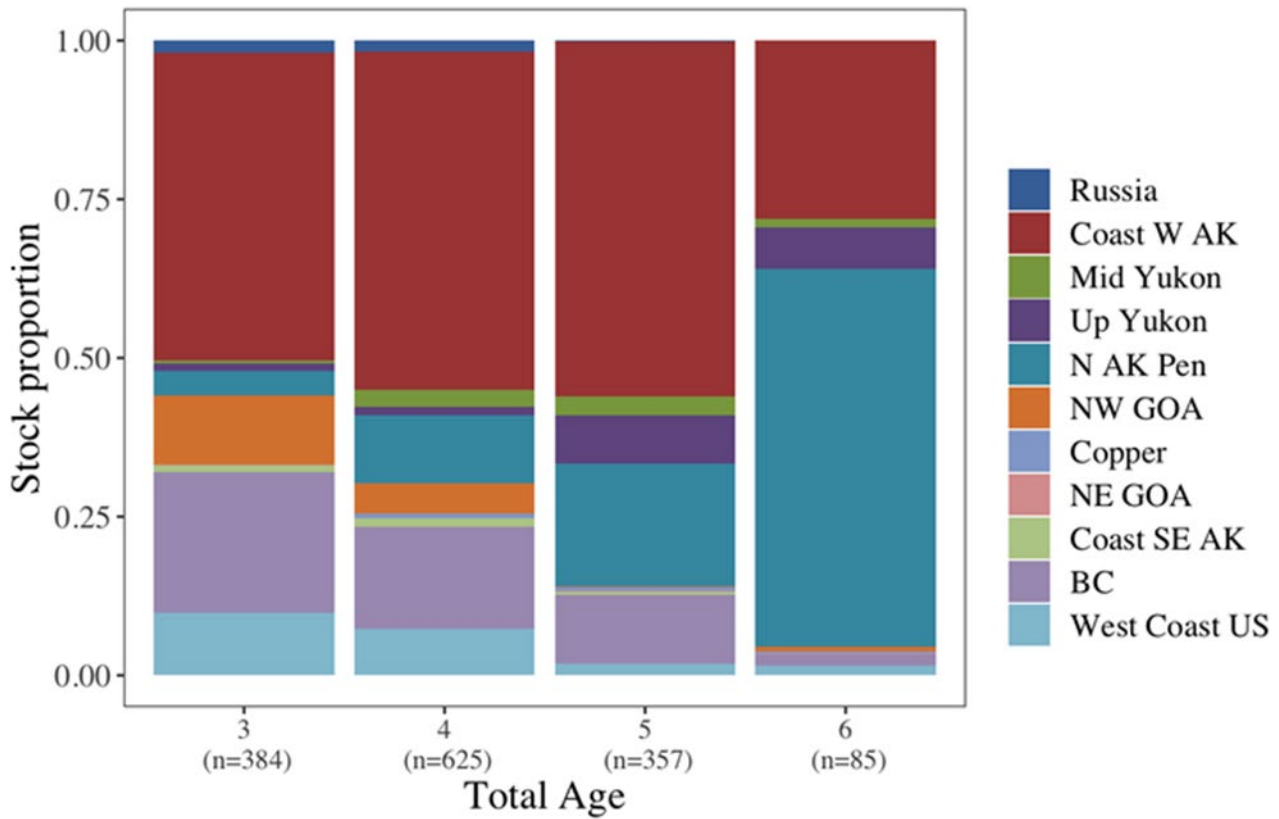


Figure 8. -- Stock Composition of the four age classes of Bering Sea Chinook salmon bycatch. The number of successfully aged samples is below the respective bars.

SUMMARY

Stock composition estimates of the Chinook salmon bycatch inform pollock and salmon fishery managers of the biological effects of the incidental take of salmon in the trawl fishery (Ianneli and Stram 2015). The incidental harvest of Chinook salmon in the Bering Sea pollock fishery averaged 34,258 salmon per year between 1991 and 2019 (29-year average), with a peak

of 121,195 in 2007 and a low of 4,961 in 2000 (Fig. 2; NMFS 2021). The Bering Sea Chinook salmon bycatch has abated somewhat in more recent years. The incidental harvest between 1991 and 2010 averaged 40,976 and after the implementation Amendment 91 between 2011 and 2019 the average dropped to 19,328 (Fig.2; NMFS 2021). In 2020, a total of 32,294 Chinook salmon were caught, which is below the 28-year average, but above the 9-year post-Amendment 91 average.

Sampling Issues

With the implementation of systematic random sampling, 2020 is the tenth year from which representative samples have been collected from the Chinook salmon bycatch. Systematic random sampling represents a substantial effort on the part of the Observer Program to develop standardized protocols for collecting sets of samples from numerous observers both at sea and in shore-based processing plants, the results of which are clearly apparent in the representative nature of the sample sets (Figs. 3). The number of successfully genotyped Chinook salmon from the Bering Sea bycatch samples was 2,614 corresponding to an effective overall sampling rate in 2020 of 8.1%, despite mishandling of samples noted earlier by a Dutch Harbor air cargo carrier.

Stock Composition Estimates

The proportions of Chinook salmon originating from Alaska rivers flowing into the Bering Sea accounted for most of the catches in early post-amendment 91 years, but southern regions have accounted for larger and larger proportions in more recent years with a maximum in 2017, where southern stocks accounted for more than half of the bycatch. The 2018-2020 data may signal a change to this pattern, with Chinook salmon originating from Alaska rivers flowing into the Bering Sea accounting for more than two-thirds of the bycatch in 2020 (Appendices 2, 3). The stock composition of the Chinook salmon bycatch from the 2019 “A” season differed

from the “B” season, demonstrating temporal changes (Appendix 2; Figs. 5 and 6). This was especially apparent for the North Alaska Peninsula (25% and 2%) region. The largest contributor to both “A” and “B” season fisheries was the Coastal Western Alaska region which increased slightly from “A” to “B” (52% to 54%).

Spatial analysis showed that the stock compositions varied within season depending upon where the salmon were caught. For example, during the “B” season a higher proportion of Coastal Western Alaska Chinook salmon were intercepted in the northwestern area of the Bering Sea, and a higher proportion of southern origin Chinook salmon were intercepted in the southeastern area of the Bering Sea (Fig. 5). Analysis of bycatch by age indicated that fish from the Coastal Western Alaska region were encountered at similar rates across the primary ages (3, 4, 5). Fish from southern stocks (NW GOA, British Columbia, and West Coast US) were encountered more frequently at younger ages. This is the first analysis year where age estimates have been widely available and more scale are currently ageing additional years to investigate temporal trends in stock compositions by age. It is notable that the North Alaska Peninsula stock group comprised the largest proportion of the oldest age class of fish.

Application of Estimates

Stock composition estimates for the 2020 Bering Sea Chinook salmon bycatch were mostly representative of the overall bycatch for this year and are presented in relative contributions as well as estimated numbers of fish. The extent to which any salmon stock group is impacted by the bycatch of the Bering Sea trawl fishery is dependent on many stock-specific factors including 1) the overall numbers of the stock in the bycatch, 2) the ages of the salmon caught in the bycatch by stock group, 3) the ages of the returning salmon by stock group, and 4) the total annual run-size of the affected stock groups. Because the effect of stock-specific

numbers of Chinook salmon in the bycatch is moderated by several factors, a higher contribution of a particular stock group in one year does not necessarily imply greater impact than a smaller estimate the next.

ACKNOWLEDGMENTS

We are grateful for the help from the AFSC's Fisheries Monitoring and Analysis Division, and the many participating observers who provided genetic samples. We appreciate the efforts of Rob Ames and Bob Ryznar for developing AKFIN Answer reports that helped us develop new strata for genetic analyses. We also appreciate the work of Bev Agler, Jodi Neil and the rest of the MTA Lab staff for conducting age analysis accurately and efficiently, and Dave Nicolls ABL for mounting and pressing the scales. We are grateful to Dani Evenson and Tyler Dann of ADF&G for their thoughtful reviews of this report.

CITATIONS

- Campbell, N. R., Harmon, S. A., & Narum, S. R. (2015). Genotyping-in-Thousands by sequencing (GT-seq): A cost effective SNP genotyping method based on custom amplicon sequencing. *Molecular Ecology Resources*, 15(4), 855-867. doi:10.1111/1755-0998.12357.
- Davis, N. D., A. V. Volkov, A. Y. Efimkin, N. A. Kuznetsova, J. L. Armstrong, and O. Sakai. 2009. Review of BASIS salmon food habits studies. *N. Pac. Anadr. Fish. Comm. Bull.* 5:197-208.
- Gelman, A., and D. B. Rubin. 1992. Inference from iterative simulation using multiple sequences. *Stat. Sci.* 7:457-511.
- Guthrie, C. M. III, Hv. Nguyen, and J. R. Guyon. 2012. Genetic stock composition analysis of Chinook salmon bycatch samples from the 2010 Bering Sea trawl fisheries. U.S. Dep. Commer., NOAA Tech. Memo. NMFS-AFSC-232, 22 p.
- Guthrie, C. M. III, Hv. Nguyen, and J. R. Guyon. 2013. Genetic stock composition analysis of Chinook salmon bycatch samples from the 2011 Bering Sea and Gulf of Alaska trawl fisheries. U.S. Dep. Commer., NOAA Tech. Memo. NMFS-AFSC-244, 28 p.
- Guthrie, C. M. III, Hv. Nguyen, and J. R. Guyon. 2014. Genetic stock composition analysis of Chinook salmon bycatch samples from the 2012 Bering Sea and Gulf of Alaska trawl fisheries. U.S. Dep. Commer., NOAA Tech. Memo. NMFS-AFSC-270, 33 p.
- Guthrie, C. M. III, Nguyen, Hv.T., and J. R. Guyon. 2015. Genetic stock composition analysis of the Chinook salmon bycatch from the 2013 Bering Sea walleye pollock (*Gadus chalcogrammus*) trawl fishery. U.S. Dep. Commer., NOAA Tech. Memo. NMFS-AFSC-290, 21 p.
- Guthrie, C. M. III, Nguyen, Hv.T., and J. R. Guyon. 2016. Genetic stock composition analysis of the Chinook salmon bycatch from the 2014 Bering Sea walleye pollock (*Gadus chalcogrammus*) trawl fishery. U.S. Dep. Commer., NOAA Tech. Memo. NMFS-AFSC-310, 25 p.
- Guthrie, C. M. III, Nguyen, Hv.T., A. E. Thomson, and J. R. Guyon. 2017. Genetic stock composition analysis of the Chinook salmon bycatch from the 2015 Bering Sea walleye pollock (*Gadus chalcogrammus*) trawl fishery. U.S. Dep. Commer., NOAA Tech. Memo. NMFS-AFSC-342, 33 p.
- Guthrie, C. M. III, Hv. T. Nguyen, A. E. Thomson, K. Hauch, and J. R. Guyon. 2018. Genetic stock composition analysis of the Chinook salmon (*Oncorhynchus tshawytscha*) bycatch from the 2016 Bering Sea walleye pollock (*Gadus chalcogrammus*) trawl fishery. U.S. Dep. Commer., NOAA Tech. Memo. NMFS-AFSC-365, 32 p.

- Guthrie III, C. M., Hv. T. Nguyen, M. Marsh, J. T. Watson, and J. R. Guyon. 2019. Genetic stock composition analysis of the Chinook salmon bycatch samples from the 2017 Bering Sea trawl fisheries. U.S. Dep. Commer., NOAA Tech. Memo. NMFS-AFSC-391, 36 p.
- Guthrie III, C. M., Hv. T. Nguyen, M. Marsh and J. R. Guyon. 2020. Genetic stock composition analysis of Chinook salmon bycatch samples from the 2018 Gulf of Alaska trawl fisheries. U.S. Dep. Commer., NOAA Tech. Memo. NMFS-AFSC-405, 33 p.
- Guthrie III, C. M., Hv. T. Nguyen, K. Karpan, J. T. Watson, and W. A. Larson. 2021. Genetic stock composition analysis of Chinook salmon (*Oncorhynchus tshawytscha*) bycatch samples from the 2019 Bering Sea trawl pollock trawl fishery. U.S. Dep. Commer., NOAA Tech. Memo. NMFS-AFSC-418, 33 p.
- Guyon, J. R., C. M. Guthrie, and H. Nguyen. 2010a. Genetic stock composition analysis of Chinook salmon bycatch samples from the 2008 Bering Sea pollock fishery, 32 p. Report to the North Pacific Fishery Management Council, 605 W. 4th Avenue, Anchorage, AK 99510.
- Guyon, J. R., C. M. Guthrie, and H. Nguyen. 2010b. Genetic stock composition analysis of Chinook salmon bycatch samples from the 2007 “B” season and 2009 Bering Sea trawl fisheries, p. 32. Report to the North Pacific Fishery Management Council, 605 W. 4th Avenue, Anchorage, AK 99510.
- Ianelli, J. N., and Stram, D. L. 2015. Estimating impacts of the pollock fishery bycatch on western Alaska Chinook salmon. ICES J. Mar. Sci. 72: 1159–1172.
- Larson, W. A., F. M. Utter, K. W. Myers, W. D. Templin, J. E. Seeb, C. M. Guthrie III, A. V. Bugaev, and L. W. Seeb. 2013. Single-nucleotide polymorphisms reveal distribution and migration of Chinook salmon (*Oncorhynchus tshawytscha*) in the Bering Sea and North Pacific Ocean. Can. J. Fish. Aquat. Sci. 70(1):128-141.
- Magoč, T., & Salzberg, S. L. (2011). FLASH: fast length adjustment of short reads to improve genome assemblies. Bioinformatics 27(21): 2957-2963.
doi:10.1093/bioinformatics/btr507
- Moran, B.M., and E.C. Anderson. 2019. Bayesian Inference from the Conditional Genetic Stock Identification Model. Canadian Journal of Fisheries and Aquatic Sciences 76 (4): 551–60.
doi:[10.1139/cjfas-2018-0016](https://doi.org/10.1139/cjfas-2018-0016).
- Myers, K. W., N. V. Klovach, O. F. Gritsenko, S. Urawa, and T. C. Royer. 2007. Stock-specific distributions of Asian and North American salmon in the open ocean, interannual changes, and oceanographic conditions. N. Pac. Anadr. Fish. Comm. Bull. 4: 159-177.

- NMFS (National Marine Fisheries Service). 2009. Bering Sea Chinook salmon bycatch management - Volume 1, Final Environmental Impact Statement, National Oceanic and Atmospheric Administration, National Marine Fisheries Service, Alaska Regional Office, Juneau, AK.
- NMFS (National Marine Fisheries Service). 2022. Catch Accounting System data. NMFS Alaska Regional Office. Data compiled by Alaska Fisheries Information Network for Alaska Fisheries Science Center, Juneau. [URL not publicly available as some information is confidential.]
- NMFS (National Marine Fisheries Service). 2021. BSAI Chinook salmon mortality estimates, 1991-present, National Oceanic and Atmospheric Administration, National Marine Fisheries Service, Alaska Regional Office, Juneau, AK.
https://alaskafisheries.noaa.gov/sustainablefisheries/inseason/chinook_salmon_mortality.pdf
- NPFMC (North Pacific Fishery Management Council). 2017a. Fishery management plan for groundfish of the Bering Sea and Aleutian Islands management area. North Pacific Fishery Management Council, 605 W. 4th Ave., Anchorage, Alaska, 99501.
<https://www.npfmc.org/wp-content/PDFdocuments/fmp/BSAI/BSAIfmp.pdf> .
- Pella, J., and H. J. Geiger. 2009. Sampling considerations for estimating geographic origins of Chinook salmon bycatch in the Bering Sea pollock fishery. Alaska Dep. Fish Game Spec. Pub. No. SP 09-08. 58 p.
- Plummer M., N. Best, K. Cowles, and K. Vines. 2006. CODA: Convergence Diagnosis and Output Analysis for MCMC. R News 6:7–11
- Templin, W. D., J. E. Seeb, J. R. Jasper, A. W. Barclay, and L. W. Seeb. 2011. Genetic differentiation of Alaska Chinook salmon: the missing link for migratory studies. Mol. Ecol. Res. 11 (Suppl. 1):226–246.

APPENDICES

Appendix 1. -- Chinook salmon populations in the ADF&G SNP baseline with the regional designations used in the analyses of this report. S. = South, R. = River, H. = Hatchery, and L. = Lake.

Population name	Reg Num.	Region	Population name	Reg Num.	Region
Bistraya River	1	Russia	Henshaw Creek	3	Mid Yukon
Bolshaya River	1	Russia	Kantishna River	3	Mid Yukon
Kamchatka River late	1	Russia	Salcha River	3	Mid Yukon
Pakhatcha River	1	Russia	Sheenjok River	3	Mid Yukon
Andreafsky River	2	Coast W AK	S. Fork Koyukuk River	3	Mid Yukon
Aniak River	2	Coast W AK	Big Salmon River	4	Up Yukon
Anvik River	2	Coast W AK	Blind River	4	Up Yukon
Arolik River	2	Coast W AK	Chandindu River	4	Up Yukon
Big Creek	2	Coast W AK	Klondike River	4	Up Yukon
Cheeneetnu River	2	Coast W AK	Little Salmon River	4	Up Yukon
Eek River	2	Coast W AK	Mayo River	4	Up Yukon
Gagaryah River	2	Coast W AK	Nisutlin River	4	Up Yukon
George River	2	Coast W AK	Nordenskiold River	4	Up Yukon
Gisasa River	2	Coast W AK	Pelly River	4	Up Yukon
Golsovia River	2	Coast W AK	Stewart River	4	Up Yukon
Goodnews River	2	Coast W AK	Takhini River	4	Up Yukon
Kanektok River	2	Coast W AK	Tatchun Creek	4	Up Yukon
Kisaralik River	2	Coast W AK	Whitehorse Hatchery	4	Up Yukon
Kogrukluk River	2	Coast W AK	Black Hills Creek	5	N AK Pen
Kwethluk River	2	Coast W AK	King Salmon River	5	N AK Pen
Mulchatna River	2	Coast W AK	Meshik River	5	N AK Pen
Naknek River	2	Coast W AK	Milky River	5	N AK Pen
Nushagak River	2	Coast W AK	Nelson River	5	N AK Pen
Pilgrim River	2	Coast W AK	Steelhead Creek	5	N AK Pen
Salmon R. -Pitka Fork	2	Coast W AK	Anchor River	6	NW GOA
Stony River	2	Coast W AK	Ayakulik River	6	NW GOA
Stuyahok River	2	Coast W AK	Benjamin Creek	6	NW GOA
Takotna River	2	Coast W AK	Chignik River	6	NW GOA
Tatlawiksuk River	2	Coast W AK	Crescent Creek	6	NW GOA
Togiak River	2	Coast W AK	Crooked Creek	6	NW GOA
Tozitna River	2	Coast W AK	Deception Creek	6	NW GOA
Tuluksak River	2	Coast W AK	Deshka River	6	NW GOA
Unalakleet River	2	Coast W AK	Funny River	6	NW GOA
Beaver Creek	3	Mid Yukon	Juneau Creek	6	NW GOA
Chandalar River	3	Mid Yukon	Karluk River	6	NW GOA
Chena River	3	Mid Yukon	Kasilof River mainstem	6	NW GOA

Population name	Reg		Population name	Reg	
	Num.	Region		Num.	Region
Kenai River mainstem	6	NW GOA	Kowatua River	9	Coast SE AK
Killey Creek	6	NW GOA	Little Tatsemenie River	9	Coast SE AK
Ninilchik River	6	NW GOA	Macaulay Hatchery	9	Coast SE AK
Prairie Creek	6	NW GOA	Medvejie Hatchery	9	Coast SE AK
Slikok Creek	6	NW GOA	Nakina River	9	Coast SE AK
Talachulitna River	6	NW GOA	Tahltn River	9	Coast SE AK
Willow Creek	6	NW GOA	Unuk R.-Deer Mountain H.	9	Coast SE AK
Bone Creek	7	Copper	Unuk River - LPW	9	Coast SE AK
E. Fork Chistochina River	7	Copper	Upper Nahlin River	9	Coast SE AK
Gulkana River	7	Copper	Big Qualicum River	10	BC
Indian River	7	Copper	Birkenhead River spring	10	BC
Kiana Creek	7	Copper	Bulkley River	10	BC
Manker Creek	7	Copper	Chilko River summer	10	BC
Mendeltna Creek	7	Copper	Clearwater River summer	10	BC
Otter Creek	7	Copper	Conuma River	10	BC
Sinona Creek	7	Copper	Damdochax Creek	10	BC
Tebay River	7	Copper	Ecstall River	10	BC
Tonsina River	7	Copper	Harrison River	10	BC
Big Boulder Creek	8	NE GOA	Kateen River	10	BC
Kelsall River	8	NE GOA	Kincolith Creek	10	BC
King Salmon River	8	NE GOA	Kitimat River	10	BC
Klukshu River	8	NE GOA	Klinaklini River	10	BC
Situk River	8	NE GOA	Kwinageese Creek	10	BC
Tahini River	8	NE GOA	Louis River spring	10	BC
Tahini River - Pullen Creek H.	8	NE GOA	Lower Adams River fall	10	BC
Andrews Creek	9	Coast SE AK	Lower Atnarko River	10	BC
Blossom River	9	Coast SE AK	Lower Kalum River	10	BC
Butler Creek	9	Coast SE AK	Lower Thompson River fall	10	BC
Chickamin River	9	Coast SE AK	Marble Creek	10	BC
Chickamin River-LPW	9	Coast SE AK	Middle Shuswap R. summer	10	BC
Chickamin R. Whitman L. H.	9	Coast SE AK	Morkill River summer	10	BC
Clear Creek	9	Coast SE AK	Nanaimo River	10	BC
Cripple Creek	9	Coast SE AK	Nechako River summer	10	BC
Crystal Lake Hatchery	9	Coast SE AK	Nitinat River	10	BC
Dudidontu River	9	Coast SE AK	Oweegeee Creek	10	BC
Genes Creek	9	Coast SE AK	Porteau Cove	10	BC
Hidden Falls Hatchery	9	Coast SE AK	Quesnel River summer	10	BC
Humpy Creek	9	Coast SE AK	Quinsam River	10	BC
Kerr Creek	9	Coast SE AK	Robertson Creek	10	BC
Keta River	9	Coast SE AK	Salmon River summer	10	BC
King Creek	9	Coast SE AK	Sarita River	10	BC

Population name	Reg		Population name	Reg	
	Num.	Region		Num.	Region
Stuart River summer	10	BC	Lower Deschutes R. fall	11	West Coast US
Sustut River	10	BC	Lyons Ferry H. summer/fall	11	West Coast US
Torpy River summer	10	BC	Makah National Fish H. fall	11	West Coast US
Wannock River	10	BC	McKenzie River spring	11	West Coast US
Alsea River fall	11	West Coast US	Sacramento River winter	11	West Coast US
Carson Hatchery spring	11	West Coast US	Siuslaw River fall	11	West Coast US
Eel River fall	11	West Coast US	Soos Creek Hatchery fall	11	West Coast US
Forks Creek fall	11	West Coast US	Upper Skagit River summer	11	West Coast US
Hanford Reach	11	West Coast US			
Klamath River	11	West Coast US			

Appendix 2. -- Regional *Rubias* stock composition percentage estimates, standard deviations (SD), 95% credible intervals (CI), and estimated numbers of Chinook salmon from the the 2020 Bering Sea pollock trawl fisheries. Sample sizes are adjacent to the stratum designation. Total catch is the census for each stratum from AKFIN reports (NMFS 2021). Estimated numbers of fish for aged fish are for only the number of fish aged.

Region	"A" Season (N=1,371)				"B" Season (N=1,243)				Bering Sea all (N=3,241)			
	Est. #	Mean	SD	95% CI	Est. #	Mean	SD	95% CI	Est. #	Mean	SD	95% CI
Russia	435	2.4	0.48	(1.5,3.4)	123	0.9	0.28	(0.4,1.5)	552	1.7	0.30	(1.2,2.3)
Coast W AK	9,469	51.5	1.64	(48.3,54.7)	7,467	53.6	1.68	(50.3,56.9)	16,796	52.0	1.21	(49.6,54.4)
Mid Yukon	281	1.5	0.49	(0.7,2.6)	318	2.3	0.73	(1.0,3.8)	670	2.1	0.47	(1.2,3.0)
Up Yukon	557	3.0	0.54	(2.1,4.2)	130	0.9	0.41	(0.3,1.8)	729	2.3	0.36	(1.6,3.0)
N AK Pen	4,553	24.8	1.41	(22.1,27.6)	208	1.5	0.48	(0.7,2.5)	4,247	13.1	0.84	(11.5,14.8)
NW GOA	143	0.8	0.53	(0.3,2.1)	1,295	9.3	1.12	(7.2,11.6)	1,825	5.7	0.68	(4.4,7.1)
Copper	0	0.0	0.11	(0.0,0.4)	7	0.0	0.08	(0.0,0.3)	0	0.0	0.06	(0.0,0.2)
NE GOA	3	0.0	0.10	(0.0,0.3)	12	0.1	0.15	(0.0,0.5)	14	0.0	0.10	(0.0,0.3)
Coast SE AK	297	1.6	0.55	(0.7,2.8)	249	1.8	0.73	(0.5,3.3)	497	1.5	0.47	(0.7,2.6)
BC	2,138	11.6	1.01	(9.7,13.6)	2,548	18.3	1.25	(15.9,20.8)	4,824	14.9	0.84	(13.3,16.6)
West Coast US	494	2.7	0.47	(1.9,3.7)	1,569	11.3	0.95	(9.5,13.2)	2,141	6.6	0.52	(5.7,7.7)
Total Catch	18,369				13,925				32,294			
Region	CVOA "A" (N=659)				CVOA "B" (N=766)				CVOA (N=1,325)			
	Est. #	Mean	SD	95% CI	Est. #	Mean	SD	95% CI	Est. #	Mean	SD	95% CI
Russia	0	0.0	0.05	(0.0,0.1)	88	1.0	0.41	(0.3,1.9)	65	0.4	0.20	(0.0,0.8)
Coast W AK	4,696	47.3	2.29	(42.8,51.8)	3,796	42.6	2.16	(38.3,46.8)	8,035	44.6	1.64	(41.4,47.8)
Mid Yukon	56	0.6	0.38	(0.1,1.5)	0	0.0	0.08	(0.0,0.2)	42	0.2	0.18	(0.0,0.7)
Up Yukon	20	0.2	0.28	(0.0,1.0)	2	0.0	0.09	(0.0,0.3)	23	0.1	0.13	(0.0,0.5)
N AK Pen	2,538	25.6	2.05	(21.6,29.7)	60	0.7	0.51	(0.0,1.9)	2,199	12.2	1.16	(10.0,14.5)
NW GOA	36	0.4	0.48	(0.1,1.8)	1,175	13.2	1.64	(10.1,16.5)	1,421	7.9	1.09	(5.9,10.2)
Copper	0	0.0	0.12	(0.0,0.4)	3	0.0	0.10	(0.0,0.3)	0	0.0	0.07	(0.0,0.3)
NE GOA	4	0.0	0.17	(0.0,0.6)	14	0.2	0.25	(0.0,0.9)	16	0.1	0.14	(0.0,0.5)
Coast SE AK	272	2.7	1.06	(0.9,5.0)	105	1.2	0.88	(0.0,3.2)	370	2.1	0.96	(0.4,4.2)
BC	1,818	18.3	1.81	(14.9,21.9)	2,150	24.1	1.91	(20.5,27.9)	3,934	21.8	1.48	(18.9,24.7)
West Coast US	486	4.9	0.87	(3.4,6.8)	1,514	17.0	1.57	(14.1,20.2)	1,917	10.6	0.90	(8.9,12.5)
Total Catch	9,925				8,907				18,022			
Region	NW Bering S. "A" (N=579)				NW Bering S. "B" (N=571)				NW Bering S. (N=1,150)			
	Est. #	Mean	SD	95% CI	Est. #	Mean	SD	95% CI	Est. #	Mean	SD	95% CI
Russia	394	6.0	1.10	(4.0,8.3)	50	0.8	0.38	(0.3,1.7)	522	4.1	0.65	(2.9,5.4)
Coast W AK	3,808	58.1	2.49	(53.1,62.8)	4,177	66.7	2.28	(62.2,71.1)	7,785	60.8	1.77	(57.2,64.2)
Mid Yukon	201	3.1	1.00	(1.4,5.3)	347	5.5	1.33	(3.1,8.3)	488	3.8	0.85	(2.3,5.6)
Up Yukon	367	5.6	1.03	(3.7,7.8)	106	1.7	0.89	(0.3,3.7)	526	4.1	0.71	(2.8,5.6)
N AK Pen	1,369	20.9	2.00	(17.1,25.0)	127	2.0	0.82	(0.7,3.9)	1,511	11.8	1.22	(9.5,14.3)
NW GOA	32	0.5	0.63	(0.1,2.4)	316	5.0	1.27	(2.8,7.8)	428	3.3	0.91	(1.7,5.3)
Copper	20	0.3	0.42	(0.1,1.6)	5	0.1	0.17	(0.0,0.6)	16	0.1	0.19	(0.0,0.7)
NE GOA	1	0.0	0.25	(0.0,0.7)	5	0.1	0.25	(0.0,0.9)	7	0.1	0.19	(0.0,0.7)
Coast SE AK	29	0.4	0.51	(0.0,1.8)	123	2.0	0.75	(0.7,3.7)	168	1.3	0.46	(0.5,2.3)
BC	305	4.7	0.95	(2.9,6.7)	675	10.8	1.36	(8.3,13.6)	1,027	8.0	0.85	(6.4,9.8)
West Coast US	29	0.4	0.32	(0.0,1.3)	327	5.2	0.97	(3.5,7.3)	336	2.6	0.50	(1.7,3.7)
Total Catch	6,557				6,258				12,815			
Region	SE Bering S. "A" (N=792)				SE Bering S. "B" (N=672)				SE Bering S. (N=1,464)			
	Est. #	Mean	SD	95% CI	Est. #	Mean	SD	95% CI	Est. #	Mean	SD	95% CI
Russia	0	0.0	0.11	(0.0,0.4)	75	1.0	0.40	(0.3,1.9)	67	0.3	0.19	(0.0,0.8)
Coast W AK	5,431	46.6	2.07	(42.5,50.6)	3,282	42.5	2.19	(38.2,46.7)	8,725	45.0	1.54	(42.0,48.0)
Mid Yukon	132	1.1	0.49	(0.4,2.3)	0	0.0	0.08	(0.0,0.2)	114	0.6	0.26	(0.2,1.2)
Up Yukon	131	1.1	0.53	(0.3,2.3)	2	0.0	0.09	(0.0,0.3)	116	0.6	0.28	(0.2,1.2)
N AK Pen	3,214	27.6	1.91	(23.9,31.4)	68	0.9	0.54	(0.1,2.1)	2,772	14.3	1.15	(12.1,16.6)
NW GOA	48	0.4	0.48	(0.1,1.7)	1,024	13.3	1.64	(10.2,16.6)	1,355	7.0	0.96	(5.2,9.0)
Copper	0	0.0	0.09	(0.0,0.3)	2	0.0	0.10	(0.0,0.3)	0	0.0	0.06	(0.0,0.2)
NE GOA	4	0.0	0.14	(0.0,0.4)	14	0.2	0.25	(0.0,0.9)	15	0.1	0.11	(0.0,0.4)
Coast SE AK	303	2.6	0.99	(0.8,4.7)	86	1.1	0.84	(0.0,3.0)	378	2.0	0.82	(0.4,3.6)
BC	1,905	16.3	1.62	(13.3,19.7)	1,877	24.3	1.87	(20.8,28.1)	3,939	20.3	1.29	(17.9,23.0)
West Coast US	491	4.2	0.79	(2.8,5.9)	1,295	16.8	1.57	(13.8,19.9)	1,904	9.8	0.82	(8.3,11.5)
Total Catch	11,659				7,726				19,385			

Appendix 2. -- Continued

Region	Area 509 "A" (N=578)				Area 509 (N=607)				Bering Sea Age 3 (N=384)			
	Est. #	Mean	SD	95% CI	Est. #	Mean	SD	95% CI	Est. #	Mean	SD	95% CI
Russia	0	0.0	0.00	(0.1,0.0)	0	0.0	0.00	(0.1,0.0)	7	1.9	0.76	(0.7,3.6)
Coast W AK	3,912	45.7	40.95	(2.4,45.7)	3,843	43.4	38.79	(2.4,43.4)	187	48.6	2.94	(42.8,54.3)
Mid Yukon	46	0.5	0.04	(0.4,0.4)	51	0.6	0.11	(0.4,0.5)	2	0.4	0.50	(0.0,1.8)
Up Yukon	8	0.1	0.01	(0.2,0.0)	7	0.1	0.00	(0.2,0.0)	5	1.2	0.66	(0.2,2.8)
N AK Pen	2,249	26.3	22.08	(2.2,26.3)	2,254	25.5	21.43	(2.1,25.4)	14	3.8	1.32	(1.5,6.7)
NW GOA	24	0.3	0.06	(0.4,0.1)	49	0.6	0.16	(0.6,0.2)	42	10.9	2.23	(6.9,15.6)
Copper	0	0.0	0.00	(0.1,0.0)	0	0.0	0.00	(0.1,0.0)	0	0.0	0.11	(0.0,0.3)
NE GOA	2	0.0	0.00	(0.2,0.0)	0	0.0	0.00	(0.2,0.0)	1	0.2	0.39	(0.0,1.4)
Coast SE AK	202	2.4	0.66	(1.1,2.2)	221	2.5	0.65	(1.2,2.3)	4	1.0	0.64	(0.0,2.5)
BC	1,729	20.2	16.51	(1.9,20.2)	1,847	20.9	17.01	(2.0,20.8)	85	22.1	2.25	(17.9,26.7)
West Coast US	383	4.5	3.02	(0.8,4.4)	582	6.6	4.77	(1.0,6.5)	38	9.9	1.65	(6.9,13.4)
Total Catch	8,554				8,854				384			
Region	Bering Sea Age 4 (N=384)				Bering Sea Age 5 (N=384)				Bering Sea Age 6 (N=384)			
	Est. #	Mean	SD	95% CI	Est. #	Mean	SD	95% CI	Est. #	Mean	SD	95% CI
Russia	11	1.7	0.58	(0.7,3.0)	0	0.1	0.23	(0.0,0.8)	0	0.0	0.36	(0.0,1.1)
Coast W AK	333	53.3	2.36	(48.6,57.9)	200	56.0	3.04	(49.9,61.9)	24	28.1	5.87	(17.2,40.1)
Mid Yukon	17	2.7	1.10	(0.8,5.0)	10	2.9	1.14	(1.0,5.5)	1	1.3	2.06	(0.0,7.0)
Up Yukon	8	1.3	0.81	(0.2,3.1)	27	7.7	1.61	(4.8,11.0)	6	6.6	3.17	(1.6,13.9)
N AK Pen	67	10.7	1.60	(7.8,14.0)	69	19.3	2.50	(14.6,24.3)	51	59.5	6.10	(47.3,71.1)
NW GOA	30	4.8	1.31	(2.6,7.7)	1	0.3	0.64	(0.0,2.2)	1	0.8	1.61	(0.0,5.8)
Copper	5	0.7	0.56	(0.3,2.1)	2	0.5	0.49	(0.1,1.8)	0	0.2	0.78	(0.0,2.7)
NE GOA	0	0.0	0.18	(0.0,0.6)	1	0.2	0.71	(0.0,2.6)	0	0.1	0.77	(0.0,2.6)
Coast SE AK	8	1.3	0.88	(0.0,3.3)	1	0.4	0.58	(0.0,2.0)	0	0.0	1.00	(0.0,3.5)
BC	100	16.1	1.62	(13.0,19.4)	39	10.9	1.71	(7.7,14.4)	2	1.9	1.67	(0.3,6.2)
West Coast US	46	7.3	1.05	(5.4,9.5)	7	1.9	0.72	(0.7,3.5)	1	1.5	1.41	(0.0,5.2)
Total Catch	625				357				85			

Appendix 3. -- Regional BAYES stock composition percentage estimates and estimated numbers of previous years of Chinook salmon from the Bering Sea pollock trawl fisheries. The BAYES mean estimates are also provided with standard deviations (SD), and the 95% credible intervals (CI). Sample sizes are adjacent to stratum designation. Total catch is the actual catch for that year.

2019													
Region	"A" Season (N=1499)				"B" Season (N=811)				Bering Sea all (N=2,310)				
	Est. #	Mean	SD	95% CI	Est. #	Mean	SD	95% CI	Est. #	Mean	SD	95% CI	
Russia	8	0.1	0.09	(0.0,0.3)	47	0.5	0.27	(0.1,1.1)	60	0.2	0.13	(0.1,0.6)	
Coast W AK	7,055	44.8	1.67	(41.5,48.1)	2,812	30.4	1.88	(26.8,34.1)	9,901	39.6	1.32	(37.0,42.2)	
Mid Yukon	6	0.0	0.11	(0.0,0.4)	126	1.4	0.57	(0.5,2.6)	122	0.5	0.21	(0.2,1.0)	
Up Yukon	39	0.3	0.20	(0.0,0.7)	55	0.6	0.35	(0.0,1.4)	105	0.4	0.18	(0.1,0.8)	
N AK Pen	3,420	21.7	1.50	(18.8,24.7)	32	0.4	0.48	(0.0,1.6)	3,635	14.6	1.12	(12.4,16.8)	
NW GOA	36	0.2	0.37	(0.0,1.3)	1,036	11.2	1.43	(8.5,14.1)	964	3.9	0.73	(2.5,5.4)	
Copper	3	0.0	0.07	(0.0,0.2)	17	0.2	0.25	(0.0,0.9)	10	0.0	0.09	(0.0,0.3)	
NE GOA	2	0.0	0.05	(0.0,0.1)	6	0.1	0.21	(0.0,0.7)	5	0.0	0.07	(0.0,0.2)	
Coast SE AK	318	2.0	0.55	(1.0,3.2)	264	2.9	0.75	(1.5,4.4)	550	2.2	0.43	(1.4,3.1)	
BC	3,827	24.3	1.18	(22.0,26.7)	2,392	25.9	1.60	(22.8,29.1)	6,236	25.0	0.96	(23.1,26.9)	
West Coast US	1,025	6.5	0.67	(5.3,7.9)	2,461	26.6	1.59	(23.5,29.8)	3,395	13.6	0.74	(12.2,15.1)	
Total Catch	15,738				9,246				24,984				
2018													
Region	"A" Season (N=827)				"B" Season (N=470)				Bering Sea all (N=1,297)				
	Est. #	Mean	SD	95% CI	Est. #	Mean	SD	95% CI	Est. #	Mean	SD	95% CI	
Russia	0	0.0	0.03	(0.0,0.1)	41	0.8	0.46	(0.1,1.9)	43	0.3	0.19	(0.0,0.8)	
Coast W AK	2,974	34.8	2.01	(31.0,38.8)	1,613	31.1	2.50	(26.2,36.0)	4,635	33.8	1.64	(30.6,37.0)	
Mid Yukon	36	0.4	0.51	(0.0,1.7)	65	1.3	1.14	(0.0,3.8)	62	0.5	0.51	(0.0,1.6)	
Up Yukon	69	0.8	0.38	(0.2,1.7)	55	1.1	0.79	(0.0,2.8)	122	0.9	0.31	(0.4,1.6)	
N AK Pen	2,187	25.6	1.86	(22.1,29.3)	153	2.9	1.05	(1.2,5.2)	2,395	17.5	1.29	(15.0,20.0)	
NW GOA	126	1.5	0.84	(0.1,3.3)	209	4.0	1.34	(1.8,7.0)	312	2.3	0.69	(1.1,3.8)	
Copper	2	0.0	0.06	(0.0,0.2)	26	0.5	0.37	(0.0,1.4)	33	0.2	0.16	(0.0,0.6)	
NE GOA	6	0.1	0.20	(0.0,0.6)	2	0.0	0.20	(0.0,0.5)	4	0.0	0.09	(0.0,0.3)	
Coast SE AK	279	3.3	0.79	(1.9,5.0)	273	5.3	1.66	(2.2,8.7)	509	3.7	0.70	(2.4,5.2)	
BC	2,333	27.3	1.62	(24.2,30.6)	1,715	33.0	2.56	(28.1,38.1)	4,060	29.6	1.35	(27.0,32.3)	
West Coast US	526	6.2	0.89	(4.5,8.0)	1,039	20.0	1.91	(16.4,23.9)	1,550	11.3	0.91	(9.6,13.1)	
Total Catch	8,535				5,191				13,726				
2017													
Region	"A" Season (N=1,866)				"B" Season (N=753)				Bering Sea all (N=2,619)				
	Est. #	Mean	SD	95% CI	Est. #	Mean	SD	95% CI	Est. #	Mean	SD	95% CI	
Russia	35	0.2	0.12	(0.0,0.5)	19	0.2	0.19	(0.0,0.7)	54	0.2	0.10	(0.1,0.4)	
Coast W AK	6,118	28.3	1.23	(25.9,30.8)	1,019	12.0	1.33	(9.5,14.7)	7,113	23.7	0.99	(21.7,25.6)	
Mid Yukon	136	0.6	0.26	(0.2,1.2)	29	0.3	0.33	(0.0,1.1)	162	0.5	0.21	(0.2,1.0)	
Up Yukon	156	0.7	0.27	(0.3,1.3)	1	0.0	0.04	(0.0,0.1)	162	0.5	0.20	(0.2,1.0)	
N AK Pen	4,465	20.7	1.15	(18.5,23.0)	154	1.8	0.59	(0.8,3.1)	4,490	14.9	0.87	(13.3,16.7)	
NW GOA	78	0.4	0.39	(0.0,1.4)	231	2.7	0.79	(1.3,4.4)	406	1.4	0.45	(0.6,2.3)	
Copper	2	0.0	0.04	(0.0,0.1)	10	0.1	0.18	(0.0,0.6)	3	0.0	0.03	(0.0,0.1)	
NE GOA	13	0.1	0.12	(0.0,0.4)	2	0.0	0.08	(0.0,0.2)	9	0.0	0.07	(0.0,0.3)	
Coast SE AK	691	3.2	0.54	(2.2,4.3)	575	6.8	1.24	(4.5,9.3)	1,221	4.1	0.52	(3.1,5.1)	
BC	7,609	35.2	1.18	(32.9,37.6)	3,141	37.1	2.01	(33.2,41.0)	10,812	36.0	1.03	(34.0,38.0)	
West Coast US	2,303	10.7	0.75	(9.2,12.2)	3,291	38.8	1.87	(35.2,42.5)	5,642	18.8	0.81	(17.2,20.4)	
Total Catch	21,603				8,473				30,076				
2016													
Region	"A" Season (N=1,488)				"B" Season (N=422)				Bering Sea all (N=1,910)				
	Est. #	Mean	SD	95% PI	Est. #	Mean	SD	95% PI	Est. #	Mean	SD	95% PI	
Russia	108	0.6	0.25	(0.2,1.2)	12	0.2	0.24	(0.0,0.9)	114	0.5	0.19	(0.2,1.0)	
Coast W AK	6,570	39.0	1.46	(36.2,41.9)	843	16.5	2.14	(12.5,20.8)	7,372	33.6	1.28	(31.2,36.2)	
Mid Yukon	283	1.7	0.40	(1.0,2.5)	18	0.4	0.60	(0.0,2.0)	327	1.5	0.34	(0.9,2.2)	
Up Yukon	365	2.2	0.43	(1.4,3.1)	34	0.7	0.48	(0.0,1.8)	406	1.9	0.35	(1.2,2.6)	
N AK Pen	2,839	16.9	1.17	(14.6,19.2)	56	1.1	0.72	(0.0,2.8)	2,927	13.4	0.96	(11.5,15.3)	
NW GOA	94	0.6	0.46	(0.0,1.6)	298	5.9	1.54	(3.1,9.1)	458	2.1	0.62	(1.0,3.4)	
Copper	3	0.0	0.06	(0.0,0.2)	90	1.8	0.73	(0.6,3.4)	75	0.3	0.18	(0.1,0.8)	
NE GOA	2	0.0	0.07	(0.0,0.2)	2	0.0	0.13	(0.0,0.3)	2	0.0	0.07	(0.0,0.1)	
Coast SE AK	663	3.9	0.72	(2.6,5.4)	333	6.5	1.70	(3.6,10.2)	971	4.4	0.64	(3.3,5.8)	
BC	4,394	26.1	1.26	(23.7,28.6)	1,888	37.0	2.68	(31.8,42.3)	6,312	28.8	1.14	(26.6,31.0)	
West Coast US	1,506	9.0	0.81	(7.4,10.6)	1,524	29.9	2.33	(25.4,34.5)	2,960	13.5	0.82	(11.9,15.1)	
Total Catch	16,828				5,098				21,926				

Appendix 3. -- Continued

2015													
Region	"A" Season (N=1,181)				"B" Season (N=576)				Bering Sea all (N=1,757)				
	Est. #	Mean	SD	95% CI	Est. #	Mean	SD	95% CI	Est. #	Mean	SD	95% CI	
Russia	75	0.6	0.29	(0.2,1.3)	5	0.1	0.20	(0.0,0.7)	93	0.5	0.21	(0.2,1.0)	
Coast W AK	5,644	45.9	1.87	(42.2,49.5)	1,651	27.4	2.36	(22.9,32.1)	7,256	39.6	1.60	(36.4,42.7)	
Mid Yukon	119	1.0	0.76	(0.0,2.7)	97	1.6	0.67	(0.6,3.2)	304	1.7	0.71	(0.6,3.2)	
Up Yukon	448	3.6	0.68	(2.4,5.1)	65	1.1	0.55	(0.2,2.3)	502	2.7	0.48	(1.9,3.7)	
N AK Pen	1,785	14.5	1.33	(12.0,17.2)	60	1.0	0.85	(0.0,3.0)	1,943	10.6	1.00	(8.7,12.6)	
NW GOA	349	2.8	0.82	(1.4,4.6)	496	8.2	1.95	(4.6,12.3)	724	4.0	0.83	(2.5,5.7)	
Copper	21	0.2	0.36	(0.0,1.3)	3	0.1	0.12	(0.0,0.4)	11	0.1	0.18	(0.0,0.7)	
NE GOA	2	0.0	0.10	(0.0,0.2)	4	0.1	0.22	(0.0,0.7)	4	0.0	0.11	(0.0,0.3)	
Coast SE AK	475	3.9	0.72	(2.6,5.4)	381	6.3	1.39	(3.8,9.3)	828	4.5	0.67	(3.3,5.9)	
BC	2,355	19.1	1.21	(16.8,21.6)	1,603	26.6	2.06	(22.6,30.7)	3,998	21.8	1.08	(19.7,24.0)	
West Coast US	1,030	8.4	0.84	(6.8,10.1)	1,659	27.5	1.95	(23.8,31.4)	2,665	14.5	0.88	(12.9,16.3)	
Total Catch	12,304				6,025				18,329				
2014													
Region	"A" Season (N=1,066)				"B" Season (N=319)				Bering Sea all (N=1,385)				
	Est. #	Mean	SD	95% CI	Est. #	Mean	SD	95% CI	Est. #	Mean	SD	95% CI	
Russia	74	0.6	0.26	(0.2,1.2)	13	0.4	0.50	(0.0,1.7)	96	0.6	0.23	(0.3,1.2)	
Coast W AK	6,301	54.6	2.17	(50.4,58.8)	1,109	31.8	3.09	(25.8,37.9)	7,314	48.7	1.79	(45.2,52.2)	
Mid Yukon	380	3.3	1.24	(1.2,5.9)	58	1.7	0.98	(0.1,3.9)	484	3.2	0.91	(1.5,5.1)	
Up Yukon	477	4.1	0.79	(2.7,5.8)	55	1.6	0.86	(0.3,3.6)	564	3.8	0.66	(2.6,5.1)	
N AK Pen	2,624	22.7	1.58	(19.7,25.9)	3	0.1	0.31	(0.0,1.0)	2,666	17.7	1.35	(15.2,20.4)	
NW GOA	16	0.1	0.32	(0.0,1.1)	642	18.4	2.68	(13.4,23.9)	630	4.2	1.00	(2.4,6.3)	
Copper	1	0.0	0.05	(0.0,0.1)	5	0.1	0.37	(0.0,1.3)	5	0.0	0.09	(0.0,0.3)	
NE GOA	1	0.0	0.05	(0.0,0.1)	3	0.1	0.32	(0.0,1.1)	3	0.0	0.08	(0.0,0.2)	
Coast SE AK	68	0.6	0.36	(0.0,1.4)	124	3.6	1.41	(1.3,6.7)	207	1.4	0.43	(0.6,2.3)	
BC	1,174	10.2	0.98	(8.3,12.2)	855	24.5	2.59	(19.6,29.7)	2,049	13.6	1.01	(11.7,15.7)	
West Coast US	422	3.7	0.63	(2.5,5.0)	624	17.9	2.21	(13.8,22.4)	1,013	6.7	0.76	(5.2,8.3)	
Total Catch	11,539				3,492				15,031				
2013													
Region	"A" Season (N=792)				"B" Season (N=454)				Bering Sea all (N=1,246)				
	Est. #	Mean	SD	95% CI	Est. #	Mean	SD	95% CI	Est. #	Mean	SD	95% CI	
Russia	74	0.9	0.40	(0.4,1.7)	43	0.9	0.50	(0.2,2.0)	117	0.9	0.30	(0.4,1.5)	
Coast W AK	4,135	50.2	2.20	(46.0,54.5)	2,490	51.9	2.80	(46.4,57.3)	6,530	50.1	1.80	(46.7,53.5)	
Mid Yukon	91	1.1	0.60	(0.0,2.6)	91	1.9	1.00	(0.4,4.2)	235	1.8	0.70	(0.6,3.1)	
Up Yukon	593	7.2	1.10	(5.1,9.4)	67	1.4	0.90	(0.0,3.4)	652	5.0	0.80	(3.5,6.7)	
N AK Pen	1,573	19.1	1.80	(15.7,22.8)	283	5.9	1.50	(3.4,9.0)	1,851	14.2	1.40	(11.6,17.0)	
NW GOA	41	0.5	0.70	(0.0,2.4)	331	6.9	1.80	(3.5,10.7)	443	3.4	1.00	(1.8,5.5)	
Copper	8	0.1	0.10	(0.0,0.5)	5	0.1	0.30	(0.0,0.9)	13	0.1	0.20	(0.0,0.7)	
NE GOA	0	0.0	0.10	(0.0,0.4)	0	0.0	0.20	(0.0,0.4)	0	0.0	0.10	(0.0,0.3)	
Coast SE AK	157	1.9	0.70	(0.8,3.4)	91	1.9	1.10	(0.1,4.5)	313	2.4	0.60	(1.3,3.6)	
BC	1,400	17.0	1.40	(14.2,19.8)	686	14.3	1.90	(10.8,18.2)	2,020	15.5	1.10	(13.4,17.8)	
West Coast US	165	2.0	0.60	(1.0,3.3)	710	14.8	1.70	(11.6,18.2)	873	6.7	0.80	(5.2,8.2)	
Total Catch	8,237				4,797				13,034				
2012													
Region	"A" Season (N=759)				"B" Season (N=352)				Bering Sea all (N=1,111)				
	Est. #	Mean	SD	95% CI	Est. #	Mean	SD	95% CI	Est. #	Mean	SD	95% CI	
Russia	42	0.5	0.27	(0.2,1.2)	86	2.4	0.83	(1.1,4.3)	126	1.1	0.32	(0.6,1.8)	
Coast W AK	5,266	67.8	2.22	(63.4,72.1)	1,863	52.1	2.92	(46.3,57.7)	7,152	63.1	1.83	(59.4,66.6)	
Mid Yukon	92	1.2	0.82	(0.0,3.1)	6	0.2	0.32	(0.0,1.1)	115	1.0	0.59	(0.0,2.3)	
Up Yukon	241	3.1	0.82	(1.6,4.8)	35	1.0	0.64	(0.1,2.5)	271	2.4	0.60	(1.3,3.7)	
N AK Pen	1,256	16.2	1.88	(12.7,20.0)	3	0.1	0.25	(0.0,0.8)	1,227	10.8	1.35	(8.3,13.6)	
NW GOA	19	0.2	0.35	(0.0,1.2)	135	3.8	1.44	(1.3,6.9)	155	1.4	0.73	(0.2,3.1)	
Copper	2	0.0	0.12	(0.0,0.3)	2	0.1	0.17	(0.0,0.5)	2	0.0	0.07	(0.0,0.2)	
NE GOA	6	0.1	0.26	(0.0,0.9)	2	0.1	0.20	(0.0,0.6)	6	0.1	0.17	(0.0,0.6)	
Coast SE AK	128	1.7	0.78	(0.3,3.4)	292	8.2	1.84	(4.5,11.9)	381	3.4	0.73	(2.0,4.9)	
BC	568	7.3	1.12	(5.2,9.6)	547	15.3	2.24	(11.2,20.0)	1,159	10.2	1.01	(8.3,12.3)	
West Coast US	146	1.9	0.51	(1.0,3.0)	609	17.0	2.09	(13.1,21.3)	749	6.6	0.78	(5.1,8.2)	
Total Catch	7,765				3,579				11,344				

Appendix 3. -- Continued

Region	2011				"A" Season (N=695)				"B" Season (N=1,778)				Bering Sea all (N=2,473)			
	Est. #	Mean	SD	95% CI	Est. #	Mean	SD	95% CI	Est. #	Mean	SD	95% CI				
Russia	12	0.2	0.16	(0.0,0.6)	184	1.0	0.25	(0.6,1.6)	196	0.8	0.19	(0.5,1.2)				
Coast W AK	3,856	54.0	2.28	(49.6,58.5)	13,549	73.8	1.28	(71.3,76.2)	17,421	68.3	1.16	(66.0,70.6)				
Mid Yukon	127	1.8	0.76	(0.6,3.6)	233	1.3	0.46	(0.5,2.2)	411	1.6	0.46	(0.8,2.5)				
Up Yukon	526	7.4	1.12	(5.3,9.7)	119	0.7	0.35	(0.1,1.4)	627	2.5	0.47	(1.6,3.4)				
N AK Pen	1,556	21.8	1.94	(18.1,25.7)	628	3.4	0.65	(2.2,4.8)	2,201	8.6	0.81	(7.1,10.3)				
NW GOA	41	0.6	0.60	(0.0,2.2)	654	3.6	0.89	(2.0,5.5)	663	2.6	0.67	(1.4,4.1)				
Copper	1	0.0	0.07	(0.0,0.2)	105	0.6	0.30	(0.0,1.2)	69	0.3	0.24	(0.0,0.8)				
NE GOA	1	0.0	0.09	(0.0,0.2)	26	0.1	0.24	(0.0,0.8)	13	0.1	0.12	(0.0,0.4)				
Coast SE AK	218	3.1	0.86	(1.6,4.9)	259	1.4	0.46	(0.6,2.4)	459	1.8	0.41	(1.1,2.6)				
BC	515	7.2	1.13	(5.1,9.6)	1,425	7.8	0.71	(6.4,9.2)	1,984	7.8	0.62	(6.6,9.0)				
West Coast US	283	4.0	0.78	(2.6,5.6)	1,181	6.4	0.61	(5.3,7.7)	1,461	5.7	0.49	(4.8,6.7)				
Total Catch	7,137				18,362				25,504							

Appendix 4. -- 37 SNP DNA markers represented in the Chinook salmon baseline								
Locus	Ploidy	SNPpos	Allele1	Allele2	Probe1	Probe2	Primer	Primer Conc. (uM)
Ots_AsnRS-60	2	1	T	C	TGAGTCCCTGACCAGC	AGTCCCGGACCAGC	CCGACGCCTCACTGAGT	0.16
Ots_E2-275	2	1	A	G	CCCCCATATTGCTG	CCCCACATTGCTG	GGTGCCACTTTAGTATAGCTGCTTA	0.16
Ots_ETIF1A	2	1	A	C	CAACTGAAGAAAATAATATG	CTGAAGAAAAGAATATG	TCTGAACTACCAAAGGAACACTTG	0.16
Ots_FARSLA-220	2	1	G	A	CCTTGGATGGGATGFG	CCTTGGATAGGATGFG	GTTCTGGGATTGTTCAATGTTTCAAT	0.16
Ots_FGF6A	2	1	G	T	CACGATTAGCAATGAACAA	CACGATTAGCAATGAACAA	TCAAAAATGCTATCCAACAAATACTCTGAAAAATATTG	0.16
Ots_GH2	2	1	A	T	TGACTCTCAGCA[TA]CTG	TGACTCTCTGCA[TA]CTG	GCGTACTGAGCCTGGATGACA	0.08
Ots_GPDH-338	2	1	G	A	CCACTACTTAACGTGCTTT	CCACTACTTAAACATGCTTT	CACTAAAATTCCTTATCATTTCATACTAAGTCTGAAGAA	0.32
Ots_GPH-318	2	1	C	T	ATCAAGCTGACGAAACCA	CAAGCTGACAAACCA	GGTGATAACAGGTGTGCAACCA	0.08
Ots_GST-207	2	1	C	T	ATGAGAGAGTCTTTCTCTGTT	ATGAGAGAGTCTTTTCTGTT	GGAGAACATGCATCAACCAATCAAG	0.16
Ots_GST-375	2	1	C	T	TTTCTGTAGGCGTCAGAG	TCTTGTAGGCATCAGAG	CAGCCCGTCCCAAAATCAAG	0.16
Ots_GTH2B-550	2	1	C	G	ATAACAATCTGCAGCATTA	ATAACAATGTCAGCATTA	CACAGGAAGGACGTGTTTGTATG	0.32
Ots_hnRNPL-533	2	1	A	T	CATTTACCAGTTCACACAC	TTTACCAGTTCACACAC	TCTTTGATATTGAGCTCATAAAGCAAGGT	0.16
Ots_HSP90B-100	2	1	C	T	TCTATGGTGTGATTCAAT	TTCTATGGTGTAAATCAAT	CACCTTAGTTCACGCAACATG	0.16
Ots_IGF-1.1-76	2	1	A	T	CTGCCTAGTAAATAAAATA	CTGCCTAGTAAATAAAATA	GGTAGGCCGTCAAGTGTAAATAAAGT	0.32
Ots_Ikaros-250	2	1	G	A	ACAGAAGATTTTCGGCTGC	ACAGAAGATTTTCGACTGC	GAGGCTGACTTGGACTTTGC	0.16
Ots_LEI-292	2	1	G	A	CATCATGTCCAGGCTG	ATCATGTCAAGGCTG	CACCTGAACCTCCACTGTGT	0.16
Ots_LWSop-638	2	1	T	C	TTAACAAGAAAATTATACATTC	CAAGAAAGTTATACATTC	CAATTACTCTTCTCAGCCCTGTGT	0.16
Ots_MHC1	2	1	G	A	CATCATCCCCTGAGCAG	TCATCATCCCATGAGCAG	GTCCACATCTCCAGTACATGTATGG	0.16
Ots_MHC2	2	1	T	G	CTGGAGCGTCTCTGTA	CTGGAGCGTCTCTGTA	GTCTCAGCTGGGTCAAGAG	0.16
Ots_NOD1	2	1	C	G	CCAACGCGGACTTG	CCAACGCGGACTTG	GTGCTGCAAGCAACCATGTG	0.08
Ots_P450	2	1	T	A	CCCCGAAGTACTTTT	CCCCGAAGAATTTT	TGAGCGAGATTTATCAAAGTGTCAAGA	0.32
Ots_Pr12	2	1	A	G	ATGTATTGTTCAATTAATG	TGTATTGTTGTTAATG	CCTGGTCTGTTGTTGATCAAGATG	0.16
Ots_RAG3	2	1	C	T	CTCTACAGTATGAACTATG	CTCTACAATATGAACTATG	CATTTCCACGAAAAGCCAGATGAC	0.32
Ots_RFC2-558	2	1	A	-	TGCATGTAACAAAATAACAT	TGCATGTAACATAACAT	AAGGTCTACTCCGGTGTATTGGT	0.08
Ots_S7-1	2	1	T	C	TACAGGAGATAAGGTCGCA	CAGGAGATAAGGTCGCA	TGCCATCATAAACAACCTAACAAGTAACT	0.32
Ots_SCIkF2R2-135	2	1	A	T	ATTCAAAGTCAAATTTT	ATTCAAAGTCAAATTTT	CCAAAACAGACCAGCTACTGTGT	0.16
Ots_SERPC1-209	2	1	A	T	CATTCAGCTTTTTTTC	ATTTCAGCTTTTTTTC	CTAAGTCTTCTCTGCCTAATGTGGAT	0.16
Ots_SL	2	1	A	G	TCAAAGATATGATTCAATTA	AAGATATGGTCAATTA	AATATTGGCTTCTGAGAATGCATTTGG	0.16
Ots_SWS1op-182	2	1	T	A	ATGTAATTTAACGATTCATTT	ATGTAATTTAACGATTCATTT	TCAAAGACATCGAACACAAGAACGA	0.32
Ots_TAPBP	2	1	C	T	CAGCTGCCAGTCTG	CAGTGTGCCAGTCTG	TTTCTCATCCTTCTCTCTCCAGTCT	0.08
Ots_Tnsf	2	1	A	G	TGCTCCAGATCTC	TGCTCCAGGCTC	GCCAAACGGGTCTGAACTGT	0.16
Ots_u202-161	2	1	T	A	AGCTAGTGCTTAGCAGCTA[AC]	AGCTAGTGCTTAGCAGCTA[AC]	CACTTTTGACTTTACATGGAACCTAACTCAT	0.32
Ots_u211-85	2	1	C	T	TCCCAAAGTCGAGTGTG	CCCAAAGTCAAGTGTG	TGGTGAGAGCAGCTTTAAATGTCTT	0.16
Ots_U212-158	2	1	G	A	CTGGAAAGAGGCTC	CTGGAAAAGGCTC	CCCCATATGAGACGCTACAGTAATG	0.16
Ots_u4-92	2	1	T	C	CTGTGTTGAATTTAACATAAT	TCTGTGTTGAATTTAACGTAAT	ATCCAAGGAGCCCAATTAAGATTT	0.16
Ots_u6-75	2	1	C	T	TTAGTCAACTGTGTTTTT	TTAGTCAACTGTATTTTTT	GAAAAAGTAAAGTAAAGTAAAGTATTATACCACTAAAGACAAT	0.32
Ots_zP3b-215	2	1	G	T	CCAAATATCCTACCCGTGATG	CAAAATATCCTACCAAGTATG	TGCTGAGGACCATCTGCAATTC	0.16



U.S. Secretary of Commerce

Gina M. Raimondo

Under Secretary of Commerce for
Oceans and Atmosphere

Dr. Richard W. Spinrad

Assistant Administrator, National Marine
Fisheries Service. Also serving as
Acting Assistant
Secretary of Commerce for Oceans
and Atmosphere, and Deputy NOAA
Administrator

Janet Coit

August 2022

www.nmfs.noaa.gov

OFFICIAL BUSINESS

**National Marine
Fisheries Service**

Alaska Fisheries Science Center
7600 Sand Point Way N.E.
Seattle, WA 98115-6349

Review of Salmon Bycatch in the Pacific Region 2022/23 Groundfish Trawl Fishery and Preliminary Results of an Enhanced Monitoring Program

Cory R. Lagasse, Kathryn A. Fraser, Rob Houtman, Erik Grundmann,
Nicholas Komick, Michael O'Brien, Emily Braithwaite, A. Maria Cornthwaite

Fisheries and Oceans Canada
Pacific Biological Station
3190 Hammond Bay Rd
Nanaimo, BC V9T 6N7

2024

**Canadian Manuscript Report of
Fisheries and Aquatic Sciences 3273**



Fisheries and Oceans
Canada

Pêches et Océans
Canada

Canada

Canadian Manuscript Report of Fisheries and Aquatic Sciences

Manuscript reports contain scientific and technical information that contributes to existing knowledge but which deals with national or regional problems. Distribution is restricted to institutions or individuals located in particular regions of Canada. However, no restriction is placed on subject matter, and the series reflects the broad interests and policies of Fisheries and Oceans Canada, namely, fisheries and aquatic sciences.

Manuscript reports may be cited as full publications. The correct citation appears above the abstract of each report. Each report is abstracted in the data base *Aquatic Sciences and Fisheries Abstracts*.

Manuscript reports are produced regionally but are numbered nationally. Requests for individual reports will be filled by the issuing establishment listed on the front cover and title page.

Numbers 1-900 in this series were issued as Manuscript Reports (Biological Series) of the Biological Board of Canada, and subsequent to 1937 when the name of the Board was changed by Act of Parliament, as Manuscript Reports (Biological Series) of the Fisheries Research Board of Canada. Numbers 1426 - 1550 were issued as Department of Fisheries and Environment, Fisheries and Marine Service Manuscript Reports. The current series name was changed with report number 1551.

Rapport manuscrit canadien des sciences halieutiques et aquatiques

Les rapports manuscrits contiennent des renseignements scientifiques et techniques qui constituent une contribution aux connaissances actuelles, mais qui traitent de problèmes nationaux ou régionaux. La distribution en est limitée aux organismes et aux personnes de régions particulières du Canada. Il n'y a aucune restriction quant au sujet; de fait, la série reflète la vaste gamme des intérêts et des politiques de Pêches et Océans Canada, c'est-à-dire les sciences halieutiques et aquatiques.

Les rapports manuscrits peuvent être cités comme des publications à part entière. Le titre exact figure au-dessus du résumé de chaque rapport. Les rapports manuscrits sont résumés dans la base de données *Résumés des sciences aquatiques et halieutiques*.

Les rapports manuscrits sont produits à l'échelon régional, mais numérotés à l'échelon national. Les demandes de rapports seront satisfaites par l'établissement auteur dont le nom figure sur la couverture et la page du titre.

Les numéros 1 à 900 de cette série ont été publiés à titre de Manuscrits (série biologique) de l'Office de biologie du Canada, et après le changement de la désignation de cet organisme par décret du Parlement, en 1937, ont été classés comme Manuscrits (série biologique) de l'Office des recherches sur les pêcheries du Canada. Les numéros 901 à 1425 ont été publiés à titre de Rapports manuscrits de l'Office des recherches sur les pêcheries du Canada. Les numéros 1426 à 1550 sont parus à titre de Rapports manuscrits du Service des pêches et de la mer, ministère des Pêches et de l'Environnement. Le nom actuel de la série a été établi lors de la parution du numéro 1551.

Canadian Manuscript Report of
Fisheries and Aquatic Sciences 3273

2024

Review of Salmon Bycatch in the Pacific Region 2022/23 Groundfish Trawl Fishery and
Preliminary Results of an Enhanced Monitoring Program

Cory R. Lagasse, Kathryn A. Fraser, Rob Houtman, Erik Grundmann, Nicholas Komick,
Michael O'Brien, Emily Braithwaite, A. Maria Cornthwaite

Fisheries and Oceans Canada
Pacific Biological Station
3190 Hammond Bay Rd
Nanaimo, BC
V9T 6N7

© His Majesty the King in Right of Canada, as represented by the Minister of the
Department of Fisheries and Oceans, 2024.
Cat. No. Fs97-4/3273E-PDF ISBN 978-0-660-69095-7 ISSN 1488-5387

Correct Citation for this publication:

Lagasse, C.R., Fraser, K.A., Houtman, R., Grundmann, E., Komick, N., O'Brien, M., Braithwaite, E., Cornthwaite, A. M. 2024. Review of Salmon Bycatch in the Pacific Region 2022/23 Groundfish Trawl Fishery and Preliminary Results of an Enhanced Monitoring Program. Can. Manuscr. Rep. Fish. Aquat. Sci. 3273: v + 35 p.

TABLE OF CONTENTS

Introduction	1
Methods.....	1
Salmon Bycatch Monitoring and Sampling.....	1
Catch Data Analysis.....	3
Coded Wire Tag and Stock Composition Analysis.....	4
CWT Analysis.....	5
Stock Composition Analysis	5
Results.....	6
Salmon Catch	6
Coded Wire Tag and Stock Composition Results	7
Discussion.....	9
Acknowledgements.....	11
References	12
Tables	13
Appendix A - 2022/23 Option A Groundfish Trawl Fleet Enhanced Salmon Monitoring, Bycatch Reporting & Biological Sampling Program Requirements	23
Appendix B - DFO Option A Trawl Salmon Head Sampling Instructions for Vessels Landing Catch Frozen25	
Appendix C - Table and map of Regions for defining catch strata.....	27
Appendix D - CWT Exploitation Rate Indicator Stocks used in Exploitation Rate Analysis.....	29
Appendix E - SMU-CU-Reporting Units Tables.....	32
Appendix F - Salmon catch by Pacific Fishery Management Area for 2022	35

ABSTRACT

Lagasse, C.R., Fraser, K.A., Houtman, R., Grundmann, E., Komick, N., O'Brien, M., Braithwaite, E., Cornthwaite, A. M. 2024. Review of Salmon Bycatch in the Pacific Region 2022/23 Groundfish Trawl Fishery and Preliminary Results of an Enhanced Monitoring Program. Can. Manuscr. Rep. Fish. Aquat. Sci. 3273: v + 35 p.

The Pacific Region groundfish trawl fishery is one of the largest fisheries in British Columbia by catch volume and value, operating throughout the year with all fishing trips subject to at-sea electronic monitoring and independent validation of landings via a dockside monitoring program. An enhanced monitoring and sampling program for salmon bycatch was initiated for all Option A trawl licence holders on September 26, 2022 to improve the accuracy of estimates of salmon catch by species and collect coded wire tag (CWT) and stock composition information to assess potential impacts on Chinook salmon (*Oncorhynchus tshawytscha*) stocks of concern. This report summarizes estimates of Pacific salmon bycatch in the groundfish trawl fishery since 2008, with a focus on the 2022/23 fishery. Catch of Pacific salmon in the 2022/23 fishery was the highest recorded since 2008 with a total catch of 28,117 Pacific salmon, including 26,273 Chinook salmon. Most of this catch occurred during the enhanced monitoring period from September 26, 2022 to February 20, 2023, with 15,234 Chinook salmon sampled during this period for CWT analysis and estimation of stock composition. The enhanced monitoring program will continue to be implemented through the 2023/24 fishery with additional results described in future reports.

RÉSUMÉ

Lagasse, C.R., Fraser, K.A., Houtman, R., Grundmann, E., Komick, N., O'Brien, M., Braithwaite, E., Cornthwaite, A. M. 2024. Review of Salmon Bycatch in the Pacific Region 2022/23 Groundfish Trawl Fishery and Preliminary Results of an Enhanced Monitoring Program. Can. Manuscr. Rep. Fish. Aquat. Sci. 3273: v + 35 p.

Les pêches au chalut des poissons de fond dans la Région du Pacifique est l'une des plus importantes pêcheries de la Colombie-Britannique en termes de volume et de valeur des prises, opérant tout au long de l'année avec toutes les sorties de pêche étant soumises à une surveillance électronique en mer et à une validation indépendante des débarquements via un programme de surveillance à quai. Pour améliorer l'exactitude des estimations des prises de saumon par espèce et recueillir des données sur la composition des stocks afin d'évaluer les impacts potentiels sur les stocks préoccupants de saumon quinnat (*Oncorhynchus tshawytscha*), un programme amélioré de surveillance et d'échantillonnage des prises de saumon a été lancé pour tous les titulaires de permis de chalutage de l'option A le 26 septembre 2022. Ce rapport résume les estimations des prises de saumon du Pacifique dans la pêche au chalut du poisson de fond depuis 2008, en mettant l'accent sur la pêche de 2022-23. Les prises de saumon du Pacifique dans la pêche de 2022-2023 ont été les plus élevées enregistrées depuis 2008 avec une capture totale de 28 117 saumons du Pacifique, dont 26 273 saumons quinnat. La plupart de ces prises ont eu lieu pendant la période de surveillance accrue du 26 septembre 2022 au 20 février 2023, avec 15 234 saumons quinnat échantillonnés au cours de cette période pour l'analyse étiquette de fil codée (CWT) et l'estimation de la composition du stock. Le programme de surveillance améliorée continuera d'être mis en œuvre tout au long de la pêche de 2023-2024 et une période de données plus longue sera décrite dans les prochains rapports.

INTRODUCTION

The Pacific Region groundfish trawl fishery is one of the largest fisheries in British Columbia by catch volume and value, operating year-round using either mid-water or bottom trawl gear to target various flatfish, rockfish, and other groundfish species. The fishery consists of approximately 45 active vessels that are managed under an individual transferable quota / individual vessel quota system with each vessel individually accountable for their catch (Fisheries and Oceans Canada 2023a). Management of the fishery is informed by a comprehensive catch monitoring program with all fishing trips requiring logbook records and independent validation via at-sea electronic monitoring (EM) and a dockside monitoring program (DMP).

Recent estimates from catch monitoring data in the groundfish trawl fishery indicated that thousands of Pacific salmon (*Oncorhynchus spp.*) were being caught on an annual basis, with most bycatch occurring using mid-water trawl gear and Chinook salmon (*Oncorhynchus tshawytscha*) the main species of salmon being caught. While existing monitoring programs in the trawl fishery provide comprehensive estimates of catch weights of groundfish species, they were not targeted towards accurate estimation of salmon piece counts by species or assessment of potential impacts on stocks of concern. Over the past decades, there have been widespread declines for many stocks of Chinook salmon, and a growing number of populations are now assessed as at risk by the Committee on the Status of Endangered Wildlife in Canada (COSEWIC 2018, 2020), and designated as stocks of concern by DFO (Fisheries and Oceans Canada 2023b). In salmon-directed fisheries, monitoring programs require the collection of samples for genetic analysis and coded wire tag (CWT) recovery to estimate stock composition and impacts on stocks of concern. This information supports the assessment of fisheries management objectives for stocks of concern, including for Fraser Chinook stocks (Dobson et al. 2020).

Beginning in 2021, DFO engaged with industry representatives and monitoring service providers to review monitoring procedures and develop an enhanced monitoring and sampling program for salmon bycatch. The program was initiated on September 26, 2022, and is ongoing during the 2023/24 fishery. This report summarizes estimates of bycatch of Pacific salmon in the groundfish trawl fishery since 2008, with a focus on the 2022/23 groundfish fishing year, which began on February 21, 2022, and ended on February 20, 2023. Preliminary results from the enhanced monitoring program are also provided including CWT and stock composition analysis.

METHODS

Salmon Bycatch Monitoring and Sampling

Monitoring requirements for the groundfish trawl fishery are detailed in Appendix 8 of the Groundfish Integrated Fisheries Management Plan (Fisheries and Oceans Canada 2023a). This section provides a brief overview of monitoring requirements with a focus on changes to catch monitoring and sampling of Pacific salmon that occurred during the 2022/23 groundfish trawl fishery for Option A licence holders (see Table 1). Groundfish trawl license holders may choose one of two license options at the beginning of each fishing year that determines allowable fishing locations and gear type: Option B vessels must fish exclusively within PFMA 12 to 20 and 29 using bottom trawl gear, while Option A vessels may fish in all other areas and inside PFMA 12 to 20 and 29 using mid-water trawls only. Option A licences represents approximately 40 of the 45 active commercial groundfish trawl licences and the only licence type permitted to use mid-

water trawl gear, and thus this licence type was the focus for changes to monitoring and sampling of Pacific salmon.

Commercial groundfish trawl catch is monitored and reported using a combination of fisher logbooks, independent at-sea EM auditing, and DMP validation of landed catch. While at sea, all vessels must keep accurate records of fishing activities in an electronic fishing logbook while ensuring that the at-sea EM systems are fully operational. EM system requirements are specified by DFO and include video cameras, global positioning systems (GPS), and hydraulic sensors. EM information is used to verify the accuracy of information recorded in fisher logbooks via audits of a random subset of tows from each trip. If fisher reported information does not meet accuracy requirements, logbook data may be replaced by EM results and additional audits conducted. Prior to March 2020, independent at-sea monitoring requirements for Option A trips were fulfilled by the at-sea observer program (ASOP), with the exception of trips targeting Pacific hake using midwater trawl gear and landing fresh product; however, the ASOP has been suspended since the Covid pandemic. At the end of each fishing trip, landed catch must be independently validated by the DMP during offload to ensure accurate catch weights for each species.

Prior to implementation of the enhanced monitoring program, there were no requirements for monitoring Pacific salmon in the groundfish trawl fishery, other than the requirements that apply to all species encountered in the fishery. As a prohibited species, Pacific salmon were not allowed to be targeted and were required to be released at-sea if caught. Therefore, available estimates of Pacific salmon catch were based on fisher logbook information, with DMP validation only when Pacific salmon were landed incidentally. Before March 2020, the ASOP provided independent monitoring of retained and released catch of Pacific salmon as described above. In addition, opportunistic at-sea or shoreside biological sampling, including the retention of heads from adipose clipped Chinook and Coho and the recording of lengths and weights, occurred as a lower priority to other groundfish catch monitoring duties.

A review of monitoring procedures beginning in 2021 led to the development of an enhanced monitoring program for salmon bycatch that revised retention and monitoring requirements in order to provide more accurate estimates of bycatch counts by species and collect CWT and genetic samples. The enhanced monitoring program was developed collaboratively with representatives from DFO Pacific Region Science and Fisheries Management, the groundfish trawl industry, the David Suzuki Foundation, and monitoring service providers from Archipelago Marine Research Ltd. and J.O. Thomas and Associates Ltd. In consideration of information needs for assessment and management, the following four objectives were used to guide development of the program:

1. Accurately estimate fishery catch counts (pieces) of fish of each Pacific salmon species;
2. Ensure sufficiently precise and representative CWT sampling to quantify the fishery mortality for Chinook CWT exploitation rate indicator stocks;
3. Use genetic stock identification to identify the stock composition of Chinook catch, including for populations that do not have CWT exploitation rate indicator stocks; and
4. Estimate the spatial and temporal distribution of Chinook catch to determine when and where mortality on stocks of concern may be occurring.

Objectives 2 to 4 were focused on Chinook salmon as these were the most prevalent salmon bycatch species, and where potential impacts on stocks of concern were considered most likely. Coho salmon were also sampled for CWTs and DNA, but represented a much smaller portion of salmon catch. The program was targeted towards all Option A trawl vessels, but did not include trawl vessels fishing under Option B,

which represent a smaller component of the fishery and do not capture significant amounts of salmon bycatch because they are not permitted to fish using mid-water trawl gear.

The changes to retention and sampling requirements were implemented via scientific licences under Section 52 of the Fisheries (General) Regulations (1993). Scientific licences were issued to all Option A Groundfish trawl vessels authorizing the retention of salmon to enable independent validation of catch numbers by species and collection of DNA and CWTs. Changing to mandatory retention was not expected to significantly increase mortality from trawl bycatch; although there are no established mortality rates for salmon released at-sea caught with trawl gear, all species entering a receiving tank vessel (those landing catch frozen) have a 100% mortality rate applied and it was assumed that most salmon do not survive being caught in a trawl net regardless of retention status. The sale, trade, or personal use of any retained salmon remained prohibited in the licence requirements.

Most Option A trawl vessels land catch fresh and whole, while a few vessels are fitted to process and freeze landed catch at sea. Different catch retention requirements and sampling procedures were developed for vessels landing catch fresh versus frozen to achieve monitoring objectives (see Appendix A for a detailed description of requirements). For vessels landing fresh catch, all Pacific salmon were required to be retained and landed whole, where they would be subject to DMP validation of catch numbers and weight by species on all trips. 25% of trips were also targeted for collection of Chinook and Coho salmon heads by the dockside observer, with sampling of trips randomly selected after vessel hail-in. A target of 25% was chosen to correspond with the 20% standard sampling rate to recover CWT indicator stocks in salmon-directed fisheries, plus a 5% buffer for potential implementation error.

For vessels landing frozen catch, which consisted of six active licence holders in the 2022/23 groundfish Option A trawl fishery, scientific licences required the retention of heads only in recognition of the limited freezer space available for storage of non-marketable fish. Vessels were responsible for retaining heads, including gills and collars, and bagging and labelling them on all trips according to instructions provided by DFO (Appendix B). The requirements specified that salmon heads from each tow should be bagged and labelled separately so that samples could be matched to tow information such as location and date. At the end of each trip, heads were to be packaged in larger trip bags and received by the DMP. The 100% sampling rate was chosen to ensure representative sampling of the small number of vessels that were able to fish over long periods and wide areas.

After landing, salmon head bags were collected and labelled by dockside observers to allow the bags to be traced back to the trip, placed in cold storage, and shipped to the sampling service provider, J.O. Thomas and Associates Ltd. Every head was identified to species, counted, and checked for the presence of a CWT using specialized electronic detection equipment. CWTs were recovered from all heads that scanned positive. DNA tissue samples were initially collected from the operculum and then later changed to cheek tissue to improve success rates of DNA amplification for genetic analysis.

Catch Data Analysis

Summaries of salmon catch information presented in this report are based on commercial groundfish trawl catch monitoring data, with adjustment of salmon catch using information from the enhanced monitoring program beginning on September 26, 2022. Commercial groundfish fisher log, ASOP, and DMP data are housed in the Fishery Operations Systems (FOS) database, DFO's centralized repository for commercial fishery data in the Pacific Region. DFO Pacific Science maintains a 'Groundfish views of FOS' (GFFOS) database that restructures the data for convenient access for Groundfish scientists.

During the standard monitoring period, prior to September 26, 2022, estimates of salmon bycatch were compiled from the GFFOS Official Catch table, which summarizes the best available data for each fishing event (i.e. trawl tow) using fisher logbook, ASOP, and DMP sources. Landed catch for each tow is calculated by prorating the DMP landed catch at trip offload over the retained catch from logbook and ASOP sources, such that landed catch for a species added across all tows for a trip will equal the DMP landed catch for that trip. If there are DMP records for a species that is not recorded in ASOP or fisher logbook data for a trip, it will be associated with the trip but not assigned to a specific tow, and therefore catch location and other data may be unavailable. Since 2020, ASOP data has been based on fisher reported information that is corrected using EM data where the audit reveals consistent differences between EM and fisher reported catches.

For the enhanced monitoring period, from September 26, 2022 onward, different methods for determining best estimates of salmon catch by species were applied for landed fresh catch versus frozen catch corresponding with the different collection methods and sampling requirements. For vessels landing catch fresh, salmon catch was compiled from the GFFOS Official Catch table and based upon DMP validation of landed catch. DMP validation occurred on all retained fresh salmon catch due to new retention requirements, whereas during the standard monitoring period only salmon retained incidentally would have been validated by the DMP. For the subset of trips where DMP collected Chinook and Coho salmon heads, the DMP counts of catch by species at offload were compared to counts of salmon heads by species conducted by J.O. Thomas to confirm accuracy.

For vessels landing catch frozen during the enhanced monitoring period, salmon catch estimates were derived from lab counts of salmon heads identified to species and matched to trips and tows. If salmon heads were unable to be matched to tows using label information, salmon catch was estimated from lab counts over the entire trip and not associated at the tow level, analogous to the method for applying DMP validation of landed catch. Salmon catch from logbooks in GFFOS were not used to estimate salmon catch by species, however, they provided information on tows where salmon catch occurred for trips with missing label information.

The location of salmon catch was determined for individual tows or across a trip using logbook information. Salmon heads that could be matched to specific tows were assigned to PFMA from the GFFOS Official Catch table based on tow start and end locations. For salmon heads that could not be matched to a specific tow, including most catch landed fresh and unlabeled catch landed frozen, catch locations were inferred for broader regions based on the locations of all tows within a trip. Regions consisted of geographic groupings of PFMA (e.g. West Coast Vancouver Island South) and were identified based upon fishing patterns by catch type and areas of salmon encounters (see Appendix C for correspondence between Regions, PFMA, and groundfish management areas). Where logbook records of species catch by tow occurred within the same Region throughout a trip, all salmon catch from that trip was assigned to the Region. Using this method, almost all salmon catch during the 2022/23 groundfish trawl fishery could be assigned to a Region, with only a small proportion of catch remaining in an “unassigned” category.

Coded Wire Tag and Stock Composition Analysis

A key component of the enhanced monitoring program was the collection of CWTs and DNA tissue from Chinook salmon to estimate recoveries of CWT exploitation rate indicator stocks and estimate stock composition. To develop these estimates, salmon bycatch in the trawl fishery was divided into catch strata that represented different fishing areas, catch type, and time periods. More specifically, each catch

stratum consisted of a combination of Region, whether catch was landed fresh or frozen, and whether catch occurred from September 26 to December 31, 2022, or from January 1 to February 20, 2023. CWT Analysis relied on CWT recoveries from all head samples, while stock composition analysis used CWT recoveries and DNA.

CWT Analysis

CWTs are tiny lengths of metal wire inscribed with a numeric code that are implanted in the snout of groups of Chinook and Coho salmon juveniles before their ocean migration. When recovered, read with a microscope and associated with CWT release data, CWTs accurately identify the stock of origin, brood year, and other associated rearing information of the CWT release group. The Chinook Technical Committee (CTC) of the Pacific Salmon Commission uses CWTs to perform an annual exploitation rate analysis (CTC 1988), and currently monitors 45 Chinook CWT exploitation rate indicator stocks within Canada and the US (see Appendix D for geographic locations, stock acronyms, and full stock names). Recovery of CWT indicator stocks in salmon-directed fisheries and escapement is used to assess survival, maturation rates, exploitation, and fishery mortality rates in Canada and United States fisheries, as required under Chapter 3 of the Pacific Salmon Treaty and reported on annually (e.g. CTC 2023).

To estimate total CWT recoveries for Canadian Chinook CWT exploitation rate indicator stocks, the CWTs recovered were expanded by the inverse of the sample rate within each catch stratum. Sample rates corresponded to the number of Chinook salmon heads collected and scanned for CWTs, divided by the total Chinook salmon catch in each catch stratum. Total CWT recoveries are reported separately by 2022 and 2023 calendar years for consistency with CWT recovery estimates developed by the CTC for Canadian salmon-directed fisheries.

CWT analytical methods and stock information presented in this report were created from the Mark Recovery Program Information System (MRPIS). MRPIS is maintained by Salmon Stock Assessment and is DFO's centralized repository for salmon coded wire tag data in the Pacific Region.

Stock Composition Analysis

Stock composition of Chinook salmon catch in each stratum was estimated using both CWT and genetic methods to identify fish to population or conservation unit of origin, which were rolled up to the stock management unit (SMU) level for reporting (see Appendix E for SMU assignment tables). CWT recoveries can determine the stock of origin to high accuracy and resolution; however, they cannot be used to determine stock composition for hatchery or wild fish that do not have CWTs. Therefore, for fish that did not contain a CWT, DNA tissue samples were analyzed to determine stock of origin using parentage-based tagging (PBT) and genetic stock identification (GSI) assignment methods.

GSI assignment matches genetic markers to baselines collected from spawning grounds to identify the population of origin for wild or hatchery fish, while PBT assignment matches hatchery produced fish back to their parents, allowing determination of the hatchery of origin and age of sampled fish (Beacham et al. 2018). PBT analysis can only be conducted for populations in which all hatchery brood stock is genotyped, and therefore can only be applied to fish produced in Canadian hatcheries that have PBT programs in place. PBT results provide better accuracy than GSI and were used instead of GSI to determine stock of origin where available, with the combined application of both methods denoted by PBT-GSI.

To determine stock composition of Chinook salmon catch, each stratum was partitioned into fish containing CWTs and fish that did not contain CWTs, and separate stock proportions for each partition were calculated using CWT and genetic (PBT-GSI) stock assignments respectively. The overall stock

composition estimate for each catch stratum was calculated by weighting each set of stock proportions according to their respective catch. The CWT partition represented the proportion of catch estimated to have CWTs and was equal to the number of CWTs recovered divided by the number of heads scanned for CWTs within each catch stratum. The PBT-GSI partition consisted of all Chinook salmon estimated to not have CWTs within the catch strata, and was calculated as the remaining proportion of catch after subtracting the CWT partition. The sample rate for the PBT-GSI partition was the number of PBT-GSI samples successfully analyzed divided by the estimated catch without CWTs within each catch stratum, while the sample rate for the CWT partition was equal to the number of heads scanned for CWTs divided by the total catch.

In addition to stock identification, results from the PBT analysis provided information on brood year composition, which can be used to calculate salmon age by subtracting the year a fish was caught from the brood year. Chinook salmon from the 2020 brood year would represent age 2 fish if caught in 2022 and age 3 fish if caught in 2023. While CWTs can also provide brood year information, most Canadian CWT indicator stocks from the 2019 brood year were not tagged due to the Covid pandemic. Therefore, brood year compositions based upon CWTs are not reported due to expected bias.

RESULTS

Salmon Catch

Catch of Pacific salmon was estimated from the standard monitoring program beginning in 2008, the first full year where data are stored in the Fishery Operations System (FOS) database, up until September 25, 2022, while catch between September 26, 2022 to February 20, 2023 was estimated from the enhanced monitoring program procedures. Annual totals of salmon bycatch by species, numbers of fishing trips, tows using mid-water gear type, and total landed catch weights are summarized by groundfish fishing year from 2008/09 to 2022/23 in Table 2. Annual salmon bycatch by calendar year from 2008 to 2022 are summarized in Table 3. Monthly catch of salmon by species for the 2022/23 fishery is provided in Table 4. Table 5 provides salmon catch by species for the 2022/23 fishery within each Region, catch type, and time period strata (for catch by PFMA in the 2022 calendar year see Appendix F). Key catch results are summarized below:

- Estimated bycatch of Pacific salmon in the groundfish trawl fishery for the 2022/23 groundfish fishing year was the highest recorded among recent years with a total catch of 28,117 salmon (Table 2). The second highest fishing year was 2020/21 with a total catch of 12,354 salmon.
- Chinook salmon was the primary salmon species caught in the 2022/23 groundfish fishing year with an estimated catch of 26,273, representing 93% of total salmon catch. Chinook salmon represent greater than 80% of Pacific salmon bycatch in most groundfish fishing years from 2008/09 to 2022/23.
- Estimated catch of other salmon species caught in the 2022/23 groundfish fishing year was 625 Coho salmon, 1097 Chum salmon, 18 Pink Salmon, and 42 Sockeye salmon. There were 123 salmon that were reported as Pacific salmon and trout that could not be identified to species either by fisher or independent monitoring programs.
- Most salmon bycatch in the 2022/23 groundfish fishing year occurred during the enhanced monitoring period, with 18,867 salmon caught between September 26, 2022 and February 20,

2023. The highest monthly catch occurred in October and February, with 8,268 and 3,272 salmon caught in these months respectively (Table 4).

- The Regions with the highest salmon catch in 2022/23 were Queen Charlotte and Johnstone Strait with 12,176 salmon caught, followed by WCVI South with 10,428 salmon, and Strait of Georgia with 3,264 salmon (Table 5). There were only 540 salmon caught in the North Coast Region, while 1,065 salmon were caught in the WCVI North Region. 644 salmon were unassigned and could not be associated to a specific Region.
- There were 6 active licences for vessels landing frozen catch in 2022/23 that caught 74% of salmon in the trawl fishery, corresponding to 20,745 salmon pieces including 19,026 Chinook salmon. All of the 12,176 salmon caught in the Queen Charlotte and Johnstone Strait Region were landed frozen catch, while the remaining landed frozen catch of salmon mostly occurred in the WCVI South Region where 7,135 salmon were caught by these vessels.
- For vessels landing fresh catch, 3,293 pieces or 45% of this salmon catch in 2022/23 occurred in the southern West Coast Vancouver Island Region, while 3,264 pieces or 44% of salmon catch occurred in the Strait of Georgia.
- 96% of salmon were caught using midwater trawl gear during the 2022/23 fishery. 26,907 salmon were caught in tows with midwater trawl gear as the reported gear type, while 807 salmon were caught with bottom trawl gear. 403 salmon were caught with an unspecified or unavailable gear type.
- There were 847 unique trawl fishing trips and 3,424 tows with mid-water trawl gear that occurred in the 2022/23 groundfish fishing year (Table 2). This was lower than the annual average from 2008/09 to 2022/23 of 1,316 trips and 3,699 mid-water tows. Total landed catch of Pacific Hake (*Merluccius productus*) in 2022/23 was among the lowest in the time series at 38,560,000 kg compared to the average of 66,402,000 kg; however, landed catch of Walleye Pollock (*Gadus chalcogrammus*) was the highest in the time series at 9,412,000 kg compared to the average of 4,945,000 kg.
- Salmon catch was concentrated within a small proportion of trawl fishing trips and tows. Out of the 847 trips in the 2022/23 groundfish fishery, the 10 trips with the highest salmon catch caught 15,145 salmon, or 54% of the total salmon catch. Out of the 3,424 tows using mid-water trawl gear in 2022/23, 42 tows caught more than 100 salmon, while no salmon catch was recorded in 2,616 or 76% of tows.

Coded Wire Tag and Stock Composition Results

Estimates of the catch of Canadian exploitation rate indicator stocks and stock composition for Chinook salmon cover the enhanced monitoring period from September 26, 2022 to February 20, 2023. Although this period represents less than 5 months of sample collection, it coincided with the period of highest salmon bycatch in recent years within the groundfish trawl fishery, with a total of 15,642 Chinook salmon heads collected.

Every Chinook salmon head collected was scanned for CWTs, yielding 2,051 CWTs from Canadian and US tagging projects, and 298 CWTs from Canadian exploitation rate indicator stocks. More than 35% of catch

was sampled from all catch strata, except in the WCVI North, WCVI South, and North Coast Regions where smaller catches occurred. There were 1,913 DNA samples that were successfully analyzed for PBT-GSI among sampled Chinook salmon without CWTs, out of which 362 were identified to stock of origin by PBT and 1,555 were identified by GSI. PBT-GSI sample sizes and sample rates varied considerably and not all catch strata were sufficiently represented to accurately estimate stock composition, particularly those catch strata occurring in the WCVI North and WCVI South Regions where sample rates were 2% or less.

The number of Chinook salmon sampled, numbers and proportions of CWTs, and sample rates for CWT and PBT-GSI are summarized by catch strata in Table 6. Estimates of total CWT recoveries of Canadian exploitation rate indicator stocks are provided in Table 7, including a comparison to 2022 estimates of CWT indicator stock recoveries in Canadian marine salmon-directed fisheries. Stock composition estimates using combined CWT and PBT-GSI stock assignments are provided for southern BC Chinook salmon SMUs in Table 8 and for northern BC SMUs in Table 9. The brood year composition of PBT samples is summarized by catch strata in Table 10.

Key observations from CWT and genetic analysis are as follows:

- The highest estimated CWT recoveries for Canadian exploitation rate indicator stocks were from Chilliwack, Harrison, and Cowichan stocks, with estimates of 76.1, 40.5, and 37.6 respectively during the 2022 calendar year (Table 7). By comparison, total estimated CWT recoveries for the 2022 calendar year from Canadian salmon-directed fisheries in marine areas was 178.1, 87.8, and 276.6 for Chilliwack, Harrison, and Cowichan stocks respectively. Comparisons between estimated CWT recoveries in fisheries are based on CWT sampling over the entire year in salmon-directed fisheries, while trawl CWT sampling occurred from September 26 to December 31, 2022 and has not been expanded to represent catch prior to the enhanced monitoring period.
- Other Canadian exploitation rate indicator stocks in trawl samples included Big Qualicum River, Nicola River, Robertson Creek, Puntledge River, and Quinsam River. Estimated CWT recoveries of the US Samish River indicator stock, included as a proxy for Boundary Bay Chinook, was 63.1 in 2022. There were no CWT recoveries of the Similkameen River stock, which is used as a proxy for Canadian Okanagan Chinook. Proxies were used to provide an indication of potential fisheries catch for Boundary Bay and Canadian Okanagan Chinook because there is no Canadian indicator stock for these populations (Dionne et al. 2023, Matylewich et al. 2019).
- The stock composition of Chinook salmon represented by Canadian-origin stocks, as estimated based upon combined CWT and PBT-GSI information, varied from 21% to 83% among catch strata. The highest proportions of Canadian-origin stocks were estimated in the Strait of Georgia Region, with estimates of 82% to 83%. In the Queen Charlotte & Johnstone Strait Region, where the largest amount of Chinook salmon catch occurred, the Canadian proportion was estimated at 37% for bycatch occurring between September 26 to December 31, 2022, and 60% for bycatch occurring between January 1 to February 20, 2023.
- Most of the Canadian-origin Chinook salmon catch originated from the Fraser Fall 4(1), Lower Georgia Strait, and Middle Georgia Strait SMUs according to stock composition estimates (Table 8). Fraser Fall 4(1), which includes Chilliwack and Harrison Chinook CUs, was the highest proportion of catch among Canadian SMUs, representing 21% to 51% of Chinook catch within the Queen Charlotte & Johnstone Strait and Strait of Georgia Regions. Stocks of concern that

were represented by smaller proportions in some catch strata included Fraser Spring 4(2), Fraser Spring 5(2), Fraser Summer 5(2), and WCVI Chinook. Central Coast, Skeena, and Nass were the only northern BC SMUs detected and represented a much smaller proportion of the catch than southern BC SMUs (Table 9).

- Most Canadian-origin Chinook salmon that could be assigned to brood year using PBT belonged to the 2020 brood year, which represented 69% of the 141 PBT observations from catch occurring between September 26 and December 31, 2022 and 91% of the 226 PBT observations from catch occurring between January 1 and February 20, 2023 (Table 10).

DISCUSSION

This report summarizes estimates of salmon bycatch in the groundfish trawl fishery since 2008, with a focus on estimates for the 2022/23 fishery and results from an enhanced monitoring program that was implemented beginning on September 26, 2022. As this is a new monitoring program, the results may be subject to change and further revisions. There are also several sources of uncertainty and limitations that should be considered when interpreting results.

Known sources of uncertainty and limitations in the results include:

- Catch counts (pieces) for salmon may be incomplete or lower accuracy prior to the enhanced monitoring program. Catch weight by species is the primary metric for quota management and catch reporting used in the groundfish trawl fishery, however, piece counts of fish are used throughout this report as they are the metric used to manage salmon-directed fisheries. Salmon piece counts of released catch were not subject to DMP, auditing, or verification of species, except by the ASOP prior to March 2020.
- Estimates of CWT recoveries of Canadian Chinook indicator stocks (Table 7) do not include fish from the 2019 brood year for most stocks because they were not tagged with CWTs due to the Covid pandemic. Estimates may therefore be lower than would otherwise have occurred if CWT tagging had included the 2019 brood year. For exploitation rate analysis, the Chinook Technical Committee has developed infilling methods to compensate for this missing information using the long time series of CWT data (CTC 2023); however, this was not possible for the trawl fishery.
- Estimates of CWT recoveries of Chinook indicators are provided irrespective of age and have not been adjusted into adult equivalent mortalities according to models developed and applied by the CTC when reporting on CWT-based exploitation rates in salmon-directed fisheries (see CTC 2019, page 9). By adjusting fishery catches into adult equivalent mortality based on age and stock, CTC models are intended to more accurately represent the numbers of fish of a given age that would, in the absence of fishing, leave the ocean and return to terminal areas to spawn. Available information from PBT brood year assignments (Table 10), while limited in its representation of the fishery, suggests that most Chinook salmon caught in the trawl fishery during the enhanced monitoring period were from the 2020 brood year or 2-3 year olds. This is younger than most Chinook salmon catch in salmon-directed fisheries and therefore catch numbers in trawl and salmon fisheries may not be directly comparable in terms of adult equivalent mortality.

- Estimates of CWT recoveries of Chinook indicators and stock composition only represent the enhanced monitoring period occurring in the final 5 months of the 2022/23 groundfish fishery year. Fishing activity in the trawl fishery changes throughout the season and across years in response to various factors, therefore, the results should not be considered representative of the entire fishery or other years. Stock and age composition may also vary considerably between years and during the year as a result of changing distributions and abundances of Chinook salmon populations.
- Stock proportions of Chinook salmon SMUs (Table 8 and 9) are derived from PBT-GSI results that have low sample rates for some catch strata, particularly for bycatch occurring in October and November 2022 and in WCVI Regions.
- During the first few months of the enhanced monitoring program, PBT-GSI analysis had low success rates because DNA tissue collected from the operculum was inadequate quality. As a result, sampling rates were lower for PBT-GSI stock assignments at the beginning of the enhanced monitoring program. DNA sampling protocols were revised to collect samples from cheek tissue for the remainder of the program, resulting in improved rates for successful PBT-GSI analysis.

Despite potential sources of uncertainty, monitoring data shows that bycatch of Pacific salmon in the groundfish trawl fishery were the highest on record during the 2022/23 fishery, as estimated using a combination of standard and enhanced monitoring procedures. Most bycatch occurred around the southern West Coast Vancouver Island and the Queen Charlotte & Johnstone Strait Regions during a small number of fishing trips, primarily from vessels landing frozen catch. Most salmon were caught using mid-water trawl gear, with less than 4% of salmon caught when using bottom trawl gear. Many of these mid-water trawl tows with salmon bycatch targeted Pacific Hake and Walleye Pollock, though detailed information on target species associated with salmon bycatch was not examined.

There are many factors that may influence the prevalence and distribution of salmon bycatch in the trawl fishery. An analysis of these factors and the spatiotemporal dynamics of salmon encounters was not included in this report; however, information on total landed catch of groundfish species and the number of fishing trips and mid-water tows suggest that overall fishing activity in the 2022/23 groundfish fishing year did not increase compared to previous years, with the exception of landed catch of Walleye Pollock. Further analyses could explore the use of spatiotemporal models as a forecasting tool to predict Chinook salmon bycatch associations with target species, locations, depths, times, and other fishing characteristics (e.g. Shirk et al. 2023).

Stock composition estimates and recoveries of CWT indicators during the enhanced monitoring period indicate that the Fraser Fall 4(1) SMU is the largest proportion of catch among Canadian-origin stocks, followed by Lower Georgia Strait and Middle Georgia Strait SMUs. Due to sampling gaps and the limited time series represented by these results, stock composition estimates were not applied to Chinook salmon catch to calculate catches by SMU or determine exploitation rate indices, as has been applied to salmon-directed fisheries to assess achievement of fisheries management objectives for Fraser Chinook stocks of concern (Dobson et al. 2020); however, estimates of total CWT recoveries are provided for Canadian exploitation rate indicator stocks to compare with marine salmon-directed fisheries, albeit with some limitations and differences. These comparisons show that estimates of CWT indicators in the groundfish

trawl fishery for Chilliwack and Harrison River Chinook between September 26 to December 31, 2022 were more than 40% of CWT recoveries from salmon-directed fisheries in Canadian marine waters in 2022. Relative proportions between groundfish trawl catch and marine salmon-directed fisheries were variable for other indicator stocks, and these comparisons do not include estimates of CWT recoveries that occur in freshwater or terminal fisheries.

Implementation of the enhanced monitoring program will continue through the 2023/24 Option A groundfish trawl fishery and mandatory retention requirements to collect head samples have been ongoing since the program was initiated. Results from the enhanced monitoring program that include 2023/24 will be described in future reports. Additional monitoring information will support more comprehensive assessments of groundfish trawl fishery bycatch of Chinook salmon stocks of concern compared to the limited time series represented in this report.

ACKNOWLEDGEMENTS

Development and implementation of the groundfish trawl salmon bycatch enhanced monitoring program has been a collaborative initiative that benefited greatly from the expertise and contributions of Brian Mose from the Groundfish Trawl Industry, Bruce Turriss from the Canadian Groundfish Research and Conservation Society, Doug Tallman and Sylvia Chow from JO Thomas and Associates Ltd, Scott Buchanan from Archipelago Marine Research Ltd, and Deirdre Finn, Rob Tadey, Lindsay Richardson-Deranger, Trevor Ruelle, Mike Hawkshaw, Chuck Parken, and Rachel Rickaby from DFO. Thanks to Malcolm Wyeth, Norm Olsen and Jonathan Faris for their work developing and maintaining the GFFOS database. We would also like to acknowledge the work accomplished by those that collected data and samples for the enhanced monitoring program, including dockside observers with Archipelago Marine Research, fisheries and lab technicians with JO Thomas and Associates Ltd, and fishers in the groundfish trawl industry. Funding for the enhanced monitoring program was provided by DFO via the Harvest Transformation Pillar of the Pacific Salmon Strategy Initiative. The David Suzuki Foundation also provided funding to support a pilot program to test sampling procedures prior to fleetwide program implementation.

REFERENCES

- Beacham, T.D., Wallace, C., Macconnachie, C., Jonsen, K., McIntosh, B., Candy, J.R., and Withler, R.E. 2018. Population and individual identification of Chinook salmon in British Columbia through parentage-based tagging and genetic stock identification with single nucleotide polymorphisms. *Can. J. Fish. Aquat. Sci.* **75**(7): 1096–1105. doi:10.1139/cjfas-2017-0168.
- COSEWIC. 2018. COSEWIC assessment and status report on the Chinook Salmon *Oncorhynchus tshawytscha*, Designatable Units in Southern British Columbia (Part One - Designatable Units with no or low levels of artificial releases in the last 12 years), in Canada. *In* Committee on the Status of Endangered Wildlife in Canada, Ottawa. Available from <https://www.canada.ca/en/environment-climate-change/services/species-risk-public-registry.html>.
- COSEWIC. 2020. COSEWIC assessment and status report on the Chinook Salmon *Oncorhynchus tshawytscha*, Designatable Units in Southern British Columbia (Part Two – Designatable Units with High Levels of Artificial Releases in the Last 12 Years), in Canada. *In* Committee on the Status of Endangered Wildlife in Canada, Ottawa. Available from <https://www.canada.ca/en/environment-climate-change/services/species-risk-public-registry.html>.
- CTC (Chinook Technical Committee). 1988. 1987 Annual Report. Pacific Salmon Commission Joint Chinook Technical Committee Report TCCHINOOK (88)-2. Vancouver, BC.
- CTC (Chinook Technical Committee). 2019. 2018 Exploitation Rate Analysis and Model Calibration, Volume One. Pacific Salmon Commission Joint Chinook Technical Committee Report TCCHINOOK (19)-02. Vancouver, BC.
- CTC (Chinook Technical Committee). 2023. 2022 Exploitation Rate Analysis. Pacific Salmon Commission Joint Chinook Technical Committee Report TCCHINOOK (23)-01. Vancouver, BC.
- Dionne, K., Rachinski, T., Parken, C., Weir, L., Doutaz, D., Ritchie, L., Bailey, R., Jenewein, B., Miller-Saunders, K., Labelle, M., Manson, M., Welch, P., Trouton, N., Mozin, P., and Walsh, M. 2023. Recovery Potential Assessment for Southern British Columbian Chinook Populations, Fraser and Southern Mainland Chinook Designatable Units (1, 6, 13 and 15). DFO Can. Sci. Advis. Sec. Res. Doc. 2023/042. xvii + 291 p.
- Dobson, D., Holt, K., and Davis, B. 2020. A Technical Review of the Management Approach for Stream-Type Fraser River Chinook. DFO Can. Sci. Advis. Sec. Res. Doc: x +281 pp.
- Fisheries and Oceans Canada. 2023a. Groundfish Integrated Fisheries Management Plan 2023/24.
- Fisheries and Oceans Canada. 2023b. Southern Salmon Integrated Fisheries Management Plan 2023/24.
- Fishery (General) Regulations*, SOR/93-53.
- Matylewich, M., M. Oatman, C. Parken, B. Riddell, B. Tweit, H. Wright, C. Baldwin, T. Garrison, R. Lothrop, and E. McGrath. 2019. A Summary of Okanagan Chinook Information Requested by the Pacific Salmon Commission. Pacific Salmon Comm. Tech. Rep. No. 42: 89 p.
- Shirk, P.L., Richerson, K., Banks, M., and Tuttle, V. 2023. Predicting bycatch of Chinook salmon in the Pacific hake fishery using spatiotemporal models. *ICES J. Mar. Sci.* **80**(1): 133–144. Oxford Academic. doi:10.1093/ICESJMS/FSAC219.

TABLES

Table 1 – Summary of salmon bycatch monitoring and sampling requirements in the Option A groundfish trawl fishery for the standard and enhanced monitoring periods.

		Standard Monitoring Period	Enhanced Monitoring Period
Time period		<ul style="list-style-type: none"> All catch monitoring results prior to September 26, 2022 	<ul style="list-style-type: none"> September 26, 2022 to February 20, 2023, ongoing as of report publication
Retention requirements by catch type	Vessels landing fresh catch	<ul style="list-style-type: none"> Retention of salmon prohibited 	<ul style="list-style-type: none"> 100% retention of entire salmon to enable accurate enumeration and sampling
	Vessels landing frozen catch	<ul style="list-style-type: none"> Retention of salmon prohibited 	<ul style="list-style-type: none"> 100% retention of salmon heads only, vessels responsible for cutting and bagging heads
Species identification and counts	Vessels landing fresh catch	<ul style="list-style-type: none"> Fisher logbook reporting of at-sea released salmon catch ASOP catch monitoring up until March 2020 DMP counts of any landed salmon by species 	<ul style="list-style-type: none"> Fisher logbook reporting of counts and weights of retained salmon catch. DMP counts and weights of all landed salmon catch by species 25% of trips randomly selected for collection of Chinook and Coho salmon heads by DMP Lab: Counts and speciation of all salmon heads
	Vessels landing frozen catch	<ul style="list-style-type: none"> Fisher logbook reporting of at-sea released salmon catch ASOP catch monitoring up until March 2020 DMP counts of any landed salmon by species 	<ul style="list-style-type: none"> Fisher logbook reporting of counts and weights of at-sea retained salmon catch with EM auditing 100% of trips targeted for collection of salmon heads (all species) Lab: Counts and speciation of all salmon heads
Coded wire tag sampling	Vessels landing fresh catch	<ul style="list-style-type: none"> No random/representative requirement for sampling of CWTs ASOP opportunistic sampling of CWTs 	<ul style="list-style-type: none"> 25% of trips randomly selected for collection of Chinook and Coho salmon heads at offload Lab: All heads sampled for CWTs
	Vessels landing frozen catch	<ul style="list-style-type: none"> No random/representative requirement for sampling of CWTs ASOP opportunistic sampling of CWTs 	<ul style="list-style-type: none"> 100% of trips targeted for collection of salmon heads, bagged and labelled by tow Lab: All heads sampled for CWTs.
DNA sampling	Vessels landing fresh catch	<ul style="list-style-type: none"> No requirements for DNA sampling 	<ul style="list-style-type: none"> Lab: All heads sampled for DNA; Sub-sample of Chinook salmon heads selected for genetic analysis
	Vessels landing frozen catch	<ul style="list-style-type: none"> No requirements for DNA sampling 	<ul style="list-style-type: none"> Lab: All heads sampled for DNA; Sub-sample of Chinook salmon heads selected for genetic analysis

Table 2 – Summary of annual coastwide salmon catch (numbers of fish retained and released) by species, number of fishing trips, tows with mid-water gear type, and landed catches (kg) in the groundfish trawl fishery reported by groundfish fishing year (February 21 of the starting year to February 20 of the subsequent year). Unidentified salmon catch was reported as Pacific salmon and trout and represents salmonids that could not be identified to species either by fisher or independent monitoring programs.

Groundfish fishing year	All salmon (# of fish)	Chinook (# of fish)	Coho (# of fish)	Chum (# of fish)	Pink (# of fish)	Sockeye (# of fish)	Unidentified salmon (# of fish)	# of trawl trips	# of mid-water tows	Total landed catch (kg)	Landed catch Pacific Hake (kg)	Landed catch Walleye Pollock (kg)
2008/09	3,470	3,121	56	195	19	0	79	1,882	4,029	103,600,000	73,800,000	1,606,000
2009/10	9,611	8,628	95	191	566	32	99	1,586	2,967	85,280,000	55,780,000	3,570,000
2010/11	7,364	6,973	62	185	44	21	79	1,537	3,333	85,760,000	56,020,000	3,706,000
2011/12	11,193	9,808	242	457	328	22	336	1,534	3,500	90,780,000	55,400,000	3,866,000
2012/13	8,062	7,119	418	253	25	18	229	1,369	3,286	81,190,000	46,910,000	5,807,000
2013/14	4,813	3,034	292	218	700	16	553	1,395	3,415	90,790,000	54,060,000	4,063,000
2014/15	7,668	6,641	234	240	125	23	405	1,151	2,671	79,640,000	37,440,000	7,006,000
2015/16	7,645	6,319	193	794	122	80	137	1,049	2,673	80,470,000	45,420,000	3,984,000
2016/17	3,510	2,469	403	296	21	28	293	1,268	3,454	109,800,000	74,610,000	2,340,000
2017/18	8,265	7,320	113	394	157	39	242	1,374	3,988	124,300,000	90,780,000	3,363,000
2018/19	8,886	8,290	123	284	46	16	127	1,403	4,741	133,200,000	102,400,000	3,275,000
2019/20	7,680	6,776	199	294	80	59	272	1,304	5,063	132,200,000	98,830,000	7,587,000
2020/21	12,354	11,848	27	197	30	2	250	1,141	5,030	127,300,000	102,100,000	6,006,000
2021/22	11,627	9,635	695	708	572	17	0	907	3,912	98,350,000	63,930,000	8,588,000
2022/23	28,117	26,273	625	1,097	18	42	123	847	3,424	74,710,000	38,560,000	9,412,000

Table 3 – Estimated annual coastwide salmon catch (numbers of fish retained and released) by species in the groundfish trawl fishery reported by calendar year.

Calendar year	Total salmon catch	Chinook catch	Coho catch	Chum catch	Pink catch	Sockeye catch	Unidentified salmon catch
2008	3,209	2,871	26	191	19	0	102
2009	9,646	8,666	121	178	566	32	83
2010	7,582	7,097	65	205	44	20	151
2011	11,081	9,753	242	456	325	23	282
2012	8,299	7,404	378	254	28	18	217
2013	4,681	2,898	289	212	701	14	567
2014	7,299	6,303	247	244	121	24	360
2015	8,171	6,731	211	795	119	81	234
2016	3,157	2,211	400	290	28	28	200
2017	6,839	5,944	129	394	93	39	240
2018	9,218	8,514	119	288	85	16	196
2019	7,828	6,945	146	292	96	55	294
2020	10,002	9,442	83	178	39	6	254
2021	14,270	12,255	697	729	572	17	0
2022	24,457	22,624	613	1,101	16	42	122

Table 4 – Coastwide monthly catch by salmon species (numbers of fish retained and released) in the groundfish trawl fishery for the 2022/23 Groundfish Fishing Year (February 21, 2022 to February 20, 2023). The number of salmon heads collected represents heads that were counted and identified to species by independent lab verification as part of the enhanced monitoring program, and are included in monthly catches by species.

Month	Total salmon catch	# salmon heads collected	Chinook catch	Coho catch	Chum catch	Pink catch	Sockeye catch	Steelhead catch	Unidentified salmon catch
Feb 21 – Feb 28	67	0	67	0	0	0	0	0	0
Mar	514	0	514	0	0	0	0	0	0
Apr	267	0	189	13	61	1	3	0	0
May	1,117	0	1,044	7	66	0	0	0	0
Jun	495	0	464	2	29	0	0	0	0
Jul	1,978	0	1,963	6	3	4	0	0	2
Aug	2,704	0	2,053	547	90	1	13	0	0
Sep	2,227	1	2,029	33	53	9	25	0	78
Oct	8,268	7,129	7,518	4	767	1	0	0	39
Nov	2,625	2,124	2,594	1	27	0	1	0	2
Dec	2,827	2,556	2,825	0	1	0	0	0	1
Jan	1,756	1,585	1,755	1	0	0	0	0	0
Feb 1- Feb 20	3,272	3,057	3,258	11	0	2	0	0	1

Table 5 – Total salmon catch (numbers of fish retained and released) by species, Region (see Appendix C for included PFMA) and catch type for the 2022/23 groundfish fishery year (February 21, 2022 to February 20, 2023). Catch in the Unassigned Region could not be associated to a single geographic Region.

Region	Catch type	Total salmon catch	Total heads sampled	Chinook catch	Coho catch	Chum catch	Pink catch	Sockeye catch	Unidentified salmon catch
North Coast	FRESH	87	4	44	15	20	5	3	0
	FROZEN	453	346	427	11	8	1	0	6
QC & JSt Strait	FRESH	0	0	0	0	0	0	0	0
	FROZEN	12,176	11,987	11,649	4	513	2	25	3
Strait of Georgia	FRESH	3,264	1,162	3,220	4	40	0	0	0
	FROZEN	0	0	0	0	0	0	0	0
WCVI NORTH	FRESH	360	2	355	1	0	0	0	4
	FROZEN	705	393	383	27	309	0	1	11
WCVI SOUTH	FRESH	3,293	105	3,280	12	1	0	0	0
	FROZEN	7,135	1,965	6,299	550	179	10	13	99
Unassigned	FRESH	368	216	348	1	19	0	0	0
	FROZEN	276	272	268	0	8	0	0	0
TOTAL	FRESH	7,372	1,489	7,247	33	80	5	3	4
	FROZEN	20,745	14,963	19,026	592	1,017	13	39	119
TOTAL		28,117	16,452	26,273	625	1,097	18	42	123

Table 6 – Summary of Chinook catch (numbers of fish), sample sizes of CWTs and PBT-GSI, and sample rates for CWT and stock composition analysis in the Groundfish Trawl Fishery during the enhanced monitoring period (September 26, 2022 to February 20, 2023). The CWT sample rate is equal to the proportion of Chinook catch that had heads collected and scanned for CWTs, while the CWT Partition is the proportion of heads that contained CWTs from those that were scanned. The PBT-GSI partition is the remaining fraction without CWTs where stock composition is estimated from PBT-GSI samples. The PBT-GSI partition sample rate is the proportion of Chinook catch without CWTs that have been analyzed using PBT-GSI, while the CWT partition sample rate is the same as the CWT sample rate.

Time period	Region	Catch type	Chinook catch (# of fish)	Chinook sampled (# heads collected)	CWT Analysis			Stock Composition Analysis			
					CWT Sample Rate	# CWTs recovered	# Indicator CWTs from Canadian Stocks	CWT Partition	PBT-GSI Partition	# PBT-GSI analyzed	PBT-GSI Partition Sample Rate
Sep 26 – Dec 31 2022	North Coast	FRESH	23	2	9%	0	0	0.0%	100.0%	0	0%
		FROZEN	342	339	99%	67	1	19.8%	80.2%	38	14%
	QC & JSt Strait	FROZEN	7212	7212	100%	1088	116	15.1%	84.9%	306	5%
	Strait of Georgia	FRESH	2606	1037	40%	95	17	9.2%	90.8%	315	13%
		FROZEN	178	0	0%	0	0				
	WCVI North	FRESH	178	0	0%	0	0				
		FROZEN	193	190	98%	28	1	14.7%	85.3%	47	29%
	WCVI South	FRESH	271	96	35%	5	0	5.2%	94.8%	5	2%
FROZEN		1941	1941	100%	203	15	10.5%	89.5%	18	1%	
Jan 1 - Feb 20 2023	North Coast	FRESH	0	0		0	0				
		FROZEN	2	0	0%	0	0			0	
	QC & JSt Strait	FROZEN	4287	4287	100%	558	144	13.0%	87.0%	1068	29%
	Strait of Georgia	FRESH	247	120	49%	6	4	5.0%	95.0%	111	47%
		FROZEN	43	2	5%	0	0	0.0%	100.0%	0	0%
	WCVI North	FRESH	43	2	5%	0	0				
		FROZEN	0	0		0	0			0	
	WCVI South	FRESH	332	7	2%	1	0	14.3%	85.7%	5	2%
FROZEN		1	1	100%	0	0			0		

Table 7 – Estimates of CWT recoveries of Canadian exploitation rate indicator stocks in the Groundfish Trawl Fishery during the enhanced monitoring period (September 26, 2022 to February 20, 2023). The CWT sample rate is equal to the proportion of Chinook catch that had heads collected and scanned for CWTs for each combination of Region, catch type and calendar year. Regions without any CWTs recovered from indicator stocks are excluded from the table. Estimates of CWT recoveries of indicator stocks for 2022 salmon-directed fisheries in BC marine waters are provided for comparative purposes. For consistency with trawl estimates, estimates for salmon-directed fisheries do not include incidental mortality, do not represent adult equivalents, and have not been infilled to compensate for missing observations on 2019 brood years due to lack of tagging. These estimates may therefore differ from numbers reported in PSC Chinook Technical Committee reports.

Canadian CWT stock codes are as follows: CHI = Chilliwack River; HAR = Harrison River; BQR = Big Qualicum River; COW = Cowichan River; NIC = Nicola River; RBT = Robertson Creek; PPS = Puntledge River; QUI = Quinsam River

Time Period	Region	Catch Type	CWT Sample Rate	CHI	HAR	BQR	COW	NIC	RBT	PPS	QUI	SAM ¹	SMK ²
Sep 26 - Dec 31 2022	North Coast	FROZEN	99%	1	0	0	0	0	0	0	0	3	0
	QC & JSt Strait	FROZEN	100%	57	31	12	14	1	1	0	0	36	0
	Strait of Georgia	FRESH	40%	10.1	2.5	5	22.6	2.5	0	0	0	15.1	0
	WCVI North	FROZEN	98%	1	0	0	0	0	0	0	0	1	0
	WCVI South	FROZEN	100%	7	7	0	1	0	0	0	0	8	0
	TOTAL				76.1	40.5	17	37.6	3.5	1	0	0	63.1
Estimated CWT recoveries in 2022 BC marine salmon-directed fisheries retained catch				178.1	87.8	7.2	276.6	21.5	2609	5.1	275.3	412.8	87.9
Jan 1 – Feb 20 2023	QC & JSt Strait	FROZEN	100%	56	73	5	7	1	0	1	1	10	0
	Strait of Georgia	FRESH	49%	2.1	4.1	0	2.1	0	0	0	0	0	0
	TOTAL				58.1	77.1	5	9.1	1	0	1	1	10

¹ SAM = Samish River is a US stock and has been included as a proxy for Boundary Bay Chinook

² SMK = Similkameen River is a US stock and has been included as a proxy for Okanagan Summer Chinook

Table 8 – Stock composition for Southern BC Canadian stock management units of Chinook salmon during the enhanced monitoring period (September 26, 2022 to February 20, 2023) across Region, catch type, and time period strata. Stock proportions are estimated using weighted proportions from CWT and PBT-GSI samples, with CWT stock proportions applied to fish with CWTs and PBT-GSI proportions applied to the remaining subset of fish without CWTs. Stock composition estimates from strata with less than 5% CWT or PBT-GSI sample rates have not been estimated due to low sample sizes.

Time period	Region	Catch type	Chinook catch (# of fish)	% Canadian origin	Fraser Fall 4(1)	Fraser Sum. 4(1)	Fraser Sum. 5(2)	Fraser Spring 4(2)	Fraser Spring 5(2)	Lower Georgia Strait	Middle Georgia Strait	Upper Georgia Strait	WCVI	SC Mainland Inlet
Sep 26 - Dec 31 2022	North Coast	FRESH	23											
		FROZEN	342	23.5%	6.6%	2.1%	2.1%	0.0%	0.0%	2.1%	4.2%	0.0%	4.2%	0.0%
	QC & JSt Strait	FROZEN	7212	36.9%	21.4%	0.0%	0.0%	0.0%	0.6%	4.4%	10.2%	0.3%	0.0%	0.0%
	Strait of Georgia	FRESH	2606	82.2%	49.5%	0.0%	0.0%	0.4%	0.3%	17.6%	13.5%	0.4%	0.0%	0.3%
	WCVI North	FRESH	178											
		FROZEN	193	36.8%	27.7%	0.0%	1.8%	0.0%	0.0%	3.6%	3.6%	0.0%	0.0%	0.0%
	WCVI South	FRESH	271											
		FROZEN	1941											
Jan 1 – Feb 20 2023	QC & JSt Strait	FROZEN	4287	60.2%	51.1%	0.0%	0.0%	0.0%	0.0%	2.6%	5.6%	0.1%	0.2%	0.3%
	Strait of Georgia	FRESH	247	82.8%	41.4%	0.0%	0.0%	0.0%	0.0%	17.2%	22.5%	0.0%	0.0%	0.0%
	WCVI North	FRESH	43											
	WCVI South	FRESH	332											

Table 9 - Stock composition for Northern BC Canadian stock management units of Chinook salmon during the enhanced monitoring period (September 26, 2022 to February 20, 2023) across Region, catch type, and time period strata. Stock proportions are estimated using weighted proportions from CWT and PBT-GSI samples, with CWT stock proportions applied to fish with CWTs and PBT-GSI proportions applied to the remaining subset of fish without CWTs. Stock composition estimates from strata with less than 5% CWT or PBT-GSI sample rates have not been estimated due to low sample sizes.

Time period	Region	Catch type	Chinook Catch (# of fish)	% Canadian origin	Central Coast	Skeena	Nass
Sep 26 - Dec 31 2022	North Coast	FRESH	23				
		FROZEN	342	23.5%	0.0%	2.1%	0.0%
	QC & JSt Strait	FROZEN	7212	36.9%	0.0%	0.0%	0.0%
	Strait of Georgia	FRESH	2606	82.2%	0.0%	0.0%	0.0%
	WCVI North	FRESH	178				
		FROZEN	193	36.8%	0.0%	0.0%	0.0%
WCVI South	FRESH	271					
	FROZEN	1941					
Jan 1 – Feb 20 2023	QC & JSt Strait	FROZEN	4287	60.2%	0.1%	0.1%	0.1%
	Strait of Georgia	FRESH	247	82.8%	0.0%	0.0%	0.0%
	WCVI North	FRESH	43				
	WCVI South	FRESH	332				

Table 10 – Brood year composition of Canadian-origin Chinook salmon samples based on parentage-based tags (PBTs) collected during the enhanced monitoring period from September 26, 2022 to February 20, 2023. Regions not shown did not contain any PBT samples. Salmon age may be calculated by subtracting the year a fish was caught from the brood year.

Time period	Region	# PBT	2018 brood year (# of Chinook)	2019 brood year (# of Chinook)	2020 brood year (# of Chinook)	% 2018 brood year	% 2019 brood year	% 2020 brood year
Sep 26 - Dec 31 2022	North Coast	6	0	2	4	0%	33%	67%
	QC & JSt Strait	47	0	3	44	0%	6%	94%
	Strait of Georgia	85	1	37	47	1%	44%	55%
	WCVI North	3	0	1	2	0%	33%	67%
	TOTAL	141	1	43	97	1%	30%	69%
Jan 1 – Feb 20 2023	QC & JSt Strait	192	0	8	184	0%	4%	96%
	Strait of Georgia	29	1	11	17	3%	38%	59%
	TOTAL	221	1	20	200	1%	17%	82%

Appendix A - 2022/23 Option A Groundfish Trawl Fleet Enhanced Salmon Monitoring, Bycatch Reporting & Biological Sampling Program Requirements

Introduction

Aug 30, 2022

Program requirements were developed by DFO in consultation with the Groundfish Trawl Salmon Bycatch Technical Working Group with representatives from the GTAC, and dockside monitoring service providers. **The requirements apply to all salmon bycatch, including steelhead.**

A pilot program for the groundfish trawl fleet was conducted on the F/V Pacific Legacy No. 1 between September 2021 and February 2022. Lessons learned from the pilot have informed sampling procedures and further development of the monitoring program.

Separate requirements have been developed for Receiving Tank Vessels (RTVs) that freeze product at sea and vessels that land fresh product.

Vessels Freezing Catch at Sea

Vessel Requirements

For all trips:

1. For each tow,
 - a. Remove the heads from **all salmon bycatch according to sampling instructions**. Do not mix heads from separate tows.
 - b. Package all heads into bags.
 - c. Using TOW bag labels in sequence, record the vessel name, **packing date and time**, and tow # (if known) **using pencil**, on a TOW bag label.
 - d. Put a completed TOW bag label into **each** bag of heads and seal with a zip tie.
 - e. In the at-sea observer logbook, record the total estimated retained pieces and weights of all salmon by species. If species cannot be determined, record as “salmonids (106)”.
2. Freeze salmon heads in tow bags until delivery.
3. Transfer all frozen samples in tow bags to the dockside monitor at the end of the offload.

Sampling kits will be provided by the dockside monitor and will contain:

- Detailed sampling instructions, including salmon head cut requirements
- Bags for samples and zip ties
- TOW bag labels and pencils

Throughout the season, more supplies will be available from the dockside monitor. Please verify sufficient supply as part of your pre-departure checklist.

AMR Dockside Monitor Procedures

For all landings:

1. Receive all tow bags containing heads from the vessel.
2. Ask the vessel crew if they need a resupply of any items they are running low on.
3. Fill in the Groundfish Salmon Head DMP form using pencil.

4. Pack all tow bags containing salmon heads into larger trip bags to consolidate the samples. If the vessel used large bags for tows there is no need to consolidate the tow bags, but each tow bag will need to be labelled with a TRIP bag label.
5. Record essential information for the landing on TRIP bag labels **using pencil**.
6. Close all trip bags and attach a TRIP bag label **to each bag** using zip ties.
7. Create a record of each bag of salmon heads in the “tagged fish” form of the Trawler dockside monitor application noting the hail number and TRIP bag label number.
8. Coordinate cold storage and direct shipment of trip bags to the CWT lab in Vancouver or to DFO’s Pacific Biological Station in Nanaimo.

Vessels Landing Fresh Product

Vessel Requirements

For all trips:

1. Retain all salmon bycatch.
2. In the at-sea observer logbook, record the total estimated retained pieces and weights of all salmon by species. If species cannot be determined, record as “salmonids (106)”.
3. All salmon retained must be landed at the conclusion of each trip.

AMR Dockside Monitor Procedures

Dockside Monitors will be responsible for the collection of salmon heads from 25% of the landings. The dockside monitoring data management system will be used to randomly select vessels and notify dockside monitors which landings require salmon head sampling.

For all landings:

1. In the trawler platform, record the pieces and weights of all salmon by species.

For landings randomly selected for salmon head sampling:

1. Remove the heads from all Chinook and Coho salmon.
2. Package salmon heads into bags.
3. Using TRIP bag labels in sequence, record essential information for the landing on TRIP bag labels **using pencil**.
4. Take a digital photo of the first TRIP bag label used and the last TRIP bag label used to associate the TRIP label series used to the hail number.
5. Close all trip bags and attach a TRIP bag label **to each bag** of heads using zip ties.
6. Fill in the Groundfish Salmon Head DMP form using pencil.
7. Create a record of each bag of salmon heads in the “tagged fish” form of the Trawler dockside monitor application noting the hail number and TRIP bag label number.
8. Coordinate storage or direct shipment of trip bags to the CWT lab in Vancouver or to DFO’s Pacific Biological Station in Nanaimo.
9. Send all salmon bodies to offal after heads have been removed.

For landings not selected for salmon head sampling, send all salmon to offal.

Appendix B - DFO Option A Trawl Salmon Head Sampling Instructions for Vessels Landing Catch Frozen



Fisheries and Oceans Canada / Pêches et Océans Canada



Option A Trawl RTV Salmon Head Sampling Instructions (for Receiving Tank Vessels that freeze their product at sea)

According to the scientific licence conditions, all Option A Trawl Receiving Tank Vessels *that freeze their product at sea* are required to remove and retain heads from all salmon caught as bycatch prior to landing. The bags and labels provided with these instructions must be used to store these heads.


1. Remove the heads from **all salmon species** with a straight cut running square to the lateral line, at least 1 cm behind the operculum, and include the gills and pectoral fins.



2. Heads must be packed by the tow in which they were caught. Do not mix heads from separate tows.
3. Use as many bags as needed for storing heads from a given tow. Three sizes of bags are provided so that you can choose the appropriate sized bag for the quantity of heads being packed – do not overfill medium and large bags as they may break during handling or transport.

Large Bags	18 x 30 inches	Leave approx. 12 inches (30 cm) of space at top before closing
Medium Bags	14 x 24 inches	Leave approx. 8 inches (20 cm) of space at top before closing
Small Bags	12 x 18 inches	Leave enough space at top to securely zip-tie

4. Every bag must have a completed tow bag label inside. Fill out a tow bag label: record the vessel name, tow number (if known), and packing date and time on the label. Put the label inside the tow bag, then close the bag securely with a zip tie.

SALMON HEAD <i>TOW</i> BAG LABEL			GROUND FISH										
(Instructions on back)													
Vessel Name: _____	Tow#: _____	Unknown: <input type="checkbox"/>	<div style="display: flex; align-items: center; justify-content: center;"> <div style="writing-mode: vertical-rl; transform: rotate(180deg); font-size: 8px; margin-right: 5px;">Lab Use</div> <div style="text-align: center;">  1509001 <div style="display: flex; justify-content: space-around; font-size: 10px;"> P <input type="checkbox"/> H <input type="checkbox"/> C <input type="checkbox"/> </div> <div style="display: flex; justify-content: space-around; font-size: 8px;"> 15 24 NP FM LF LP </div> </div> </div>										
Packing Date & Time:	<table border="1" style="border-collapse: collapse; width: 100%;"> <tr> <td style="width: 20px; text-align: center;">D</td> <td style="width: 20px; text-align: center;">D</td> <td style="width: 20px; text-align: center;">M</td> <td style="width: 20px; text-align: center;">M</td> <td style="width: 20px; text-align: center;">2</td> <td style="width: 20px; text-align: center;">0</td> <td style="width: 20px; text-align: center;">:</td> <td style="width: 20px; text-align: center;">AM</td> <td style="width: 20px; text-align: center;"><input type="checkbox"/></td> <td style="width: 20px; text-align: center;">PM</td> <td style="width: 20px; text-align: center;"><input type="checkbox"/></td> </tr> </table>	D		D	M	M	2	0	:	AM	<input type="checkbox"/>	PM	<input type="checkbox"/>
D	D	M	M	2	0	:	AM	<input type="checkbox"/>	PM	<input type="checkbox"/>			

5. Heads in bags must be frozen until delivery to preserve samples.
6. Transfer all bags containing heads to the designated Archipelago Marine Research (AMR) dockside monitor **at the end of the offload.**
7. Let the AMR dockside monitor know if there aren't enough supplies for your next trip and they will resupply you.

For further assistance call the DFO Salmon Head Recovery Program at **1-866-483-9994.**

Appendix C - Table and map of Regions for defining catch strata

Table C1 – Correspondence between Regions and PFMA's and groundfish management areas. Regions were used to define strata for reporting, CWT analysis, and stock composition estimation.

Region	Abbreviation	Pacific Fishery Management Areas (PFMA's)	Groundfish Management Areas
West Coast Vancouver Island South	WCVI South	20 to 24, 121 to 124	3C, portions of 4B and 3D
West Coast Vancouver Island North	WCVI North	25 to 27, 125 to 127	3D, portions of 5A
Strait of Georgia	SoG	14 to 19, 28, 29	Portions of 4B
Queen Charlotte & Johnstone Strait	QC & JSt Strait	11, 12	Portions of 4B and 5A
North Coast	NC	3 to 10, 101 to 11, 127, 130, 142	5B, 5C, 5D, 5E, portions of 5A
Unassigned	UN	Unknown or multiple PFMA's	

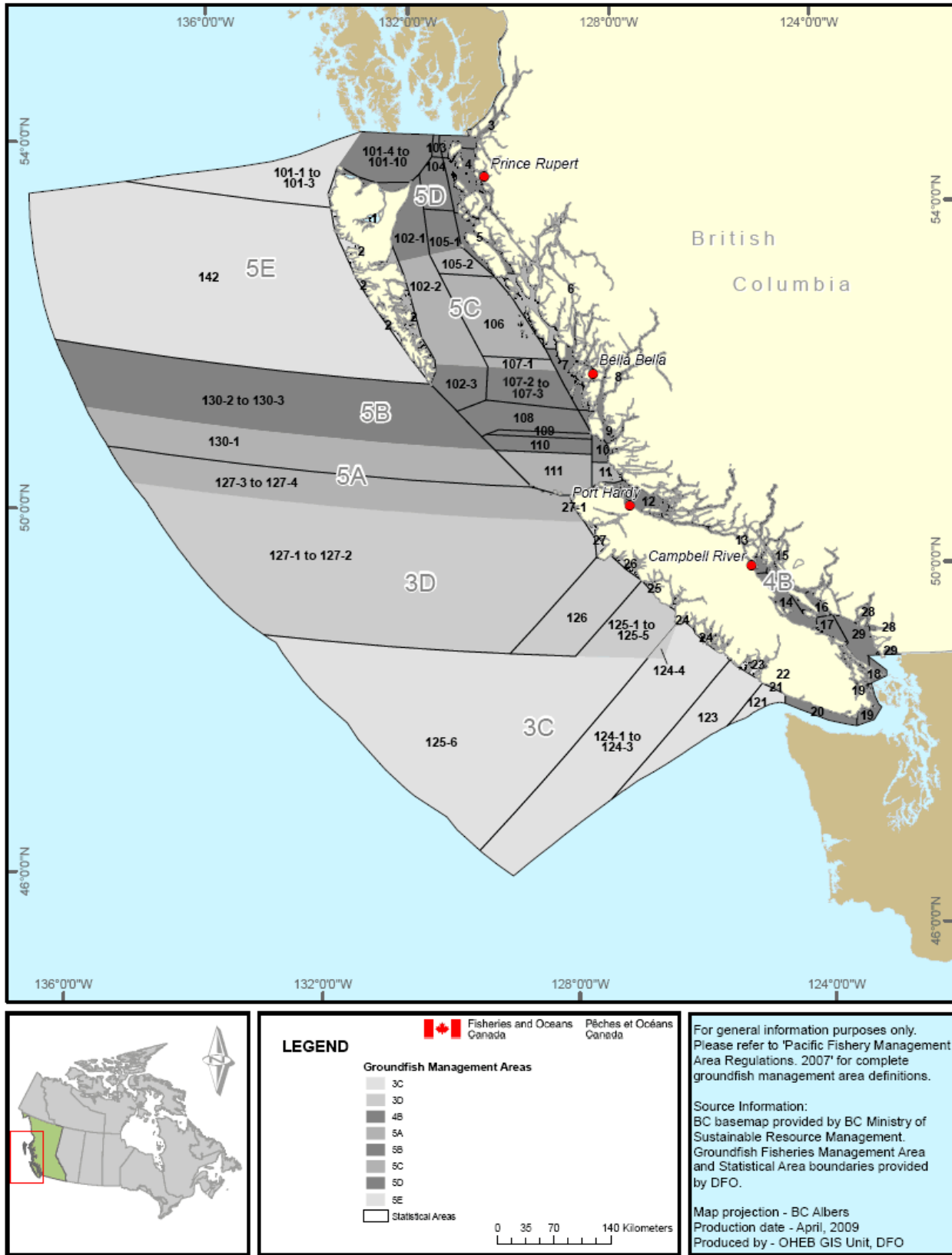


Figure C1 – Map of Groundfish Management Areas and PFMA. Adapted from <https://www.pac.dfo-mpo.gc.ca/fm-gp/maps-cartes/ground-fond/index-eng.html>

Appendix D - CWT Exploitation Rate Indicator Stocks used in Exploitation Rate Analysis

Figure D1—Geographical locations of historic and current Chinook salmon coded wire tag (CWT) exploitation rate indicator stocks. See Table D1 for the full stock names associated with each number. The southern B.C. and Puget Sound area, where concentration of the CWT indicators is greatest, is shown in the expanded view. Adapted from CTC 2023, Page 3

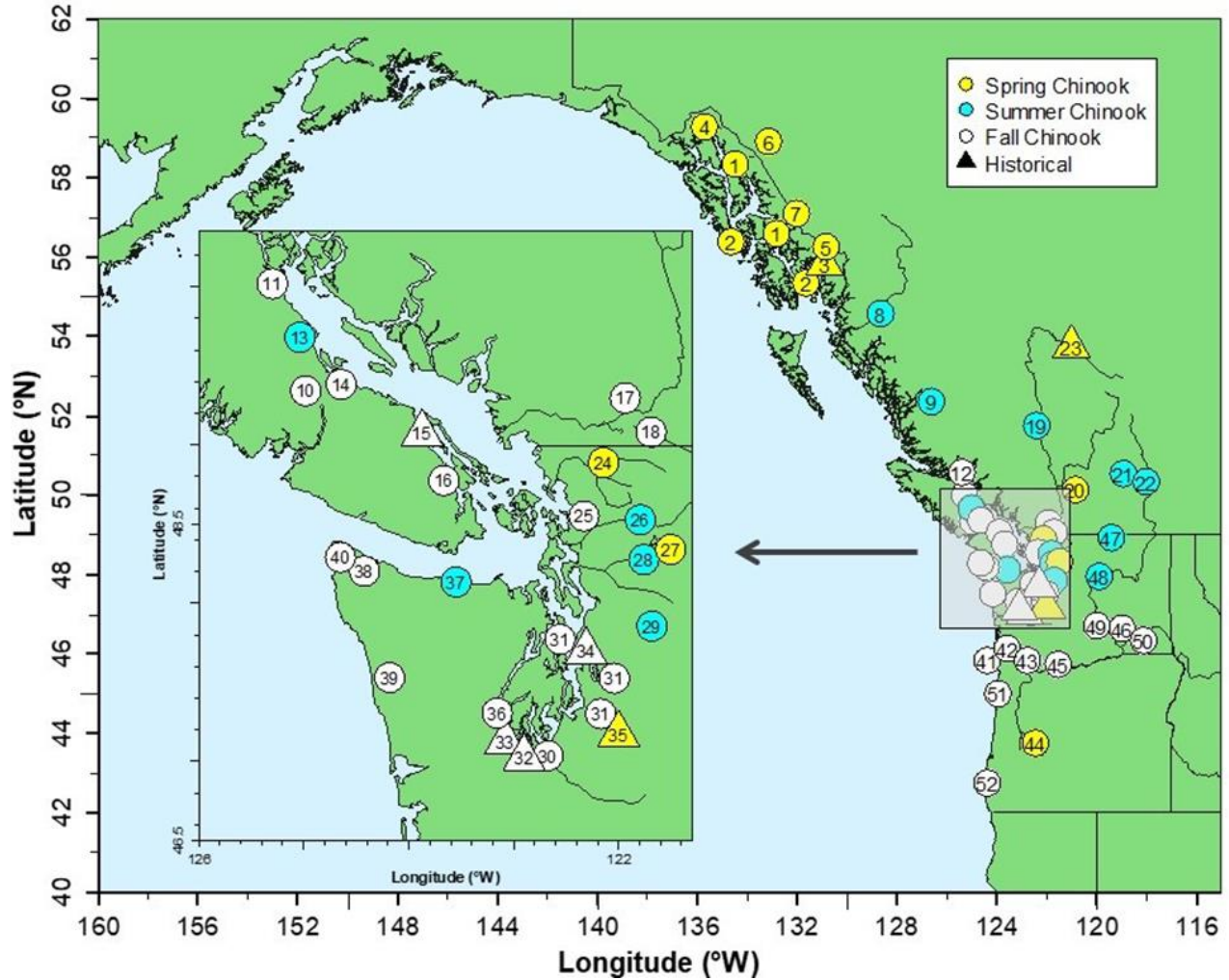


Table D1—Summary of current and historic (last tagged brood year in brackets) coded wire tag (CWT) exploitation rate indicator stocks, location, run type, and smolt age. Adapted from CTC 2023, Pages 4-5.

Stock/Area	Exploitation Rate Indicator Stock	Hatchery	Run Type	Smolt Age	Map No.	Status
Southeast Alaska	Northern Southeast Alaska (NSA)	Crystal Lake (ACI), Macaulay (AMC)	Spring	Age 1	1	Current
	Southern Southeast Alaska (SSA)	Herring Cove (AHC), Little Port Walter (ALP), Deer Mountain (ADM), Neets Bay (ANB)	Spring	Age 1	2	Current
	Chickamin (CHM)	Wild	Spring	Age 1	3	Historical (2005)
	Chilkat (CHK)	Wild	Spring	Age 1	4	Current
	Unuk (UNU)	Wild	Spring	Age 1	5	Current
Transboundary Rivers	Taku (TAK)	Wild	Spring	Age 1	6	Current
	Stikine (STI)	Wild	Spring	Age 1	7	Current
North/Central B.C.	Kitsumkalum (KLM)	Deep Creek	Summer	Age 1	8	Current
	Atnarko (ATN)	Snootli	Summer	Age 0	9	Current
WCVI	Robertson Creek (RBT)	Robertson Creek	Fall	Age 0	10	Current
Strait of Georgia	Quinsam (QUI)	Quinsam	Fall	Age 0	11	Current
	Phillips (PHI)	Gillard Pass	Summer/Fall	Age 0	12	Current
	Puntledge (PPS)	Puntledge	Summer	Age 0	13	Current
	Big Qualicum (BQR)	Big Qualicum	Fall	Age 0	14	Current
	Nanaimo (NAN)	Nanaimo	Fall	Age 0	15	Historical (2004)
	Cowichan (COW) ₁	Cowichan	Fall	Age 0	16	Current
Fraser River	Harrison (HAR)	Chehalis	Fall	Age 0	17	Current
	Chilliwack (CHI) ₁	Chilliwack	Fall	Age 0	18	Current
	Chilko (CKO)	Spius Creek, Chehalis	Summer	Age 1	19	In development
	Nicola (NIC)	Spius Creek	Spring	Age 1	20	Current
	Lower Shuswap (SHU) ₁	Shuswap Falls	Summer	Age 0	21	Current
	Middle Shuswap (MSH)	Shuswap Falls	Summer	Age 0	22	Current
	Dome (DOM)	Penny Creek	Spring	Age 1	23	Historical (2002)
North Puget Sound	Nooksack Spring Fingerling (NSF)	Kendall Creek	Spring	Age 0	24	Current
	Nooksack Spring Yearling (NKS)	Kendall Creek	Spring	Age 1		Historical (1996)
	Samish Fall Fingerling (SAM) ₂	Samish	Summer/Fall	Age 0	25	Current
	Skagit Summer Fingerling (SSF)	Marblemount	Summer	Age 0	26	Current
	Skagit Spring Fingerling (SKF)	Marblemount	Spring	Age 0	27	Current
	Skagit Spring Yearling (SKS) ₂	Marblemount	Spring	Age 1		Historical (2010)
Central Puget Sound	Stillaguamish Fall Fingerling (STL) ₃	Stillaguamish Tribal	Summer/Fall	Age 0	28	Current

Stock/Area	Exploitation Rate Indicator Stock	Hatchery	Run Type	Smolt Age	Map No.	Status
	Skykomish Summer Fingerling (SKY) _{2,3}	Wallace	Summer/Fall	Age 0	29	Current
South Puget Sound	Nisqually Fall Fingerling (NIS) ₂	Clear Creek	Summer/Fall	Age 0	30	Current
	South Puget Sound Fall Fingerling (SPS) ₂	Soos/Grovers/Is saquah creeks	Summer/Fall	Age 0	31	Current
	South Puget Sound Fall Yearling (SPY)	Tumwater Falls	Summer/Fall	Age 1	32	Historical (2013)
	Squaxin Net Pens Fall (SQP)	Squaxin Net Pen			33	Historical (1997)
	University of Washington Accelerated (UWA)	University of Washington			34	Historical (1988)
	White River Spring Yearling (WRY) ₄	White River	Spring	Age 1	35	Historical (2015)
Hood Canal	George Adams Fall Fingerling (GAD) ₂	George Adams	Summer/Fall	Age 0	36	Current
Juan de Fuca	Elwha Fall Fingerling (ELW)	Lower Elwha	Summer/Fall	Age 0	37	Current
North Washington Coast	Hoko Fall Fingerling (HOK)	Hoko Makah National Hatchery	Fall	Age 0	38	Current
	Queets Fall Fingerling (QUE)	Wild, Salmon River (WA)	Fall	Age 0	39	Current
	Tsoo-Yess Fall Fingerling (SOO) ₅	Makah National Fish Hatchery	Fall	Age 0	40	Current
Lower Columbia River	Columbia Lower River Hatchery (LRH) ₂	Big Creek	Fall Tule	Age 0	41	Current
	Cowlitz Tule (WA) (CWF)	Cowlitz	Fall Tule	Age 0	42	Current
	Lewis River Wild (LRW)	Wild	Fall Bright	Age 0	43	Current
	Willamette Spring (WSH) ₁	Willamette Hatcheries	Spring	Age 1	44	Current
	Spring Creek Tule (WA) (SPR) ₂	Spring Creek National Hatchery	Fall Tule	Age 0	45	Current
Upper Columbia River	Hanford Wild (HAN)	Wild	Fall Bright	Age 0	46	Current
	Similkameen Summer Yearling (SMK)	Similkameen and Omak Pond	Summer	Age 1	47	Current
	Columbia Summers (WA) (SUM)	Wells	Summer	Age 0/1	48	Current
	Columbia Upriver Brights (URB) ₂	Priest Rapids	Fall Bright	Age 0	49	Current
Snake River	Lyons Ferry Fingerling (LYF) ₆	Lyons Ferry	Fall Bright	Age 0	50	Current
	Lyons Ferry Yearling (LYY) ₂	Lyons Ferry	Fall Bright	Age 1		Current
North Oregon Coast	Salmon (SRH)	Salmon	Fall	Age 0	51	Current
Mid Oregon Coast	Elk River (ELK)	Elk River	Fall	Age 0	52	Current

Appendix E - SMU-CU-Reporting Units Tables

Table E1 – PBT-GSI reporting units and corresponding CU and SMU assignments used for stock composition estimates in this report.

Reporting Unit	CU #	Conservation Unit (CU) name	Stock Management Unit (SMU)
DOCEE	36	Docee	Central Coast
RI	37	Rivers Inlet	Central Coast
WANN	38	Wannock	Central Coast
BCR-BENT	39	Bella Coola-Bentinck	Central Coast
DEAN	40	Dean River	Central Coast
NCC-lake	41	North and Central Coast-late timing	Central Coast
NCC-stream	42	North and Central Coast-early timing	Central Coast
BB	2	Boundary Bay_FA_0.3	Fall 41 Boundary Bay
LFR-fall	3	Lower Fraser River_FA_0.3	Fraser Fall 41
STh-BESS	16	South Thompson-Bessette Creek_SU_1.2	Fraser Spring 42
LTh	17	Lower Thompson_SP_1.2	Fraser Spring 42
MFR-spring	10	Middle Fraser River_SP_1.3	Fraser Spring 52
UFR-spring	12	Upper Fraser River_SP_1.3	Fraser Spring 52
NTh-spr	18	North Thompson_SP_1.3	Fraser Spring 52
LFR-spring	4	Lower Fraser River_SP_1.3	Fraser Spring 52
LFR-UPITT	5	Lower Fraser River-Upper Pitt_SU_1.3	Fraser Spring 52
FRcanyon	8	Middle Fraser-Fraser Canyon_SP_1.3	Fraser Spring 52
STh-0.3	13	South Thompson_SU_0.3	Fraser Summer 41
STh-SHUR	15	Shuswap River_SU_0.3	Fraser Summer 41
Maria	7	Maria Slough_SU_0.3	Fraser Summer 41
MFR-summer	11	Middle Fraser River_SU_1.3	Fraser Summer 52
STh-1.3	14	South Thompson_SU_1.3	Fraser Summer 52
NTh-sum	19	North Thompson_SU_1.3	Fraser Summer 52
LFR-summer	6	Lower Fraser River_SU_1.3	Fraser Summer 52
Portage	9	Middle Fraser River-Portage_FA_1.3	Fraser Summer 52
LFR-suppl	9006	Fraser-Cross-CU Supplementation Exclusion<<Bin>>	Fraser-Cross
HGN	43	Haida Gwaii-North	Haida Gwaii
CWCH-KOK	22	East Vancouver Island-Cowichan and Koksilah_FA_0.x	Lower Georgia Strait
EVI-fall	25	East Vancouver Island-Nanaimo and Chemainus_FA_0.x	Lower Georgia Strait
SMn-SFj	28	Southern Mainland-Southern Fjords_FA_0.x	Mainland Inlet
HOMATH	34	Homathko_SU_x.x	Mainland Inlet
KLINA	35	Klinaklini_SU_1.3	Mainland Inlet
SMn-GStr	20	Southern Mainland-Georgia Strait_FA_0.x	Middle Georgia Strait
QP-fall	27	East Vancouver Island-Qualicum and Puntledge_FA_0.x	Middle Georgia Strait

Reporting Unit	CU #	Conservation Unit (CU) name	Stock Management Unit (SMU)
EVIGStr-sum	83	East Vancouver Island-Georgia Strait_SU_0.3	Middle Georgia Strait
LNR-P	57	Portland Sound-Observatory Inlet-Lower Nass	Nass
UNR	58	Upper Nass	Nass
SKEst	45	Skeena Estuary	Skeena
ECST	46	Ecstall	Skeena
LSK	48	Lower Skeena	Skeena
KALUM-E	49	Kalum_early timing	Skeena
KALUM-L	50	Kalum_late timing	Skeena
MSK-LGLKS	53	Middle Skeena-large lakes	Skeena
MSK-M_S	54	Middle Skeena-mainstem tributaries	Skeena
MSK-UprBulk	55	Upper Bulkley River	Skeena
USK	56	Upper Skeena	Skeena
ZYM	80	Zymoetz	Skeena
SIC	81	Sicintine	Skeena
NEVI	29	East Vancouver Island-North_FA_0.x	Upper Georgia Strait
SWVI	31	West Vancouver Island-South_FA_0.x	WCVI
NoKy	32	West Vancouver Island-Nootka and Kyuquot_FA_0.x	WCVI
NWVI	33	West Vancouver Island-North_FA_0.x	WCVI

Table E2 – CWT exploitation rate indicator stock codes and corresponding Chinook salmon CUs and SMUs used for stock composition estimates. Canadian CWTs that did not belong to an indicator stock are not included in this table, but were matched to CU and SMU through a table provided by the Enhancement Planning and Assessment Database (EPAD). EPAD is maintained by the Salmonid Enhancement Program and is DFO’s centralized repository for enhancement data in the Pacific Region.

Stock code	Stock name	Conservation Unit (CU)	Stock Management Unit (SMU)
SHU	Lower Shuswap	Shuswap River_SU_0.3	Fraser Summer 41
MSH	Middle Shuswap	Shuswap River_SU_0.3	Fraser Summer 41
HAR	Harrison River	Lower Fraser River_FA_0.3	Fraser Fall 41
RBT	Robertson Creek	West Vancouver Island-South_FA_0.x	WCVI
KLM	Kitsumkalum	Kalum_late timing	Skeena
PHI	Phillips River Fall	Southern Mainland-Southern Fjords_FA_0.x	Mainland Inlet
ATN	Atnarko	Bella Coola-Bentinck	Central Coast
BQR	Big Qualicum River	East Vancouver Island-Qualicum and Puntledge_FA_0.x	Middle Georgia Strait
KLY	Kitsumkalum	Kalum_late timing	Skeena
QUI	Quinsam River	East Vancouver Island-North_FA_0.x	Upper Georgia Strait
PPS	Puntledge River	East Vancouver Island-Georgia Strait_SU_0.3	Middle Georgia Strait
NIC	Nicola River	Lower Thompson_SP_1.2	Fraser Spring 42
COW	Cowichan River	East Vancouver Island-Cowichan and Koksilah_FA_0.x	Lower Georgia Strait
CHI	Chilliwack River	Fraser-Harrison Fall Transplant_FA_0.3	Fraser Fall 41

Appendix F - Salmon catch by Pacific Fishery Management Area for 2022

Table F1 – Estimated annual salmon catch (pieces retained and released) by Pacific Fishery Management Area (PFMA) in the groundfish trawl fishery during the 2022 calendar year. *Catches are confidential when fewer than 3 distinct vessels fished in an area over the time period.

PFMA	All salmon	Chinook	Coho	Chum	Pink	Sockeye	Unidentified salmon
0	4,235	4,191	2	34	0	0	5
3*							
7	228	216	7	1	1	0	3
11	3,819	3,350	0	455	0	13	1
12	2,340	2,291	0	57	0	12	0
14	2,854	2,816	0	38	0	0	0
15	38	38	0	0	0	0	0
17*							
18	123	123	0	0	0	0	0
20	206	145	32	29	0	0	0
21*							
29	49	49	0	0	0	0	0
101	183	173	0	7	2	0	1
104	32	31	1	0	0	0	0
105	1	1	0	0	0	0	0
107	10	1	6	1	0	0	2
108	24	15	4	4	1	0	0
109	12	4	3	3	2	0	0
110	5	2	0	3	0	0	0
111	17	11	2	4	0	0	0
121	4,911	4,337	374	99	9	13	79
123	3,175	3,004	138	33	0	0	18
124	902	860	17	22	1	0	2
125	526	457	4	64	0	1	11
126	54	42	0	12	0	0	0
127	548	306	23	234	0	0	0
130	2	2	0	0	0	0	0
142	3	0	0	0	0	3	0
Total	24,457	22,624	613	1,101	16	42	122